

Utah State University

DigitalCommons@USU

All Graduate Theses and Dissertations

Graduate Studies

12-2013

Substrate Binding and Reduction Mechanism of Molybdenum Nitrogenase

Zhiyong Yang
Utah State University

Follow this and additional works at: <https://digitalcommons.usu.edu/etd>

 Part of the [Chemistry Commons](#)

Recommended Citation

Yang, Zhiyong, "Substrate Binding and Reduction Mechanism of Molybdenum Nitrogenase" (2013). *All Graduate Theses and Dissertations*. 2052.
<https://digitalcommons.usu.edu/etd/2052>

This Dissertation is brought to you for free and open access by the Graduate Studies at DigitalCommons@USU. It has been accepted for inclusion in All Graduate Theses and Dissertations by an authorized administrator of DigitalCommons@USU. For more information, please contact digitalcommons@usu.edu.



SUBSTRATE BINDING AND REDUCTION MECHANISM OF MOLYBDENUM
NITROGENASE

by

Zhiyong Yang

A dissertation submitted in partial fulfillment
of the requirements for the degree

of

DOCTOR OF PHILOSOPHY

in

Biochemistry

Approved:

Dr. Lance C. Seefeldt
Major Professor

Dr. Lisa M. Berreau
Committee Member

Dr. Sean J. Johnson
Committee Member

Dr. Joan M. Hevel
Committee Member

Dr. Korry Hintze
Committee Member

Dr. Mark R. McLellan
Vice President for Research and
Dean of the School of Graduate Studies

UTAH STATE UNIVERSITY
Logan, Utah

2013

Copyright © Zhiyong Yang 2013

All Rights Reserved

ABSTRACT

Substrate Binding and Reduction Mechanism of Molybdenum Nitrogenase

by

Zhiyong Yang, Doctor of Philosophy

Utah State University, 2013

Major Professor: Dr. Lance C. Seefeldt
Department: Chemistry and Biochemistry

Nitrogenase is responsible for biological nitrogen fixation. The most studied nitrogenase is molybdenum nitrogenase. Combining genetic, biochemical, and spectroscopic methods, several advances toward understanding substrate binding and reduction mechanism of nitrogenase have been achieved.

One major goal of this dissertation was aimed at understanding the N_2 binding and reduction mechanism catalyzed by nitrogenase. A dihydride intermediate with two bridging hydrides bound to the FeMo-cofactor at E_4 state was proposed as the key intermediate for N_2 binding and activation. The ^{95}Mo -ENDOR characterization of this E_4 intermediate revealed that the Mo ion does not interact with the hydride ligands, suggesting that each hydride ligand bridges two Fe ions. When N_2 binds to the FeMo-cofactor, one equivalent of H_2 is produced. The N_2 -dependent incorporation of

D₂-derived deuterium into ethylene product of acetylene reduction during nitrogenase turnover strongly supports the proposed reductive elimination mechanism for N₂ binding and activation at E₄ state and confirms the mechanistic role of obligatory H₂ loss.

Once bound to the FeMo-cofactor, N₂ was proposed to be stepwise reduced to ammonia through diazene and hydrazine intermediates. Two EPR-active common intermediates have been freeze-trapped during turnover of an altered MoFe protein with diazene, methyldiazene, and hydrazine as substrates. Pulsed ENDOR characterization of these two intermediates led to the assignment of the FeMo-cofactor bound ligands as –NH₂ and NH₃, respectively. These results support a proposed N₂ reduction mechanism with unification of Lowe-Thorneley kinetic model and the alternating pathway.

The other major goal was aimed at expanding nitrogenase catalysis toward other substrates. It was found that the α -70 amino acid residue of MoFe protein has a steric effect on the carbon monoxide (CO) coordination to the FeMo-cofactor. Further study revealed that CO can be reduced and coupled to form hydrocarbons by remodeled molybdenum nitrogenase. Moreover, carbon dioxide (CO₂) was also found to be catalytically reduced to form methane by a remodeled molybdenum nitrogenase. The unprecedented formation of both propane and propylene was observed from the reductive coupling of CO₂ and acetylene, supporting a plausible coupling mechanism based on two adjacent substrate binding sites.

PUBLIC ABSTRACT

Substrate Binding and Reduction Mechanism of Molybdenum Nitrogenase

by

Zhiyong Yang, Doctor of Philosophy

Utah State University, 2013

Major Professor: Dr. Lance C. Seefeldt
Department: Chemistry and Biochemistry

As a key constituent of proteins, nucleic acids, and other biomolecules, nitrogen is essential to all living organisms including human beings. Dinitrogen represents the largest pool of nitrogen, about 79% of the Earth's atmosphere, yet it is unusable by most living organisms due to its inertness. There are two ways to fix this inert dinitrogen to usable ammonia. One is the industrial Haber-Bosch process, which needs to be conducted at high temperature and pressure. This process uses a lot of the non-renewable fossil fuel as the energy source. The other major pathway is the biological nitrogen fixation carried out by some microorganisms called diazotrophs. The usable nitrogen output from this biological pathway ultimately supports an estimated 60% of the human population's demand for nitrogen.

The catalyst responsible for the biological nitrogen fixation is called nitrogenase, the most studied form of which contains molybdenum and iron in its active center, so

called molybdenum nitrogenase. The work in this dissertation attempts to understand how this biological catalyst breaks down dinitrogen to ammonia by application of different modern techniques. Firstly, an approach was developed to understand the stepwise reduction mechanism of dinitrogen to ammonia by molybdenum nitrogenase.

The second goal of my research is to understand the roles of iron and molybdenum centers in nitrogenase function. My results using carbon monoxide as a probe for genetically modified molybdenum nitrogenase indicate that iron should be the metal sites functioning for nitrogen fixation. This is further supported by another study aimed at understanding the role of molybdenum during nitrogenase functioning.

Moreover, an approach was developed to understand the mechanism for the obligatory production of hydrogen gas when nitrogenase activates dinitrogen for reduction. The same study also suggests possible pathways for the addition of hydrogenous species to nitrogen to produce ammonia.

As part of this work, we also found that remodeled nitrogenases can use poisonous carbon monoxide and greenhouse-gas carbon dioxide to produce useful hydrocarbons by coupling one or more small molecules, which is hard to be achieved by other catalysts. Further study of these new reactions might give us deep insights on nitrogenase mechanism and inspire scientists to design better catalysts for relevant industrial processes.

DEDICATION

To Yang Weitian and Wang Zhuangyu, my dear parents, who gave me the chance to experience a great journey of life.

ACKNOWLEDGMENTS

Since the first chemical observation of fermentation of dough as a middle school student, my curiosity about chemistry never stopped. On my way of scientific exploration, there are many people who have helped me to get to this point and I appreciate them all forever. First and foremost, I thank my mentor both in science and life, Professor Lance C. Seefeldt, for everything in the past six years. I first met Dr. Seefeldt at Nankai University in China. It was that “twenty-minute” meeting with him that gave me this great opportunity to continue my science adventure in his lab at Utah State University. There were many challenges in the starting phase of my Ph.D. program, from both my biochemistry background and English. No matter how hard it was, Dr. Seefeldt was the one who gave me enough patience and helped me out of that stage. I appreciate his help for not only teaching me to be a better experimenter and writer, but also guiding me on how to cogitate science, which might be the most important thing for being a scientist. I have also benefitted from his example of scientific leadership, and his spirit of collaboration and friendship.

I also would like to take this chance to thank my committee members, Dr. Sean J. Johnson, Dr. Lisa M. Berreau, Dr. Joan M. Hevel, and Dr. Korry Hintze, for their kind advice and suggestions. I would not forget to thank Dr. Vernon D. Parker for his recommendation and kind help during my Ph.D. study.

I have been extremely fortunate to have been able to collaborate “closely” with many great scientists. Professor Brian M. Hoffman and Dr. Dmitriy Lukoyanov at Northwestern University, Professor Dennis R. Dean and his colleagues at Virginia Polytechnic Institute and State University, and Professor Stephen P. Cramer and Dr. Simon J. George at Lawrence Berkeley National Laboratory and University of California (Davis) are all invaluable collaborators and colleagues. I thank them all not only for publishing together, but also for the friendship we build up together.

I would never have been possible to complete my journey through this Ph.D. program without having help from the members of the Seefeldt lab. I was very fortunate to have Dr. Brett M. Barney as my mentor in the lab and learn from him. I’d like to thank Karamatullah Danyal, Miguel Alejandro Pabon, Dr. Bradley Wahlen, Robert Willis, Alex McCurdy, Dr. Simon Duval, Sudipta Shaw, and all others not named here for making a pleasant lab to work in. I especially thank Dr. Vivian Moure, Nimesh Khadka, and Dr. Andrew Fielding for working with me on those great projects. Their hard work saved me a lot of time to accomplish this dissertation. After working in the lab for six years, Dr. Bradley Wahlen and Karamatullah Danyal do deserve my special credits for everything we experienced together.

I would love to thank my colleagues in the department, especially Anna Lytle, Caleb Allpress, Stacey Anderson, Jeremy Bakelar, Sushma Saraf, Qian Zhang, and Shanying Gui, for their kind help and discussion to improve this dissertation. I thank Dr.

Alvan C. Hengge and his wife, Maribeth Evensen-Hengge, for their kind help during the last six years.

I appreciate all the good times my friends created for me. I could never imagine meeting Jer Pin Chong, Tiago Brando, and his wife, Andreia Suzuki, and becoming good friends in Logan, UT. I am very grateful to Dr. Dong Chen and his wife, Ningling Yin, for taking care of me all the time, no matter when I was “hungry or bored.” I also thank many other good friends I could not name one by one for being part of my life.

Finally and most importantly, I would like to thank my parents for their constant love and support through this time in my life. Without my parents’ constant love and encouragement, I would not have made it this far. I thank my brother and his family for taking care of my parents and having two brilliant granddaughters for the family. Thank my ex-wife, Yuan Chu, for her almost eight years’ support, patience, and love.

Life is tough. The life to be a scientist is even tougher, but fair enough for everybody. I am very happy that I never gave up on the way to be a scientist. Thankfully, I learned from both positive and negative sides of life.

Zhiyong Yang

CONTENTS

	Page
ABSTRACT.....	iii
PUBLIC ABSTRACT	v
DEDICATION.....	vii
ACKNOWLEDGMENTS	viii
LIST OF TABLES.....	xiii
LIST OF FIGURES	xiv
LIST OF SCHEMES AND CHARTS	xviii
ABBREVIATIONS	xix
CHAPTER	
1. INTRODUCTION	1
2. ENDOR/HYSCORE STUDIES OF THE COMMON INTERMEDIATE TRAPPED DURING NITROGENASE REDUCTION OF N_2H_2 , CH_3N_2H , AND N_2H_4 SUPPORT AN ALTERNATING REACTION PATHWAY FOR N_2 REDUCTION	56
3. UNIFICATION OF REACTION PATHWAY AND KINETIC SCHEME FOR N_2 REDUCTION CATALYZED BY NITROGENASE.....	91
4. IS MO INVOLVED IN HYDRIDE BINDING BY THE FOUR-ELECTRON REDUCED (E_4) INTERMEDIATE OF THE NITROGENASE MOFE PROTEIN?	112
5. ACETYLENE INTERCEPTION OF INTERMEDIATES REVEALS IMPORTANT ROLES OF METAL HYDRIDES IN NITROGENASE CATALYSIS.....	120
6. STERIC CONTROL OF THE HI-CO MOFE NITROGENASE COMPLEX REVEALED BY STOPPED-FLOW INFRARED SPECTROSCOPY	144

7.	MOLYBDENUM NITROGENASE CATALYZES THE REDUCTION AND COUPLING OF CO TO FORM HYDROCARBONS.....	155
8.	CARBON DIOXIDE REDUCTION TO METHANE AND COUPLING WITH ACETYLENE TO FORM PROPYLENE CATALYZED BY REMODELED NITROGENASE.....	171
9.	SUMMARY AND FUTURE DIRECTIONS.....	191
	APPENDICES	204
	APPENDIX A.....	205
	APPENDIX B.....	244
	APPENDIX C.....	253
	APPENDIX D.....	255
	CURRICULUM VITAE.....	261

LIST OF TABLES

Table	Page
1-1 Substrates for nitrogenases	15
1-2 Important variants of MoFe protein and and EPR parameters of the resulting intermediates with different substrates in the turnover state	23
6-1 Assignment of observed IR bands	149

LIST OF FIGURES

Figure	Page
1-1	Mo-nitrogenase with cofactors4
1-2	Structure of P-cluster in oxidized and reduced states8
1-3	FeMo-cofactor and key residues10
1-4	The deficit-spending model for electron transfer events in Mo-dependent nitrogenase12
1-5	Position of α -69 ^{Gly} and α -70 ^{Val}21
1-6	Modified Lowe-Thorneley kinetic scheme for reduction of N ₂26
1-7	Metal hydrides and the FeMo-cofactor30
1-8	Stepwise reduction of N ₂ following the “distal” (D) (left) and “alternating” (A) pathways (right)33
2-1	Structure of FeMo-cofactor.....58
2-2	EPR spectra of intermediate I (l(N ₂ H ₄)) detected by various techniques.....64
2-3	35 GHz CW ¹ H ENDOR spectra of I (l(N ₂ H ₄))66
2-4	Contour presentations of the ¹ H HYSCORE spectra of the l(N ₂ H ₄) intermediate (magnetic field 332.0 mT (A) and 345.0 mT (B)).....70
2-5	(A) Comparison of 35 GHz ReMims pulsed ¹⁵ N ENDOR spectra of intermediates trapped during turnover of the α -70 ^{Ala} / α -195 ^{Gln} MoFe protein with ¹⁵ N ₂ H ₄ , ¹⁵ N ₂ H ₄ , and ¹⁵ NH=N-CH ₃ (denoted ¹⁵ MD). (B) 2D Field-Frequency plot of 35 GHz pulsed ¹⁵ N ENDOR spectra of l(¹⁵ N ₂ H ₄) intermediate71
2-6	35 GHz Mims ¹⁵ N ENDOR spectra detected at the maximum of EPR signal intensity ($g_2 = 2.018$) for l(¹⁵ N ₂ H ₄) (black) and m(¹⁵ N ₂ H ₂) (red) intermediates....75
2-7	Contour presentations of the ^{14,15} N HYSCORE spectra of the l(N ₂ H ₄) intermediate with ¹⁴ N ₂ H ₄ (A) and ¹⁵ N ₂ H ₄ (B)77

2-8	Contour (A, C) and stacked (B, D) presentations of the cross-features 3 from the HYSCORE spectra of the I(¹⁵ N ₂ H ₄) intermediate	82
3-1	Q-band CW EPR spectrum of α -70 ^{Val→Ala} , α -195 ^{His→Gln} MoFe protein in resting state ($S = 3/2$) and trapped during turnover with ¹⁴ N ₂ H ₄	95
3-2	ESEEM traces for non-Kramers intermediate H of α -70 ^{Val→Ala} , α -195 ^{His→Gln} MoFe protein under turnover.....	98
3-3	Integration of LT kinetic scheme with Alternating pathways for N ₂ reduction ...	106
3-4	Proposed pathways for reduction of N ₂ H ₂ and N ₂ H ₄	108
4-1	FeMo-cofactor from PDB coordinate file 1M1N.pdb	112
4-2	(Left) Davies ⁹⁵ Mo-ENDOR spectra of ⁹⁵ Mo-enriched (black) and natural-abundance (red) α -70 ^{lle} MoFe protein in the resting state, and (Right) CW ⁹⁵ Mo -ENDOR spectra of ⁹⁵ Mo-enriched (black) and natural-abundance (red) α -70 ^{lle} MoFe protein in E ₄ intermediate state.....	116
5-1	FeMo-cofactor and key mechanistic steps	123
5-2	Time-dependent formation of mono- and di-deutero ¹³ C-ethylene catalyzed by nitrogenase	126
5-3	Deuterated ethylene formation as a function of acetylene partial pressure	127
5-4	Deuterated ethylene formation as a function of D ₂ partial pressure	128
5-5	Deuterated ethylene formation as a function of N ₂ partial pressure	129
5-6	Deuterated ethylene formation as a function of electron flux.....	130
5-7	Proposed acetylene interception mechanisms.....	132
5-8	A full reaction pattern for acetylene interception of deuteride containing nitrogenase intermediates.....	137
6-1	FeMo-cofactor showing the position and potential steric influence of the α -70 residue over the Fe 6 atom on the Fe 2, 3, 6, 7 face	145
6-2	Transient IR spectra of the <i>A. vinelandii</i> MoFe nitrogenase hi-CO complex showing the effect of varying the size of the α -70 sidechain.....	148

7-1	Time course of hydrocarbon production by the α -Ala ⁷⁰ and α -Gly ⁷⁰ substituted MoFe proteins	160
7-2	Time course of hydrocarbon production by the α -Ala ⁷⁰ / α -His ⁹⁶ and α -Ala ⁷⁰ / α -Ala ¹⁹¹ substituted MoFe proteins.....	162
7-3	Time course of hydrocarbon production by the α -Ala ⁷⁰ and α -Ala ⁷⁰ / α -Gln ¹⁹⁵ substituted MoFe proteins.....	163
7-4	Electron flux dependence on CO reduction product profile	164
7-5	CO pressure dependence on CO reduction product profile	165
7-6	Schematic representation of a possible CO-derived hydrocarbon formation at the nitrogenase active site	167
8-1	The FeMo-cofactor with some key amino acid residues	173
8-2	CH ₄ formation as a function of time for different MoFe proteins	175
8-3	Electron flux dependence for CO ₂ reduction to CH ₄	177
8-4	Propylene formation from CO ₂ and acetylene as a function of electron flux	179
8-5	Propylene formation from CO ₂ and acetylene	180
9-1	Standard Gibbs free energy change diagrams for N ₂ reduction.....	192
9-2	Mo-EXAFS spectra for α -70 ^{Ala} / α -195 ^{Gln} MoFe protein at different states.....	200
9-3	CO inhibition of proton reduction catalyzed by different MoFe proteins	201
B-S1	Two-pulse field-sweep ESE spectra of intermediate I (I(N ₂ H ₄)) recorded with $\tau = 200$ ns	245
B-S2	Field dependence of 35 GHz CW ¹ H ENDOR spectra of I (I(N ₂ H ₄)) obtained for samples prepared in H ₂ O (black) and D ₂ O (red) buffers	246
B-S3	Stacked presentations of sets of four-pulse ESEEM spectra of I(N ₂ H ₄) intermediate.....	249
B-S4	¹ H HYSORE.....	250
B-S5	¹ H HYSORE.....	251

C-S1	Time courses from transient IR spectra of the <i>A. vinelandii</i> MoFe nitrogenase hi-CO complex showing the effect of varying the size of the α -70 side chain....	254
D-S1	Dependence of CH ₄ formation on partial pressure of CO ₂	256
D-S2	Dependence of CH ₄ formation on concentration of HCO ₃ ⁻	257
D-S3	GC-MS analysis of methane	258
D-S4	Effect of hemoglobin on CH ₄ formation.....	259
D-S5	GC-MS analysis of propylene.....	260

LIST OF SCHEMES AND CHARTS

	Page
Scheme 2-1 N ₂ reduction pathways	59
Chart 4-1 Representative hydrides bridging modes	114

ABBREVIATIONS

a	isotropic hyperfine tensor in ENDOR
A	hyperfine coupling constant
Å	angstrom
ADP	adenosine 5'-diphosphate
ADP-AlF ₄ ⁻	a complex of adenosine 5'-diphosphate and aluminum tetrafluoride
ATP	adenosine 5'-triphosphate
Bis-Tris	bis(2-hydroxyethyl)amino-tris(hydroxymethyl)methane
BSA	bovine serum albumin
CW	continuous wave
DNA	deoxyribose nucleic acid
EDC	1-ethyl-3-(3-dimethylaminopropyl)carbodiimide, crosslinking chemical reagent
EDTA	ethylenediaminetetraacetic acid
EI	electron ionization, an ionization method for mass spec technique
E_m	midpoint redox potential
ENDOR	electron nuclear double resonance, a pulsed EPR technique
EPR	electron paramagnetic resonance spectroscopy
ESEEM	electron spin echo envelope modulation, a pulsed EPR technique
ET	electron transfer
EXAFS	extended X-ray absorption fine structure

FeMo-co	iron-molybdenum cofactor, also called FeMo-cofactor or M-cluster, the active site for substrate binding and reduction in Mo-dependent nitrogenase
Fe protein	iron protein, dinitrogenase reductase
Fe ^{Red}	dithionite reduced iron protein
Fe ^{Ox}	one electron oxidized state of dithionite reduced Fe protein
FID	flame ionization detector
<i>g</i> -factor	<i>g</i> value, dimensionless magnetic moment, also called Landé <i>g</i> -factor splitting
GC	gas chromatograph
HEPES	<i>N</i> -2-hydroxyethylpiperazine- <i>N'</i> -2-ethane sulfonic acid
HYSCORE	hyperfine sublevel correlation spectroscopy
IR	infrared spectroscopy
K_d	dissociation constant
K_m	Michaelis constant
MCD	magnetic circular dichroism
MES	2-(<i>N</i> -morpholino)ethanesulfonic acid
mg	milligram
MgADP	complex of Mg ²⁺ and adenosine 5'-diphosphate
MgATP	complex of Mg ²⁺ and adenosine 5'-triphosphate
mL	milliliter
M ^N	dithionite reduced oxidation state or resting state of the FeMo-cofactor
MoFe protein	molybdenum iron protein, dinitrogenase
MOPS	3-(<i>N</i> -morpholino)propanesulfonic acid

M^{Ox}	one electron oxidized state of resting state FeMo-cofactor
M^R	one electron reduced state of resting state FeMo-cofactor
MS	mass spectrometry
m/z	mass over charge ratio
<i>nifD</i>	gene coding for the alpha-subunit of MoFe protein
<i>nifH</i>	gene coding for the gamma-subunit of Fe protein
<i>nifK</i>	gene coding for the beta-subunit of MoFe protein
NK-EPR	non-Kramers state EPR
NMR	nuclear magnetic resonance
NRVS	nuclear resonance vibrational spectroscopy
P^{1+}	one electron oxidized state of dithionite-reduced P-cluster
P^{2+}	two electron oxidized state of dithionite-reduced P-cluster
P-cluster	[8Fe-7S] cluster in MoFe protein, responsible for electron transfer
PDB ID	the 4-character unique identifier of every entry in the Protein Data Bank
P_i	inorganic phosphate
P^N	dithionite reduced state or resting state of P-cluster
P^{Ox}	oxidized state of P-cluster, refer to P^{2+} and/or P^{1+}
PTV	programmed temperature vaporization
Q-band	a segment of microwave frequency range from 30-50 GHz
ReMims ENDOR	refocused Mims electron nuclear double resonance
RF	radio frequency
RFQ	rapid freeze quench

SAM	<i>S</i> -adenosyl methionine
SAXS	small-angle X-ray scattering
S-band	a segment of microwave frequency range from 2-4 GHz
SDS-PAGE	sodium dodecyl sulfate-polyacrylamide gel electrophoresis
SF-FTIR	stopped-flow Fourier transform infrared spectroscopy
SIM	selected ion monitoring mode of mass spec technique
τ	time interval between two microwave pulses in pulsed ENDOR experiments
TAPS	<i>N</i> -tris(hydroxymethyl)methyl-3-aminopropanesulfonic acid
TRIS	tris(hydroxymethyl)aminomethane
WT	wild-type or wild type
ν_N	Larmor frequency
XES	X-ray emission spectroscopy
X-band	a segment of microwave frequency range from 8-12 GHz

CHAPTER 1

INTRODUCTION¹

Nitrogen Fixation

Fixed nitrogen (N) is a fundamental constituent of basic building blocks of life such as nucleotides for DNA and amino acids for proteins (1). Dinitrogen (N₂) is the major constituent (79%) of the Earth's atmosphere, representing the largest global pool of nitrogen. While nitrogen is essential to all life, the vast reservoir of dinitrogen in the atmosphere is unusable by most organisms (1, 2). This is largely a consequence of the high bond dissociation energy for the N₂ triple bond (3), making the breaking of this bond and "fixation" of the nitrogen to a form usable to living organisms energetically challenging. Dinitrogen can be fixed with considerable energy input by addition of electrons and protons to yield two ammonia (NH₃) molecules, so called nitrogen fixation. In the industrial Haber-Bosch process for fixing dinitrogen, the reaction is carried out at high temperatures (~ 450 °C) and pressures (> 200 atm) in the presence of an iron catalyst, with the electrons and protons coming from H₂ (2, 4–6). This process is extremely energy demanding, utilizing approximately 1% of the total fossil fuel used globally (7). However, the ammonia produced through this process is the precursor of the majority of nitrogenous fertilizers produced today.

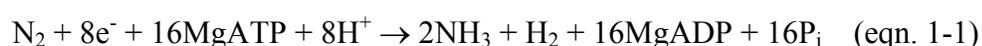
¹ Part of text and figures in this chapter is reproduced from these publications: (1) Coauthored by Zhi-Yong Yang, Karamatullah Danyal, and Lance C. Seefeldt (2011) Mechanism of Mo-dependent nitrogenase, *Methods in Molecular Biology* **766**, 9-29 as a chapter in *Nitrogen Fixation: Methods and Protocols* edited by Markus W. Ribbe. Copyright 2011 Springer Science+Business Media, LLC. With kind permission of Springer Science+Business Media; and (2) Coauthored by Lance C. Seefeldt, Zhi-Yong Yang, Simon Duval, and Dennis R. Dean (2013) Nitrogenase reduction of carbon-containing compounds, *Biochimica et Biophysica Acta (BBA) – Bioenergetics* <http://dx.doi.org/10.1016/j.bbabi.2013.04.003>. Copyright (2013), with permission from Elsevier.

The other major pathway for nitrogen fixation is through the action of microorganisms (called diazotrophs (8)) that carry out a process called biological nitrogen fixation (6, 8) discovered more than 120 years ago (9, 10). The fixed nitrogen (N) from this process accounts for approximately 60% of the total fixed N input from N₂ into the global biogeochemical nitrogen cycle (11) with the most of the remaining from the Haber-Bosch process (2, 12, 13). Biological nitrogen fixation is catalyzed by a complex metalloenzyme called nitrogenase (14, 15), found in the bacterial and archaeal domains of life (16, 17). The biosynthesis of nitrogenases is a complex process requiring the participation of many gene products (*Nif*, *Vnf*, or *Anf*) (18–23).

Three major classes of nitrogenase have been reported, with a key difference among the classes being the identity of the heterometal contained in their active site metal cluster (14, 15, 24). The most widely distributed and best-studied class of nitrogenase is the molybdenum (Mo)-dependent nitrogenase (or Mo-nitrogenase), which appears to be the paradigm for nitrogenases (14, 20, 22, 25–35). The active site of Mo-dependent nitrogenase, an iron and molybdenum containing metal cluster, is designated to “FeMo-cofactor” (FeMo-co) (36–38). The other two classes of nitrogenase contain V or Fe atom in place of Mo (15, 39), which are often referred to “alternative” nitrogenases. The alternative nitrogenases are less efficient at N₂ reduction when compared to Mo-dependent nitrogenase (15, 39, 40). Given that most of the mechanistic information known about nitrogenases is for the Mo-dependent enzyme, this dissertation will focus on this enzyme.

Mo-dependent Nitrogenase: Overview

The two component proteins of the Mo-dependent nitrogenase are called the iron (Fe) protein (or dinitrogenase reductase) and the molybdenum-iron (MoFe) protein (or dinitrogenase) (**Figure 1-1**). These two component proteins work together to catalyze the reduction of dinitrogen in a complex reaction with an ideal reaction stoichiometry shown in equation 1-1 (41).



Since the first report of the cell-free enzyme preparation in 1960 (42), a breakthrough in understanding nitrogenase mechanism came from the X-ray crystal structures of the component proteins solved individually (43–63) and in couple (64–67). In this section, general information about the Fe protein, the MoFe protein, and the interaction between the two proteins will be reviewed.

Fe Protein

The Fe protein is a homodimer (coded by the *nifH* gene) with a molecular mass of approximately 64,000 Da (47, 68). It contains two nucleotide (MgATP or MgADP) binding sites, one on each subunit, and a single [4Fe-4S] cluster that bridges the two subunits (**Figure 1-1**) (47, 68). The Fe protein is the physiological reductant of the MoFe protein that catalyzes substrate reduction. In addition to delivering electrons to the MoFe protein, the Fe protein also is known to function in the maturation of the MoFe protein and in the bioassembly of the active site metal cluster called FeMo-cofactor (20, 69). This maturation role for the Fe protein does not appear to require electron transfer or the ATP hydrolysis function (14).

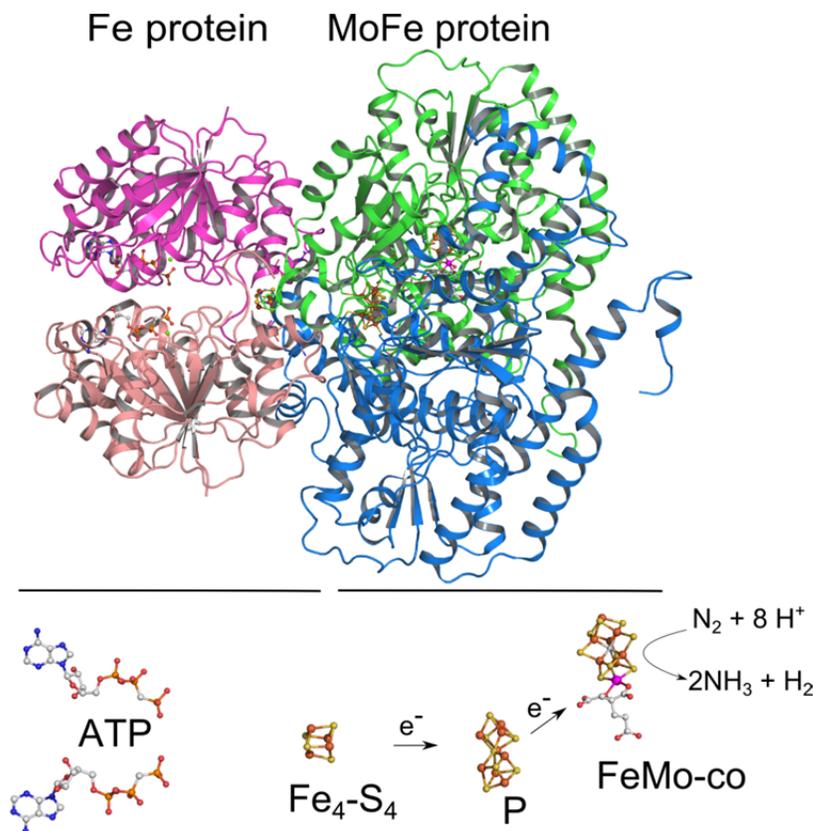
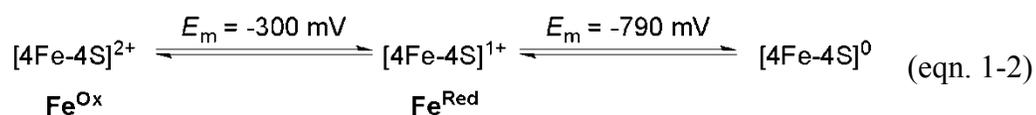


Figure 1-1. Mo-nitrogenase with cofactors. Shown is one functioning half of the Mo-dependent nitrogenase. The top shows the Fe protein (left) and an $\alpha\beta$ -dimer half of the MoFe protein (right). Shown below are the metal clusters and ATP, with Fe in rust, S in yellow, C in gray, O in red, N in blue, and Mo in magenta. Reproduced from PDB 2AFK.

Redox properties of the [4Fe-4S] cluster—The Fe protein contains a single [4Fe-4S] cluster that serves as a carrier of electrons. The X-ray structure of the Fe protein revealed that this cluster is symmetrically ligated between the two Fe protein subunits, with each subunit contributing two cysteine ligands (**Figure 1-1**). The [4Fe-4S] is known to access three redox states (eqn. 1-2) (14, 70–72).



The 1+ oxidation state (Fe^{Red}) of the [4Fe-4S] cluster is the dominant state of the purified enzyme in the presence of the reductant dithionite ($\text{S}_2\text{O}_4^{2-}$) (73–75). The 1+ oxidation state of the [4Fe-4S] cluster can be reversibly oxidized by the removal of one electron, achieving the 2+ oxidation state (Fe^{Ox}), with the iron atoms distributed as 2Fe^{2+} and 2Fe^{3+} (75–77). This reversibility allows the establishment of the midpoint reduction potential (E_m) for the $[4\text{Fe-4S}]^{2+/1+}$ redox couple using voltametric and coulometric methods (78–80). The values of E_m are dependent on the organism from which the Fe protein is purified and the presence or absence of bound nucleotides (14). The E_m for the $[4\text{Fe-4S}]^{2+/1+}$ couple of the Fe protein from *Azotobacter vinelandii* is measured to be -300 mV in the absence of nucleotides (eqn. 1-2) (77, 81). Upon addition of MgATP and MgADP, the E_m value shifts negative to -430 and -440 mV, respectively (81). It is well established from kinetic and spectroscopic studies that the $[4\text{Fe-4S}]^{2+/1+}$ redox couple of the [4Fe-4S] cluster in the Fe protein is functional during nitrogenase catalysis (14, 28, 70).

The Fe protein binds nucleotides—Early work on nitrogenase revealed that the Fe protein could bind nucleotides and that the hydrolysis of nucleotides by the nitrogenase complex was critical to the transfer of an electron from the Fe protein to the MoFe protein (28, 82). The Fe protein binds two nucleotides, one to each subunit. The nucleotide binding sites on the Fe protein are on the opposite end of the Fe protein from the [4Fe-4S] cluster (51, 53, 58, 59, 61, 64–67). A divalent metal is required for the binding of nucleotides to the Fe protein. While a number of different metals will work, it

is thought that Mg^{2+} is the physiologically relevant metal (83). While the Fe protein binds MgATP, it shows undetectable rates of hydrolysis in the absence of the MoFe protein (70). It is only after the Fe protein binds to the MoFe protein that hydrolysis is activated. This observation has been explained from examination of X-ray structures of the Fe protein with bound nucleotides as the movement of a likely catalytic base into place to activate hydrolysis following Fe protein binding to the MoFe protein.

Nucleotide binding induces protein conformational changes in the Fe protein—There is ample evidence showing that the binding of nucleotides to the Fe protein induces conformational changes to the protein structure that impact many aspects of its function. For example, the binding of MgATP or MgADP to the Fe protein shifts the E_m for the $[4Fe-4S]^{2+/1+}$ redox couple to more negative potentials by about -120 mV (described above). It is clear that these changes are not the result of nucleotides binding directly to the $[4Fe-4S]$ cluster, but rather a result of nucleotide induced protein conformational changes impacting the cluster over a distance. The nucleotide binding sites are located approximately 15 Å away from the $[4Fe-4S]$ cluster (51, 53, 58, 59, 61, 64–67). Recent studies using both small angle X-ray scattering (SAXS) and X-ray crystallography provide clearer pictures of the larger structural changes induced in the Fe protein upon nucleotide binding (84).

MoFe Protein

The MoFe protein is an $\alpha_2\beta_2$ heterotetramer ($M_r \sim 240,000$ Da) with the α and β subunits encoded by the *nifD* and *nifK* genes, respectively (14, 20, 32, 68, 69). Each $\alpha\beta$ dimeric unit contains two unique metalloclusters: a P-cluster ($[8Fe-7S]$) and a FeMo-

cofactor ([7Fe-9S-Mo-C-(R)-homocitrate]) (27, 44, 49, 60). The FeMo-cofactor is embedded solely in the α -subunit, while the P-cluster is located at the interface between the α and β subunits (43, 46) (**Figure 1-1**). Each $\alpha\beta$ -unit appears to function as a catalytic half.

P-cluster—Early Mössbauer spectroscopic studies of the MoFe protein revealed that the P-cluster was composed of eight ferrous Fe atoms in the resting state in the presence of dithionite (termed the P^N state) (85). The X-ray structures revealed the nature of this unusual cluster (**Figure 1-2**) as being composed of two cubic [4Fe-4S] subclusters sharing a common sulfide ligand at one corner (43, 44, 46, 54, 63). Each Fe atom is coordinated by two or three sulfide ligands and one terminal or bridging cysteinyl ligand from a cysteine residue in the α or β subunit. Upon oxidation, one of the cubic units is opened up with two Fe-S bonds (Fe5-S1 and Fe6-S1) being cleaved and two novel Fe6-O and Fe5-N bonds being formed. Further, a serinate-O (β -188^{Ser}) and a backbone amide-N (α -88^{Cys}) become ligands to Fe atoms (**Figure 1-2**) (63).

From *in vitro* studies using dye oxidants, it has been shown that the resting state of the P cluster (P^N) can be oxidized by up to three electrons (P^{1+} , P^{2+} , and P^{3+}) (eqn. 1-3) (86–89). The E_m values measured for these redox couples are shown for the *A. vinelandii* MoFe protein in equation 1-3 (77, 90, 91).



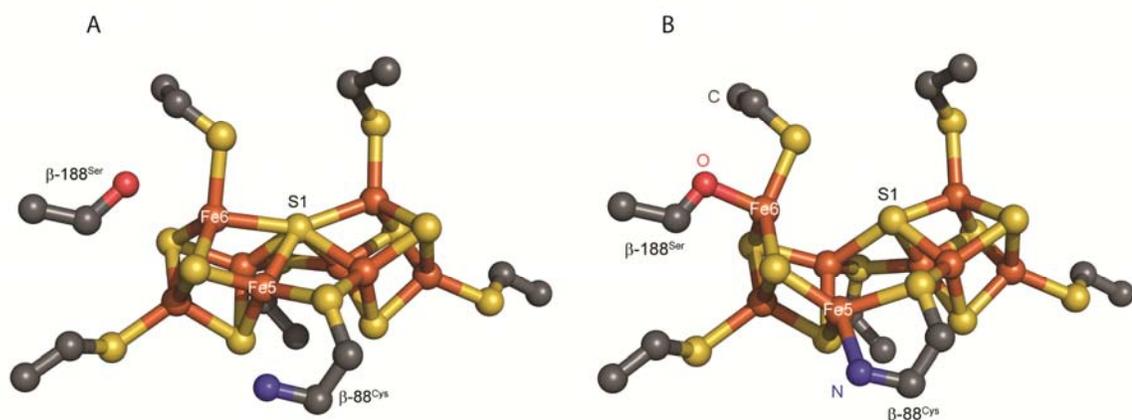


Figure 1-2. Structure of P-cluster in oxidized and reduced states. The reduced state (P^N) of the P-cluster (panel A) and the oxidized state (P^{OX}) of the P-cluster (panel B) are shown (3MIN.pdb and 2MIN.pdb, respectively).

Because both P^{1+} and P^{2+} oxidation states are usually populated in oxidized states of the MoFe protein, these two oxidation states are often collectively referred to as the P^{OX} state. The P^{3+} oxidation state is not reversible, so is not believed to be functioning during catalysis. Recently, magnetic circular dichroism (MCD) spectroscopic study of the P^{1+} state from a MoFe protein variant (92) suggested that the P-cluster could be viewed as two coupled 4Fe clusters and that it could donate either one or two electrons to FeMo-cofactor by using one or both of its 4Fe halves (93).

FeMo-cofactor—the active site of nitrogenase—The FeMo-cofactor (36), also called the M-cluster (**Figure 1-3**), is the site for substrate binding and reduction of Mo-dependent nitrogenase. The structure of FeMo-cofactor was established when the X-ray structure of the MoFe protein was solved (27). The early structure revealed a

heterometallocluster with a composition [7Fe-9S-Mo-X-(R)-homocitrate] with the first assignment of the interstitial X as a light atom (C, N, or O) bound to each of the central 6 Fe atoms (48). ENDOR studies have suggested that it is not an exchangeable N atom, but have left open the possibility that it is a non-exchanging N or C atom (94–96). Likewise, a number of previous calculations support the presence of X, but do not provide a definitive assignment for X (97–101). Recently, the interstitial atom has been conclusively assigned to a C atom by a 1.0 Å-resolution structure and ESEEM spectroscopy (49), X-ray emission spectroscopy (XES) of MoFe protein (102) with the methyl group in *S*-adenosyl methionine (SAM) as the C-source (103). The results from tracing the fate of the ¹³C- and ¹⁴C-labeled interstitial carbide ligand in the protein under turnover conditions showed that this carbide is non-exchangeable (94) and cannot be used as a substrate and incorporated into the products (104).

The FeMo-cofactor is ligated to the peptide matrix through one cysteine ligand (α -275^{Cys}) bound to the Fe atom at one end and through one histidine ligand (α -442^{His}) bound to the Mo atom at the other end. The six Fe atoms in the middle part are arranged as a prismatic structure with each Fe atom coordinated by three sulfide atoms. Homocitrate provides two oxygen atom (C1 carboxylate and C3 hydroxylate) ligands to the Mo (105, 106). Thus, the overall structure of the FeMo-cofactor can be viewed as one [4Fe-3S-C] cubane and one [Mo-3Fe-3S-C] cubane that are connected by three bridging sulfides with one shared μ_6 -C atom at the center.

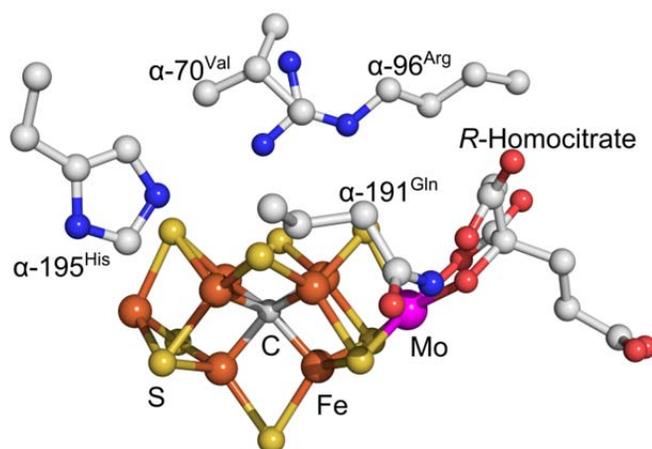


Figure 1-3. FeMo-cofactor and key residues. Shown is the FeMo-cofactor with key MoFe protein amino acid side chains. Colors are Fe in rust, S in yellow, C in gray, O in red, N in blue, and Mo in magenta. PDB: 2AFK.

FeMo-cofactor can be reversibly oxidized or reduced from its resting state. The resting state of FeMo-cofactor (M^N) occurs in the MoFe protein isolated in the presence of dithionite. This state is paramagnetic with a rhombic $S = 3/2$ spin EPR signal (107). Treatment of the MoFe protein with oxidizing dyes results in the one electron oxidation to the M^{Ox} state (85, 86). The M^{Ox} state is diamagnetic ($S = 0$) and EPR silent. The E_m for the $M^{Ox/N}$ redox couple is about -40 mV (108). The M^N state can be reduced. Incubation with the Fe protein in the presence of MgATP and dithionite results in the reduction of FeMo-cofactor to an M^R state with an interger spin ($S \geq 1$) state that is EPR silent (109, 110). The E_m for the $M^{N/R}$ redox couple has not been measured, but has been estimated as -465 mV (111). The oxidation states of the Fe atoms and the Mo atom in the resting state of FeMo-cofactor (M^N) have been examined by Mössbauer and ENDOR spectroscopies.

The Mössbauer study suggested an assignment of $[\text{Mo}^{4+}, 3\text{Fe}^{3+}, 4\text{Fe}^{2+}, 9\text{S}^{2-}]$ (110), which is supported by calculations using a model with the interstitial atom (112). The ^{57}Fe ENDOR study suggested an assignment of $[\text{Mo}^{4+}, 1\text{Fe}^{3+}, 6\text{Fe}^{2+}, 9\text{S}^{2-}]$ for two electron reduced state relative to the resting state FeMo-cofactor (113, 114). In Chapter 5 of this dissertation, we found that the oxidation state of Mo is +4 after accumulations of four electrons as two bridging hydrides to FeMo-cofactor.

Fe Protein-MoFe Protein Complex Formation and Electron Transfer

During the catalytic cycle, an Fe protein binds transiently to one MoFe protein $\alpha\beta$ unit. Several structures of the complex of the Fe protein bound to the MoFe protein reveal the interfaces where the Fe protein and MoFe protein dock (64–67). These structures place the P cluster directly in-line and between the Fe protein [4Fe-4S] cluster and the FeMo-cofactor (**Figure 1-1**). The distance between the [4Fe-4S] cluster and the P-cluster varies depending on the nucleotide bound state of the Fe protein, leading to a model wherein one role of nucleotides is to alter this electron transfer distance and therefore the electron transfer rate. The arrangement of the three metalloclusters suggests an electron transfer chain from the [4Fe-4S] cluster to the P-cluster and from P-cluster to the FeMo-cofactor, with P-cluster as an mediator during electron transfer (67).

Recently, a proposed model for the nitrogenase macroscopic mechanism indicates that Fe protein binding to the MoFe protein induces large protein conformational changes ($\sim 800 \text{ \AA}^2$) within the two proteins that gate the electron transfer (ET) events (33, 115). The first ET event is proposed to involve intramolecular ET from the resting P cluster (P^{N}) to the resting FeMo-cofactor (M^{N}), resulting in an oxidized P cluster ($\text{P}^{\text{I}+}$) and a reduced

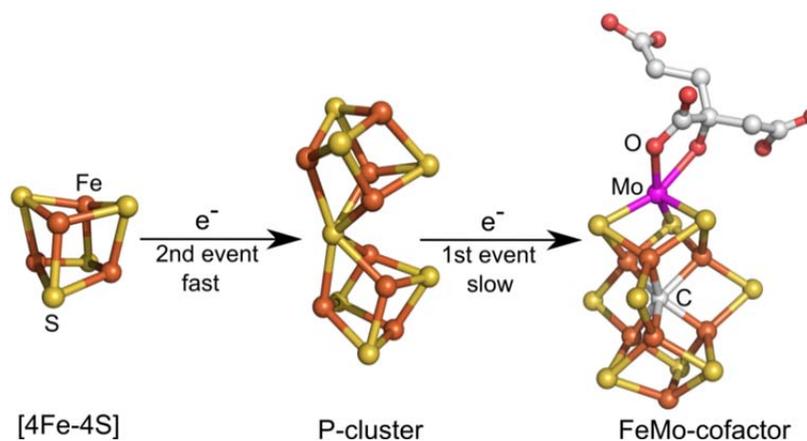


Figure 1-4. The deficit-spending model for electron transfer events in Mo-dependent nitrogenase. Colors are Fe in rust, S in yellow, C in gray, O in red, N in blue, and Mo in magenta. PDB: 1FP6 and 2AFK.

FeMo-cofactor (M^R) (116) (**Figure 1-4**). In the second ET event, Fe protein transfers an electron to the oxidized P^{1+} cluster, resulting in reduction of the P cluster back to the P^N state and oxidized Fe protein. This model has been designated the “deficit-spending” model to reflect the creation of an electron deficit at the P cluster that is then backfilled. Recent results support ATP hydrolysis following the electron transfer events (117), although this sequence has yet to be definitively established. The cycle is completed by the dissociation of the Fe protein from the MoFe protein (118). A reduced and MgATP-bound Fe protein then associates again to the partially reduced MoFe protein, and the cycle of electron transfer and ATP hydrolysis is repeated to accomplish the accumulation of sufficient electrons to affect substrate binding and reduction (32).

Mo-dependent Nitrogenase: Substrates and Inhibitors

Mo-dependent nitrogenase can catalyze the reduction of a wide range of substrates using multiple electron/proton (e^-/H^+) transfer via the association-dissociation process of the Fe protein and MoFe-protein. While the physiological substrates for nitrogenase are N_2 and protons, a variety of other small compounds containing multiple bonds have been demonstrated to be substrates (14, 32, 119, 120). Nitrogenase-catalyzed substrate reduction is summarized in **Table 1-1**. Substrates relevant to this dissertation research will be discussed in this section.

N-Compounds as Substrates

Dinitrogen (N_2)—The most important physiological substrate for all nitrogenases is N_2 , which can be quantitatively reduced to two NH_3 with no observed “leaked” intermediates for Mo-dependent nitrogenase (**Table 1-1**) (121). During N_2 reduction by the V-nitrogenase, a trace amount of hydrazine has been reported as one product other than NH_3 (122). One key feature of N_2 reduction catalyzed by Mo-dependent nitrogenase is the obligatory evolution of one H_2 per N_2 reduced (41). The mechanism for this obligatory H_2 evolution will be discussed in the following sections and in Chapter 5.

Diazene ($HN=NH$)—In 2007, diazene was reported as a substrate for Mo-dependent nitrogenase by using a *in situ* generation method from azodiformate (123). The $4 e^-/H^+$ reduction of diazene produced two equivalents of NH_3 (**Table 1-1**). The reduction of diazene is inhibited by H_2 , which is also a competitive inhibitor of N_2 reduction. This result indicates that diazene enters at an early step in the N_2 reduction pathway for nitrogenase. Previous studies demonstrated that diazene analogs methyldiazene (CH_3-

N=NH), dimethyldiazene ($\text{CH}_3\text{-N=N-CH}_3$) and diazirine (CH_2N_2) are also substrates for nitrogenase (**Table 1-1**) (124, 125).

Hydrazine ($\text{H}_2\text{N-NH}_2$)—The $2\text{ e}^-/\text{H}^+$ reduction of hydrazine to produce two equivalents of NH_3 was confirmed by Davis in 1980 (**Table 1-1**) (126). Recently, it was shown that substitution of the α -70^{Val} residue around FeMo-cofactor with a smaller side chain can enhance the specific activity of hydrazine reduction catalyzed by Mo-dependent nitrogenase (127).

The application of diazene, methyldiazene, and hydrazine as substrates in understanding N_2 reduction mechanism will be discussed in the following sections and in Chapters 2 and 3.

Proton (H^+) Reduction and HD Formation Reactions

Protons are the other physiological substrate of all nitrogenases (14, 15).

Dihydrogen (H_2) is the only product of nitrogenase-catalyzed two-electron reduction of two protons in the absence of other substrates (**Table 1-1**). Furthermore, H_2 is directly involved in nitrogenase catalysis in two other ways (14): (i) H_2 is a competitive inhibitor of N_2 reduction (128, 129) and an inhibitor of diazene (HN=NH) reduction (123).

However, H_2 does not inhibit the reduction of any other nitrogenase substrates (130); (ii) H_2 evolution appears to be obligately associated with N_2 binding and/or reduction with a stoichiometry of one H_2 released when one N_2 reduced to two NH_3 (equation 1-1) (41).

Table 1-1. Substrates for nitrogenases.

Substrate	Reaction	Nitrogenase	References
<i>Nitrogen-nitrogen substrate reduction</i>			
Dinitrogen	$N\equiv N + 6H^+ + 6e^- \rightarrow 2NH_3$	Mo, V, Fe	(14, 15)
	$N\equiv N + 4H^+ + 4e^- \rightarrow H_2N-NH_2$	V	(122)
Diazene	$HN=NH + 4H^+ + 4e^- \rightarrow 2NH_3$	Mo	(123)
Hydrazine	$H_2N-NH_2 + 2H^+ + 2e^- \rightarrow 2NH_3$	Mo	(126)
Azide	$N_3^- + 3H^+ + 2e^- \rightarrow N\equiv N + NH_3$	Mo and V	(131–133)
	$N_3^- + 9H^+ + 8e^- \rightarrow 3NH_3$	Mo and V	(130, 133, 134)
Hydrazoic acid	$HN_3 + 6H^+ + 6e^- \rightarrow H_2N-NH_2 + NH_3$	Mo	(134, 135)
Nitrous oxide	$N_2O + 2H^+ + 2e^- \rightarrow N\equiv N + H_2O$	Mo	(129, 136, 137)
Nitrite	$NO_2^- + 7H^+ + 6e^- \rightarrow NH_3 + 2H_2O$	Mo	(138)
<i>Hydrogenous substrate reduction</i>			
Proton	$2H^+ + 2e^- \rightarrow H_2$	Mo, V, Fe	(14, 15)
Dideuterium	$D_2 + 2H^+ + 2e^- + 'M-N_2' \rightarrow 2HD + M + N_2$	Mo	(137)
<i>Carbon-carbon substrate reduction</i>			
Acetylene	$HC\equiv CH + 2H^+ + 2e^- \rightarrow CH_2=CH_2$	Mo, V, Fe	(139–143)
	$HC\equiv CH + 4H^+ + 4e^- \rightarrow CH_3-CH_3$	Mo, V, Fe	(140–146)
Propyne	$CH_3C\equiv CH + 2H^+ + 2e^- \rightarrow CH_3CH=CH_2$	Mo	(147–149)
1-Butyne	$C_2H_5C\equiv CH + 2H^+ + 2e^- \rightarrow C_2H_5CH=CH_2$	Mo	(147, 148, 150)
2-Butyne	$CH_3C\equiv CCH_3 + 2H^+ + 2e^- \rightarrow cis-CH_3CH=CHCH_3$	Mo	(151)
Propargyl alcohol	$HC\equiv CCH_2OH + 2H^+ + 2e^- \rightarrow CH_2=CHCH_2OH$	Mo	(149)
Propargyl amine	$HC\equiv CCH_2NH_2 + 2H^+ + 2e^- \rightarrow CH_2=CHCH_2NH_2$	Mo	(152)
Allene	$CH_2=C=CH_2 + 2H^+ + 2e^- \rightarrow CH_3CH=CH_2$	Mo	(153)
Ethylene	$CH_2=CH_2 + 2H^+ + 2e^- \rightarrow CH_3-CH_3$	Mo and V	(154, 155)
Cyclopropene	$\begin{array}{c} H_2 \\ \diagup \quad \diagdown \\ C \\ \diagdown \quad \diagup \\ HC=CH \end{array} + 2H^+ + 2e^- \longrightarrow \begin{array}{c} H_2 \\ \diagup \quad \diagdown \\ C \\ \diagdown \quad \diagup \\ H_2C-CH_2 \end{array} \text{ or } CH_3CH=CH_2$	Mo	(156)
	3,3-Difluorocyclopropene	$\begin{array}{c} F_2 \\ \diagup \quad \diagdown \\ C \\ \diagdown \quad \diagup \\ HC=CH \end{array} + 4H^+ + 4e^- \longrightarrow CH_3CF=CH_2 + HF$	Mo
	$\begin{array}{c} F_2 \\ \diagup \quad \diagdown \\ C \\ \diagdown \quad \diagup \\ HC=CH \end{array} + 6H^+ + 6e^- \longrightarrow CH_3CH=CH_2 + 2HF$		
<i>Carbon-nitrogen substrate reduction</i>			
Hydrogen cyanide	$HC\equiv N + 2H^+ + 2e^- \rightarrow [CH_2=NH] + H_2O \rightarrow CH_2O + NH_3$	Mo and V	(133, 158)
	$HC\equiv N + 4H^+ + 4e^- \rightarrow CH_3-NH_2$	Mo and V	(131, 133, 148, 158)
	$HC\equiv N + 6H^+ + 6e^- \rightarrow CH_4 + NH_3$	Mo and V	(131, 133, 148, 158)
	$2HC\equiv N + 8H^+ + 8e^- \rightarrow C_2H_4 + 2NH_3$	Mo	(158, 159)
	$2HC\equiv N + 10H^+ + 10e^- \rightarrow C_2H_6 + 2NH_3$	Mo	(158, 159)
Cyanamide	$N\equiv C-NH_2 + 6H^+ + 6e^- \rightarrow CH_3-NH_2 + NH_3$	Mo and V	(160)
	$N\equiv C-NH_2 + 8H^+ + 8e^- \rightarrow CH_4 + 2NH_3$	Mo and V	(160)
Alkyl nitriles	$RC\equiv N + 6H^+ + 6e^- \rightarrow RCH_3 + NH_3$ (R = CH ₃ , C ₂ H ₅ and n-C ₃ H ₇)	Mo and V	(147, 148, 161)
	$CH_3CH_2C\equiv N + 4H^+ + 4e^- \rightarrow CH_2=CH-CH_3 + NH_3$	Mo	(148)
Acrylonitrile	$CH_2=CH-C\equiv N + 6H^+ + 6e^- \rightarrow CH_2=CH-CH_3 + NH_3$	Mo and V	(148, 161, 162)
	$CH_2=CH-C\equiv N + 8H^+ + 8e^- \rightarrow CH_3-CH_2-CH_3 + NH_3$	Mo and V	(148, 161, 162)
<i>cis</i> -But-2-ene-1-nitrile	$cis-CH_3CH=CH-C\equiv N + 6H^+ + 6e^- \rightarrow cis\text{- or } trans-CH_3CH=CHCH_3$ or $CH_3CH_2CH=CH_2 + NH_3$	Mo	(147)
	$cis-CH_3CH=CH-C\equiv N + 8H^+ + 8e^- \rightarrow CH_3CH_2CH_2CH_3 + NH_3$	Mo	(147)
<i>trans</i> -But-2-ene-1-nitrile	$trans-CH_3CH=CH-C\equiv N + 6H^+ + 6e^- \rightarrow trans-CH_3CH=CHCH_3$ or $CH_3CH_2CH=CH_2 + NH_3$	Mo	(147)
	$trans-CH_3CH=CH-C\equiv N + 8H^+ + 8e^- \rightarrow CH_3CH_2CH_2CH_3 + NH_3$		(147)
But-3-ene-1-nitrile	$CH_2=CHCH_2-C\equiv N + 6H^+ + 6e^- \rightarrow CH_3CH_2CH=CH_2 + NH_3$	Mo	(147)
	$CH_2=CHCH_2-C\equiv N + 8H^+ + 8e^- \rightarrow CH_3CH_2CH_2CH_3 + NH_3$	Mo	(147)

Isonitriles	$\text{RN}\equiv\text{C} + 4\text{H}^+ + 4\text{e}^- \rightarrow \text{RNH}-\text{CH}_3$ (R = CH ₃)	Mo	(135)
	$\text{RN}\equiv\text{C} + 6\text{H}^+ + 6\text{e}^- \rightarrow \text{RNH}_2 + \text{CH}_4$ (R = CH ₃ , C ₂ H ₅ , and CH ₂ =CH-)	Mo	(148, 159, 163)
	$2\text{RN}\equiv\text{C} + 8\text{H}^+ + 8\text{e}^- \rightarrow 2\text{RNH}_2 + \text{CH}_2=\text{CH}_2$ (R = CH ₃ , C ₂ H ₅ , and CH ₂ =CH-)	Mo	(135, 148, 159, 164)
	$2\text{RN}\equiv\text{C} + 10\text{H}^+ + 10\text{e}^- \rightarrow 2\text{RNH}_2 + \text{CH}_3-\text{CH}_3$ (R = CH ₃ , C ₂ H ₅ , and CH ₂ =CH-)	Mo	(135, 148, 159, 164)
	$3\text{CH}_3\text{N}\equiv\text{C} + 12\text{H}^+ + 12\text{e}^- \rightarrow 3\text{CH}_3\text{NH}_2 + \text{CH}_3\text{CH}=\text{CH}_2$	Mo	(165)
	$3\text{CH}_3\text{N}\equiv\text{C} + 14\text{H}^+ + 14\text{e}^- \rightarrow 3\text{CH}_3\text{NH}_2 + \text{CH}_3-\text{CH}_2-\text{CH}_3$	Mo	(165)
	$\text{CH}_3\text{C}\equiv\text{N} + 2\text{H}^+ + 2\text{e}^- \rightarrow [\text{CH}_3\text{N}=\text{CH}_2] + \text{H}_2\text{O} \rightarrow \text{CH}_2\text{O}?? + \text{CH}_3\text{NH}_2$	Mo	(135)
	$\text{CH}_3\text{N}\equiv\text{C} + \text{CO} + 8\text{H}^+ + 8\text{e}^- \rightarrow \text{CH}_3\text{NH}_2 + \text{CH}_2=\text{CH}_2 + \text{H}_2\text{O} (???)$	Mo	(135, 159, 166)
	$\text{CH}_3\text{N}\equiv\text{C} + \text{CO} + 10\text{H}^+ + 10\text{e}^- \rightarrow \text{CH}_3\text{NH}_2 + \text{CH}_3-\text{CH}_3 + \text{H}_2\text{O} (???)$	Mo	(135, 159, 166)
	Diazirine	 + 6H ⁺ + 6e ⁻ → CH ₃ NH ₂ + NH ₃	Mo
 + 8H ⁺ + 8e ⁻ → CH ₄ + 2NH ₃		Mo	(125)
Dimethyldiazene	$\text{CH}_3\text{N}=\text{NCH}_3 + 6\text{H}^+ + 6\text{e}^- \rightarrow \text{CH}_3\text{NH}_2 + \text{NH}_3 + \text{CH}_4$	Mo	(125)
<i>Carbon-chalcogen substrate reduction</i>			
Carbon monoxide	$\text{C}\equiv\text{O} + 6\text{H}^+ + 6\text{e}^- \rightarrow \text{CH}_4 + \text{H}_2\text{O}$	Mo and V	(167)
	$2\text{C}\equiv\text{O} + 8\text{H}^+ + 8\text{e}^- \rightarrow \text{CH}_2=\text{CH}_2 + 2\text{H}_2\text{O}$	Mo and V	(167, 168)
	$2\text{C}\equiv\text{O} + 10\text{H}^+ + 10\text{e}^- \rightarrow \text{CH}_3-\text{CH}_3 + 2\text{H}_2\text{O}$	Mo and V	(167, 168)
	$3\text{C}\equiv\text{O} + 12\text{H}^+ + 12\text{e}^- \rightarrow \text{CH}_3\text{CH}=\text{CH}_2 + 3\text{H}_2\text{O}$	Mo and V	(167, 168)
	$3\text{C}\equiv\text{O} + 14\text{H}^+ + 14\text{e}^- \rightarrow \text{CH}_3\text{CH}_2\text{CH}_3 + 3\text{H}_2\text{O}$	Mo and V	(167-169)
	$4\text{C}\equiv\text{O} + 16\text{H}^+ + 16\text{e}^- \rightarrow \text{CH}_3\text{CH}_2\text{CH}=\text{CH}_2$ or $(\text{CH}_3)_2\text{C}=\text{CH}_2 + 4\text{H}_2\text{O}$	Mo and V	(167)
	$4\text{C}\equiv\text{O} + 18\text{H}^+ + 18\text{e}^- \rightarrow \text{CH}_3\text{CH}_2\text{CH}_2\text{CH}_3 + 4\text{H}_2\text{O}$	Mo and V	(167)
Carbonyl sulfide	$\text{S}=\text{C}=\text{O} + 2\text{H}^+ + 2\text{e}^- \rightarrow \text{CO} + \text{H}_2\text{S}$	Mo	(170)
Carbon dioxide	$\text{O}=\text{C}=\text{O} + 2\text{H}^+ + 2\text{e}^- \rightarrow \text{CO} + \text{H}_2\text{O}$	Mo	(170)
	$\text{O}=\text{C}=\text{O} + 2\text{H}^+ + 2\text{e}^- \rightarrow \text{HCOOH}$	Mo	(119)
Carbon disulfide	$\text{S}=\text{C}=\text{S} + ?\text{H}^+ + ?\text{e}^- \rightarrow \text{C}?? + ?\text{H}_2\text{S}$	Mo	(171)
Thiocyanate	$\text{S}=\text{C}=\text{N}^- + 3\text{H}^+ + 2\text{e}^- \rightarrow \text{HC}\equiv\text{N} + \text{H}_2\text{S}$	Mo	(171)
Cyanate	$\text{O}=\text{C}=\text{N}^- + 3\text{H}^+ + 2\text{e}^- \rightarrow \text{HC}\equiv\text{N} + \text{H}_2\text{O}$	Mo	(171)
	$\text{O}=\text{C}=\text{N}^- + 3\text{H}^+ + 2\text{e}^- \rightarrow \text{CO} + \text{NH}_3$	Mo	(171)

In the presence of D₂, nitrogenase can catalyze the N₂-dependent HD formation (128, 130, 172, 173, 137). In the presence of any other nitrogenase substrates, no HD formation was observed (137, 174). There are three key constraints for nitrogenase catalyzed N₂-dependent HD formation reaction: (i) For every two equivalents of HD formed under turnover conditions in the presence of N₂ and D₂, two electrons diverted from N₂ reduction and two H⁺ from solvent are required (**Table 1-1**) (14, 128, 172, 174);

(ii) During the formation of HD, only a negligible amount of D^+ (~2% D of the produced HD) is released to solvent (174); (iii) HD formation under N_2/D_2 requires the enzyme with a FeMo-co-bound N-N species at the level of N_2H_2 or beyond (130), which was proposed since the discovery of the HD exchange reaction (14, 137).

In Chapter 5 of this dissertation, a proposed reductive elimination mechanism has been developed to explain the obligatory H_2 evolution upon N_2 binding, H_2 inhibition of N_2 reduction, and all constraints for HD formation catalyzed by Mo-nitrogenase.

C-Compounds as Substrates

Alkynes as substrates—Among the earliest studies on isolated nitrogenase was the observation by Dilworth that nitrogenase could reduce acetylene ($HC\equiv CH$) by two electrons and two protons to yield ethylene ($H_2C=CH_2$) (**Table 1-1**) (139, 175). This discovery contributed to the realization that nitrogenase could reduce a number of “alternative” substrates other than just the physiological substrates N_2 and protons (14). It was observed that Mo-dependent nitrogenase has the capacity to reduce acetylene by two electrons to yield ethylene, with very little production of the four electron reduced product ethane (H_3C-CH_3) (144–146, 176). In contrast, it has been shown that both the V- and Fe-dependent forms of nitrogenase can catalyze the reduction of acetylene by either two or four electrons, yielding ethylene or ethane, respectively (140–143, 155). Nevertheless, ethylene is the most abundant reduction product for all of the nitrogenases when acetylene is used as the substrate. Although the Mo-dependent nitrogenase does not have a significant ability to reduce acetylene by four electrons to yield ethane, the enzyme can be remodeled by amino acid substitution such that it gains the capacity for measurable formation of ethane as a reduction product (177).

Early investigations of the stereochemistry of H-atom addition to acetylene catalyzed by nitrogenase also provide important mechanistic insights about how acetylene is bound and reduced. Analysis of the stereochemistry of the product (*cis*- or *trans*-) 1,2-dideuteroethylene (HDC=CDH) formed during reduction of acetylene in the presence of D₂O or during the reduction of dideuteroacetylene (DC≡CD) in H₂O revealed primarily the *cis*-product (139, 155, 166, 178). The stereo-selectivity of this reaction is dependent on the concentration of acetylene concentration (179). This observation revealed that reduction of bound acetylene occurs by the addition of both protons to the same side of the bound acetylene (180). An enzyme-bound η^2 -vinyl intermediate has been proposed to explain this stereochemistry, with H atom addition to one face of the bound acetylene. This stereospecificity can be perturbed by amino acid substitutions around the active site of Mo-nitrogenase (130). In Chapter 5 of this dissertation, the proposed hydrogenation mechanisms of acetylene will be presented.

In addition to acetylene, several other alkynes have been investigated as substrates for nitrogenase (**Table 1-1**). For example, both propyne (CH₃-C≡CH) and 1-butyne (CH₃CH₂-C≡CH) were found to be reduced by 2 e⁻/H⁺ to the corresponding alkenes at very slow rates (147, 148, 181). The triple bonds in propargyl alcohol and propargyl amine are also reduced by nitrogenase to yield the corresponding double-bond compounds (**Table 1-1**), which have provided valuable probes for gaining insight into where and how alkyne substrates interact with FeMo-cofactor during catalysis (149, 152, 182).

Carbon-chalcogen substrates—Nitrogenase can also reduce carbon-chalcogen substrates such as carbon dioxide (CO₂), carbonyl sulfide (COS), carbon disulfide (CS₂),

thiocyanite (CSN^-) and cyanite (CON^-) (**Table 1-1**) (170, 171). It was shown that nitrogenase can reduce both C=S and C=O bonds (210). The observation that COS interacts with nitrogenase as an inhibitor of acetylene reduction (183) led to the study of the reduction of COS by nitrogenase (171). These studies demonstrated that nitrogenase could catalyze the $2 e^-/\text{H}^+$ reduction of a new class of compounds. The C=S bond in COS is reduced to form the products CO and H_2S . In light of these observations it was shown by kinetic analysis and EPR spectroscopy for the COS structural analogues, that the $2 e^-/\text{H}^+$ reduction of the C=S bond of CSN^- results in H_2S and HCN, and the $2 e^-/\text{H}^+$ reduction of the C=O and C=N in CON^- results in H_2O , HCN and CO, NH_3 , respectively (171). Finally it was demonstrated that CS_2 can be an inhibitor of nitrogenase reduction reaction and total electron flow but also be reduced to H_2S and an unknown CS species (170, 171). Before this dissertation research, there is no other product characterized from CO_2 reduction. In Chapter 8, CO_2 reduction to methane and coupling with acetylene to form propylene using remodeled nitrogenase as catalyst will be presented.

In addition to these C-containing substrates, carbon monoxide (CO) was early shown to be an inhibitor of wild type molybdenum nitrogenase-catalyzed reactions except for proton reduction (14, 184, 185). In the presence of CO, electron flux through nitrogenase is diverted to proton reduction. CO has been known as an inhibitor of nitrogenase-catalyzed substrate reduction for a long time, but not as a substrate of nitrogenase. Recently, it was found that vanadium nitrogenase is able to catalyze the reduction and coupling of two or three CO molecules at very low rates forming C2 (ethylene, $\text{H}_2\text{C}=\text{CH}_2$, and ethane, CH_3-CH_3) and C3 (propane, $\text{H}_3\text{C}-\text{CH}_2-\text{CH}_3$)

hydrocarbons (168). Shortly after, propylene ($\text{H}_3\text{C}-\text{CH}=\text{CH}_2$) was found as an additional product of CO reduction by V-nitrogenase in D_2O assays (169).

In this dissertation, the steric effect around FeMo-cofactor on CO binding was studied using stopped-flow FTIR (SF-FTIR) (see Chapter 6). Moreover, it was found that remodeled molybdenum nitrogenase can reduce and couple CO to produce hydrocarbons (see Chapter 7).

Remodeling Nitrogenase: Effect of Amino Acid Substitution on Nitrogenase Catalysis

A key recent advance in understanding nitrogenase reduction of substrates has been the recognition that it is possible to change the size of substrates that can be reduced by Mo-nitrogenase by remodeling the MoFe protein environment surrounding the FeMo-cofactor (29, 30, 32). In the genetic screen for an altered form of the MoFe protein that has the ability to discriminate between binding of acetylene (excluded) and N_2 (unaffected), it was surprising that one substitution yielding this phenotype resulted in replacement of the α -69^{Gly} residue by 69^{Ser} (186). The reason this result was surprising was because α -69^{Gly} is not in the first shell of non-covalent interactions with the FeMo-cofactor. Rather, it is located adjacent to α -70^{Val}, which closely approaches a particular Fe-S face of the FeMo-cofactor (**Figure 1-5**). This led us to suspect that α -69^{Gly} serves as part of a switch mechanism that exquisitely controls the position of the α -70^{Val} side chain, thereby controlling access to the active site. Indeed, when the side chain of α -70^{Val} was

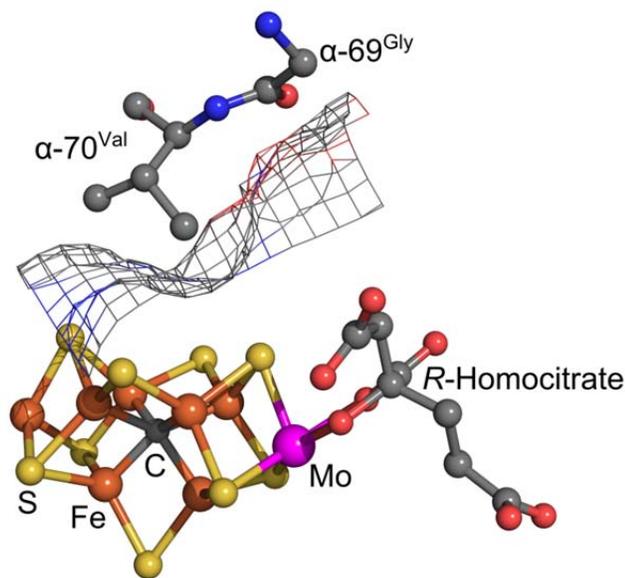


Figure 1-5. Position of α -69^{Gly} and α -70^{Val}. Shown are the locations of α -69^{Gly} and α -70^{Val} near the FeMo-cofactor, with the van der Waals surface of the surrounding protein shown as mesh. Colors are Fe in rust, S in yellow, C in gray, O in red, N in blue, and Mo in magenta. PDB: 2AFK.

progressively shortened by substitution with Ala or Gly, (without substitution of α -69^{Gly}), progressively larger alkynes (propyne and butyne) were able to access the active site and be reduced (149, 151, 152, 187). It was also found that as access to the active site for reduction of larger substrates was increased, the ability to reduce smaller substrates was diminished. Thus, it appears there are three possible roles for the amino acid “shrubby” surrounding the FeMo-cofactor in the reduction process. The first of these is to make the “hot spot(s)” for catalysis available to a particular substrate. The second could be to lock the substrate in place for progressive reduction steps, indicating a dynamic role for the α -69^{Gly} and α -70^{Val} residue positions. Recent work with MoFe proteins containing amino

acid substitutions are providing strong evidence that the 4Fe-4S face gated by α -70^{Val} and α -96^{Arg} is the site of substrate (or inhibitor) binding on FeMo-cofactor (**Figure 1-3** and **1-5**) (25, 30, 32). For example, substitution of the arginine (Arg) at α -96 position by leucine (Leu) in MoFe protein resulted in the interaction of acetylene and cyanide with the resting state FeMo-cofactor (188). A third related aspect could involve intermediate stabilization through amino acid chain functional groups. It would appear that locking down the substrate is particularly important for those substrates that must accept a relatively large number of electrons for complete reduction, such as N₂.

Several early studies examined the roles of α -195^{His} in nitrogenase catalysis (**Figure 1-3**) (130, 144, 189–191). Substitution of the α -195^{His} residue by glutamine resulted in a variant of the MoFe protein that cannot effectively reduce N₂ or azide (N₃⁻), but which retained full rates of reduction of acetylene and protons. From these studies, it was concluded that α -195^{His} might participate in delivery of protons during reduction of nitrogen containing substrates. Using freeze quench technique, slowing down proton delivery by substituting for α -195^{His} has been exploited to trap presumed intermediate states during the reduction of a number of substrates including hydrazine (N₂H₄) (127, 192), diazene (HN=NH) (123), and methyldiazene (MeN=NH) (124, 192) (**Table 1-2**), which are important for understanding the N₂ reduction mechanism of nitrogenase (see the following section and Chapter 2 and Chapter 3). It is clear that α -195^{His} is not the sole source of protons for substrate reduction as the rates of reduction of other substrates remain undisturbed when this residue is substituted (130). Moreover, substitution of the valine (Val) at α -70 position by isoleucine (Ile) can help to trap a hydride-bound intermediate (**Table 1-2**) during turnover under Ar (193).

Table 1-2. Important variants of MoFe protein and and EPR parameters of the resulting intermediates with different substrates in the turnover state.

MoFe protein	Substrate	EPR parameters	References
Wild type	Dinitrogen (N ₂)	$S = 1/2, g = 2.08, 1.99, 1.97$	(192, 194)
Wild type	Carbon monoxide (lo-CO)	$S = 1/2, g = 2.09, 1.97, 1.93$	(195–197)
Wild type	Carbon monoxide (hi-CO)	$S = 1/2, g = 2.17, 2.06$	(195–197)
α -70 ^{Val→Ile}	Proton (H ⁺)	$S = 1/2, g = 2.14, 2.00, 1.96$	(193)
α -70 ^{Val→Ala}	Propargyl alcohol (HC≡CCH ₂ OH)	$S = 1/2, g = 2.12, 2.00, 1.99$	(182, 198)
α -195 ^{His→Gln}	Acetylene (HC≡CH)	$S = 1/2, g(a) = 2.12, 1.98, 1.95$	(199)
α -195 ^{His→Gln}	Methyldiazene (CH ₃ N=NH)	$S = 1/2, g = 2.08, 2.02, 1.99$	(124, 192)
α -70 ^{Val→Ala} / α -195 ^{His→Gln}	Diazene (HN=NH)	$S = 1/2, g = 2.09, 2.01, 1.93$	(123)
α -70 ^{Val→Ala} / α -195 ^{His→Gln}	Hydrazine (H ₂ N-NH ₂)	$S = 1/2, g = 2.09, 2.01, 1.93$	(127, 192)

In this dissertation, remodeling nitrogenase is a key method used to understand the N₂ reduction mechanism (see the following section, Chapter 2 and Chapter 3) and substrate binding sites (see Chapter 4 and Chapter 6). It is also used to expand the reactivity of molybdenum nitrogenase toward reduction and coupling reactions of CO and CO₂ (see Chapter 7 and Chapter 8).

Mo-Dependent Nitrogenase: Mechanistic Aspects on Substrate

Binding and Reduction

Important aspects of the nitrogenase mechanism includes: (i) defining exactly how and where substrates bind; (ii) understanding how electrons are accumulated; (iii) defining the N₂ reduction mechanism with characterization of the redox state of FeMo-cofactor and chemical nature of the reduced nitrogenous species along the reduction

pathway; (iv) figuring out the mechanism of hydrogenation of substrate reduction; and (v) understanding the roles of the peptide matrix during nitrogenase catalysis.

Substrate/Inhibitor Binding Sites

Earlier studies indicate that the FeMo-cofactor has multiple binding sites for some substrates and inhibitors (14, 200), but the precise location of substrate binding is still being pursued (29, 30, 32). For example, kinetic studies with the substrate acetylene were interpreted as the FeMo-cofactor presenting two binding sites (179, 200).

There are many possibilities for the substrate binding sites: (i) the Mo atom; (ii) one or more of the central Fe atom(s); and (iii) some combination of Fe, S and Mo atoms. All these hypotheses can find support from either experimental or theoretical studies (29). For example, studies of biomimetic Mo complexes (201, 202) and the isolated FeMo-cofactor (203) indicate that the Mo atom might be involved in substrate binding in nitrogenase function. However, Fe is the catalytic metal in the catalyst used for the industrial Haber-Bosch process for NH_3 formation, and there are V and Fe-only nitrogenases that reduce N_2 but do not have Mo (15). Recently, based on the combined genetic, biochemical, spectroscopic (*e.g.*, ENDOR, EXAFS and IR) and molecular dynamic modeling approaches (30, 32), there is growing evidence for the binding of carbon monoxide (113, 204–208), hydrides (127), alkynes (182, 186, 198), and nitrogenous compounds (123, 124, 127, 192, 194) to one or more of the Fe atoms in the central portion of FeMo-cofactor (**Figure 1-5**). As yet, no experimental results have illustrated binding of any substrate or intermediate to Mo, although this possibility has not been ruled out. The role of Mo ion during nitrogenase catalysis is still not clear. The role of Mo and Fe in FeMo-cofactor for substrate binding will be further explored in

Chapter 4 and Chapter 6 of this dissertation using ^{95}Mo -ENDOR and SF-FTIR, respectively.

Accumulating Electrons on FeMo-cofactor

One of the key challenges in understanding the nitrogenase mechanism is to explain how the FeMo-cofactor accumulates multiple electrons to activate the system for the binding and subsequent reduction of N_2 and other substrates. A simple notation to designate how many electrons have been transferred into the resting MoFe protein is helpful (called the Lowe-Thorneley (abbreviated as LT) kinetic model) (**Figure 1-6**) (209–214). The number of electrons accumulated within one half of the MoFe protein (one $\alpha\beta$ dimeric unit) is designated by the nomenclature E_n ($n = 0-8$) with the subscript n indicating the number of electrons received from Fe protein and E_0 representing the resting state MoFe protein (M^{N}). A condition of the deficit-spending ET model described above (116) is that all electrons passed to the MoFe protein from the Fe protein must accumulate on the FeMo-cofactor or one of its bound activated intermediate states (34).

The results of a number of kinetic studies have allowed construction of a MoFe-protein cycle as shown in **Figure 1-6**. As noted in the cycle, there is good evidence indicating that different substrates bind to different reduction states (E_n) of the MoFe protein. In the absence of other substrates, H_2 is released from E_2 , E_3 , and E_4 state (**Figure 1-6**). Dinitrogen is modeled to bind to E_3 or E_4 state (209), which is accompanied by the release of one equivalent of H_2 (41, 215). In the absence of N_2 , the less reduced E_1 and E_2 states are achieved, which are sufficient for proton binding and reduction to H_2 .

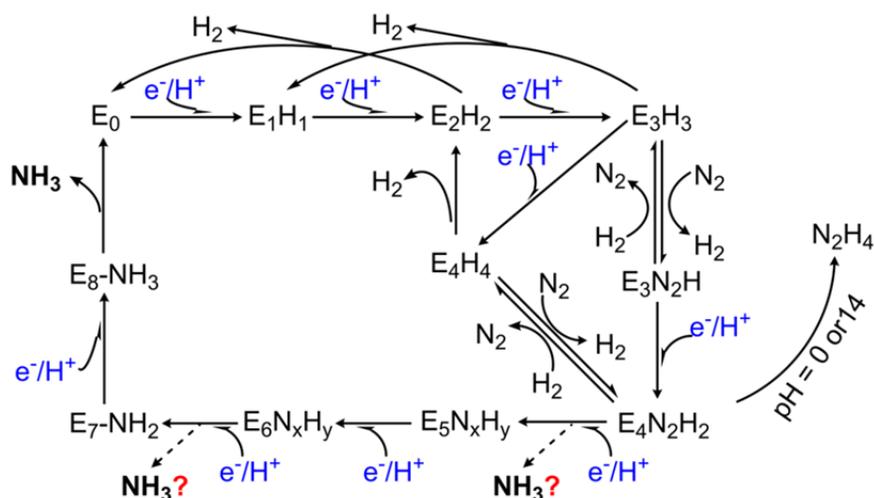


Figure 1-6. Modified Lowe-Thorneley (LT) kinetic scheme for reduction of N_2 . In this scheme, the E_n represents one functional $\alpha\beta$ dimeric unit, which has been reduced by n electrons relative to the resting state E_0 . The composition and molecular structures of nitrogenous intermediate at different E_n states, such as E_5 and E_6 , are unknown and represented by N_xH_y with $x = 1$ or 2 , and $y = 0-4$. The possible steps to release the first NH_3 are indicated by dashed arrows and red question marks.

The non-physiological substrate acetylene is modeled to bind to the E_1 or E_2 state for reduction to ethylene (216). The binding of different substrates to different redox states and binding sites of the MoFe protein can result in confusing inhibition patterns (29). For example, the inhibition of N_2 reduction by acetylene appears to be non-competitive, while the inhibition of acetylene reduction by N_2 appears to be competitive (185). This apparent contradiction can be explained by the fact that acetylene binds to the less reduced E_2 state whereas N_2 binds to more reduced states (209). Thus, acetylene appears to be a non-competitive inhibitor of N_2 reduction and N_2 a competitive inhibitor of acetylene

reduction. Experimental evidence explaining these observations at a molecular level can be found in Chapter 5 of this dissertation.

Spectroscopic Characterization of Freeze-Trapped Intermediates

The shortcomings of the kinetic-study-based LT kinetic model include that there is no information about (i) the molecular structure of individual intermediates, (ii) the mechanism of accumulation of electrons/protons on FeMo-cofactor and addition to bound substrates, and (iii) the partition of accumulated electrons between the P clusters, FeMo-cofactor, and bound intermediates. These features limit the understanding of substrate binding and reduction mechanism of nitrogenase at a molecular level.

As described before, a number of important intermediates have been trapped and characterized as EPR-active complexes with FeMo-cofactor bound substrate-derived ligands (**Table 1-2**). Characterization of the E_n states of these intermediates and fitting them into the LT kinetic model is the key to understanding the substrate reduction mechanism. Pulsed EPR spectroscopy has been widely used in the characterization of these trapped intermediates during turnover (31). ENDOR/ESEEM analysis of nuclei (*e.g.*, ^1H -, ^{13}C -, or ^{15}N -ENDOR, and $^{14/15}\text{N}$ -ESEEM) can determine the molecular structure of the substrate-derived ligands and the number of electrons residing on the ligands in the EPR active intermediates (31, 114, 123). ^{57}Fe - and ^{95}Mo -ENDOR study of the intermediates can give information about the valences of the metal ions in the FeMo-cofactor and the redox states of the cofactor, which in turn give information about the electrons residing on the FeMo-cofactor (31, 114, 217). This information directly contributes to establishing the “electron inventory,” seeking to determine the number (n) of electrons and protons that have been delivered to the MoFe protein to form an E_n state

in LT model (**Figure 1-6**) by partitioning n into four parts: (i) those that reside on the substrate-derived ligand bound to FeMo-cofactor; (ii) those reside on FeMo-cofactor; (iii) the number of released protons and electrons through liberation of H₂ and reduced substrate (e.g., NH₃); and (iv) the electrons that P cluster has donated to FeMo-cofactor (31, 114). Recently, a relaxation protocol using a temperature step annealing of the trapped states as a way to gradually and systematically observe a trapped intermediate relax while monitoring the appearance of new intermediates and ultimately the reappearance of the FeMo cofactor resting state (31, 218) was developed. This relaxation approach compensates for the difficulty of analyzing the ⁵⁷Fe ENDOR spectra caused by the slow ⁵⁷Fe nuclear relaxation (31). These spectroscopic techniques are applied to understand the reduction mechanisms of nitrogenous substrates (see Chapter 2 and 3, and the following sections) and the role of Mo (see Chapter 4) in this dissertation.

Application of the methods described above has led to key understanding of some of the freeze-trapped intermediates (**Table 1-2**). For example, the intermediate ($S = 1/2$) trapped under low-CO condition is a complex with one bridging CO bound to two Fe atoms of FeMo-cofactor with the enzyme at E₂ state (31, 114). However, the trapped intermediate in the presence of acetylene is a complex with an ethylene ligand bound “side-on” to one of Fe atom of two-electron reduced FeMo-cofactor, that is, the enzyme is at E₄ state (31, 114).

Other spectroscopic methods, such as Mössbauer (110) and EXAFS (219) spectroscopies, have also been used to characterize the freeze trapped nitrogenase intermediates. A recent Mo- and Fe-EXAFS study of freeze trapped samples with propargyl alcohol as substrate clearly suggests that the product allyl alcohol binds to one

of the Fe atom, not Mo atom of the FeMo-cofactor (219). Because both EPR active and silent intermediates exist in the freeze trapped samples, it is very hard to interpret the spectra from these studies and assign the E_n state for a specific intermediate. IR-monitored photolysis and SF-FTIR have also been applied to understand the nitrogenase mechanism (207, 208, 220–222). A study using SF-FTIR to understand CO binding to FeMo-cofactor can be found in Chapter 6.

N₂ Binding and Reduction Mechanism

To understand the molecular mechanism of N₂ reduction of nitrogenase, three features must be established: (i) the “reaction pathway,” an enumeration of the states that arise during the conversion of reactants to products, (ii) the molecular structures of these intermediates, and (iii) a kinetic scheme, in this case the LT scheme, that incorporates information about the kinetics/dynamics of conversion among these intermediates and the electron inventory of each intermediate. Combining the understanding of the binding sites and binding mode of the intermediates along the reaction pathway, a fully understood mechanism could be established.

The coupling of electron transfer to protonation to yield metal hydride(s) at the FeMo-cofactor is a key postulate in the LT kinetic model for nitrogenase catalysis (210), especially for N₂ binding and subsequent reduction (**Figure 1-6**). But there has been no direct experimental evidence for such intermediates. Until recently, the first observation of the metal hydride(s) intermediate is from the proton-trapped state by the α -70^{lle} substituted MoFe protein during turnover under Ar (193), which has been definitively assigned to the 4-electron reduced state of the FeMo-cofactor (E_4) (217, 218, 223). Surprisingly, it was found that in this multiply reduced state, the metal core of the FeMo-

cofactor, is in the same oxidation state as the resting state (E_0) (223). This apparent contradiction was explained when it was discovered that the trapped E_4 state under Ar has two Fe-bound bridging hydrides (see Chapter 4 and **Figure 1-7**) (223). Thus, it appears that electrons are located on the bound metal-hydrides, leaving the metal core of the FeMo-cofactor in the resting oxidation state. Such “parking” of electron pairs on metal bound hydrides indicates that FeMo-cofactor might formally access only two oxidation states during the catalytic process (33). Temperature step annealing study monitored by EPR revealed that the relaxation of this E_4 hydride intermediate to the resting E_0 state is through an E_2 intermediate by stepwise releasing of two H_2 (**Figure 1-6**) (218).

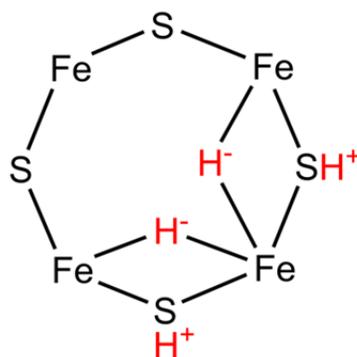


Figure 1-7. Metal hydrides and the FeMo-cofactor. Shown are provisional binding sites for bridging hydrides (H^-) and protons (H^+) on one 4Fe-4S face of the FeMo-cofactor. All hydrogen species are highlighted in red.

Recently, a “reductive elimination” model has been proposed wherein N_2 binding to the E_4 state involves the loss of two metal-bound hydrides as H_2 , with electron and proton addition to the bound N_2 resulting in a metal-bound diazene (34). Experimental evidence supporting this model has been obtained in Chapter 5 of this dissertation.

Once N_2 binds to FeMo-cofactor (designated as **M**, **Figure 1-8**), it will be subsequently reduced by hydrogenation with e^-/H^+ (H-atom). Recently, the N_2 reduction pathways have been divided into two major classes. In a “distal” (**D**) pathway, the formation of two NH_3 is completed through two cycles of sequential addition of three H-atoms to each nitrogen atom with the N-N bond cleaved after the first three H-atoms addition (**Figure 1-8**). This **D** pathway (also called Chatt cycle (201)) is supported by inorganic Fe and Mo metal complexes (201, 202, 224). This contrasts with an “alternating” (**A**) pathway in which H-atoms add alternately to the two nitrogen atoms of N_2 before the N-N bond cleavage when one H-atom addition to the metal-bound hydrazine intermediate (31, 32). The **A** pathway is favored by computational studies (225–227) and several hints from biological studies of the Mo-dependent nitrogenase as described next.

One of the most important features of the nitrogenase N_2 reduction mechanism is the observation that, once bound, N_2 is quantitatively converted to 2 NH_3 , with no observed “leaked” intermediates for Mo-nitrogenase (121). However, trace amount of N_2H_4 was detected as a product from acid or base quenching of the intermediate during N_2 reduction (121, 212). During N_2 reduction by the V-nitrogenase, a trace amount of hydrazine has been reported (122). Thus, Mo-dependent nitrogenase is designed to bind N_2 and conduct multiple rounds of reduction and protonation without the release of semi-

reduced states. However, this feature, the ability to capture a substrate for multiple rounds of reduction, can be changed when $\text{HC}\equiv\text{N}$, the isoelectronic counterpart of N_2 , is used as the substrate. The reduction of HCN by Mo-dependent nitrogenase can produce $\text{CH}_2=\text{NH}$, $\text{CH}_3\text{-NH}_2$, and CH_4 and NH_3 as products (158, 228), which are isoelectronic to the $\text{HN}=\text{NH}$, $\text{H}_2\text{N-NH}_2$, and two NH_3 intermediate and products on the **A** pathway for N_2 reduction (**Figure 1-8**). Moreover, both diazene (123) and hydrazine (126) are substrates for Mo-dependent nitrogenase. A diazene-bound state has been suggested as a key intermediate for N_2 -dependent HD formation reaction (130). All these biological studies favor the **A** pathway for N_2 reduction catalyzed by Mo-dependent nitrogenase.

Due to the different molecular structures of the N_2 -derived ligands and possible redox state of metal centers between the “diazenido” $\text{M-N}=\text{NH}$ and “amido” M-NH_2 along the two reduction pathways (**Figure 1-8**), the enzymatic pathway of N_2 reduction would be revealed if these intermediates could be characterized by spectroscopic methods, such as EPR and ENDOR. The breakthrough in freeze-trapping the EPR-active intermediates of nitrogenous substrates (*e.g.* N_2) during turnover makes this strategy feasible (**Table 1-2**). Before this dissertation research, four such EPR-active ($S = 1/2$) intermediates have been trapped for different nitrogenous substrates and different MoFe protein variants during steady-state turnover: (i) N_2 as an early stage substrate for wild type MoFe protein (192, 194); (ii) $\text{CH}_3\text{N}=\text{NH}$ (124, 192) and $\text{HN}=\text{NH}$ (123) as middle stage substrates for $\alpha\text{-}^{195}\text{Gln}$ and $\alpha\text{-}^{70}\text{Ala}/\alpha\text{-}^{195}\text{Gln}$ MoFe protein, respectively; (iii) $\text{H}_2\text{N-NH}_2$ as late stage substrate for $\alpha\text{-}^{70}\text{Ala}/\alpha\text{-}^{195}\text{Gln}$ MoFe protein (127, 192). Further characterization using pulsed ENDOR spectroscopies leads to some key features of these

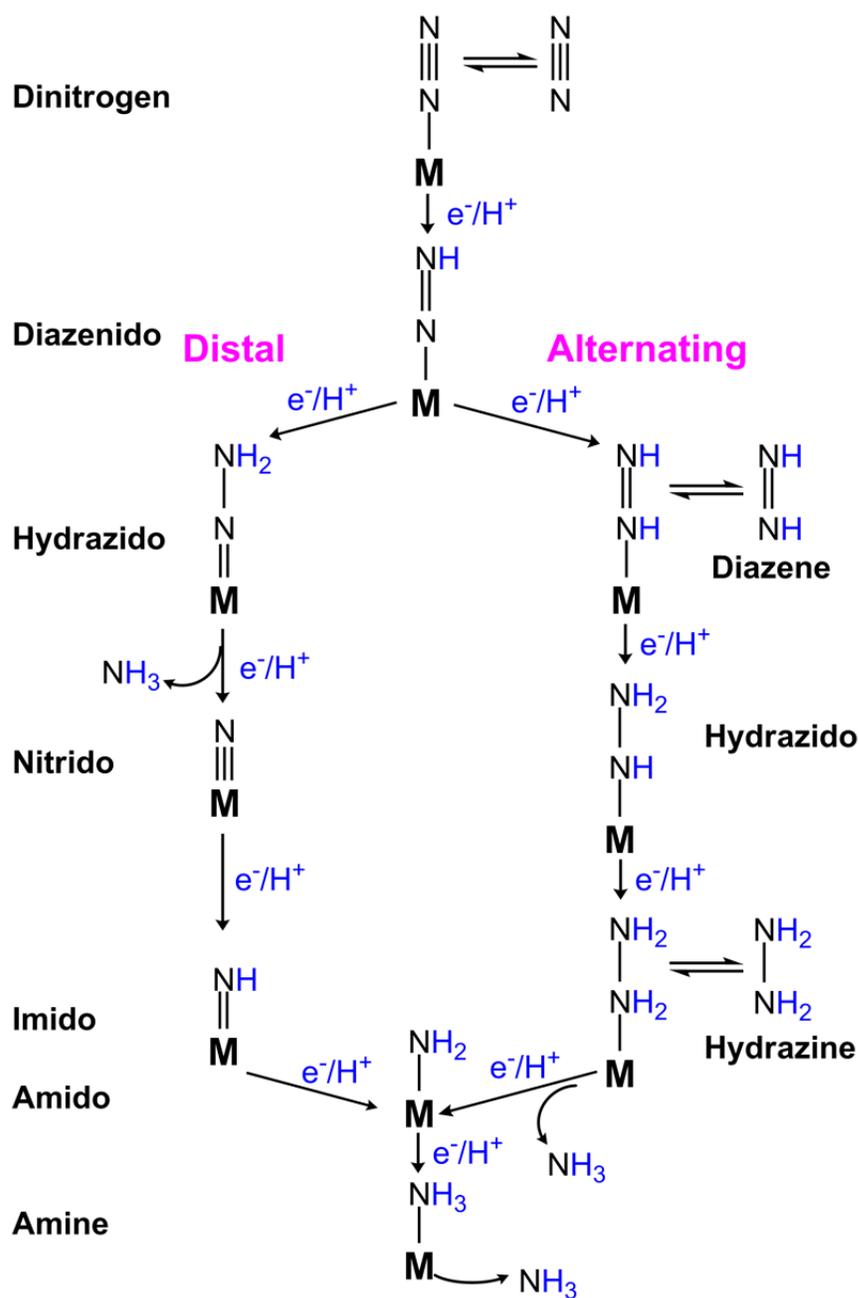


Figure 1-8. Stepwise reduction of N_2 following the “distal” (D) (left) and “alternating” (A) pathways (right). **M** represents FeMo-cofactor without specifying the change of the redox state. The representations do not imply specific binding modes and the source of electrons and protons (e^-/H^+). The proposed entry points for N_2 , diazene and hydrazine are shown to the right.

intermediates (31, 32): (i) The trapped intermediate complex during N_2 reduction appears to be a nonprotonated N bound to FeMo-cofactor, which would represent an earlier stage intermediate in the pathway (192, 194). (ii) The other three intermediate complexes trapped during reduction of $CH_3N=NH$, $HN=NH$, and H_2N-NH_2 reduction contain a substrated-derived $[-NH_x]$ moiety bound to FeMo-cofactor (123, 124, 127, 192). (iii) The $[-NH_x]$ moieties in trapped intermediates with diazene and hydrazine substrates has very indistinguishable ^{15}N and 1H ENDOR spectroscopic characteristics (123). These observations suggest that diazene and hydrazine enter the *A* reduction pathway evidenced by generating a common intermediate during Mo-dependent nitrogenase-catalyzed N_2 reduction (31, 32).

These studies have advanced our understanding of where and how substrates interact with the nitrogenase active site. Many other mechanistic insightful questions remain to be resolved. For example, is the N-N bond broken (**Figure 1-6 and 1-8**) in the trapped nitrogenous species characterized so far? What is the binding mode (*e.g.* side-on or end-on) of the substrate-derived ligands if the N-N bond is not cleaved? What is the level of reduction of the trapped states? What is the level of hydrogenation of the substrate-derived ligands in these intermediates? Does any intermediate migrate among the metals (Fe and Mo) during the course of substrate binding or reduction? Answers to some of these outstanding questions mentioned above have been solved in Chapter 2 and Chapter 3 of this dissertation using ENDOR/ESEEM/HYSCORE techniques.

Possible Mechanisms for Hydrogenation of Substrates

There are several different possible mechanisms for how substrates could be reduced by nitrogenase including through hydride insertion at an electron-deficient center, protonation of an electron-rich center, or reductive elimination reactions between the adjacent metal-hydride (M-H) and metal-ligand (M-X, X = C, N, O, or S *etc.*) bond. Enzyme bound hydride has been suggested as a key intermediate for N₂ reduction (121) for a long time and is the basis for the LT kinetic model (210). The recent discovery of bridging metal-hydrides (193) in nitrogenase suggests a reductive elimination mechanism for H₂ evolution upon N₂ binding (34), although a direct role has yet to be established (226, 227, 229).

Thus, several questions remain to be answered about the roles of such hydrides including: (i) do hydrides attack bound substrates? (ii) Is there a stepwise proton coupled electron transfer of the bound substrate or protonation of the reduced substrate-derived anionic ligand bound to the metallic active center? And (iii) is there a reductive elimination reaction of the M-H and M-X to form X-H species? As these different possible mechanisms are considered, it is important to appreciate that nitrogenase catalysis might use different hydrogenation mechanisms at different steps for different substrates. For example, the production of both *cis*- and *trans*-isomer products from acetylene reduction (180) can be explained by the insertion of an acetylene molecule into an M-H on FeMo-cofactor. This mechanism might also explain the observation that acetylene completely inhibits proton reduction (147), by intercepting the M-H that is destined to make H₂. Recently, molecular-level mechanisms for hydrogenation of acetylene have been supported by experimental results in Chapter 5 of this dissertation.

Summary

In summary, the nitrogenase mechanism has been significantly expanded in the past 50 years. An understanding of different mechanistic aspects at a molecular level is not yet crystal clear. Guided by those outstanding questions described above, my dissertation research will focus on understanding the substrate binding and reduction mechanism of molybdenum nitrogenase using a combination of genetic, biochemical and spectroscopic approach. The data presented in this dissertation are usually diverse, covering several aspects to understand: (i) the metal sites for substrate/inhibitor binding and reduction on FeMo-cofactor (Chapter 4 and Chapter 6); (ii) the mechanism of N₂ binding and reduction (Chapter 2, 3, and 5); (iii) the hydrogenation mechanism of Mo-dependent nitrogenase-catalyzed substrate reduction (Chapter 5); (iv) the effects of amino acid substitution around FeMo-cofactor on substrate/inhibitor binding and reduction of Mo-dependent nitrogenase (Chapter 2, 3, 4, 6, 7, and 8).

References

1. Ferguson, S. J. (1998) Nitrogen cycle enzymology. *Curr. Opin. Chem. Biol.* **2**, 182–193
2. Smil, V. (2004) *Enriching the Earth: Fritz Haber, Carl Bosch, and the Transformation of World Food Production*, MIT Press, Cambridge, MA
3. Fryzuk, M. D., and MacKay, B. A. (2004) Dinitrogen coordination chemistry: On the biomimetic borderlands. *Chem. Rev.* **104**, 385–401
4. Haber, F. (1922) The production of ammonia from nitrogen and hydrogen. *Naturwissenschaften* **10**, 1041–1049
5. Haber, F. (1923) The history of the ammonia process. *Naturwissenschaften* **11**, 339–340
6. Cheng, Q. (2008) Perspectives in biological nitrogen fixation research. *J. Integr. Plant. Biol.* **50**, 786–798

7. Smith, B. E. (2002) Nitrogen reveals its inner secrets. *Science* **297**, 1654–1655
8. Raymond, J., Siefert, J. L., Staples, C. R., and Blankenship, R. E. (2004) The natural history of nitrogen fixation. *Mol. Biol. Evol.* **21**, 541–554
9. Beijerinck, M. W. (1888) Die bakterien der *Papilionaceen-Knölchen*. *Bot. Ztg.* **46**, 797–804
10. Hellriegel, H., and Wilfarth, H. (1888) Untersuchungen über die stickstoffnahrung der gramineen und leguminosen. *Beil. Z. Ver. dt ZuchInd*, 1–234
11. Thamdrup, B. (2012) New pathways and processes in the global nitrogen cycle. *Annu. Rev. Ecol. Evol. Syst.* **43**, 407–428
12. Canfield, D. E., Glazer, A. N., and Falkowski, P. G. (2010) The evolution and future of earth's nitrogen cycle. *Science* **330**, 192–196
13. Gruber, N., and Galloway, J. N. (2008) An Earth-system perspective of the global nitrogen cycle. *Nature* **451**, 293–296
14. Burgess, B. K., and Lowe, D. J. (1996) Mechanism of molybdenum nitrogenase. *Chem. Rev.* **96**, 2983–3011
15. Eady, R. R. (1996) Structure-function relationships of alternative nitrogenases. *Chem. Rev.* **96**, 3013–3030
16. McGlynn, S. E., Boyd, E. S., Peters, J. W., and Orphan, V. J. (2013) Classifying the metal dependence of uncharacterized nitrogenases. *Front. Microbiol.* **3**, 419
17. Dos Santos, P. C., Fang, Z., Mason, S. W., Setubal, J. C., and Dixon, R. (2012) Distribution of nitrogen fixation and nitrogenase-like sequences amongst microbial genomes. *BMC Genomics* **13**, 162
18. Dos Santos, P. C., and Dean, D. R. (2011) Co-ordination and fine-tuning of nitrogen fixation in *Azotobacter vinelandii*. *Mol. Microbiol.* **79**, 1132–1135
19. Setubal, J. C., Dos Santos, P., Goldman, B. S., Ertesvag, H., Espin, G., Rubio, L. M., Valla, S., Almeida, N. F., Balasubramanian, D., Cromes, L., Curatti, L., Du, Z., Godsy, E., Goodner, B., Hellner-Burris, K., Hernandez, J. A., Houmiel, K., Imperial, J., Kennedy, C., Larson, T. J., Latreille, P., Ligon, L. S., Lu, J., Maerk, M., Miller, N. M., Norton, S., O'Carroll, I. P., Paulsen, I., Raulfs, E. C., Roemer, R., Rosser, J., Segura, D., Slater, S., Stricklin, S. L., Studholme, D. J., Sun, J., Viana, C. J., Wallin, E., Wang, B., Wheeler, C., Zhu, H., Dean, D. R., Dixon, R., and Wood, D. (2009) Genome sequence of *Azotobacter vinelandii*, an obligate aerobe specialized to support diverse anaerobic metabolic processes. *J. Bacteriol.* **191**, 4534–4545

20. Rubio, L. M., and Ludden, P. W. (2008) Biosynthesis of the iron-molybdenum cofactor of nitrogenase. *Annu. Rev. Microbiol.* **62**, 93–111
21. Dos Santos, P. C., Dean, D. R., Hu, Y., and Ribbe, M. W. (2004) Formation and insertion of the nitrogenase iron–molybdenum cofactor. *Chem. Rev.* **104**, 1159–1174
22. Hu, Y., and Ribbe, M. W. (2011) Biosynthesis of the metalloclusters of molybdenum nitrogenase. *Microbiol. Mol. Biol. Rev.* **75**, 664–677
23. Hu, Y., and Ribbe, M. W. (2011) Biosynthesis of nitrogenase FeMoco. *Coord. Chem. Rev.* **255**, 1218–1224
24. Hu, Y., Lee, C. C., and Ribbe, M. W. (2012) Vanadium nitrogenase: A two-hit wonder? *Dalton Trans.* **41**, 1118–1127
25. Barney, B. M., Lee, H.-I., Dos Santos, P. C., Hoffman, B. M., Dean, D. R., and Seefeldt, L. C. (2006) Breaking the N₂ triple bond: Insights into the nitrogenase mechanism. *Dalton Trans.*, 2277–2284
26. Rees, D. C., and Howard, J. B. (2000) Nitrogenase: Standing at the crossroads. *Curr. Opin. Chem. Biol.* **4**, 559–566
27. Rees, D. C., Tezcan, F. A., Haynes, C. A., Walton, M. Y., Andrade, S., Einsle, O., and Howard, J. B. (2005) Structural basis of biological nitrogen fixation. *Phil. Trans. R. Soc. A* **363**, 971–984
28. Seefeldt, L. C., and Dean, D. R. (1997) Role of nucleotides in nitrogenase catalysis. *Acc. Chem. Res.* **30**, 260–266
29. Seefeldt, L. C., Dance, I. G., and Dean, D. R. (2004) Substrate interactions with nitrogenase: Fe versus Mo. *Biochemistry* **43**, 1401–1409
30. Dos Santos, P. C., Igarashi, R. Y., Lee, H.-I., Hoffman, B. M., Seefeldt, L. C., and Dean, D. R. (2005) Substrate interactions with the nitrogenase active site. *Acc. Chem. Res.* **38**, 208–214
31. Hoffman, B. M., Dean, D. R., and Seefeldt, L. C. (2009) Climbing nitrogenase: Toward a mechanism of enzymatic nitrogen fixation. *Acc. Chem. Res.* **42**, 609–619
32. Seefeldt, L. C., Hoffman, B. M., and Dean, D. R. (2009) Mechanism of Mo-dependent nitrogenase. *Annu. Rev. Biochem.* **78**, 701–722
33. Seefeldt, L. C., Hoffman, B. M., and Dean, D. R. (2012) Electron transfer in nitrogenase catalysis. *Curr. Opin. Chem. Biol.* **16**, 19–25

34. Hoffman, B. M., Lukoyanov, D., Dean, D. R., and Seefeldt, L. C. (2013) Nitrogenase: A draft mechanism. *Acc. Chem. Res.* **46**, 587–595
35. Hu, Y., and Ribbe, M. W. (2010) Decoding the nitrogenase mechanism: The homologue approach. *Acc. Chem. Res.* **43**, 475–484
36. Shah, V. K., and Brill, W. J. (1977) Isolation of an iron-molybdenum cofactor from nitrogenase. *Proc. Natl. Acad. Sci. U.S.A.* **74**, 3249–3253
37. Burgess, B. K. (1990) The iron-molybdenum cofactor of nitrogenase. *Chem. Rev.* **90**, 1377–1406
38. Smith, B. E., Durrant, M. C., Fairhurst, S. A., Gormal, C. A., Grönberg, K. L. C., Henderson, R. A., Ibrahim, S. K., Le Gall, T., and Pickett, C. J. (1999) Exploring the reactivity of the isolated iron-molybdenum cofactor of nitrogenase. *Coord. Chem. Rev.* **185**, 669–687
39. Zhao, Y., Bian, S.-M., Zhou, H.-N., and Huang, J.-F. (2006) Diversity of nitrogenase systems in diazotrophs. *J. Integr. Plant. Biol.* **48**, 745–755
40. Masepohl, B. (2002) in *Nitrogenase Fixation at the Millenium* (Leigh, G. J., ed.) pp. 191–222, Elsevier, Amsterdam, The Netherlands
41. Simpson, F. B., and Burris, R. H. (1984) A nitrogen pressure of 50 atmospheres does not prevent evolution of hydrogen by nitrogenase. *Science* **224**, 1095–1097
42. Carnahan, J. E., Mortenson, L. E., Mower, H. F., and Castle, J. E. (1960) Nitrogen fixation in cell-free extracts of *Clostridium pasteurianum*. *Biochim. Biophys. Acta* **44**, 520–535
43. Kim, J., and Rees, D. C. (1992) Structural models for the metal centers in the nitrogenase molybdenum-iron protein. *Science* **257**, 1677–1682
44. Chan, M. K., Kim, J., and Rees, D. C. (1993) The nitrogenase FeMo-cofactor and P-cluster: 2.2 Å resolution structures. *Science* **260**, 792–794
45. Kim, J., Woo, D., and Rees, D. C. (1993) X-ray crystal structure of the nitrogenase molybdenum-iron protein from *Clostridium pasteurianum* at 3.0 Å resolution. *Biochemistry* **32**, 7104–7115
46. Kim, J., and Rees, D. C. (1992) Crystallographic structure and functional implications of the nitrogenase molybdenum-iron protein from *Azotobacter vinelandii*. *Nature* **360**, 553–560
47. Georgiadis, M. M., Komiya, H., Chakrabarti, P., Woo, D., Kornuc, J. J., and Rees, D. C. (1992) Crystallographic structure of the nitrogenase iron protein from *Azotobacter vinelandii*. *Science* **257**, 1653–1659

48. Einsle, O., Tezcan, F. A., Andrade, S. L. A., Schmid, B., Yoshida, M., Howard, J. B., and Rees, D. C. (2002) Nitrogenase MoFe-protein at 1.16 Å resolution: A central ligand in the FeMo-cofactor. *Science* **297**, 1696–1700
49. Spatzal, T., Aksoyoglu, M., Zhang, L., Andrade, S. L. A., Schleicher, E., Weber, S., Rees, D. C., and Einsle, O. (2011) Evidence for interstitial carbon in nitrogenase FeMo cofactor. *Science* **334**, 940–940
50. Sørli, M., Christiansen, J., Lemon, B. J., Peters, J. W., Dean, D. R., and Hales, B. J. (2001) Mechanistic features and structure of the nitrogenase α -Gln¹⁹⁵ MoFe protein. *Biochemistry* **40**, 1540–1549
51. Jang, S. B., Seefeldt, L. C., and Peters, J. W. (2000) Insights into nucleotide signal transduction in nitrogenase: Structure of an iron protein with MgADP bound. *Biochemistry* **39**, 14745–14752
52. Jang, S. B., Seefeldt, L. C., and Peters, J. W. (2000) Modulating the midpoint potential of the [4Fe-4S] cluster of the nitrogenase Fe protein. *Biochemistry* **39**, 641–648
53. Jang, S. B., Jeong, M. S., Seefeldt, L. C., and Peters, J. W. (2004) Structural and biochemical implications of single amino acid substitutions in the nucleotide-dependent switch regions of the nitrogenase Fe protein from *Azotobacter vinelandii*. *J. Biol. Inorg. Chem.* **9**, 1028–1033
54. Mayer, S. M., Lawson, D. M., Gormal, C. A., Roe, S. M., and Smith, B. E. (1999) New insights into structure-function relationships in nitrogenase: A 1.6 Å resolution X-ray crystallographic study of *Klebsiella pneumoniae* MoFe-protein. *J. Mol. Biol.* **292**, 871–891
55. Mayer, S. M., Gormal, C. A., Smith, B. E., and Lawson, D. M. (2002) Crystallographic analysis of the MoFe protein of nitrogenase from a *nifV* mutant of *Klebsiella pneumoniae* identifies citrate as a ligand to the molybdenum of Iron molybdenum cofactor (FeMoco). *J. Biol. Chem.* **277**, 35263–35266
56. Bolin, J. T., Campobasso, N., Muchmore, S. W., Morgan, T. V., and Mortenson, L. E. (1993) in *Molybdenum Enzymes, Cofactors and Model Systems* (Stiefel, E. I., Coucouvanis, D., and Newton, W. E., eds.) pp. 186–195, ACS, Washington DC
57. Bolin, J. T., Ronco, A. E., Mortenson, L. E., Morgan, T. V., Williamson, M., and Xuong, N. H. (1990) in *Nitrogen Fixation: Achievements and Objectives* (Gresshoff, P. M., Roth, L. E., Stacey, G., and Newton, W. E., eds.) pp. 117–122, Chapman and Hall, New York
58. Sen, S., Krishnakumar, A., McClead, J., Johnson, M. K., Seefeldt, L. C., Szilagyi, R. K., and Peters, J. W. (2006) Insights into the role of nucleotide-dependent conformational change in nitrogenase catalysis: Structural characterization of the

- nitrogenase Fe protein Leu127 deletion variant with bound MgATP. *J. Inorg. Biochem.* **100**, 1041–1052
59. Sen, S., Igarashi, R., Smith, A., Johnson, M. K., Seefeldt, L. C., and Peters, J. W. (2004) A conformational mimic of the MgATP-bound “on state” of the nitrogenase iron protein. *Biochemistry* **43**, 1787–1797
 60. Schmid, B., Ribbe, M. W., Einsle, O., Yoshida, M., Thomas, L. M., Dean, D. R., Rees, D. C., and Burgess, B. K. (2002) Structure of a cofactor-deficient nitrogenase MoFe protein. *Science* **296**, 352–356
 61. Jeong, M. S. (2004) Structural basis for the changes in redox potential in the nitrogenase Phe135Trp Fe protein with MgADP bound. *Mol. Cells* **18**, 374–382.
 62. Sarma, R., Barney, B. M., Keable, S., Dean, D. R., Seefeldt, L. C., and Peters, J. W. (2010) Insights into substrate binding at FeMo-cofactor in nitrogenase from the structure of an α -70^{le} MoFe protein variant. *J. Inorg. Biochem.* **104**, 385–389
 63. Peters, J. W., Stowell, M. H. B., Soltis, S. M., Finnegan, M. G., Johnson, M. K., and Rees, D. C. (1997) Redox-dependent structural changes in the nitrogenase P-cluster. *Biochemistry* **36**, 1181–1187
 64. Schindelin, H., Kisker, C., Schlessman, J. L., Howard, J. B., and Rees, D. C. (1997) Structure of ADP·AlF₄⁻-stabilized nitrogenase complex and its implications for signal transduction. *Nature* **387**, 370–376
 65. Chiu, H.-J., Peters, J. W., Lanzilotta, W. N., Ryle, M. J., Seefeldt, L. C., Howard, J. B., and Rees, D. C. (2001) MgATP-bound and nucleotide-free structures of a nitrogenase protein complex between the Leu 127 Δ -Fe-protein and the MoFe-protein. *Biochemistry* **40**, 641–650
 66. Schmid, B., Einsle, O., Chiu, H.-J., Willing, A., Yoshida, M., Howard, J. B., and Rees, D. C. (2002) Biochemical and structural characterization of the cross-linked complex of nitrogenase: Comparison to the ADP-AlF₄⁻-stabilized structure. *Biochemistry* **41**, 15557–15565
 67. Tezcan, F. A., Kaiser, J. T., Mustafi, D., Walton, M. Y., Howard, J. B., and Rees, D. C. (2005) Nitrogenase complexes: Multiple docking sites for a nucleotide switch protein. *Science* **309**, 1377–1380
 68. Winter, H. C., and Burris, R. H. (1976) Nitrogenase. *Annu. Rev. Biochem.* **45**, 409–426
 69. Hu, Y., Fay, A. W., Lee, C. C., Yoshizawa, J., and Ribbe, M. W. (2008) Assembly of nitrogenase MoFe protein. *Biochemistry* **47**, 3973–3981

70. Igarashi, R. Y., and Seefeldt, L. C. (2003) Nitrogen fixation: The mechanism of the Mo-dependent nitrogenase. *Crit. Rev. Biochem. Mol. Biol.* **38**, 351–384
71. Mitra, D., George, S. J., Guo, Y., Kamali, S., Keable, S., Peters, J. W., Pelmeshnikov, V., Case, D. A., and Cramer, S. P. (2013) Characterization of [4Fe-4S] cluster vibrations and structure in nitrogenase Fe protein at three oxidation levels via combined NRVS, EXAFS, and DFT analyses. *J. Am. Chem. Soc.* **135**, 2530–2543
72. Rupnik, K., Lee, C. C., Hu, Y., Ribbe, M. W., and Hales, B. J. (2011) [4Fe4S]²⁺ clusters exhibit ground-state paramagnetism. *J. Am. Chem. Soc.* **133**, 6871–6873
73. Hagen, W. R., Eady, R. R., Dunham, W. R., and Haaker, H. (1985) A novel $S = 3/2$ EPR signal associated with native Fe proteins of nitrogenase. *FEBS Lett.* **189**, 250–254
74. Hagen, W. R., Dunham, W. R., Braaksma, A., and Haaker, H. (1985) On the prosthetic group(s) of component II from nitrogenase: EPR of the Fe-protein from *Azotobacter vinelandii*. *FEBS Lett.* **187**, 146–50
75. Lindahl, P. A., Day, E. P., Kent, T. A., Orme-Johnson, W. H., and Münck, E. (1985) Mössbauer, EPR, and magnetization studies of the *Azotobacter vinelandii* Fe protein: Evidence for a [4Fe-4S]¹⁺ cluster with spin $S = 3/2$. *J. Biol. Chem.* **260**, 11160–11173
76. Watt, G. D., and Reddy, K. R. N. (1994) Formation of an all ferrous Fe₄S₄ cluster in the iron protein component of *Azotobacter vinelandii* nitrogenase. *J. Inorg. Biochem.* **53**, 281–294
77. Thorneley, R. N., and Ashby, G. A. (1989) Oxidation of nitrogenase iron protein by dioxygen without inactivation could contribute to high respiration rates of *Azotobacter* species and facilitate nitrogen fixation in other aerobic environments. *Biochem. J.* **261**, 181–187
78. Watt, G. D. (1979) An electrochemical method for measuring redox potentials of low potential proteins by microcoulometry at controlled potentials. *Anal. Biochem.* **99**, 399–407
79. Watt, G. D., Wang, Z. C., and Knotts, R. R. (1986) Redox reactions of and nucleotide binding to the iron protein of *Azotobacter vinelandii*. *Biochemistry* **25**, 8156–8162
80. Ryle, M. J., Lanzilotta, W. N., Mortenson, L. E., Watt, G. D., and Seefeldt, L. C. (1995) Evidence for a central role of Lysine 15 of *Azotobacter vinelandii* nitrogenase iron protein in nucleotide binding and protein conformational changes. *J. Biol. Chem.* **270**, 13112–13117

81. Lanzilotta, W. N., Ryle, M. J., and Seefeldt, L. C. (1995) Nucleotide hydrolysis and protein conformational changes in *Azotobacter vinelandii* nitrogenase iron protein: Defining the function of aspartate 129. *Biochemistry* **34**, 10713–10723
82. Peters, J. W., and Szilagyi, R. K. (2006) Exploring new frontiers of nitrogenase structure and mechanism. *Curr. Opin. Chem. Biol.* **10**, 101–108
83. Weston, M. F., Kotake, S., and Davis, L. C. (1983) Interaction of nitrogenase with nucleotide analogs of ATP and ADP and the effect of metal ions on ADP inhibition. *Arch. Biochem. Biophys.* **225**, 809–817
84. Sarma, R., Mulder, D. W., Brecht, E., Szilagyi, R. K., Seefeldt, L. C., Tsuruta, H., and Peters, J. W. (2007) Probing the MgATP-bound conformation of the nitrogenase Fe protein by solution small-angle X-ray scattering. *Biochemistry* **46**, 14058–14066
85. Zimmermann, R., Münck, E., Brill, W. J., Shah, V. K., Henzl, M. T., Rawlings, J., and Orme-Johnson, W. H. (1978) Nitrogenase X: Mössbauer and EPR studies on reversibly oxidized MoFe protein from *Azotobacter vinelandii* OP: Nature of the iron centers. *Biochim. Biophys. Acta* **537**, 185–207
86. Lindahl, P. A., Papaefthymiou, V., Orme-Johnson, W. H., and Münck, E. (1988) Mössbauer studies of solid thionin-oxidized MoFe protein of nitrogenase. *J. Biol. Chem.* **263**, 19412–19418
87. Hagen, W. R. W. (1987) Quantitative EPR of an $S = 7/2$ system in thionine-oxidized MoFe proteins of nitrogenase. *Eur. J. Biochem.* **169**, 457–465
88. Pierik, A. J. W. (1993) Redox properties and EPR spectroscopy of the P clusters of *Azotobacter vinelandii* MoFe protein. *Eur. J. Biochem.* **212**, 51–61
89. Tittsworth, R. C., and Hales, B. J. (1993) Detection of EPR signals assigned to the 1-equiv-oxidized P-clusters of the nitrogenase MoFe-protein from *Azotobacter vinelandii*. *J. Am. Chem. Soc.* **115**, 9763–9767
90. Morgan, T. V., Mortenson, L. E., McDonald, J. W., and Watt, G. D. (1988) Comparison of redox and EPR properties of the molybdenum iron proteins of *Clostridium pasteurianum* and *Azotobacter vinelandii* nitrogenases. *J. Inorg. Biochem.* **33**, 111–120
91. Lanzilotta, W. N., and Seefeldt, L. C. (1997) Changes in the midpoint potentials of the nitrogenase metal centers as a result of iron protein–molybdenum-iron protein complex formation. *Biochemistry* **36**, 12976–12983
92. Chan, J. M., Christiansen, J., Dean, D. R., and Seefeldt, L. C. (1999) Spectroscopic evidence for changes in the redox state of the nitrogenase P-cluster during turnover. *Biochemistry* **38**, 5779–5785

93. Rupnik, K., Hu, Y., Lee, C. C., Wiig, J. A., Ribbe, M. W., and Hales, B. J. (2012) P^+ state of nitrogenase P-cluster exhibits electronic structure of a $[Fe_4S_4]^+$ cluster. *J. Am. Chem. Soc.* **134**, 13749–13754
94. Lee, H.-I., Benton, P. M. C., Laryukhin, M., Igarashi, R. Y., Dean, D. R., Seefeldt, L. C., and Hoffman, B. M. (2003) The interstitial atom of the nitrogenase FeMo-cofactor: ENDOR and ESEEM show it is not an exchangeable nitrogen. *J. Am. Chem. Soc.* **125**, 5604–5605
95. Yang, T.-C., Maeser, N. K., Laryukhin, M., Lee, H.-I., Dean, D. R., Seefeldt, L. C., and Hoffman, B. M. (2005) The interstitial atom of the nitrogenase FeMo-cofactor: ENDOR and ESEEM evidence that it is not a nitrogen. *J. Am. Chem. Soc.* **127**, 12804–12805
96. Lukoyanov, D., Pelmeshnikov, V., Maeser, N., Laryukhin, M., Yang, T. C., Noodleman, L., Dean, D. R., Case, D. A., Seefeldt, L. C., and Hoffman, B. M. (2007) Testing if the interstitial atom, X, of the nitrogenase molybdenum–iron cofactor is N or C: ENDOR, ESEEM, and DFT studies of the $S = 3/2$ resting state in multiple environments. *Inorg. Chem.* **46**, 11437–11449
97. Lovell, T., Li, J., Liu, T., Case, D. A., and Noodleman, L. (2001) FeMo cofactor of nitrogenase: A density functional study of states M^N , M^{OX} , M^R , and M^I . *J. Am. Chem. Soc.* **123**, 12392–12410
98. Dance, I. (2003) The consequences of an interstitial N atom in the FeMo cofactor of nitrogenase. *Chem. Commun.*, 324–325
99. Dance, I. (2007) The mechanistically significant coordination chemistry of dinitrogen at FeMo-co, the catalytic site of nitrogenase. *J. Am. Chem. Soc.* **129**, 1076–1088
100. Pelmeshnikov, V., Case, D. A., and Noodleman, L. (2008) Ligand-bound $S = 1/2$ FeMo-cofactor of nitrogenase: Hyperfine interaction analysis and implication for the central ligand X identity. *Inorg. Chem.* **47**, 6162–6172
101. Harris, T. V., and Szilagyi, R. K. (2011) Comparative assessment of the composition and charge state of nitrogenase FeMo-cofactor. *Inorg. Chem.* **50**, 4811–4824
102. Lancaster, K. M., Roemelt, M., Ettenhuber, P., Hu, Y., Ribbe, M. W., Neese, F., Bergmann, U., and DeBeer, S. (2011) X-ray emission spectroscopy evidences a central carbon in the nitrogenase iron-molybdenum cofactor. *Science* **334**, 974–977
103. Wiig, J. A., Hu, Y., Lee, C. C., and Ribbe, M. W. (2012) Radical SAM-dependent carbon insertion into the nitrogenase M-cluster. *Science* **337**, 1672–1675

104. Wiig, J. A., Lee, C. C., Hu, Y., and Ribbe, M. W. (2013) Tracing the interstitial carbide of the nitrogenase cofactor during substrate turnover. *J. Am. Chem. Soc.* **135**, 4982–4983
105. Hoover, T. R., Robertson, A. D., Cerny, R. L., Hayes, R. N., Imperial, J., Shah, V. K., and Ludden, P. W. (1987) Identification of the V factor needed for synthesis of the iron-molybdenum cofactor of nitrogenase as homocitrate. *Nature* **329**, 855–857
106. Hoover, T. R., Imperial, J., Ludden, P. W., and Shah, V. K. (1989) Homocitrate is a component of the iron-molybdenum cofactor of nitrogenase. *Biochemistry* **28**, 2768–2771
107. Orme-Johnson, W. H., Hamilton, W. D., Jones, T. L., Tso, M. Y. W., Burris, R. H., Shah, V. K., and Brill, W. J. (1972) Electron paramagnetic resonance of nitrogenase and nitrogenase components from *Clostridium pasteurianum* W5 and *Azotobacter vinelandii* OP. *Proc. Natl. Acad. Sci. U.S.A.* **69**, 3142–3145
108. Schultz, F. A., Gheller, S. F., and Newton, W. E. (1988) Iron-molybdenum cofactor of nitrogenase: Electrochemical determination of the electron stoichiometry of the oxidized/semi-reduced couple. *Biochem. Biophys. Res. Commun.* **152**, 629–635
109. Huynh, B. H., Henzl, M. T., Christner, J. A., Zimmermann, R., Orme-Johnson, W. H., and Münck, E. (1980) Nitrogenase XII. Mössbauer studies of the MoFe protein from *Clostridium pasteurianum* W5. *Biochim. Biophys. Acta* **623**, 124–138
110. Yoo, S. J., Angove, H. C., Papaefthymiou, V., Burgess, B. K., and Münck, E. (2000) Mössbauer study of the MoFe protein of nitrogenase from *Azotobacter vinelandii* using selective ^{57}Fe enrichment of the M-centers. *J. Am. Chem. Soc.* **122**, 4926–4936
111. Watt, G. D., Burns, A., Lough, S., and Tennent, D. L. (1980) Redox and spectroscopic properties of oxidized MoFe protein from *Azotobacter vinelandii*. *Biochemistry* **19**, 4926–4932
112. Lovell, T., Liu, T., Case, D. A., and Noodleman, L. (2003) Structural, spectroscopic, and redox consequences of a central ligand in the FeMoco of nitrogenase: A density functional theoretical study. *J. Am. Chem. Soc.* **125**, 8377–8383
113. Lee, H.-I., Hales, B. J., and Hoffman, B. M. (1997) Metal-ion valencies of the FeMo cofactor in CO-Inhibited and resting state nitrogenase by ^{57}Fe Q-band ENDOR. *J. Am. Chem. Soc.* **119**, 11395–11400
114. Lee, H.-I., Sørli, M., Christiansen, J., Yang, T.-C., Shao, J., Dean, D. R., Hales, B. J., and Hoffman, B. M. (2005) Electron inventory, kinetic assignment (E_n), structure, and bonding of nitrogenase turnover intermediates with C_2H_2 and CO. *J. Am. Chem. Soc.* **127**, 15880–15890

115. Danyal, K., Mayweather, D., Dean, D. R., Seefeldt, L. C., and Hoffman, B. M. (2010) Conformational gating of electron transfer from the nitrogenase Fe protein to MoFe protein. *J. Am. Chem. Soc.* **132**, 6894–6895
116. Danyal, K., Dean, D. R., Hoffman, B. M., and Seefeldt, L. C. (2011) Electron transfer within nitrogenase: Evidence for a deficit-spending mechanism. *Biochemistry* **50**, 9255–9263
117. Mayweather, D., Danyal, K., Dean, D. R., Seefeldt, L. C., and Hoffman, B. M. (2012) Temperature invariance of the nitrogenase electron transfer mechanism. *Biochemistry* **51**, 8391–8398
118. Hageman, R. V., and Burris, R. H. (1978) Nitrogenase and nitrogenase reductase associate and dissociate with each catalytic cycle. *Proc. Natl. Acad. Sci. U.S.A.* **75**, 2699–2702
119. Newton, W. E., and Dilworth, M. J. (2011) Assays of nitrogenase reaction products. *Methods Mol. Biol.* **766**, 105–127
120. Burgess, B. K. (1985) in *Metal Ions in Biology: Molybdenum Enzymes* (Spiro, T. G., ed.) pp. 161–220, John Wiley and Sons, New York
121. Thorneley, R. N. F., Eady, R. R., and Lowe, D. J. (1978) Biological nitrogen fixation by way of an enzyme-bound dinitrogen-hydride intermediate. *Nature* **272**, 557–558
122. Dilworth, M. J., and Eady, R. R. (1991) Hydrazine is a product of dinitrogen reduction by the vanadium-nitrogenase from *Azotobacter chroococcum*. *Biochem. J.* **277**, 465–468
123. Barney, B. M., McClead, J., Lukoyanov, D., Laryukhin, M., Yang, T.-C., Dean, D. R., Hoffman, B. M., and Seefeldt, L. C. (2007) Diazene (HN=NH) Is a substrate for nitrogenase: Insights into the pathway of N₂ reduction. *Biochemistry* **46**, 6784–6794
124. Barney, B. M., Lukoyanov, D., Yang, T.-C., Dean, D. R., Hoffman, B. M., and Seefeldt, L. C. (2006) A methyl diazene (HN=N-CH₃)-derived species bound to the nitrogenase active-site FeMo cofactor: Implications for mechanism. *Proc. Natl. Acad. Sci. U.S.A.* **103**, 17113–17118
125. McKenna, C. E., Simeonov, A. M., Eran, H., and Bravo-Leerabhandh, M. (1996) Reduction of cyclic and acyclic diazene derivatives by *Azotobacter vinelandii* nitrogenase: Diazirine and trans-dimethyldiazene. *Biochemistry* **35**, 4502–4514
126. Davis, L. C. (1980) Hydrazine as a substrate and inhibitor of *Azotobacter vinelandii* nitrogenase. *Arch. Biochem. Biophys.* **204**, 270–276

127. Barney, B. M., Laryukhin, M., Igarashi, R. Y., Lee, H.-I., Dos Santos, P. C., Yang, T.-C., Hoffman, B. M., Dean, D. R., and Seefeldt, L. C. (2005) Trapping a hydrazine reduction intermediate on the nitrogenase active site. *Biochemistry* **44**, 8030–8037
128. Guth, J. H., and Burris, R. H. (1983) Inhibition of nitrogenase-catalyzed NH_3 formation by H_2 . *Biochemistry* **22**, 5111–5122
129. Lockshin, A., and Burris, R. H. (1965) Inhibitors of nitrogen fixation in extracts from *Clostridium pasteurianum*. *Biochim. Biophys. Acta* **111**, 1–10
130. Fisher, K., Dilworth, M. J., and Newton, W. E. (2000) Differential effects on N_2 binding and reduction, HD formation, and azide reduction with α -195^{His}- and α -191^{Gln}-substituted MoFe proteins of *Azotobacter vinelandii* nitrogenase. *Biochemistry* **39**, 15570–15577
131. Hardy, R. W., and Knight, E. J. (1967) ATP-dependent reduction of azide and HCN by N_2 -fixing enzymes of *Azotobacter vinelandii* and *Clostridium pasteurianum*. *Biochim. Biophys. Acta* **139**, 69–90
132. Schöllhorn, R., and Burris, R. H. (1967) Reduction of azide by the N_2 -fixing enzyme system. *Proc. Natl. Acad. Sci. U.S.A.* **57**, 1317–1323
133. Fisher, K., Dilworth, M. J., and Newton, W. E. (2006) *Azotobacter vinelandii* vanadium nitrogenase: Formaldehyde is a product of catalyzed HCN reduction, and excess ammonia arises directly from catalyzed azide reduction. *Biochemistry* **45**, 4190–4198
134. Dilworth, M. J., and Thorneley, R. N. (1981) Nitrogenase of *Klebsiella pneumoniae*: Hydrazine is a product of azide reduction. *Biochem. J.* **193**, 971
135. Rubinson, J. F., Corbin, J. L., and Burgess, B. K. (1983) Nitrogenase reactivity: Methyl isocyanide as substrate and inhibitor. *Biochemistry* **22**, 6260–6268
136. Jensen, B. B., and Burris, R. H. (1986) Nitrous oxide as a substrate and as a competitive inhibitor of nitrogenase. *Biochemistry* **25**, 1083–1088
137. Hoch, G. E., Schneider, K. C., and Burris, R. H. (1960) Hydrogen evolution and exchange, and conversion of N_2O to N_2 by soybean root nodules. *Biochim. Biophys. Acta* **37**, 273–279
138. Vaughn, S. A., and Burgess, B. K. (1989) Nitrite, a new substrate for nitrogenase. *Biochemistry* **28**, 419–424
139. Dilworth, M. J. (1966) Acetylene reduction by nitrogen-fixing preparations from *Clostridium pasteurianum*. *Biochim. Biophys. Acta* **127**, 285–294

140. Dilworth, M. J., Eady, R. R., Robson, R. I., and Miller, R. W. (1987) Ethane formation from acetylene as a potential test for vanadium nitrogenase *in vivo*. *Nature* **327**, 167–168
141. Eady, R. R., Robson, R. I., Richardson, T. H., Miller, R. W., and Hawkins, M. (1987) The vanadium nitrogenase of *Azotobacter chroococcum*: Purification and properties of the VFe protein. *Biochem. J.* **244**, 197–207
142. Schneider, K., Gollan, U., Selsemeiervoigt, S., Plass, W., and Muller, A. (1994) Rapid purification of the protein-components of a highly-active iron only nitrogenase. *Naturwissenschaften* **81**, 405–408
143. Pau, R. N., Eldridge, M. E., Lowe, D. J., Mitchenall, L. A., and Eady, R. (1993) Molybdenum-independent nitrogenases of *Azotobacter vinelandii*: A functional species of alternative nitrogenase-3 isolated from a molybdenum-tolerant strain contains an iron molybdenum cofactor. *Biochem. J.* **293**, 101–107
144. Kim, C.-H., Newton, W. E., and Dean, D. R. (1995) Role of the MoFe protein α -subunit histidine-195 residue in FeMo-cofactor binding and nitrogenase catalysis. *Biochemistry* **34**, 2798–2808
145. Schneider, K., Müller, A., Krahn, E., Hagen, W. R., Wassink, H., and Karl-Heinz, K. (1995) The molybdenum nitrogenase from wild-type *Xanthobacter autotrophicus* exhibits properties reminiscent of alternative nitrogenases. *Eur. J. Biochem.* **230**, 666–675
146. Scott, D. J., Dean, D. R., and Newton, W. E. (1992) Nitrogenase-catalyzed ethane production and CO-sensitive hydrogen evolution from MoFe proteins having amino acid substitutions in an α -subunit FeMo cofactor-binding domain. *J. Biol. Chem.* **267**, 20002–20010
147. Hardy, R. W., Burns, R. C., and Parshall, G. W. (1971) in *Bioinorganic Chemistry* (Dessy, R., Dillard, J., and Taylor, L., eds.) pp. 219–247, American Chemical Society, Washington, DC
148. Hardy, R. W. F., and Jackson, E. K. (1967) Reduction of model substrates - nitriles and acetylenes - by nitrogenase (N_2 ase). *Fed. Proc.* **28**, 725
149. Mayer, S. M., Niehaus, W. G., and Dean, D. R. (2002) Reduction of short chain alkynes by a nitrogenase α -70^{Ala}-substituted MoFe protein. *J. Chem. Soc.-Dalton Trans.*, 802–807
150. Burns, R. C., and Hardy, R. W. (1975) *Nitrogen Fixation in Bacteria and Higher Plants.*, Springer, Berlin

151. Dos Santos, P. C., Mayer, S. M., Barney, B. M., Seefeldt, L. C., and Dean, D. R. (2007) Alkyne substrate interaction within the nitrogenase MoFe protein. *J. Inorg. Biochem.* **101**, 1642–1648
152. Igarashi, R. Y., Dos Santos, P. C., Niehaus, W. G., Dance, I. G., Dean, D. R., and Seefeldt, L. C. (2004) Localization of a catalytic intermediate bound to the FeMo-cofactor of nitrogenase. *J. Biol. Chem.* **279**, 34770–34775
153. Burns, R. C., Hardy, R. W., and Phillips, W. D. (1975) in *Nitrogen Fixation in Free-Living Organisms* (Stewart, W. D. P., ed.) pp. 447–452, Cambridge University Press, Cambridge
154. Ashby, G. A., Dilworth, M. J., and Thorneley, R. N. F. (1987) *Klebsiella pneumoniae* nitrogenase. Inhibition of hydrogen evolution by ethylene and the reduction of ethylene to ethane. *Biochem. J.* **247**, 547–554
155. Dilworth, M. J., Eady, R. R., and Eldridge, M. E. (1988) The vanadium nitrogenase of *Azotobacter chroococcum*: Reduction of acetylene and ethylene to ethane. *Biochem. J.* **249**, 745–751
156. McKenna, C. E., McKenna, M. C., and Higa, M. T. (1976) Chemical probes of nitrogenase. 1. Cyclopropene. Nitrogenase-catalyzed reduction to propene and cyclopropane. *J. Am. Chem. Soc.* **98**, 4657–4659
157. McKenna, C. E., Eran, H., Nakajima, T., and Osumi, A. (1981) in *Current perspectives in nitrogen fixation* (Gibson, A. H., and Newton, W. E., eds.) p. 358, Australia Academy of Science, Canberra
158. Li, J., Burgess, B. K., and Corbin, J. L. (1982) Nitrogenase reactivity: Cyanide as substrate and inhibitor. *Biochemistry* **21**, 4393–4402
159. Kelly, M., Postgate, J. R., and Richards, R. L. (1967) Reduction of cyanide and isocyanide by nitrogenase of *Azotobacter chroococcum*. *Biochem. J.* **102**, 1C–3C
160. Miller, R. W., and Eady, R. R. (1988) Cyanamide: A new substrate for nitrogenase. *Biochim. Biophys. Acta* **952**, 290–296
161. Fuchsman, W. H., and Hardy, R. W. F. (1972) Nitrogenase-catalyzed acrylonitrile reductions. *Bioinorg. Chem.* **1**, 195–213
162. Burns, R. C., Fuchsman, W. H., and Hardy, R. W. (1971) Nitrogenase from vanadium-grown *Azotobacter*: Isolation, characteristics, and mechanistic implications. *Biochem. Biophys. Res. Commun.* **42**, 353–358
163. Hwang, J. C., and Burris, R. H. (1972) Nitrogenase-catalyzed reactions. *Biochim. Biophys. Acta* **283**, 339–350

164. Kelly, M. (1968) The kinetics of the reduction of isocyanides, acetylenes and the cyanide ion by nitrogenase preparation from *Azotobacter chroococcum* and the effects of inhibitors. *Biochem. J.* **107**, 1–6
165. Biggins, D. R., and Postgate, J. R. (1969) Nitrogen fixation by cultures and cell-free extracts of *Mycobacterium flavum* 301. *J. Gen. Microbiol.* **56**, 181–193
166. Kelly, M. (1969) Some properties of purified nitrogenase of *Azotobacter chroococcum*. *Biochim. Biophys. Acta* **171**, 9–22
167. Hu, Y., Lee, C. C., and Ribbe, M. W. (2011) Extending the carbon chain: Hydrocarbon formation catalyzed by vanadium/molybdenum nitrogenases. *Science* **333**, 753–755
168. Lee, C. C., Hu, Y., and Ribbe, M. W. (2010) Vanadium nitrogenase reduces CO. *Science* **329**, 642–642
169. Lee, C. C., Hu, Y., and Ribbe, M. W. (2011) Tracing the hydrogen source of hydrocarbons formed by vanadium nitrogenase. *Angew. Chem. Int. Ed.* **50**, 5545–5547
170. Seefeldt, L. C., Rasche, M. E., and Ensign, S. A. (1995) Carbonyl sulfide and carbon dioxide as new substrates, and carbon disulfide as a new inhibitor, of nitrogenase. *Biochemistry* **34**, 5382–5389
171. Rasche, M. E., and Seefeldt, L. C. (1997) Reduction of thiocyanate, cyanate, and carbon disulfide by nitrogenase: Kinetic characterization and EPR spectroscopic analysis. *Biochemistry* **36**, 8574–8585
172. Li, J.-L., and Burris, R. H. (1983) Influence of pN₂ and pD₂ on HD formation by various nitrogenases. *Biochemistry* **22**, 4472–4480
173. Jensen, B. B., and Burris, R. H. (1985) Effect of high pN₂ and high pD₂ on ammonia production, hydrogen evolution, and hydrogen deuteride formation by nitrogenases. *Biochemistry* **24**, 1141–1147
174. Burgess, B. K., Wherland, S., Newton, W. E., and Stiefel, E. I. (1981) Nitrogenase reactivity: Insight into the nitrogen-fixing process through hydrogen-inhibition and HD-forming reactions. *Biochemistry* **20**, 5140–5146
175. Schöllhorn, R., and Burris, R. H. (1967) Acetylene as a competitive inhibitor of N₂ fixation. *Proc. Natl. Acad. Sci. U.S.A.* **58**, 213–216
176. Dilworth, M. J., Eldridge, M. E., and Eady, R. R. (1993) The molybdenum and vanadium nitrogenases of *Azotobacter chroococcum*: Effect of elevated temperature on N₂ reduction. *Biochem. J.* **289**, 395–400

177. Fisher, K., Dilworth, M. J., Kim, C.-H., and Newton, W. E. (2000) *Azotobacter vinelandii* nitrogenases containing altered MoFe proteins with substitutions in the FeMo-cofactor environment: Effects on the catalyzed reduction of acetylene and ethylene. *Biochemistry* **39**, 2970–2979
178. Hardy, R. W., Holsten, R. D., Jackson, E. K., and Burns, R. C. (1968) The acetylene-ethylene assay for N₂ fixation: Laboratory and field evaluation. *Plant Physiol.* **43**, 1185–1207
179. Han, J., and Newton, W. E. (2004) Differentiation of acetylene-reduction sites by stereoselective proton addition during *Azotobacter vinelandii* nitrogenase-catalyzed C₂D₂ reduction. *Biochemistry* **43**, 2947–2956
180. Benton, P. M. C., Christiansen, J., Dean, D. R., and Seefeldt, L. C. (2001) Stereospecificity of acetylene reduction catalyzed by nitrogenase. *J. Am. Chem. Soc.* **123**, 1822–1827
181. McKenna, C. E., McKenna, M. C., and Huang, C. W. (1979) Low stereoselectivity in methylacetylene and cyclopropene reductions by nitrogenase. *Proc. Natl. Acad. Sci. U.S.A.* **76**, 4773–4777
182. Lee, H.-I., Igarashi, R. Y., Laryukhin, M., Doan, P. E., Dos Santos, P. C., Dean, D. R., Seefeldt, L. C., and Hoffman, B. M. (2004) An organometallic intermediate during alkyne reduction by nitrogenase. *J. Am. Chem. Soc.* **126**, 9563–9569
183. Madden, M. S., Kindon, N. D., Ludden, P. W., and Shah, V. K. (1990) Diastereomer-dependent substrate reduction properties of a dinitrogenase containing 1-fluorohomocitrate in the iron-molybdenum cofactor. *Proc. Natl. Acad. Sci. U.S.A.* **87**, 6517–6521
184. Hwang, J. C., Chen, C. H., and Burris, R. H. (1973) Inhibition of nitrogenase-catalyzed reductions. *Biochim. Biophys. Acta* **292**, 256–270
185. Rivera-Ortiz, J. M., and Burris, R. H. (1975) Interactions among substrates and inhibitors of nitrogenase. *J. Bacteriol.* **123**, 537–545
186. Christiansen, J., Seefeldt, L. C., and Dean, D. R. (2000) Competitive substrate and inhibitor interactions at the physiologically relevant active site of nitrogenase. *J. Biol. Chem.* **275**, 36104–36107
187. Barney, B. M., Igarashi, R. Y., Dos Santos, P. C., Dean, D. R., and Seefeldt, L. C. (2004) Substrate interaction at an iron-sulfur face of the FeMo-cofactor during nitrogenase catalysis. *J. Biol. Chem.* **279**, 53621–53624
188. Benton, P. M. C., Mayer, S. M., Shao, J., Hoffman, B. M., Dean, D. R., and Seefeldt, L. C. (2001) Interaction of acetylene and cyanide with the resting state of nitrogenase α -96-substituted MoFe proteins. *Biochemistry* **40**, 13816–13825

189. Scott, D. J., May, H. D., Newton, W. E., Brigle, K. E., and Dean, D. R. (1990) Role for the nitrogenase MoFe protein α -subunit in FeMo-cofactor binding and catalysis. *Nature* **343**, 188–190
190. Thomann, H., Bernardo, M., Newton, W. E., and Dean, D. R. (1991) N coordination of FeMo cofactor requires His-195 of the MoFe protein α subunit and is essential for biological nitrogen fixation. *Proc. Natl. Acad. Sci. U.S.A.* **88**, 6620–6623
191. Dilworth, M. J., Fisher, K., Kim, C.-H., and Newton, W. E. (1998) Effects on substrate reduction of substitution of histidine-195 by glutamine in the α -subunit of the MoFe protein of *Azotobacter vinelandii* nitrogenase. *Biochemistry* **37**, 17495–17505
192. Barney, B. M., Yang, T.-C., Igarashi, R. Y., Dos Santos, P. C., Laryukhin, M., Lee, H.-I., Hoffman, B. M., Dean, D. R., and Seefeldt, L. C. (2005) Intermediates trapped during nitrogenase reduction of $\text{N}\equiv\text{N}$, $\text{CH}_3\text{-N=NH}$, and $\text{H}_2\text{N-NH}_2$. *J. Am. Chem. Soc.* **127**, 14960–14961
193. Igarashi, R. Y., Laryukhin, M., Dos Santos, P. C., Lee, H.-I., Dean, D. R., Seefeldt, L. C., and Hoffman, B. M. (2005) Trapping H^- bound to the nitrogenase FeMo-cofactor active site during H_2 evolution: Characterization by ENDOR spectroscopy. *J. Am. Chem. Soc.* **127**, 6231–6241
194. Barney, B. M., Lukoyanov, D., Igarashi, R. Y., Laryukhin, M., Yang, T.-C., Dean, D. R., Hoffman, B. M., and Seefeldt, L. C. (2009) Trapping an intermediate of dinitrogen (N_2) reduction on nitrogenase. *Biochemistry* **48**, 9094–9102
195. Yates, M. G., and Lowe, D. J. (1976) Nitrogenase of *Azotobacter chroococcum*: A new electronparamagnetic-resonance signal associated with a transient species of the MoFe protein during catalysis. *FEBS Lett.* **72**, 121–126
196. Davis, L. C., Henzl, M. T., Burris, R. H., and Orme-Johnson, W. H. (1979) Iron-sulfur clusters in the molybdenum-iron protein component of nitrogenase. Electron paramagnetic resonance of the carbon monoxide inhibited state. *Biochemistry* **18**, 4860–4869
197. Lowe, D. J., Eady, R. R., and Thorneley, N. F. (1978) Electron-paramagnetic-resonance studies on nitrogenase of *Klebsiella pneumoniae*: Evidence for acetylene- and ethylene-nitrogenase transient complexes. *Biochem. J.* **173**, 277–290
198. Benton, P. M. C., Laryukhin, M., Mayer, S. M., Hoffman, B. M., Dean, D. R., and Seefeldt, L. C. (2003) Localization of a substrate binding site on the FeMo-cofactor in nitrogenase: Trapping propargyl alcohol with an α -70-substituted MoFe protein. *Biochemistry* **42**, 9102–9109

199. Sørli, M., Christiansen, J., Dean, D. R., and Hales, B. J. (1999) Detection of a new radical and FeMo-cofactor EPR signal during acetylene reduction by the α -H195Q mutant of nitrogenase. *J. Am. Chem. Soc.* **121**, 9457–9458
200. Shen, J., Dean, D. R., and Newton, W. E. (1997) Evidence for multiple substrate-reduction sites and distinct inhibitor-binding sites from an altered *Azotobacter vinelandii* nitrogenase MoFe protein. *Biochemistry* **36**, 4884–4894
201. Pickett, C. J. (1996) The Chatt cycle and the mechanism of enzymic reduction of molecular nitrogen. *J. Biol. Inorg. Chem.* **1**, 601–606
202. Schrock, R. R. (2005) Catalytic reduction of dinitrogen to ammonia at a single molybdenum center. *Acc. Chem. Res.* **38**, 955–962
203. Pickett, C. J., Vincent, K. A., Ibrahim, S. K., Gormal, C. A., Smith, B. E., Fairhurst, S. A., and Best, S. P. (2004) Synergic binding of carbon monoxide and cyanide to the FeMo cofactor of nitrogenase: Relic chemistry of an ancient enzyme? *Chem. Eur. J.* **10**, 4770–4776
204. Pollock, R. C., Lee, H.-I., Cameron, L. M., DeRose, V. J., Hales, B. J., Orme-Johnson, W. H., and Hoffman, B. M. (1995) Investigation of CO bound to inhibited forms of nitrogenase MoFe protein by ^{13}C ENDOR. *J. Am. Chem. Soc.* **117**, 8686–8687
205. Christie, P. D., Lee, H.-I., Cameron, L. M., Hales, B. J., Orme-Johnson, W. H., and Hoffman, B. M. (1996) Identification of the CO-binding cluster in nitrogenase MoFe protein by ENDOR of ^{57}Fe isotopomers. *J. Am. Chem. Soc.* **118**, 8707–8709
206. Lee, H.-I., Cameron, L. M., Hales, B. J., and Hoffman, B. M. (1997) CO binding to the FeMo cofactor of CO-inhibited nitrogenase: ^{13}C and ^1H Q-band ENDOR investigation. *J. Am. Chem. Soc.* **119**, 10121–10126
207. Yan, L., Pelmentschikov, V., Dapper, C. H., Scott, A. D., Newton, W. E., and Cramer, S. P. (2012) IR-monitored photolysis of CO-inhibited nitrogenase: A major EPR-silent species with coupled terminal CO ligands. *Chem. Eur. J.* **18**, 16349–16357
208. George, S. J., Ashby, G. A., Wharton, C. W., and Thorneley, R. N. F. (1997) Time-resolved binding of carbon monoxide to nitrogenase monitored by stopped-flow infrared spectroscopy. *J. Am. Chem. Soc.* **119**, 6450–6451
209. Thorneley, R. N. F., and Lowe, D. J. (1985) in *Molybdenum Enzymes* (Spiro, T. G., ed.) pp. 221–284, Wiley, New York
210. Lowe, D. J., and Thorneley, R. N. (1984) The mechanism of *Klebsiella pneumoniae* nitrogenase action. Pre-steady-state kinetics of H_2 formation. *Biochem. J.* **224**, 877–886

211. Lowe, D. J., and Thorneley, R. N. (1984) The mechanism of *Klebsiella pneumoniae* nitrogenase action: The determination of rate constants required for the simulation of the kinetics of N₂ reduction and H₂ evolution. *Biochem. J.* **224**, 895
212. Thorneley, R. N., and Lowe, D. J. (1984) The mechanism of *Klebsiella pneumoniae* nitrogenase action: Pre-steady-state kinetics of an enzyme-bound intermediate in N₂ reduction and of NH₃ formation. *Biochem. J.* **224**, 887
213. Thorneley, R. N., and Lowe, D. J. (1984) The mechanism of *Klebsiella pneumoniae* nitrogenase action: Simulation of the dependences of H₂-evolution rate on component-protein concentration and ratio and sodium dithionite concentration. *Biochem. J.* **224**, 903
214. Wilson, P. E., Nyborg, A. C., and Watt, G. D. (2001) Duplication and extension of the Thorneley and Lowe kinetic model for *Klebsiella pneumoniae* nitrogenase catalysis using a MATHEMATICA software platform. *Biophys. Chem.* **91**, 281–304
215. Liang, J., and Burris, R. H. (1988) Hydrogen burst associated with nitrogenase-catalyzed reactions. *Proc. Natl. Acad. Sci. U.S.A.* **85**, 9446–9450
216. Lowe, D. J., Fisher, K., and Thorneley, R. N. (1990) *Klebsiella pneumoniae* nitrogenase: Mechanism of acetylene reduction and its inhibition by carbon monoxide. *Biochem. J.* **272**, 621–625
217. Lukoyanov, D., Yang, Z.-Y., Dean, D. R., Seefeldt, L. C., and Hoffman, B. M. (2010) Is Mo involved in hydride binding by the four-electron reduced (E₄) intermediate of the nitrogenase MoFe protein? *J. Am. Chem. Soc.* **132**, 2526–2527
218. Lukoyanov, D., Barney, B. M., Dean, D. R., Seefeldt, L. C., and Hoffman, B. M. (2007) Connecting nitrogenase intermediates with the kinetic scheme for N₂ reduction by a relaxation protocol and identification of the N₂ binding state. *Proc. Natl. Acad. Sci. U.S.A.* **104**, 1451–1455
219. George, S. J., Barney, B. M., Mitra, D., Igarashi, R. Y., Guo, Y., Dean, D. R., Cramer, S. P., and Seefeldt, L. C. (2012) EXAFS and NRVS reveal a conformational distortion of the FeMo-cofactor in the MoFe nitrogenase propargyl alcohol complex. *J. Inorg. Biochem.* **112**, 85–92
220. Yan, L., Dapper, C. H., George, S. J., Wang, H., Mitra, D., Dong, W., Newton, W. E., and Cramer, S. P. (2011) Photolysis of hi-CO nitrogenase – Observation of a plethora of distinct CO species using infrared spectroscopy. *Eur. J. Inorg. Chem.* **2011**, 2064–2074
221. Yang, Z.-Y., Seefeldt, L. C., Dean, D. R., Cramer, S. P., and George, S. J. (2011) Steric control of the hi-CO MoFe nitrogenase complex revealed by stopped-flow infrared spectroscopy. *Angew. Chem. Int. Ed.* **50**, 272–275

222. Tolland, J. D., and Thorneley, R. N. F. (2005) Stopped-flow fourier transform infrared spectroscopy allows continuous monitoring of azide reduction, carbon monoxide inhibition, and ATP hydrolysis by nitrogenase. *Biochemistry* **44**, 9520–9527
223. Doan, P. E., Telser, J., Barney, B. M., Igarashi, R. Y., Dean, D. R., Seefeldt, L. C., and Hoffman, B. M. (2011) ^{57}Fe ENDOR spectroscopy and “Electron Inventory” analysis of the nitrogenase E_4 intermediate suggest the metal-ion core of FeMo-cofactor cycles through only one redox couple. *J. Am. Chem. Soc.* **133**, 17329–17340
224. Macleod, K. C., and Holland, P. L. (2013) Recent developments in the homogeneous reduction of dinitrogen by molybdenum and iron. *Nat. Chem.* **5**, 559–565
225. Kästner, J., and Blöchl, P. E. (2005) Towards an understanding of the workings of nitrogenase from DFT calculations. *ChemPhysChem* **6**, 1724–1726
226. Dance, I. (2008) The chemical mechanism of nitrogenase: calculated details of the intramolecular mechanism for hydrogenation of $\eta^2\text{-N}_2$ on FeMo-co to NH_3 . *Dalton Trans.*, 5977–5991
227. Dance, I. (2008) The chemical mechanism of nitrogenase: hydrogen tunneling and further aspects of the intramolecular mechanism for hydrogenation of $\eta^2\text{-N}_2$ on FeMo-co to NH_3 . *Dalton Trans.*, 5992–5998
228. Fisher, K., Dilworth, M. J., Kim, C.-H., and Newton, W. E. (2000) *Azotobacter vinelandii* nitrogenases with substitutions in the FeMo-cofactor environment of the MoFe protein: Effects of acetylene or ethylene on interactions with H^+ , HCN, and CN^- . *Biochemistry* **39**, 10855–10865
229. Dance, I. (2011) How does vanadium nitrogenase reduce CO to hydrocarbons? *Dalton Trans.* **40**, 5516–5527

CHAPTER 2

ENDOR/HYSCORE STUDIES OF THE COMMON INTERMEDIATE TRAPPED
DURING NITROGENASE REDUCTION OF N₂H₂, CH₃N₂H, AND N₂H₄ SUPPORT
AN ALTERNATING REACTION PATHWAY FOR N₂ REDUCTION²**ABSTRACT**

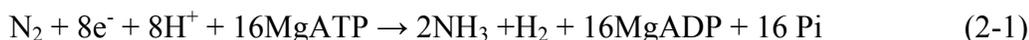
Enzymatic N₂ reduction proceeds along a reaction pathway comprised of a sequence of intermediate states generated as a dinitrogen bound to the active-site iron-molybdenum cofactor (FeMo-co) of the nitrogenase MoFe protein undergoes six steps of hydrogenation (e⁻/H⁺ delivery). There are two competing proposals for the reaction pathway, and they invoke different intermediates. In the ‘Distal’ (**D**) pathway, a single N of N₂ is hydrogenated in three steps until the first NH₃ is liberated, then the remaining nitrido-N is hydrogenated three more times to yield the second NH₃. In the ‘Alternating’ (**A**) pathway, the two N’s instead are hydrogenated alternately, with a hydrazine-bound intermediate formed after four steps of hydrogenation and the first NH₃ liberated only during the fifth step. A recent combination of X/Q-band EPR and ¹⁵N, ^{1,2}H ENDOR measurements suggested that states trapped during turnover of the α-70^{Ala}/α-195^{Gln} MoFe protein with diazene or hydrazine as substrate correspond to a common intermediate (here denoted **I**) in which FeMo-co binds a substrate-derived [N_xH_y] moiety, and measurements reported here show that turnover with methyldiazene generates the same intermediate. In the present report we describe X/Q-band EPR and ^{14/15}N, ^{1,2}H ENDOR/-

² Reproduced with permission from [Dmitriy Lukoyanov, Sergei A. Dikanov, Zhi-Yong Yang, Brett M. Barney, Rimma I. Samoilova, Kuppala V. Narasimhulu, Dennis R. Dean, Lance C. Seefeldt, and Brian M. Hoffman (2011) *Journal of The American Chemical Society* **133**(30), 11655-11664]. Copyright [2011] American Chemical Society.

HYSORE/ESEEM measurements that characterize the N-atom(s) and proton(s) associated with this moiety. The experiments establish that turnover with N_2H_2 , $\text{CH}_3\text{N}_2\text{H}$, and N_2H_4 in fact generates a common intermediate, **I**, and show that the N-N bond of substrate has been cleaved in **I**. Analysis of this finding leads us to conclude that nitrogenase reduces N_2H_2 , $\text{CH}_3\text{N}_2\text{H}$, and N_2H_4 via a common **A** reaction pathway, and that the same is true for N_2 itself, with Fe ion(s) providing the site of reaction.

INTRODUCTION

Nitrogen fixation — the reduction of N_2 to two NH_3 molecules — is essential for all life, with the lives of over one-half of today's human population depending on biologically fixed nitrogen.¹ Biological nitrogen fixation, which requires energy in the form of MgATP, is catalyzed by the enzyme nitrogenase according to the limiting stoichiometry:^{2,3}



There are three types of nitrogenases,⁴ with the best-characterized and most prevalent being the Mo-dependent enzyme studied here.^{3,5,6} It consists of two components, denoted the Fe protein and the MoFe protein. The former delivers electrons to the catalytic MoFe protein, which contains two remarkable metal clusters, the N_2 binding/reduction active site, the iron-molybdenum cofactor ([7Fe-9S-Mo-X-homocitrate]; FeMo-co, **Figure 2-1**), and the [8Fe-7S] P cluster, which is involved in electron transfer to FeMo-co.^{3,5}

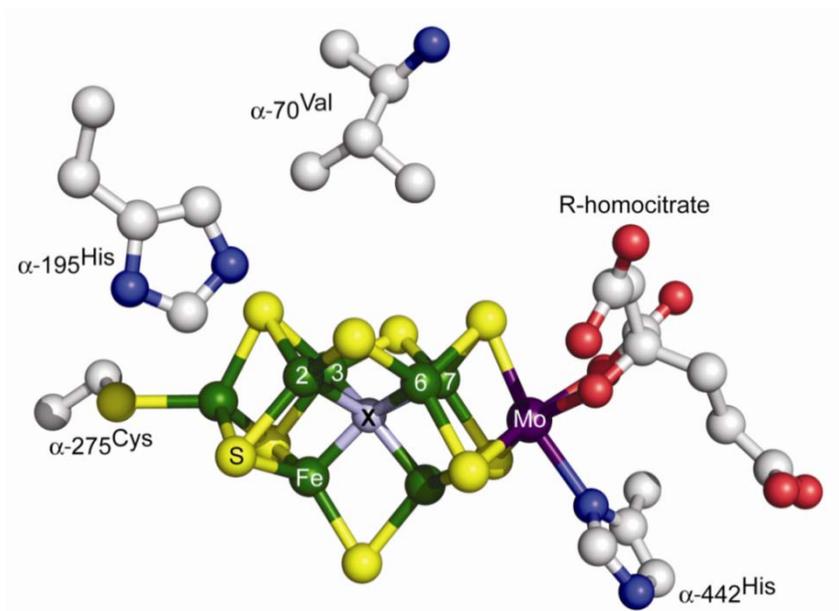
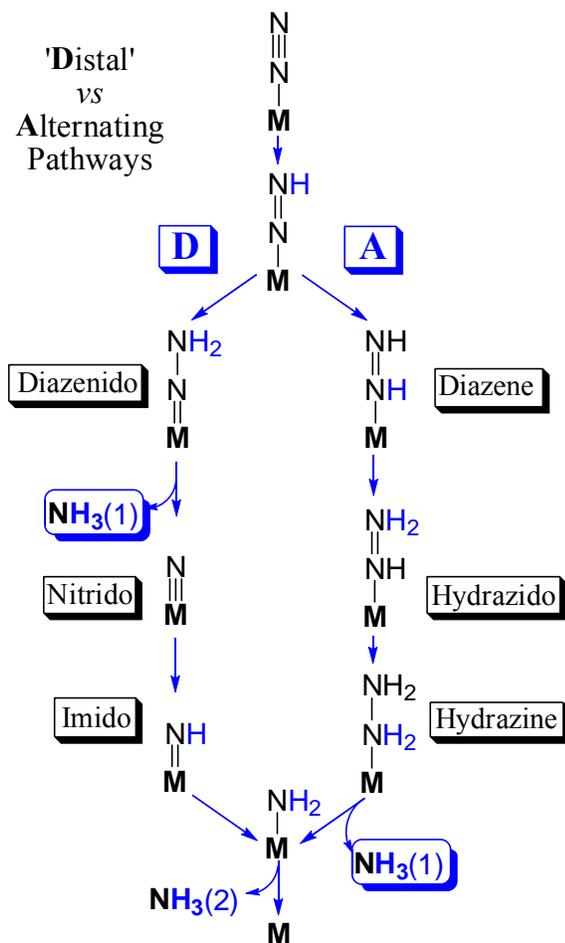


Figure 2-1. Structure of FeMo-co showing Fe green, Mo purple, S yellow, X grey.

N_2 reduction by nitrogenase proceeds along a reaction pathway comprised of the sequence of intermediate states generated as a dinitrogen bound to FeMo-co undergoes six steps of hydrogenation (e^-/H^+ delivery),^{2,3,5-8} as schematized in the Lowe-Thorneley kinetic model for nitrogenase function.^{3,9,10} We note that one can further consider whether electron/proton delivery at each stage is coupled or sequential, thereby possibly introducing additional intervening intermediates,¹¹ but such issues are beyond the scope of this report.

Two competing proposals for the reaction pathway have long been considered.^{3,6,12} They invoke distinctly different intermediates, **Scheme 2-1**, and computations suggest they likely involve different metal-ion sites on FeMo-co.¹² In the ‘Distal’ (**D**) pathway, followed by N_2 -fixing inorganic Mo complexes¹¹ and suggested to apply in reaction at Mo of FeMo-co,¹³ a single N of N_2 is hydrogenated in three steps

Scheme 2-1.



until the first NH_3 is liberated, then the remaining nitrido-N is hydrogenated three more times to yield the second NH_3 . In the ‘Alternating’ (A) pathway that has been suggested to apply to reaction at Fe of FeMo-co,¹⁴ the two N’s instead are hydrogenated alternately, with a hydrazine-bound state generated upon four steps of hydrogenation and the first NH_3 only liberated during the fifth step. Simple arguments can be made for both pathways. For example, the A route is suggested by the fact that hydrazine is both a substrate of WT nitrogenase and is released upon acid or base hydrolysis of the enzyme under turnover,^{3,8,15} and is favored in computations with reaction at Fe,^{12,14} while the D

route is suggested by the fact that the only inorganic complexes that catalytically fix N_2 employ Mo and function via the **D** route,¹¹ which is computationally favored for reaction at Mo.¹² As shown by **Scheme 2-1**, characterization of catalytic intermediates can distinguish between the two competing pathways.

Nitrogenase reduction intermediates had long eluded capture until we^{5,16,17} described the freeze-trapping and ENDOR spectroscopic studies of a number of them, each of which shows an EPR signal arising from an $S = 1/2$ state of the FeMo-co, rather than the $S = 3/2$ state of resting-state FeMo-co.⁵ These include intermediates formed during the reduction of alkyne substrates,¹⁸ the reduction of H^+ under Ar,¹⁹ and finally, four associated with N_2 fixation itself.^{17,20-24} These four include a proposed early (*e*) stage of the reduction of N_2 , $e(N_2)$, obtained from wild-type (WT) MoFe protein with N_2 as substrate,¹⁶ and three putative ‘mid-stage’ or late-stage intermediates that are the subject of this study: $m(NH=N-CH_3)$, obtained from α -195^{Gln} MoFe protein with $CH_3-N=NH$ as substrate;²³ $m(NH=NH)$, obtained from the doubly substituted, α -70^{Ala}/ α -195^{Gln} MoFe protein during turnover with *in situ*-generated $NH=NH$,¹⁷ and a ‘late’ stage, $l(N_2H_4)$, from the α -70^{Ala}/ α -195^{Gln} MoFe protein during turnover with H_2N-NH_2 ²¹ as substrate.

Both hydrazine and diazene are substrates of wild-type nitrogenase that, like N_2 , are reduced to ammonia.^{3,17,21} Substitution of the α -70^{Val} residue by α -70^{Ala} opens up the active site in the vicinity of an Fe ion at the waist of FeMo-co, Fe6, to accommodate larger substrates, increasing the rate of ammonia formation when either hydrazine or diazene is the substrate,⁵ and, implicating Fe as the site of substrate binding. Substitution of the α -195^{His} residue by α -195^{Gln}, alone or in combination with the α -70^{Ala} substitution, is thought to disrupt the delivery of protons for reduction of nitrogenous substrates,²⁵ and

facilitate the accumulation of intermediates.⁵ Recently, a combination of X/Q-band EPR and ¹⁵N, ^{1,2}H ENDOR measurements suggested that m(NH=NH) and l(N₂H₄) formed during turnover of the α-70^{Ala}/α-195^{Gln} MoFe protein with diazene or hydrazine as substrate correspond to a common intermediate (here denoted **I**) in which FeMo-co binds a substrate-derived [N_xH_y] moiety.¹⁷ However, whether or not the N-N bond in **I** had been broken ($x = 1$ or 2) was not established. The capture of a common intermediate would indicate that diazene and hydrazine both enter and ‘flow through’ the normal N₂-reduction pathway (**Scheme 2-1**), and that the diazene-derived intermediate is not ‘mid-stage’, but rather that diazene must have ‘caught up’ with the ‘later’ hydrazine reaction via additional steps of enzymatic hydrogenation.

In the present report we describe X/Q-band EPR and ^{14/15}N, ^{1,2}H ENDOR/HYSCORE/ESEEM²⁶⁻²⁸ measurements that characterize the N-atom(s) and proton(s) associated with the substrate-derived moiety of the intermediates formed during turnover with N₂H₂ and N₂H₄, and further report measurements showing that turnover with NH=N-CH₃, which can be selectively ¹⁵N labeled in either nitrogen. These measurements establish that all three substrates generate a common intermediate, **I**, in which the N-N bond of substrate has been cleaved. Consideration of this finding allows us to evaluate whether the **D** or **A** reduction pathways (**Scheme 2-1**) describes N₂ fixation by nitrogenase, and which type of metal ion, Fe or Mo, forms the reactive site.

MATERIALS AND METHODS

Samples. The preparation of the MoFe α-70^{Ala}/α-195^{Gln} protein and the freeze-trapping of intermediates for paramagnetic resonance measurements have been described.^{17,21,23}

Q-Band CW and Pulsed ENDOR Experiments. CW and pulsed 35 GHz

ENDOR spectra were recorded at 2 K as described previously.^{17,21,23} The ENDOR spectrum for a single orientation of an $I = \frac{1}{2}$ nucleus (^1H , ^{15}N) is a ν_{\pm} doublet centered at the nuclear Larmor frequency and split by the hyperfine coupling, A ; hyperfine tensors are obtained through analysis of 2D field-frequency plots comprised of spectra collected at multiple fields across the EPR envelope.^{27,29} Pulsed ENDOR spectra were detected with Mims and ReMims sequences.³⁰ Intensity of ENDOR response for Mims sequence, $[\pi/2-\tau-\pi/2-T(\text{rf})-\pi/2-\tau-\text{detect}]$, follows the relationship, $I(A) \sim 1 - \cos(2\pi A\tau)$, and as a result the signals at $A\tau = n$, $n = 0, 1, \dots$ are suppressed ('blind spots'). ReMims sequence, $[\pi/2-\tau_1-\pi/2-T(\text{rf})-\pi/2-\tau_2-\pi-(\tau_1+\tau_2)-\text{detect}]$, allows using short preparation interval τ_1 and study of wider range of hyperfine values without 'blind spots' distortions.

X-Band Pulsed EPR and ESEEM Experiments. CW EPR measurements were

performed on an ESP 300 Bruker spectrometer equipped with Oxford CF 935 cryostat. Pulsed X-band EPR measurements were carried out using a Bruker ELEXSYS E580 spectrometer with an Oxford CF 935 cryostat at 8 K. Several types of ESEEM experiments with different pulse sequences were employed, with appropriate phase-cycling schemes to eliminate unwanted features from experimental echo envelopes. Among them are two-pulse, and one-(1D) and two-dimensional (2D) four-pulse sequences. In the two-pulse experiment ($\pi/2-\tau-\pi-\tau-\text{echo}$), the intensity of the echo signal is measured as a function of the time interval τ between two microwave pulses with turning angles $\pi/2$ and π to generate an echo envelope that maps the time course of relaxation of the spin system (in ESEEM) or as a function of magnetic field at fixed τ (in field-sweep ESE). In the 2D four-pulse HYSORE experiment ($\pi/2-\tau-\pi/2-t_1-\pi-t_2-\pi/2-\tau-$

echo),³¹ the intensity of the echo after the fourth pulse was measured with t_2 and t_1 varied and τ constant. The length of a $\pi/2$ pulse was nominally 16 ns and a π pulse 32 ns. The repetition rate of pulse sequences was 1000 Hz. HYSCORE data were collected in the form of 2D time-domain patterns containing 256×256 points with steps of 20 or 32 ns. Spectral processing of ESEEM patterns, including subtraction of the relaxation decay (fitting by polynomials of 3-6 degree), apodization (Hamming window), zero filling, and fast Fourier transformation (FT), was performed using Bruker WIN-EPR software.

RESULTS

In describing results we will employ the original notation, m(NH=NH), m(NH=N-CH₃), and l(N₂H₄), when it is helpful in specifying the origin of a sample and/or its isotopic composition for ENDOR/HYSCORE measurements. As these in fact represent a common intermediate, when discussing properties we will commonly refer to it as **I**.

X- and Q-Band EPR. EPR spectra of α -70^{Ala}/ α -195^{Gln} trapped during turnover in the presence of N₂H₄ and N₂H₂ reveal a complete disappearance of the resting state spectrum and the presence of the low spin signal with almost axial **g**-tensor characteristic of the **I** intermediate. For completeness, we note that the high field part of the **I** spectrum is overlapped with the rhombic signal of the reduced 4Fe4S cluster of the Fe protein, **g** = [2.05, 1.94, 1.86]. As shown earlier, the spectrum of **I** is the sum of contributions from two conformers.¹⁷ X-band and Q-band spectra of the m(NH=N-CH₃) intermediate formed by turnover of CH₃N₂H with α -70^{Ala}/ α -195^{Gln} MoFe protein likewise show the presence of two major conformers and their **g**-values are indistinguishable from those of the

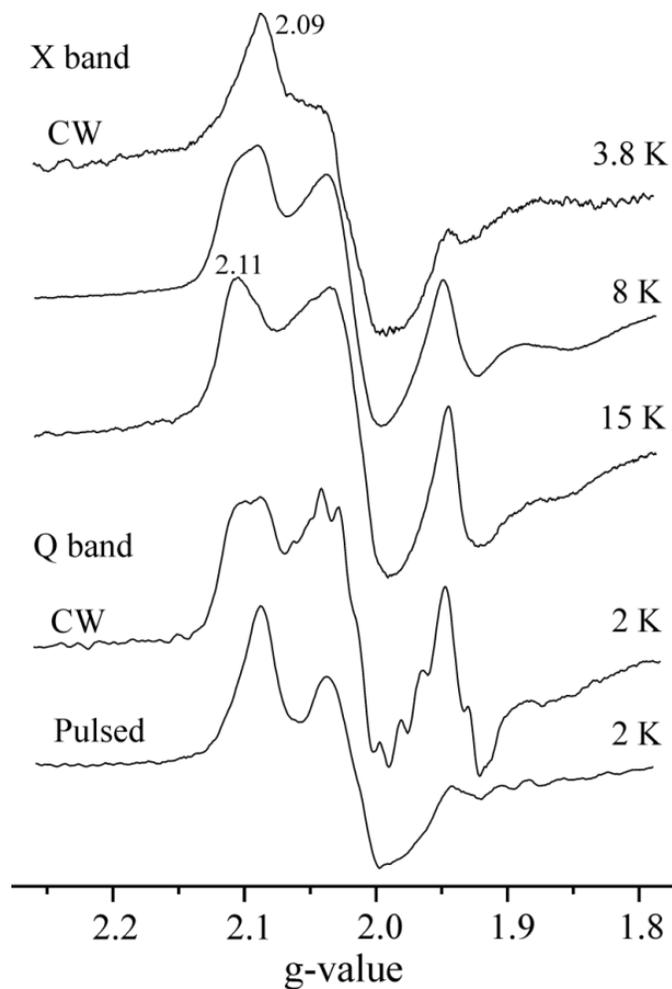


Figure 2-2. EPR spectra of intermediate **I** ($l(N_2H_4)$) detected by various techniques.

Conditions for CW X-band: microwave frequency, 9.38 GHz; microwave power, 10 mW; modulation amplitude, 7 G; time constant, 160 ms; field sweep speed, 20 G/s. Conditions for CW Q-band: microwave frequency, 35.08 GHz; microwave power, 32 μ W; modulation amplitude 4 G; time constant, 128 ms; field sweep speed, 17 G/s. Conditions for pulsed Q-band: microwave frequency, 34.79 GHz; Mims sequence, $\pi/2 = 50$ ns, $\tau = 600$ ns; repetition time 10 ms, 50 shots/point; field sweep speed, 8 G/s.

$l(\text{N}_2\text{H}_4)$, suggesting that enzymatic turnover with methyldiazene likewise generates intermediate **I**.

We have also extended the characterization of the spin properties of **I**. The temperature and microwave power dependences of the $l(\text{N}_2\text{H}_4)$ signal show that the two major conformers of the EPR-active FeMo-co in **I** have significantly different relaxation properties, **Figure 2-2**. At temperatures below 8 K the X-band signal is dominated by a conformer with $\mathbf{g} = [2.09, 2.01, 1.98]$ ($g_1 = 2.09$ signal), **Figure 2-2**. As the temperature is increased to $T \sim 15$ K, the EPR signal from a second conformer with $g_1 = 2.11$ becomes dominant. The signal intensity decreases at still higher temperatures, disappearing above $T \sim 30$ K.

Q-band CW spectra collected at $T = 2$ K show signals from both major conformers at high microwave power. As the power is lowered, the $g_1 = 2.11$ signal progressively becomes more prominent. At the microwave power settings used for 2 K Q-band CW ^1H ENDOR measurements, the conformers contribute roughly equally to the EPR spectrum, **Figure 2-2**. In contrast, the 2 K Q-band echo-detected EPR spectrum collected with the short repetition times (~ 10 ms) used for ^{15}N Mims pulsed ENDOR experiments is dominated by the $g_1 = 2.09$ conformer, which thus governs these ENDOR measurements. The contribution of the $g_1 = 2.11$ conformer becomes more noticeable with longer repetition times (~ 50 ms) but remains substantially lower in intensity.

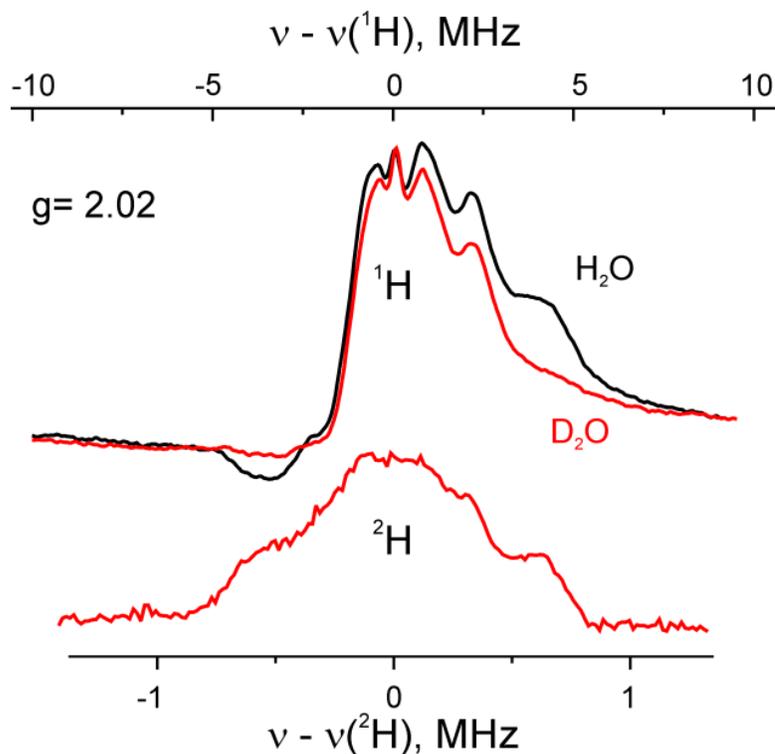


Figure 2-3: 35 GHz CW ^1H ENDOR spectra of **I** ($l(\text{N}_2\text{H}_4)$) obtained at $g = 2.02$ for samples prepared in H_2O (black) and D_2O (red) buffers. The lower spectrum shows pulsed ^2H ENDOR detected for D_2O sample. Conditions for CW ENDOR: microwave frequency, 35.002 GHz (H_2O), 35.096 GHz (D_2O); modulation amplitude, 2.5 G; time constant, 64 ms; bandwidth of RF broadened to 100 kHz; RF sweep speed, 1 MHz/s, 80 scans; temperature, 2 K. Conditions for pulsed ENDOR: microwave frequency, 34.886 GHz; Mims sequence, $\pi/2 = 52$ ns, $\tau = 452$ ns; RF 73 μs ; repetition time 12 ms, 16 shots/point, 32 scans; temperature, 2 K.

Based on the temperature dependence of the CW X-band EPR spectra, **Figure 2-2**, it is likely that the two conformers contribute roughly equally at the temperatures used to collect X-band HYSORE spectra, $T \approx 8$ K. For completeness, **Figure B-S1**

(APPENDIX B) shows the X-band field-sweep two-pulse ESE spectrum. It is a broad line between 322.0 mT and 382.0 mT with two maxima around 345.0 mT and 360.0 mT corresponding to $g = 2.01$ and 1.926 , respectively. The relative intensities of two maxima varied slightly in different samples used in this work, presumably because of slight variations in the ratio of Fe to MoFe proteins.

35 GHz ^1H CW and ^2H Pulsed ENDOR. The 35 GHz CW ^1H ENDOR spectra at $g = 2.02$ for $\text{l}(\text{N}_2\text{H}_4)$ in H_2O buffer show a peak corresponding to the higher-frequency, ν_+ , branch of the doublet for a proton(s) with $A(1) \sim 8$ MHz, a shoulder from a proton(s) with $A(2) \sim 6$ MHz, and a central, poorly resolved signal with breadth of ~ 4 MHz. The ν_- branch of the H1 and H(2) spectra are respectively distorted and absent, common observations in such low-temperature spectra. When $\text{l}(\text{N}_2\text{H}_4)$ is prepared in D_2O buffer, the H1 signal is lost, and instead is visible in the ^2H Mims pulsed ENDOR spectrum, **Figure 2-3**. Although the ^2H spectrum has a hint of a $\nu_-(2)$ feature, suggesting H(2) likewise is exchangeable, the H(2) shoulder is not lost from the sample prepared in D_2O buffer, so we conclude that H(2) is not exchangeable. In addition, although the majority of the central peak is not lost with D_2O buffer, and hence not exchangeable, the ^2H spectrum shows that a fraction of it does exchange. The coupling, $A(1)$ decreases as the field is increased/decreased towards g_3/g_1 . At these single-crystal orientations the signals are strongly overlapped with broad peak of weakly coupled protons, and minimum hyperfine coupling can only be roughly estimated as $A(1)_{\text{min}} \leq 6$ MHz. The poor resolution of the H1 ENDOR signals likely arises from the presence of multiple slightly inequivalent H1 protons plus the presence of two distinct conformers. The maximum component of the hyperfine tensor, $A(1)_{\text{max}} \sim 9$ MHz, occurs at $g \sim 2.05$ (**Figure B-S2**,

APPENDIX B). If the field dependence of the poorly resolved H1 ENDOR pattern is considered to be associated with an anisotropic interaction of the dipolar form the polar angle between dipolar direction and g_1 is estimated to be $\theta \sim 45^\circ$.

9 GHz ^1H ESEEM/HYSCORE. Weak hyperfine couplings of the protons around FeMo-co and 4Fe4S centers were studied using orientation-selective two-dimensional ESEEM, called HYSCORE. The HYSCORE experiment creates off-diagonal cross-peaks (ν_α, ν_β) and (ν_β, ν_α) from each $I = 1/2$ nucleus in 2D spectrum. Powder and orientation-selected HYSCORE spectra of $I = 1/2$ nuclei reveal, in the form of cross-ridges, the interdependence between ν_α and ν_β , in the same orientations. Analysis of the ridges in $(\nu_\alpha)^2$ vs. $(\nu_\beta)^2$ coordinates allows separate estimate of the isotropic (a) and anisotropic (T) components of the hyperfine tensors.³²

Figure 2-4 shows ^1H HYSCORE spectra of the $l(\text{N}_2\text{H}_4)$ intermediate obtained at the magnetic field 332.0 mT ($g = 2.087$) (**Figure 2-4A**) and 334.5 mT ($g = 2.008$) (**Figure 2-4B**). Spectra resolve two pairs of cross-peaks **1** and **2**. Cross-peaks **2** possess larger splitting $\sim 6\text{-}8$ MHz and visible deviation from antidiagonal indicating a significant anisotropic hyperfine component. The intensities of the cross-peaks **2** decrease relative to those of **1** as the magnetic field is increased and cross-peaks **2** are not observed above ~ 349.0 mT ($g = 1.985$). Cross-peaks **2** were also not observed in the spectra of the sample prepared in D_2O showing that they are produced by exchangeable proton(s). As discussed in detail in APPENDIX B, quantitative analysis of the cross-ridges **2** contours from the spectra recorded at different field in the coordinates $(\nu_1)^2$ vs. $(\nu_2)^2$ using methodology previously described³³ and assuming an axial anisotropic component gives two possible solutions: $T = 4.6$ MHz, $a = -0.2$ MHz and $T = 4.6$ MHz, $a = -4.3$ MHz

(signs are relative). These values for a and T correspond to $A_{\perp} = |a - T| \sim 4.8$ MHz and $A_{\parallel} = |a + 2T| \sim 9$ MHz for the first solution, and $A_{\perp} \sim 9$ MHz and $A_{\parallel} \sim 4.8$ MHz for the second. The second solution is consistent with the observation in Q-band ENDOR of an exchangeable proton(s) with maximum coupling, $A(1)_{\max} \sim 9$ MHz and minimum coupling, $A(1)_{\min} \leq 6$ MHz. Cross-peaks **1** correspond to the non-exchangeable proton shoulder seen in Q-band ENDOR and associated with the protein.

Additional information about the exchangeable proton(s) was sought from 1D four-pulse ^1H ESEEM spectra. Such spectra contain lines in the region of the double proton Larmor frequency ($2\nu_{\text{H}} \sim 28\text{-}29$ MHz) that are sum-combination harmonics ($\nu_{\alpha} + \nu_{\beta}$) of two basic frequencies ν_{α} and ν_{β} . As presented in APPENDIX B, analysis of these harmonics shows the existence of protons with the same anisotropic coupling as found for the exchangeable protons by HYSORE.

35 GHz ^{15}N ReMims ENDOR. **Figure 2-5A** presents pulsed ^{15}N ENDOR spectra collected at the three canonical g -values for the intermediates trapped during turnover with the three isotopically labeled substrates, N_2H_2 , $\text{CH}_3\text{N}_2\text{H}$, and N_2H_4 , and **Figure 2-5B** presents a 2D field-frequency plot of pulsed ^{15}N ENDOR spectra collected across the EPR envelope of $l(^{15}\text{N}_2\text{H}_4)$ prepared from the $\alpha\text{-}70^{\text{Ala}}/\alpha\text{-}195^{\text{Gln}}$ MoFe protein by freeze-quench during turnover in the presence of $^{15}\text{N}_2\text{H}_4$. Spectra were collected with the ReMims³⁰ pulse sequence. This permitted measurements with $\tau_1 = 200$ ns, which eliminates Mims ENDOR ‘blind spots’ from the frequency range of the scan. Wider ENDOR scans collected for $l(^{15}\text{N}_2\text{H}_4)$ showed no ^{15}N signal with a hyperfine coupling greater than the maximum for N1, $A_3 = 2.7$ MHz.

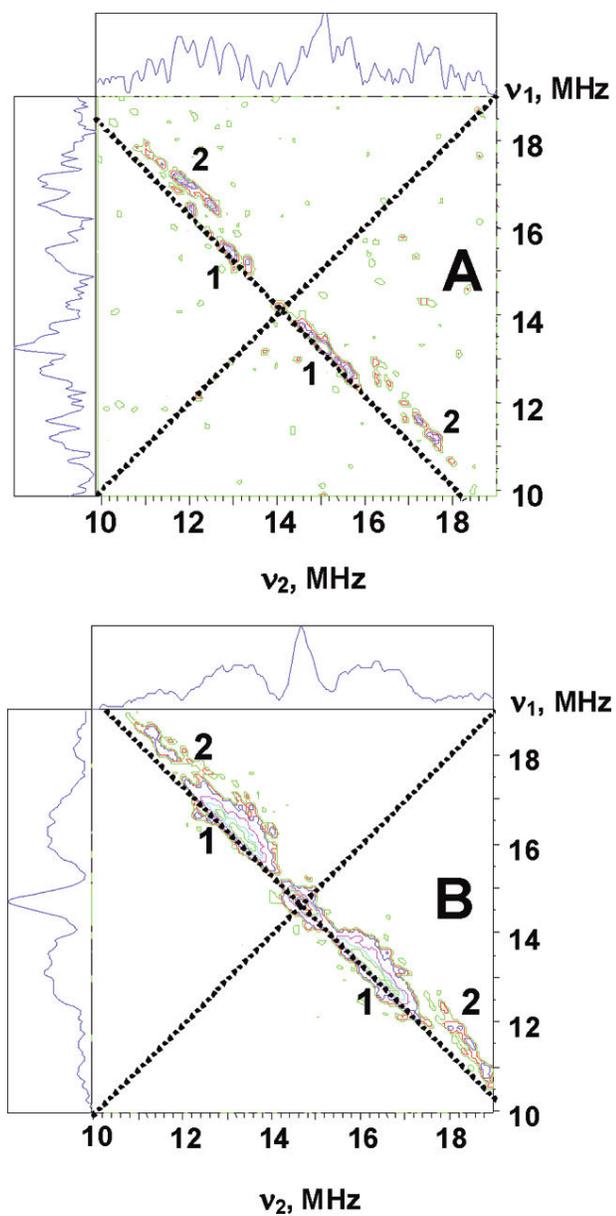


Figure 2-4. Contour presentations of the ^1H HYSORE spectra of the $l(\text{N}_2\text{H}_4)$ intermediate (magnetic field 332.0 mT (A) and 345.0 mT (B), time between first and second pulses $\tau = 136$ ns, microwave frequency 9.6982 GHz).

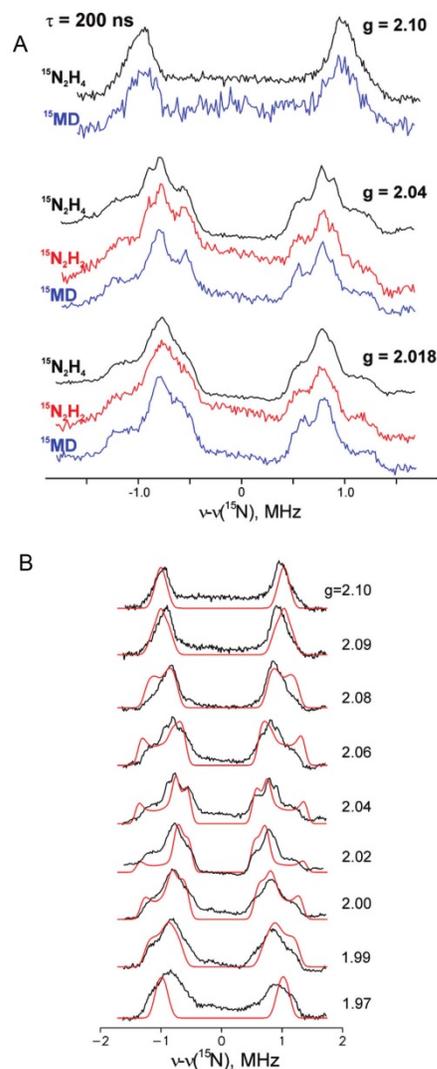


Figure 2-5. (A) Comparison of 35 GHz ReMims pulsed ^{15}N ENDOR spectra of intermediates trapped during turnover of the $\alpha\text{-}70^{\text{Ala}}/\alpha\text{-}195^{\text{Gln}}$ MoFe protein with $^{15}\text{N}_2\text{H}_4$, $^{15}\text{N}_2\text{H}_4$, and $^{15}\text{NH}=\text{N}-\text{CH}_3$ (denoted ^{15}MD). (B) 2D Field-Frequency plot of 35 GHz pulsed ^{15}N ENDOR spectra of $l(^{15}\text{N}_2\text{H}_4)$ intermediate. Conditions: microwave frequency, 34.82 GHz; ReMims sequence, $\pi/2 = 30$ ns, $\tau_1 = 200$ ns; RF 40 μs ; repetition time, 10 ms; 500-950 scans; temperature, 2 K. Spectral baselines were corrected by simple subtraction if needed. Simulation (red) parameters: $g = [2.09, 2.015, 1.98]$, hyperfine tensor $A = [1.0, 2.8, 1.5]$ MHz, Euler angles $\phi = 50^\circ$, $\theta = 60^\circ$, $\psi = 55^\circ$ with respect to g -frame.

The spectra for the three intermediates are essentially identical, **Figure 2-5A**. The observed 2D ^{15}N ENDOR patterns, as shown for $l(^{15}\text{N}_2\text{H}_4)$, **Figure 2-5B**, is consistent with the presence of a single type of ^{15}N . As shown in the figure, the 2D pattern can be described moderately well by simulations that assume a single ^{15}N with hyperfine tensor, $\mathbf{A}(^{15}\text{N1}) = \pm[1, 1.5, 2.8]$ MHz, $|a_{\text{iso}}(^{15}\text{N1})| = 1.8$ MHz, corresponding to $\mathbf{A}(^{14}\text{N1}) = \pm[0.7, 1.1, 2]$ MHz, $|a_{\text{iso}}(^{14}\text{N1})| = 1.3$ MHz. The observation of an isotropically coupled, substrate-derived ^{15}N signal, in conjunction with the observation of the exchangeable H1 ENDOR signal, establishes the presence of a substrate-derived $[\text{N}_x\text{H}_y]$ moiety bound to metal ion(s) of the cofactor of **I**. These pulsed-ENDOR measurements were performed at $T = 2$ K with a 10 ms repetition time. As shown in **Figure 2-2**, the EPR spectrum collected under these conditions is dominated by the $g_1 = 2.09$ conformer. Thus, the $^{15}\text{N1}$ hyperfine tensor derived from the ReMims pulsed ENDOR measurements are assigned to this conformer, whose **g** tensor was used in the simulation.

The imperfections to the simulations in **Figure 2-5B** in terms of a single $^{15}\text{N1}$ associated with each FeMo-co can be attributed to a combination of two factors: a distribution in the N1 tensor values for the $g_1 = 2.09$ dominant conformer; a contribution from the $^{15}\text{N1}$ associated with the $g_1 = 2.11$ conformer, whose contribution to the EPR spectrum can be discerned in **Figure 2-2**. The ^{15}N ENDOR spectra of $m(^{15}\text{NH}=\text{N}-\text{CH}_3)$, **Figure 2-5A**, confirm that the spectra do *not* instead arise from an overlap of signals from two nearly equivalent ^{15}N associated with each FeMo-co. The original study of this intermediate,²³ which employed the α - ^{195}Gln -substituted MoFe protein not the double mutant employed in this study, showed that when $m(^{15}\text{NH}=\text{N}-\text{CH}_3)$ is formed from $^{15}\text{NH}=\text{N}-\text{CH}_3$ it exhibits a ^{15}N signal comparable to those of N_2H_4 and N_2H_2 , but with a

slightly smaller coupling, $|a_{\text{iso}}(^{15}\text{N1})| \approx 1.5$ MHz. To assure proper comparisons, we here examine $m(^{15}\text{NH}=\text{N}-\text{CH}_3)$ generated with the α -70^{Ala}/ α -195^{Gln} MoFe protein, as with the other two substrates.

The EPR signal of $m(^{15}\text{NH}=\text{N}-\text{CH}_3)$ prepared with the α -70^{Ala}/ α -195^{Gln} MoFe protein is reported above to be the same as that of **I**, and **Figure 2-5A** likewise demonstrates that the ReMims ENDOR spectra of $m(^{15}\text{NH}=\text{N}-\text{CH}_3)$ are the same as those of **I** formed with $^{15}\text{N}_2\text{H}_4$ and $^{15}\text{N}_2\text{H}_2$. The EPR and ENDOR results together therefore establish that turnover with methyldiazene also generates the common intermediate, **I**. As there is only one ^{15}N in this substrate, the ^{15}N signal for **I** cannot come from two nearly equivalent ^{15}N associated with each FeMo-co, and must come from contributions from two conformers, each with a single ^{15}N bound to FeMo-co.

We may further conclude that the slight differences in hyperfine parameters for $m(^{15}\text{NH}=\text{N}-\text{CH}_3)$ prepared with the α -195^{Gln} and the α -70^{Ala}/ α -195^{Gln} MoFe proteins result from secondary influences, that turnover of $\text{NH}=\text{N}-\text{CH}_3$ indeed forms the common intermediate, **I**. With this identification, the previous study of **I** then further confirms that the signals of **Figure 2-5A** arise from a single ^{15}N bound to FeMo-co in each of two conformers: when **I** is formed from $\text{NH}=\text{N}-^{15}\text{N}-\text{CH}_3$ there is no such ^{15}N signal. The use of $\text{NH}=\text{N}-\text{CH}_3$ isotopomers thus proves that either the N-N bond has been cleaved in **I**, or an N_2H_x moiety from substrate binds end-on.

^{15}N Mims ENDOR. To test for end-on binding of N_2H_x , we examined the intermediates $l(^{15}\text{N}_2\text{H}_4)$ and $m(^{15}\text{N}_2\text{H}_2)$ for the presence of a second ^{15}N derived from substrate, but with a smaller coupling than for N1, by collecting Mims ENDOR scans with a large pulse interval, τ . Although the signal from the latter sample is weaker, it is

indistinguishable from that of the former, in keeping with the assignment of both to **I**. The intensity of the Mims ENDOR response for a signal with hyperfine coupling, A (MHz), depends on τ (μ s) through the function, $I(\tau) \sim 1 - \cos(2\pi A\tau)$. When $A\tau = n$, the intensity is null and 'blind spots' appear in the ENDOR spectrum, as seen in the Mims spectrum taken for $^{15}\text{N1}$ with $\tau = 700$ ns, **Figure 2-6**. However, in parallel, $I(\tau)$ shows sensitivity maxima at $A\tau = n + 1/2$ and overall gives the best sensitivity at $A\tau \approx 1/2$. Thus, as τ is progressively increased, the measurements become progressively more sensitive to smaller values of A . As this is a relative sensitivity, measurements were performed at the maximum of EPR signal intensity (g_2).

Setting $\tau = 700$ ns in the Mims sequence, **Figure 2-6**, not only introduces the holes in the $^{15}\text{N1}$ spectra of $l(^{15}\text{N}_2\text{H}_4)$ and $m(^{15}\text{N}_2\text{H}_2)$, but also causes what *appears* to be a ^{15}N doublet from a second, weakly-coupled ^{15}N from substrate, centered at ν_{N} , with $A(^{15}\text{N2}) \sim 0.1$ MHz. *However*, this signal remains unchanged when a corresponding spectrum is collected for $l(^{14}\text{N}_2\text{H}_4)$ (and $m(^{15}\text{N}_2\text{H}_2)$, not shown) prepared from $^{14}\text{N}_2\text{H}_4$ substrate. Thus, this ENDOR response is *not* associated with a second, weakly coupled $^{15}\text{N2}$ of substrate, and instead can be assigned as a double-quantum transition from ^{14}N associated with the MoFe protein. The narrow $\tau = 700$ ns scan, collected with extremely high signal/noise, shows *no* trace of any ^{15}N ENDOR response from a weakly coupled ^{15}N . Considering the example of nitrile hydratase (NHY)³⁴ where a weakly coupled ^{15}N ($A < 0.05$ MHz) is reliably detectable, one can conclude that hyperfine couplings ratio for metal-bound $^{15}\text{N1}$ and a possible second $^{15}\text{N2}$ of substrate must be $A(\text{N1})/A(\text{N2}) > 40$. As with the direct inferences drawn from the different isotopologs of methyldiazene, the absence of any trace of a weakly coupled $^{15}\text{N2}$ indicates that the N-N bond of substrate

N_2H_4 has been cleaved, and the $^{15}\text{N}1$ and $^1\text{H}1$ ENDOR signals are associated with an $[\text{N}_1\text{H}_y]$ species.

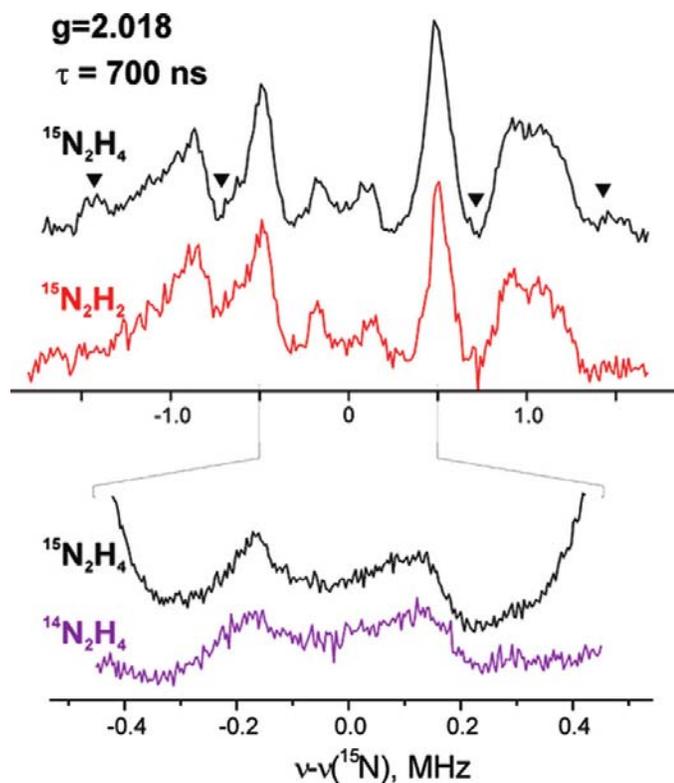


Figure 2-6. 35 GHz Mims ^{15}N ENDOR spectra detected at the maximum of EPR signal intensity ($g_2 = 2.018$) for $l(^{15}\text{N}_2\text{H}_4)$ (black) and $m(^{15}\text{N}_2\text{H}_2)$ (red) intermediates. Expanded spectra, below, compare region around ^{15}N Larmor frequency for $l(^{15}\text{N}_2\text{H}_4)$ (black) and $l(^{14}\text{N}_2\text{H}_4)$ (purple). Spectra are shown after simple baseline correction; triangles represent distortions induced by ‘blind spots’ of Mims ENDOR. Conditions: microwave frequency, ~ 34.82 GHz; Mims sequence, $\pi/2 = 50$ ns, $\tau = 700$ ns; RF 40 μs ; repetition time, 10 ms; 800-3800 scans; temperature, 2 K.

^{14,15}N HYSORE. HYSORE experiments were performed with two samples of intermediate prepared from the α -70^{Ala}/ α -195^{Gln} substituted MoFe protein by use of ¹⁴N₂H₄ or ¹⁵N₂H₄ as substrate. **Figure 2-7** shows representative HYSORE spectra of two samples in the low frequency part appropriate for the weakly coupled nitrogens. These spectra are recorded at the magnetic field corresponding to the low-field maximum $g = 2.01$ in the EPR spectrum (**Figure B-S1**, APPENDIX B). Spectrum of the sample with ¹⁴N₂H₄ (**Figure 2-7A**) shows two pairs of cross-features symmetrical relative to the diagonal. Those are extended cross-features **2** of complex shape with several maxima and cross-peaks **1** possessing symmetrical line shape with elliptic contour.

The spectrum of ¹⁵N₂H₄ (**Figure 2-7B**) shows that ¹⁵N labeling does not influence the cross-peaks **1** indicating that they are produced by protein ¹⁴N nitrogen. The labeling also leaves a pair of cross-peaks **2''** located in the area where extended cross-features **2** were observed in the spectrum of the sample with ¹⁴N₂H₄. This indicates that the cross-features **2** in **Figure 2-7A** result from the contribution of two different types of nitrogens. One contribution, denoted **2'**, is lost in the ¹⁵N sample and is from ¹⁴N of ¹⁴N₂H₄; the second (**2''**) is from ¹⁴N associated with the MoFe protein. In keeping with this assignment, ¹⁵N nitrogens of ¹⁵N₂H₄ produce new cross-peaks **3** in **Figure 2-7A**, located symmetrically around the diagonal point with ¹⁵N Larmor frequency (¹⁵ ν_N , ¹⁵ ν_N), that correspond to the lost signal **2'**.

The most important aspect of the HYSORE spectrum **Figure 2-7B** is that there is *no* signal around the diagonal point from a very weakly coupled ¹⁵N, and the same is true for spectra recorded at other fields. The limit of detectability for a small coupling in HYSORE is at least as low as that for Mims ENDOR. The absence of *any* trace of a

weakly-coupled $^{15}\text{N}_2$ in *either* experiments indicate that the N-N bond of substrate N_2H_4 has been cleaved, and the $^{15}\text{N}_1$ and $^1\text{H}_1$ ENDOR signals are associated with an $[\text{N}_1\text{H}_y]$ species. As discussed below, this conclusion is supported by earlier studies of **I** formed with isotopically labeled $\text{NH}=\text{N}-\text{CH}_3$.²³

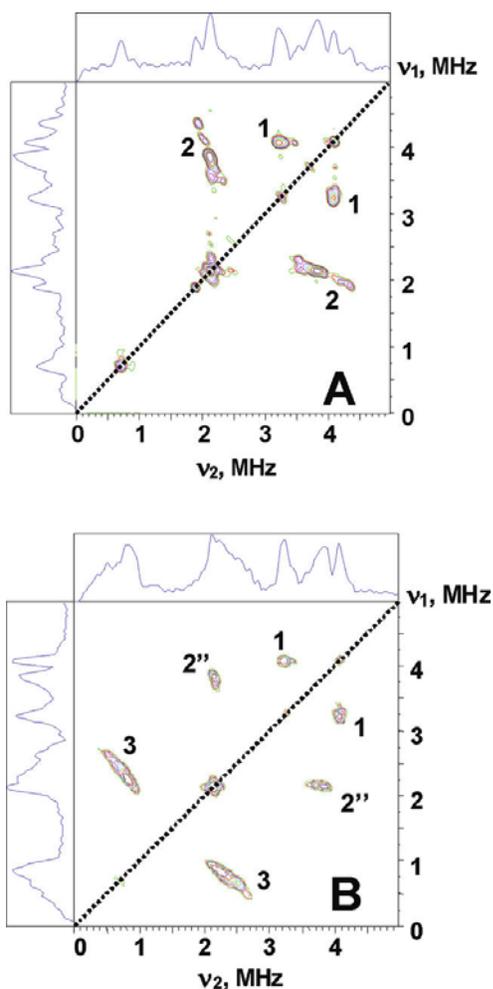


Figure 2-7. Contour presentations of the $^{14,15}\text{N}$ HYSCORE spectra of the **I**(N_2H_4) intermediate with $^{14}\text{N}_2\text{H}_4$ (**A**) and $^{15}\text{N}_2\text{H}_4$ (**B**) (magnetic field 345.9 mT ($^{14}\text{N}_2\text{H}_4$) and 346.0 mT ($^{15}\text{N}_2\text{H}_4$), time between first and second pulses $\tau = 136$ ns, microwave frequency 9.702 GHz ($^{14}\text{N}_2\text{H}_4$) and 9.707 GHz ($^{15}\text{N}_2\text{H}_4$)).

HYSCORE spectra measured for $I(^{15}\text{N}_2\text{H}_4)$ at different magnetic fields show that the cross-peaks **1** are present in spectra measured in the field interval from 332.0 mT ($g = 2.087$) up to 364.0 mT ($g = 1.90$), but decay quickly at magnetic fields below $g = 2.01$. This suggestion that the cross-peaks **1** come from nitrogen(s) associated with the 4Fe4S center of the Fe protein was confirmed by HYSCORE examination of the isolated Fe protein. In contrast, the cross-peaks **2''** are observed from the low-field edge of the EPR spectrum ($g = g_1$) up to 352.0 mT ($g = 1.97$) and the cross-peaks **3** from ^{15}N likewise are seen in this field interval, which indicates that the **2''** and **3** (and **2'**) cross-peaks are from nitrogen(s) interacting with FeMo-co of the MoFe intermediate. The width and intensity of these cross-peaks **1** and **2''** are consistent with the cross-correlation of ^{14}N double-quantum transitions from $m_S = \pm 1/2$ manifolds.

Analysis of ^{14}N HYSCORE peaks (1, and 2''). The frequency of double-quantum transition in powder spectra is well described by the following equation:³⁵

$$\nu_{dq\pm} = 2[\nu_{\text{eff}}^2 + \kappa]^2 \quad (2-2)$$

where $\kappa = K^2(3 + \eta^2)$, $\nu_{\text{eff}} = |\nu_N \pm A/2|$. We suggest that $\nu_{dq\pm}$ taken from the spectra obtained in the region of the intermediate g_2 -values, where a broad set of orientations contribute to the spectra, would allow accurate estimate of hyperfine coupling and quadrupole coupling constant $K = e^2Qq/4h$ for nitrogens producing cross-peaks **1** and **2''**. The corresponding frequencies are of (4.0, 3.1) MHz for cross-peaks **1** and (3.81, 2.14) MHz for cross-peaks **2''**. Rearrangement of eq 2-2 yields the formula:

$$A = ((\nu_{dq+})^2 - (\nu_{dq-})^2)/8 \nu_N \quad (2-3)$$

This equation, together with the corresponding ^{14}N Zeeman frequency, gives couplings $A(^{14}\text{N}) = 0.7$ MHz (**1**) and $A(^{14}\text{N}) = 1.15$ MHz (**2''**). Using the derived values of the

hyperfine coupling one can calculate the quadrupole parameter from eq 2-2: $\kappa = K^2(3+\eta^2)$ = 1.84 MHz² (**1**) and 0.9 MHz² (**2''**). Those correspond to quadrupole coupling constant (qcc) $K = 0.73 \pm 0.05$ MHz (**1**) and $K = 0.5 \pm 0.04$ MHz (**2''**), but do not permit assignment of the asymmetry parameter, $0 \leq \eta \leq 1$. The qcc (**1**) is consistent with peptide nitrogens H-bonded to the 4Fe4S cluster, which exhibit quadrupole coupling constants, $K \sim 0.7$ - 0.8 MHz.³⁶ On the other hand, the lower value of the qcc (**2''**) suggests that FeMo-co centre forms a hydrogen bond with another type of nitrogen.

The cross-features **2'** and **2''** significantly overlap in forming feature **2** of the HYSCORE spectra of the I(¹⁴N₂H₄) intermediate, but comparison of **Figure 2-7A** and **2-7B** shows that cross-features **2'** possess more a complex extended shape. However, the overlap of the **2'** and **2''** cross-peaks suggests that the values of hyperfine and quadrupole couplings for these two nitrogens are essentially the same, thereby giving for **2'**, $A(^{14}\text{N}) \approx 1.15$ MHz, $K \approx 0.5 \pm 0.04$ MHz for the cofactor-bound -NH_y fragment. This hyperfine coupling corresponds to $A(^{15}\text{N}) \approx 1.6$ MHz, in agreement with $|a_{\text{iso}}(^{15}\text{N1})| = 1.8$ MHz derived above from 35 GHz ENDOR spectra. The extended shape of the **2'** cross-peaks correlates with the features in the EPR and ¹⁵N ENDOR and ¹⁵N HYSCORE (see below) spectra that suggest the presence of several similar conformations of the paramagnetic center.

The estimate of K with an accuracy of ~15% allows its assignment to the particular type of nitrogens of the protein environment. Nevertheless, for a complete description of the nuclear-quadrupole interaction tensor, and its unambiguous assignment, direct determination of both quadrupole parameters, K and η , would be desirable. These values could be determined directly from ESEEM experiments satisfying the cancellation

condition $\nu_{ef} \sim 0$ at one of the manifolds. For hyperfine coupling $A \sim 0.67$ - 1.0 MHz, the cancellation condition is reached at ^{14}N Zeeman frequency $\nu_1 \sim 0.35$ - 0.5 MHz, that corresponds to the S-band experiment with microwave frequency ~ 3 - 4 GHz.

^{15}N HYSCORE. X-band HYSCORE spectra measured at different magnetic fields across the EPR spectrum of $\text{I}(^{15}\text{N}_2\text{H}_4)$ all show ^{15}N cross-features (**3**) centered symmetrically around the diagonal point with the ^{15}N Zeeman frequency. Their location corresponds to the ^{15}N hyperfine coupling ~ 1.5 - 2.0 MHz (**Figure 2-8**), in agreement with the ^{14}N HYSCORE (**2'**) and ^{15}N ENDOR results for the substrate-derived $[-\text{NH}_y]$. The shape of the cross-peaks for **3** significantly varies with magnetic field. For instance, the cross-peak **3** in the “single-crystal-like” spectrum recorded near g_1 is a peak with a single maximum and resolved additional shoulders (**Figure 2-8A** and **2-8B**). In contrast, two closely located but resolved ridges are seen in the spectra recorded at the fields between g_1 (low field) and g_2 , (maximum intensity) (**Figure 2-8C** and **2-8D**). The complicated shape of these ^{15}N HYSCORE ridges, **3**, corresponds to the extended shape of the ^{14}N features **2'**.

The regression lines of such ridges when plotted as $(\nu_\alpha)^2$ vs. $(\nu_\beta)^2$ must form a triangle with the apexes on the $|\nu_\alpha + \nu_\beta| = 2\nu_{\text{N}}$ curve for signals from a single ^{15}N . However, the analysis presented in detail in APPENDIX B shows that regression lines for the ridges from **Figure 2-8C** and **2-8D** (and others) do not form such a shape, indicating that the ^{15}N spectra are not consistent with a single nucleus. This is expected, as the ENDOR measurements described above show that metal ion(s) of FeMo-co in the intermediate bind a single nitrogen from substrate, but the intermediate exists in two conformations. The $(\nu_\alpha)^2$ vs. $(\nu_\beta)^2$ analysis for the ridges located closer to and farther from to the

antidiagonal in **Figure 2-8C** and **2-8D** gives the following estimate for anisotropic components for $^{15}\text{N1}$ of the two conformers, $T \sim 0.3\text{-}0.4$ and $0.6\text{-}0.7$ MHz, respectively. The isotropic couplings would be practically the same for both ridges with the value about $1.9\text{-}2.1$ MHz or $-(1.5\text{-}1.6)$ MHz, in satisfactory agreement with $|a_{\text{iso}}(^{15}\text{N1})|$ determined by ENDOR. The quantity, $2T$, can be considered as a rough estimate of the maximum component of the anisotropic tensor for these two conformations, giving $T_{\text{max}} \sim 0.6\text{-}0.8$ MHz and $1.2\text{-}1.4$ MHz, similar to $T_{\text{max}}(\text{N1}) = 1.0$ MHz seen in ENDOR.

DISCUSSION

This report describes EPR/ENDOR/HYSCORE measurements of the common intermediate, **I**, formed during freeze-quench of the $\alpha\text{-}70^{\text{Ala}}/\alpha\text{-}195^{\text{Gln}}$ substituted MoFe protein under turnover conditions using N_2H_4 , $\text{CH}_3\text{N}_2\text{H}$, or N_2H_2 as substrate. We first discuss the properties of this intermediate, then incorporate the conclusions we reach into an analysis that leads us to propose that nitrogenase functions by the **A** reaction pathway of **Scheme 1**.

Nature of Intermediate I. Earlier X/Q-band EPR and 35 GHz ENDOR measurements showed that freeze-quench of the $\alpha\text{-}70^{\text{Ala}}/\alpha\text{-}195^{\text{Gln}}$ substituted MoFe protein during turnover with N_2H_4 or N_2H_2 causes loss of the EPR signal from resting-state ($S = 3/2$) FeMo-co and the appearance of the signals from low-spin ($S = 1/2$) intermediates with almost axial g-tensors, originally denoted $\text{m}(\text{N}_2\text{H}_2)$,¹⁷ $\text{l}(\text{N}_2\text{H}_4)$,²¹ respectively. The properties of these intermediates, as measured in the previous work and extended in the present study, establish that they correspond to a common state: $[\text{m}(\text{N}_2\text{H}_2), \text{l}(\text{N}_2\text{H}_4)] = \mathbf{I}$. The temperature and microwave power dependences of the **I**

EPR signal indicate that the FeMo-co of this state has two major conformers with different g tensors ($g_1 = 2.09, 2.11$) and significantly different relaxation properties.

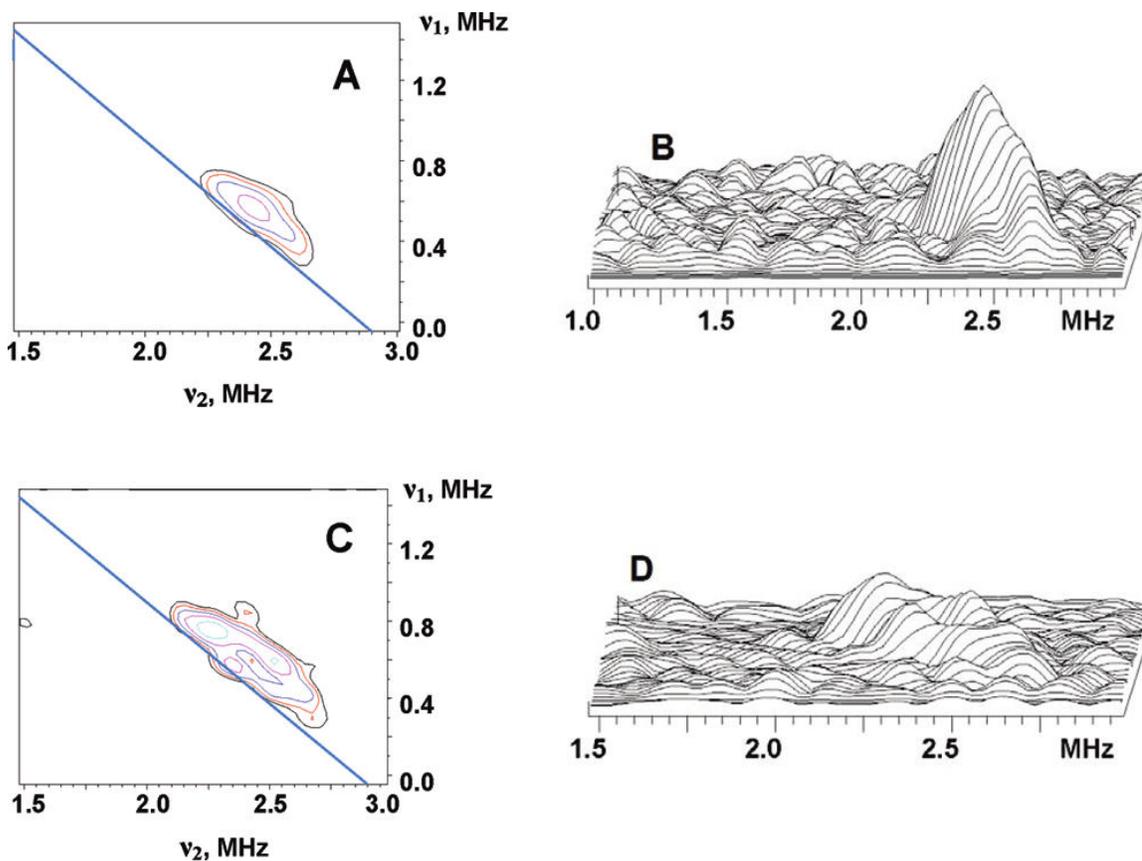


Figure 2-8. Contour (A,C) and stacked (B,D) presentations of the cross-features **3** from the HYSCORE spectra of the $l(^{15}\text{N}_2\text{H}_4)$ intermediate (magnetic field 329.5 mT (A,B) and 332.3 mT (C,D), time between first and second pulses $\tau = 136$ ns, microwave frequency 9.7034 GHz (A,B) and 9.7057 GHz (C,D)).

^1H and ^{15}N 35 GHz CW and pulsed ENDOR measurements showed that **I** has an $[\text{N}_x\text{H}_y]$ fragment bound to FeMo-co.¹⁷ The proton(s) associated with this fragment have here been investigated by 35 GHz 2 K CW ^1H ENDOR and X-band 8 K HYSCORE/ESEEM measurements with samples prepared in $\text{H}_2\text{O}/\text{D}_2\text{O}$ buffers. At the microwave power settings used for 2 K Q-band CW ^1H ENDOR measurements and at the temperature used for the HYSCORE measurements, each measurement interrogates both conformers of **I** with approximately equal sensitivity. The two techniques confirm that **I** exhibits a signal from exchangeable H1 proton(s) with a maximum hyperfine coupling, $A \sim 9$ MHz, and that the H1 signals can be interpreted in terms of an axial hyperfine tensor with $A_{\perp} = |a - T| \sim 9$ MHz and $A_{\parallel} = |a + 2T| \sim 4.8$ MHz, corresponding to $T = 4.6$ MHz, $a = -4.3$ MHz (signs are relative).

The 2 K Q-band pulsed ^{15}N ENDOR spectra are collected with short repetition times (~ 10 ms), and are dominated by the $g_1 = 2.09$ conformer of **I**. A 2D field-frequency pattern of the ^{15}N ENDOR spectra of this **I** conformer can be analyzed in terms of a single bound ^{15}N , with hyperfine tensor, $\mathbf{A}(^{15}\text{N1}) = \pm[1, 1.5, 2.8]$ MHz, although the spectra appear to be distorted by contributions from the single $^{15}\text{N1}$ of the second conformer. The 8 K X-band ^{15}N HYSCORE measurements are consistent with this tensor, but the shape of the HYSCORE signal appears to represent comparable contribution from two nitrogens with very similar couplings. As the 8 K HYSCORE measurement is equally sensitive to signals from the two conformers, these experiments are consistent with the view that the ^{15}N ENDOR and HYSCORE responses do not arise from a $[\text{N}_2\text{H}_y]$ species with roughly equivalent ^{15}N bound to FeMo-co, and instead each of the two slightly different ^{15}N is associated with one of the conformers of the FeMo-co

center. This interpretation is confirmed by experiments with **I** formed from specifically labeled $\text{CH}_3\text{-N}^{15}\text{N-H}$ and $\text{CH}_3\text{-}^{15}\text{N=N-H}$ as substrates. The ^{15}N ENDOR signals from the single ^{15}N of $\text{CH}_3\text{-N}^{15}\text{N-H}$ are identical to those of **I** formed from the other two substrates, **Figure 2-5A**, and no such signal is seen when $\text{CH}_3\text{-}^{15}\text{N=N-H}$ is employed.²³ These results prove that the two contributing ^{15}N represent a single nitrogen from substrate bound to FeMo-co metal ion(s), but with properties that differ slightly in the two conformers. The ^{14}N HYSCORE patterns for **I** further give the quadrupole coupling parameter for N1, $K \approx 0.5 \pm 0.04$ MHz.

The conclusion that the $^{15}\text{N1}$ signals originate from a single nitrogen atom bound to a metal ion(s) of FeMo-co leads to the question of whether or not the substrate-derived species retains the N-N bond of the $\text{N}_2\text{H}_4/\text{N}_2\text{H}_2$ substrates. If the second N is present but not bound to a metal ion, it would have a weaker hyperfine coupling. High-resolution 35 GHz pulsed ENDOR spectra (**Figure 2-6**) show *no* evidence of a weakly coupled $^{15}\text{N2}$. We estimate that a second $^{15}\text{N2}$ could be present only if it had a hyperfine coupling at least forty-fold smaller than that of the observed $^{15}\text{N1}$ signal; as a comparison, preliminary results indicate that the coupling constant of the remote $^{15}\text{N2}$ of $^{15}\text{N}_2\text{H}_4$ bound to the ferriheme of heme oxygenase³⁷ is roughly twenty-fold less than that of the $^{15}\text{N1}$ bound to Fe. The HYSCORE experiment likely has an even lower threshold than ENDOR for the detection of a weakly bound ^{15}N , and it also shows *no* response from a second nitrogen atom. Finally, when **I** is trapped during turnover with the selectively labeled $\text{CH}_3\text{-}^{15}\text{N=NH}$, $^{13}\text{CH}_3\text{-N=NH}$, or $\text{C}^2\text{H}_3\text{-N=NH}$ no signal is seen from the isotopic labels.²³ From these results we conclude that the N=N bonds of N_2H_2 and $\text{CH}_3\text{N}_2\text{H}$, and the N-N bond of N_2H_4 have been broken in forming the common EPR-active

intermediate **I** during enzymatic turnover. This intermediate thus contains an $[\text{NH}_y]$ moiety bound to FeMo-co, and when useful can be denoted as **I** $[\text{NH}_y]$.

The Nitrogenase Reaction Pathway. Based on the alternative reaction pathways pictured in **Scheme 2-1**, the $[\text{NH}_y]$ moiety bound to FeMo-co of **I** could be $[\text{=NH}]$, $[\text{-NH}_2]$, or even the product $[\text{NH}_3]$ (not shown). Given that two of the states that bind these fragments are reached by both pathways, the *nature* of this moiety does not in itself distinguish between **A** and **D** pathways. However, the present findings in conjunction with other considerations lead to us to propose that nitrogenase functions via the **A** reaction pathway of **Scheme 2-1** for reduction of N_2 .

Both N_2H_2 and N_2H_4 are substrates that are reduced to two NH_3 by the wild-type nitrogenase. By opening the reactive site, the $\alpha\text{-70}^{\text{Ala}}$ substitution merely enhances the reduction of these substrates, while the $\alpha\text{-195}^{\text{Gln}}$ substitution further favors the trapping of **I** $[\text{NH}_y]$. The reduction of N_2H_4 must begin by its binding to FeMo-co, and this necessarily generates a state associated only with the **A** pathway, as there is no N_2H_4 -bound intermediate along **D**. Instead, according to the **D** pathway, **Scheme 2-1**, the N-N bond is cleaved two stages of hydrogenation prior to the appearance of an intermediate at the formal reduction stage of N_2H_4 . In contrast, diazenido intermediates exist on both routes. To explain how nitrogenase could reduce each of the substrates, N_2 , N_2H_2 and N_2H_4 , to two NH_3 molecules via a common **A** reaction pathway, one need only postulate that each substrate ‘joins’ the pathway at the appropriate stage of reduction, binding to FeMo-co that has been ‘activated’ by accumulation of a sufficient number of electrons (possibly with FeMo-co reorganization) and then proceeds along that pathway. For N_2H_2 to instead join the **D** pathway would imply that it is converted to the $[\text{NH}_2=\text{N}]$ tautomeric

form upon binding to FeMo-co, a seemingly implausible process. Moreover, the strong influence of α -70^{Val} substitutions of MoFe protein *without* modification of FeMo-co reactivity strongly implicate Fe, rather than Mo, as the site of binding and reactivity,¹⁹ and energetic considerations then implicate the **A** pathway.¹² Overall, the combination of these considerations with the finding of the formation of the common intermediate **I** thus lead us to conclude that N₂H₂, CH₃N₂H, N₂H₄, all are reduced by the common **A** pathway.

Does that require N₂ reduction to follow the same pathway? Rejection of the **D** pathway contradicts the suggestions of an early study⁸ which showed that hydrazine is released upon acid or base quenching of nitrogenase actively reducing dinitrogen.⁹ This finding was interpreted as indicating that the diazenido intermediate in the **D** pathway (**Scheme 2-1**) can be viewed as accepting two electrons from FeMo-co, making it a hydrazido dianion (N-NH₂²⁻), and that this dianionic species is protonated and released as N₂H₄ upon hydrolysis by *either* acid or base. However, it is clearly more economical³⁸ to propose that the hydrazine observed during acid/base quenching of nitrogenase is merely released from the hydrazine-bound intermediate that occurs naturally as a stage along the **A** pathway, **Scheme 2-1**, and that all nitrogenous substrates, N₂ included, undergo reduction to two NH₃ molecules by the common pathway, **A**. Likewise, it is most economical to suggest that both the Mo-dependent nitrogenase studied here and the V-dependent nitrogenase⁴ reduce N₂ by the same pathway. As it has been shown that V-nitrogenase produces N₂H₄ while reducing N₂,³⁹ then according to **Scheme 2-1** this enzyme clearly functions via the **A** pathway, implying the same is true for Mo-nitrogenase.

No nitrogenous substrate binds to resting-state ($S = 3/2$) FeMo-co of nitrogenase,⁴⁰ so the activation of FeMo-co for each substrate requires the accumulation of some number of electrons. The most refractory substrate is N_2 itself, and the Lowe-Thorneley scheme states that the accumulation of three, and most effectively four, electrons is required to bind N_2 and initiate its reduction.^{3,9,10} Indeed, our previous work characterized the intermediate that has accumulated four electrons.^{19,41} Presumably, lower numbers of accumulated electrons are required to initiate reduction of N_2H_2 and N_2H_4 , as is true for reduction of C_2H_2 .^{3,9}

CONCLUSIONS

(i) EPR/ENDOR/HYSCORE measurements establish that a common intermediate, **I**, is trapped during turnover of N_2H_2 , CH_3N_2H , or N_2H_4 as substrate for the α -70^{Ala}/ α -195^{Gln} substituted MoFe protein. These measurements reveal that **I** represents a stage of N_2 fixation in which the N-N bond has been cleaved, and in which [=NH], [-NH₂], or even the product [NH₃] are bound to FeMo-co. (ii) Considerations of these findings lead us to conclude that nitrogenase reduces N_2H_2 , CH_3N_2H , N_2H_4 via the **A** reaction pathway presented in **Scheme 2-1**, and that the same is true for N_2 itself. Energetic considerations,¹² in combination with the strong influence of α -70^{Val} substitutions of MoFe protein *without* modification of FeMo-co reactivity then implicate Fe, rather than Mo, as the site of binding and reactivity.¹⁹

REFERENCES

- (1) Smil, V. *Enriching the Earth: Fritz Haber, Carl Bosch, and the Transformation of World Food Production*; MIT Press: Cambridge, MA, 2001.

- (2) Christiansen, J.; Dean, D. R.; Seefeldt, L. C. *Annu. Rev. Plant Physiol. Plant Mol. Biol.* **2001**, *52*, 269-295.
- (3) Burgess, B. K.; Lowe, D. J. *Chem. Rev. (Washington, DC, U. S.)* **1996**, *96*, 2983-3011.
- (4) Eady, R. R. *Chem. Rev. (Washington, D. C.)* **1996**, *96*, 3013-3030.
- (5) Seefeldt, L. C.; Hoffman, B. M.; Dean, D. R. *Annu. Rev. Biochem.* **2009**, *78*, 701-722.
- (6) Hoffman, B. M.; Dean, D. R.; Seefeldt, L. C. *Acc. Chem. Res.* **2009**, *42*, 609-619.
- (7) Chatt, J.; Dilworth, J. R.; Richards, R. L. *Chem. Rev.* **1978**, *78*, 589-625.
- (8) Thorneley, R. N. F.; Eady, R. R.; Lowe, D. J. *Nature* **1978**, *272*, 557-558.
- (9) Thorneley, R. N. F.; Lowe, D. J. In *Molybdenum Enzymes*; Spiro, T. G., Ed.; Wiley-Interscience: New York, 1985; Vol. 7, pp 89-116.
- (10) Wilson, P. E.; Nyborg, A. C.; Watt, G. D. *Biophys. Chem.* **2001**, *91*, 281-304.
- (11) Schrock, R. R. *Acc. Chem. Res.* **2005**, *38*, 955-962.
- (12) Neese, F. *Angew. Chem., Int. Ed.* **2006**, *45*, 196-199.
- (13) Kastner, J.; Blochl Peter, E. *J. Am. Chem. Soc.* **2007**, *129*, 2998-3006.
- (14) Hinnemann, B.; Norskov, J. K. *Top. Catal.* **2006**, *37*, 55-70.
- (15) Burgess, B. K. in *Metal Ions in Biology: Molybdenum Enzymes*; Spiro, T. G., Ed.; John Wiley and Sons; New York, 1985; pp 161-220.
- (16) Barney, B. M.; Lukoyanov, D.; Igarashi, R. Y.; Laryukhin, M.; Yang, T.-C.; Dean, D. R.; Hoffman, B. M.; Seefeldt, L. C. *Biochemistry* **2009**, *48*, 9094-9102.
- (17) Barney, B. M.; McClead, J.; Lukoyanov, D.; Laryukhin, M.; Yang, T. C.; Hoffman, B. M.; Dean, D. R.; Seefeldt, L. C. *Biochemistry* **2007**, *46*, 6784-6794.
- (18) Lee, H.-I.; Igarashi, R. Y.; Laryukhin, M.; Doan, P. E.; Dos Santos, P. C.; Dean, D. R.; Seefeldt, L. C.; Hoffman, B. M. *J. Am. Chem. Soc.* **2004**, *126*, 9563-9569.
- (19) Igarashi, R. Y.; Laryukhin, M.; Santos, P. C. D.; Lee, H.-I.; Dean, D. R.; Seefeldt, L. C.; Hoffman, B. M. *J. Am. Chem. Soc.* **2005**, *127*, 6231-6241.
- (20) Barney, B. M.; Igarashi, R. Y.; Dos Santos, P. C.; Dean, D. R.; Seefeldt, L. C. *J. Biol. Chem.* **2004**, *279*, 53621-53624.

- (21) Barney, B. M.; Laryukhin, M.; Igarashi, R. Y.; Lee, H.-I.; Santos, P. C. D.; Yang, T.-C.; Hoffman, B. M.; Dean, D. R.; Seefeldt, L. C. *Biochemistry* **2005**, *44*, 8030-8037.
- (22) Barney, B. M.; Yang, T.-C.; Igarashi, R. Y.; Santos, P. C. D.; Laryukhin, M.; Lee, H.-I.; Hoffman, B. M.; Dean, D. R.; Seefeldt, L. C. *J. Am. Chem. Soc.* **2005**, *127*, 14960-14961.
- (23) Barney, B. M.; Lukoyanov, D.; Yang, T.-C.; Dean, D. R.; Hoffman, B. M.; Seefeldt, L. C. *Proc. Natl. Acad. Sci. U. S. A.* **2006**, *103*, 17113-17118.
- (24) Seefeldt, L. C.; Dean, D. R.; Hoffman, B. M.; Dos Santos, P. C.; Barney, B. M.; Lee, H.-I. *Dalton Trans.* **2006**, 2277-2284.
- (25) Kim, C.-H.; Newton, W. E.; Dean, D. R. *Biochemistry* **1995**, *34*, 2798-2808.
- (26) Lowe, D. J. *ENDOR and EPR of Metalloproteins*; R. G. Landes Co.: Austin, TX, 1995.
- (27) Hoffman, B. M. *Acc. Chem. Res.* **2003**, *36*, 522-529.
- (28) Schweiger, A.; Jeschke, G. *Principles of Pulse Electron Paramagnetic Resonance*; Oxford University Press: Oxford, UK, 2001.
- (29) DeRose, V. J.; Hoffman, B. M. In *Methods in Enzymology*; Sauer, K., Ed.; Academic Press: New York, 1995; Vol. 246, pp 554-589.
- (30) Doan, P. E.; Hoffman, B. M. *Chem. Phys. Lett.* **1997**, *269*, 208-214.
- (31) Hoefler, P.; Grupp, A.; Nebenfuhr, H.; Mehring, M. *Chem. Phys. Lett.* **1986**, *132*, 279-282.
- (32) Dikanov, S. A.; Bowman, M. K. *J. Magn. Res. Ser. A* **1995**, *116*, 125-128.
- (33) Dikanov, S. A.; Bowman, M. K. *J. Biol. Inorg. Chem.* **1998**, *3*, 18-29.
- (34) Jin, H.; Turner, I. M., Jr.; Nelson, M. J.; Gurbiel, R. J.; Doan, P. E.; Hoffman, B. M. *J. Am. Chem. Soc.* **1993**, *115*, 5290-5291.
- (35) Dikanov, S. A.; Tsvetkov, Y. D.; Bowman, M. K.; Astashkin, A. V. *Chem. Phys. Lett.* **1982**, *90*, 149-153.
- (36) Dikanov, S. A.; Samoilova, R. I.; Kappl, R.; Crofts, A. R.; Huttermann, J. *Phys. Chem. Chem. Phys.* **2009**, *11*, 6807-6819.
- (37) Sakamoto, H.; Higashimoto, Y.; Hayashi, S.; Sugishima, M.; Fukuyama, K.; Palmer, G.; Noguchi, M. *J. Inorg. Biochem.* **2004**, *98*, 1223-1228.

- (38) "Occam's razor", *Wikipedia-Contributors Wikipedia, The Free Encyclopedia*, http://en.wikipedia.org/w/index.php?title=Occam%27s_razor&oldid=418788633 (accessed 16 March 2011).
- (39) Dilworth, M. J.; Eady, R. R. *Biochem. J.* **1991**, *277*, 465-468.
- (40) Benton, P. M. C.; Mayer, S. M.; Shao, J.; Hoffman, B. M.; Dean, D. R.; Seefeldt, L. C. *Biochemistry* **2001**, *40*, 13816-13825.
- (41) Lukoyanov, D.; Barney, B. M.; Dean, D. R.; Seefeldt, L. C.; Hoffman, B. M. *Proc. Natl. Acad. Sci. U. S. A.* **2007**, *104*, 1451-1455.

CHAPTER 3

UNIFICATION OF REACTION PATHWAY AND KINETIC SCHEME FOR N₂
REDUCTION CATALYZED BY NITROGENASE³**Abstract**

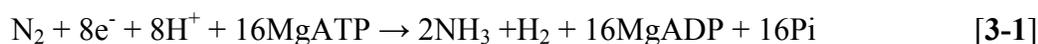
Nitrogenase catalyzes the reduction of N₂ and protons to yield two NH₃ and one H₂. Substrate binding occurs at a complex organo-metallocluster called FeMo-cofactor (FeMo-co). Each catalytic cycle involves the sequential delivery of eight electrons/protons to this cluster, and this process has been framed within a kinetic scheme developed by Lowe and Thorneley. Rapid freezing of a modified nitrogenase under turnover conditions using diazene, methyldiazene (HN=N-CH₃), or hydrazine as substrate recently was shown to trap a common S = 1/2 intermediate, designated **I**. It was further concluded that the two N-atoms of N₂ are hydrogenated alternately ('Alternating' (**A**) pathway). In the present work, Q-band CW EPR and ⁹⁵Mo ESEEM spectroscopy reveal such samples also contain a common intermediate with FeMo-co in an integer-spin state having a ground-state 'non-Kramers' doublet. This species, designated **H**, has been characterized by ESEEM spectroscopy using a combination of ^{14,15}N isotopologs plus ^{1,2}H isotopologs of methyldiazene. It is concluded that: **H** has NH₂ bound to FeMo-co and corresponds to the penultimate intermediate of N₂ hydrogenation, the state formed after the accumulation of seven electrons/protons and the release of the first NH₃; **I** corresponds to the final intermediate in N₂ reduction, the state formed after accumulation of eight electrons/protons, with NH₃ still bound to FeMo-co prior to release and

³ Coauthored by Dmitriy Lukoyanov, Zhi-Yong Yang, Brett M. Barney, Dennis R. Dean, Lance C. Seefeldt, and Brian M. Hoffman (2012) *Proceedings of the National Academy of Sciences of the United States of America* **109**(15), 5583-5587.

regeneration of resting-state FeMo-co. A proposed unification of the Lowe-Thorneley kinetic model with the ‘prompt’ alternating reaction pathway represents a draft mechanism for N₂ reduction by nitrogenase.

Introduction

Nitrogen fixation — the reduction of N₂ to two NH₃ molecules — is catalyzed by the enzyme nitrogenase according to the limiting stoichiometry (1, 2):



The Mo-dependent enzyme studied here (2-4) consists of two component proteins, denoted the Fe protein and the MoFe protein. The former delivers electrons one-at-a-time to the MoFe protein, where they are utilized at the active site iron-molybdenum cofactor ([7Fe-9S-Mo-C-R-homocitrate]; FeMo-co) to reduce substrate (2, 3). In the Lowe-Thorneley (LT) kinetic scheme for N₂ reduction by nitrogenase (2, 5, 6), the eight steps of electron/proton delivery implied by **Eq. 3-1** are denoted E_n, where *n* = 0 to 8, with E₀ representing the resting-state enzyme. It is known that N₂ binds only after the MoFe protein accumulates three or four electrons (E₃ or E₄ states), with N₂ reduction then proceeding along a reaction pathway that comprises the sequence of intermediate states generated as N₂ bound to FeMo-co undergoes six steps of hydrogenation (e⁻/H⁺ delivery to substrate) (1-4, 7). Recently, we concluded that nitrogenase follows an ‘alternating’ (A) reaction pathway, in which the two N’s are hydrogenated alternately, with a hydrazine-bound intermediate formed after four steps of hydrogenation, and with cleavage of the hydrazine N-N bond and liberation of the first NH₃ only at the fifth hydrogenation step (8). However, this conclusion left many questions unresolved, in particular the

correspondence between intermediates formed along the reaction pathway and the LT kinetic scheme for the accumulation of eight reducing equivalents during catalysis.

Intermediates formed during turnover have been trapped by freeze-quench methods and studied by paramagnetic resonance techniques. The resting-state FeMo-co of E_0 exhibits an EPR-active, $S = 3/2$ spin state. When nitrogenase is freeze-quenched during turnover, the resting-state EPR spectrum partially or fully disappears as FeMo-cofactor accumulates electrons. Accumulation of an even number of electrons generates E_n , $n = \text{even}$, intermediates with EPR-active, odd-electron (half-integer spin; Kramers) FeMo-co states ($S = 1/2, 3/2$) (3, 4). Such states have been observed upon freeze-quench of wild-type and amino-acid substituted MoFe proteins during turnover with a variety of different substrates (3, 4). However, the signals from Kramers forms of FeMo-co in the quenched samples never quantitate to the total FeMo-co present, indicating that apparently EPR-silent states of FeMo-co must also exist. These silent MoFe protein states contain FeMo-co with an even number of electrons, and correspond to E_n , $n = \text{odd}$ ($n = 2m + 1$, $m = 0-3$) intermediates in the LT scheme. These quenched samples may include states with diamagnetic FeMo-co, but Mössbauer studies indicated the presence of reduced FeMo-co in integer-spin ($S = 1, 2, \dots$), ‘non-Kramers (NK)’ states (9). Although NK-EPR signals at conventional microwave frequencies are well known for other enzymes (10, 11), until now, no EPR signal from an integer-spin form of FeMo-co has been detected.

Recently, rapid freezing during turnover of a doubly-substituted nitrogenase MoFe protein ($\alpha\text{-70}^{\text{Val}\rightarrow\text{Ala}}$, $\alpha\text{-195}^{\text{His}\rightarrow\text{Gln}}$), which favors reduction of large nitrogenous substrates (3, 4), with diazene, methyldiazene ($\text{HN}=\text{N-CH}_3$), or hydrazine as substrate

was shown to trap a common $S = \frac{1}{2}$ intermediate (denoted **I**) (8). Here, Q-band CW EPR and ^{95}Mo ESEEM (electron spin-echo envelope modulation) spectroscopy reveal that these samples also contain a second common intermediate, denoted **H**, the first to be observed in which FeMo-co is in an EPR-active integer-spin state with a ground-state NK doublet. The NK-EPR signal in samples prepared with ^{95}Mo -enriched FeMo-co and with $^{14,15}\text{N}$ -enriched substrates has been studied by pulsed-EPR measurements of the nuclear modulation of the electron spin-echo (ESE) amplitude, denoted NK-ESEEM (12). These measurements allow us to infer the state of the N-N bond in **H** and the relationship of **H** to intermediate, **I**. Most importantly, the analysis allows us to assign the correspondence of both intermediates with specific E_n states, and to infer how the hydrogenated reaction intermediates, diazene and hydrazine, join the N_2 reduction pathway. These conclusions integrate the sequence of N_2 reduction intermediates (the reaction ‘pathway’) with the LT kinetic scheme for the accumulation of the eight reducing equivalents (and protons), thereby generating a draft mechanism for nitrogen fixation by nitrogenase.

Results

The EPR spectra of the doubly substituted α -70^{Val→Ala}, α -195^{His→Gln} MoFe protein trapped during turnover in the presence of hydrazine, diazene, and methyldiazene show a significant loss of the $S=3/2$ resting state of FeMo-co and the appearance of a $S = \frac{1}{2}$ signal from intermediate **I** in the vicinity of $g = 2$, along with the spectrum from the $[\text{4Fe4S}]^{1+}$ cluster of the Fe protein (**Figure 3-1**). Recent ^1H , $^{14,15}\text{N}$ ENDOR and HYSCORE spectroscopic experiments demonstrated that **I** represents a late stage of nitrogen fixation, when the first ammonia molecule already has been released (8), and only a $[\text{NH}_x]$ ($x = 2$ or 3) fragment of substrate is bound to FeMo-co (8).

We here note that samples freeze-trapped during turnover with all three substrates also show an additional broad EPR signal at low field in Q-band spectra collected at a temperature of 2 K (**Figure 3-1**). This signal begins near zero-field and extends beyond 5000 G, where the signals from $S = 3/2$ FeMo-co in both resting state and trapped high-spin intermediates (13) appear. The low-field signal arises from an integer-spin system ($S \geq 2$) (10) that exhibits a ground-state non-Kramers doublet that is split in zero applied field by an energy, $h\Delta$ (h , Planck's constant) (14), in the range of the microwave quantum, $\nu_e = 35$ GHz; the breadth of the signal indicates that Δ exhibits a considerable distribution in values.

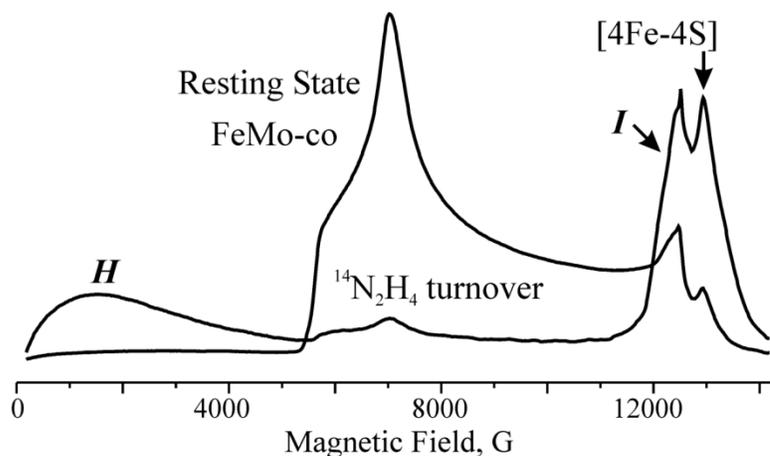


Figure 3-1. Q-band CW EPR spectrum of α -70^{Val→Ala}, α -195^{His→Gln} MoFe protein in resting state ($S = 3/2$) and trapped during turnover with $^{14}\text{N}_2\text{H}_4$. *Conditions:* microwave frequency, 35.015 GHz (resting), 35.022 GHz (turnover); modulation amplitude, 2 G; time constant, 128 ms; field sweep, 67 G/s; $T = 2$ K.

ESEEM can be used to characterize a non-Kramers doublet (NK-ESEEM) (15); we begin by discussing the ESEEM time-waves. **Figure 3-2A** presents representative 35 GHz (2 K) three-pulse NK-ESEEM time-waves collected at several relatively low fields from the nitrogenase NK intermediates generated with isotopologs of the three substrates. The electron spin-echo (ESE) amplitude from the NK intermediates is maximum at zero applied magnetic field (B) and decreases very slowly with increasing field, being observable at all fields up to ~ 5000 G, where signals from $S = 3/2$ FeMo-co begin. This slow decrease of echo intensity with field contrasts sharply with the rapid decrease for carboxylate-bridged di-ferrous centers ($S = 4$), where the echo (at X band) vanished by ~ 100 G (16). As illustrated in **Figure 3-2A, left** (upper), at the lowest applied magnetic field ($B = 18$ G) none of the nitrogenase intermediates show nuclear modulation of the ESE envelope. As the field is increased, nuclear modulation from protons first appears ($B = 296$ G), then modulation associated with hyperfine-coupled ^{14}N ($B = 362$ G). The appearance of modulation with increasing field reflects the fact that at zero applied field the electron and nuclear spins are uncoupled and so there can be no ESE modulation. Application of a field establishes the coupling and introduces modulation, with a depth that increases quadratically with B (15).

As illustrated in **Figure 3-2A**, the NK-ESEEM time-waves for the NK intermediates trapped during turnover with the corresponding ^{14}N and ^{15}N isotopologs of N_2H_2 , N_2H_4 , and HN_2CH_3 substrates are identical at all fields, indicating that a common intermediate, denoted ***H***, is trapped during turnover with all three substrates. **Figure 3-2A, left** and **Figure 3-2C, left** further show that ^{95}Mo enrichment of $\alpha\text{-}70^{\text{Val}\rightarrow\text{Ala}}$, $\alpha\text{-}195^{\text{His}\rightarrow\text{Gln}}$ MoFe protein produces significant change of the NK-ESEEM time-wave. This

establishes that the NK-EPR signal of **H** arises from the Mo-containing FeMo-co in an integer-spin state, and not the all-iron electron-transfer-active P cluster also present in the MoFe protein, or even the [4Fe-4S] cluster of the Fe protein. The absence of any signal in **Figure 3-1** from the P cluster further indicates that all electrons delivered to MoFe protein of **H** during turnover reside on FeMo-co.

The ‘turn-on’ of nuclear modulation for **H** with applied field is quite gradual in comparison with that observed for the carboxylate-bridged diiron centers (16). In addition to A_{\parallel} and g_{\parallel} , there are three factors that influence the field dependence of the modulation depth (15). First, the earlier diiron centers measurements were performed at X band ($\nu_e \sim 9$ GHz), whereas the present ones employ a four-fold higher frequency ($\nu_e \sim 35$ GHz). According to our analysis (15), this causes a four-fold decrease in the rate at which the effective hyperfine coupling (\tilde{A}_{eff}) increases with field. Second, the earlier measurements were performed with the microwave field parallel to the external field, whereas the current ones are performed in perpendicular mode, which requires a roughly three-fold higher field to achieve the same \tilde{A}_{eff} (17). Finally, the diiron centers exhibit a total spin state $S = 4$ (16); assigning intermediate **H** a total spin of $S = 2$ would further lower the rate at which \tilde{A}_{eff} increases with field by an additional factor of four (15). This value of S for **H** is supported by the finding from Q-band EPR spectroscopy (**Figure 3-1**) that $\Delta \sim 35$ GHz for **H**, not ~ 9 GHz for the diiron centers, for it is generally expected that Δ increases as S decreases (11).

Figure 3-2. (A): Three-pulse ESEEM traces for NK intermediate **H** of α -70^{Val→Ala}, α -195^{His→Gln} MoFe protein under turnover. **(A, left)** Time domain for ¹⁴N₂H₂ (black), ¹⁴N₂H₄ (red) substrates, and for ⁹⁵Mo-enriched MoFe with ¹⁴N₂H₄ (blue). Most spectra taken with τ selected to suppress the ¹H response; nonetheless, residual ¹H signals typically are observed. *Conditions:* microwave frequency, 34.756 GHz (¹⁴N₂H₂), 34.767 GHz (¹⁴N₂H₄), 34.756 GHz (⁹⁵Mo-FeMo-co, ¹⁴N₂H₄); $\pi/2 = 50$ ns, 30 ns time steps; repetition time 2 ms, 50 shots/point (10 ms, 10 shots/point for ¹⁴N₂H₂), 50-150 scans; T = 2 K. **(A, right)** Time-waves for **H** trapped with: ¹⁴NH=¹⁴NH (black), ¹⁴NH=¹⁴NCD₃ (green), ¹⁴NH₂-¹⁴NH₂ (red), ¹⁵NH=¹⁵NH (blue), ¹⁵NH=¹⁴NCH₃ (magenta). *Conditions:* as for **(A, left)**, except for microwave frequency, 34.772 GHz (¹⁴NH=¹⁴NCD₃), 34.764 GHz (¹⁵NH=¹⁵NH), 34.725 GHz (¹⁵NH=¹⁴NCH₃); 140-500 scans. Time-waves are shown after decay baseline subtraction. **(B):** Field dependence of three-pulse ESEEM **(B, left)** time and **(B, right)** frequency traces of **H** prepared with ¹⁴N₂H₂ (black) and ¹⁵N₂H₂ (red). *Conditions:* as for **(A)**. Triangles represent suppressed frequencies n/τ , $n = 1, 2, \dots$ **(C):** Time and frequency domain traces for **H** formed with ¹⁴N₂H₄ substrate: natural abundance (black) and ⁹⁵Mo-enriched (red) α -70^{Val→Ala}, α -195^{His→Gln} MoFe protein. *Conditions:* as for **(A)**.

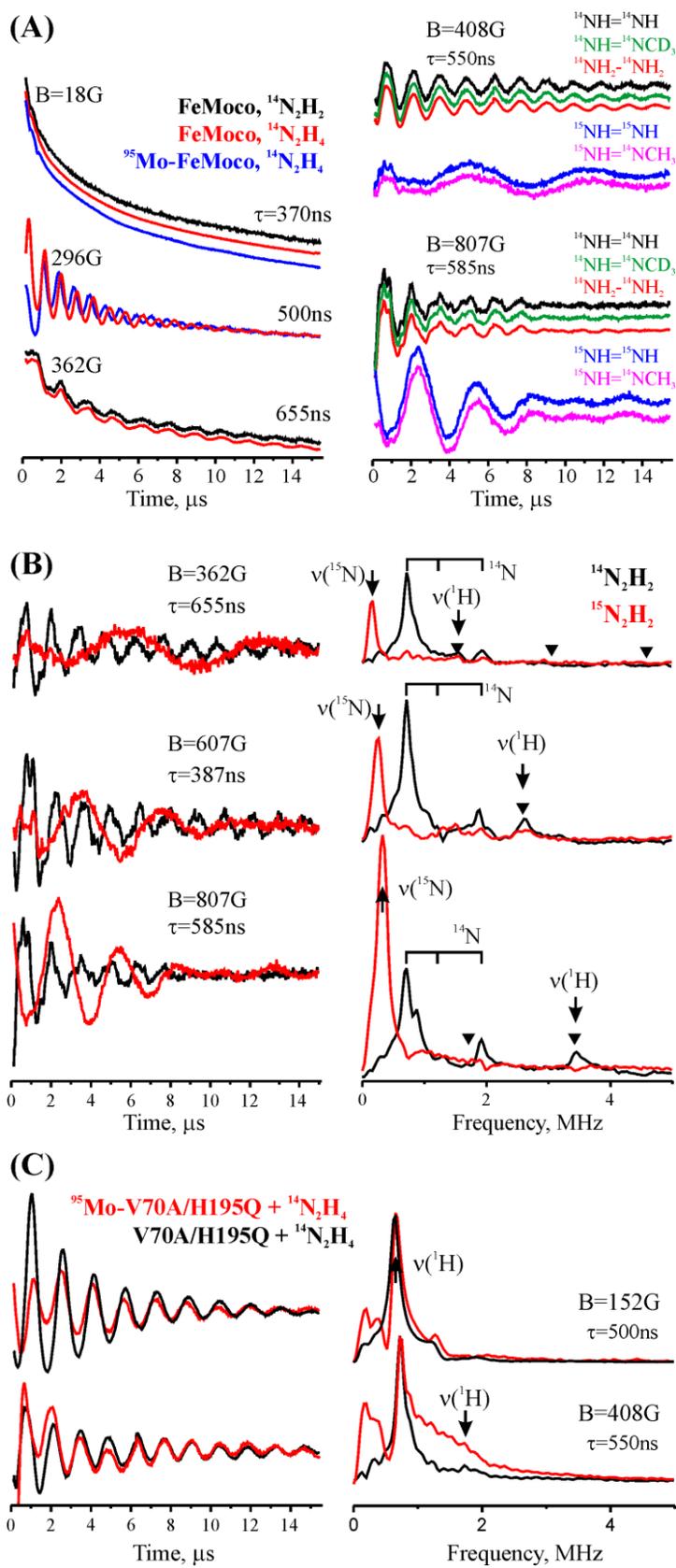


Figure 3-2A, right and **3-2B, left** show that intermediate prepared with ^{14}N and ^{15}N substrates yield quite different NK-ESEEM time-waves, demonstrating that the modulation arises from a substrate fragment bound to FeMo-co. The state of the N-N bond in **H** was revealed by the behavior of the common intermediate **H** upon isotopic substitution of the three nitrogenous substrates, in particular selective labeling of methyldiazene. The time-waves of **Figures 3-2A, right** show that the ^{14}N modulation is abolished and replaced with ^{15}N modulation not only when both nitrogens of $^{14}\text{N}_2\text{H}_2$ and $^{14}\text{N}_2\text{H}_4$ are substituted with ^{15}N , but also when $\text{H}-^{15}\text{N}=\text{N}-\text{CH}_3$ is used as substrate; furthermore, there is no added ^2H modulation from $\text{H}-^{14}\text{N}=\text{N}-\text{CD}_3$. The absence of modulation from the second ^{14}N of $\text{H}-^{14}\text{N}=\text{N}-\text{CH}_3$ or from ^2H of $\text{H}-^{14}\text{N}=\text{N}-\text{CD}_3$ indicates that the N-N bond has been cleaved prior to the formation of **H**, which thus contains an NH_x fragment bound to FeMo-co. This conclusion parallels the conclusion that the common $S = 1/2$ intermediate, **I**, formed during turnover with the same substrates (see **Figure 3-1**) likewise is formed after the first ammonia is released.

To characterize the NH_x substrate fragment of **H**, frequency-domain NK-ESEEM spectra were obtained by Fourier transform of the time-waves. At low applied fields the electron-nuclear coupling for ^{14}N ($I = 1$) is effective in introducing ESEEM, but the effects of hyperfine couplings on the frequency-domain spectrum are small, and a ^{14}N frequency spectrum exhibits transitions at the three pure nuclear-quadrupole frequencies, denoted ($\bar{\nu}_+ > \bar{\nu}_- > \bar{\nu}_0$, $\bar{\nu}_+ = \bar{\nu}_- + \bar{\nu}_0$), with relative intensities determined by the relative orientations of the quadrupole and zero-field splitting tensors (15). The frequencies yield the quadrupole coupling constant, e^2qQ/h and asymmetry parameter, η (usual symbols).

In contrast, the low-field measurements of nuclei with $I = \frac{1}{2}$ (^1H , ^{15}N) exhibit only a single line at the nuclear Larmor frequency.

Examination of spectra taken at multiple fields for \mathbf{H} prepared by turnover with $^{14}\text{N}_2\text{H}_2$ discloses two ^{14}N peaks whose frequencies 0.71 and 1.92 MHz change little with field from ~ 250 G up to at least 1200 G, and that can be assigned as part of ^{14}N quadrupole triplet. As expected from the change in the time-waves upon generating \mathbf{H} with ^{15}N -labeled substrate (**Figure 3-2A, right, 3-2B**), the ^{14}N quadrupole peaks are abolished in the NK-ESEEM spectra of \mathbf{H} prepared with $^{15}\text{N}_2\text{H}_2$, and replaced by a single peak at the ^{15}N Larmor frequency (**Figure 3-2B**). As the frequencies of the three peaks obey the relationship, $\bar{\nu}_+ = \bar{\nu}_- + \bar{\nu}_0$, there are two options for the frequency of the unobserved peak: 1.21 and 2.63 MHz. This peak could go unobserved either because it lies at 1.21 MHz, where features presumed to arise from the natural abundance molybdenum isotopes with non-zero nuclear spin could obscure the ^{14}N signal, or because the relative orientation of quadrupole and zero-field splitting tensors causes it to have negligible intensity (15). Assignment of the quadrupole frequencies as $\bar{\nu}_0 = 0.71$ MHz, $\bar{\nu}_- = 1.21$ MHz, and $\bar{\nu}_+ = 1.92$ MHz gives the quadrupole coupling parameters: $e^2qQ/h = 2.08$ MHz, $\eta = 0.68$; the alternative assignment of the missing peak as $\bar{\nu}_+ = 2.63$ MHz gives: $e^2qQ/h = 3.04$ MHz, $\eta = 0.47$. A cofactor-bound NH_3 would have $\eta \sim 0$, so the NH_x fragment of \mathbf{H} cannot be NH_3 ; as bound $-\text{NH}$ does not appear on the \mathbf{A} pathway, this fragment therefore must be NH_2 .

The frequency-domain NK-ESEEM spectra obtained from \mathbf{H} prepared with ^{95}Mo -enriched $\alpha\text{-70}^{\text{Val}\rightarrow\text{Ala}}$, $\alpha\text{-195}^{\text{His}\rightarrow\text{Gln}}$ MoFe protein give information about the environment

of the molybdenum of FeMo-co in that intermediate. **Figure 3-2C** shows that ^{95}Mo enrichment introduces a doublet centered at ~ 0.3 MHz in the low-field spectrum, as well as an additional, unresolved broad signal between one and two MHz at higher fields. As the doublet is barely observable in the natural-abundance samples and the broad signal is not seen, the new signals arise from ^{95}Mo of FeMo-co. Although the ^{14}N signal is not detectable below 250 G, the ^{95}Mo signal clearly is present in spectrum at 150 G, and likely could be detected even at lower fields but for overlap with the strong ^1H signal. This difference can be explained by a larger hyperfine coupling to ^{95}Mo in comparison with ^{14}N (15), combined with differences in the dependence of the spectrum on magnetic field for nuclei with $I = 5/2$ (^{95}Mo) and $I = 1$ (^{14}N) that will be discussed elsewhere.

The low-frequency ^{95}Mo doublet observed is provisionally assigned to two pure-quadrupole transitions. The quadrupole interaction of a ^{95}Mo ($I = 5/2$) in zero applied field splits the $2I + 1 = 6$ m_I sublevels into three doublets for each electron-spin manifold. As with ^{14}N ($I = 1$), this yields three pure-nuclear quadrupole transitions, which we denote as $\bar{\nu}_3 > \bar{\nu}_2 > \bar{\nu}_1$. Matrix diagonalization of the full electron-nuclear Hamiltonian and examination of the calculated modulation depth parameters (12) suggests that the highest frequency peak, $\bar{\nu}_3$ will generally be of low intensity, so we further assign the observed doublet as $\bar{\nu}_1 \sim 0.2\text{MHz}$, $\bar{\nu}_2 \sim 0.35\text{MHz}$. This assignment yields, $e^2qQ/h \sim 1.2$ MHz, $\eta \sim 0.2$, values comparable to those found for $(\text{M}^+)_2(\text{MoO}_4)$ salts (18). The higher-frequency feature seen at higher field presumably arises through the influence of the larger ^{95}Mo hyperfine interaction and nuclear spin.

Discussion

The key experimental findings of this report can be summarized as follows.

(i) CW EPR and ^{95}Mo NK-ESEEM spectroscopy reveal that samples of the α -70^{Val→Ala}, α -195^{His→Gln} substituted nitrogenase MoFe protein trapped during turnover in the presence of hydrazine, diazene and methyldiazene each contain a common intermediate, **H**, with FeMo-co in an even-electron, integer-spin state (plausibly $S = 2$) characterized by a low-lying NK doublet. The NK-ESEEM measurements yield quadrupole coupling parameters for the ^{95}Mo of FeMo-co in **H**.

(ii) $^{14}\text{N}/^{15}\text{N}$ NK-ESEEM of **H** formed with substrate isotopologs indicates that a nitrogen of the substrate is directly bound to FeMo-co of α -70^{Val→Ala}, α -195^{His→Gln} MoFe protein.

(iii) The absence of modulation from either a second ^{14}N of substrate, in particular from $\text{H}-^{15}\text{N}=\text{N}-^{14}\text{N}-\text{CH}_3$, or from ^2H of $\text{H}-^{14}\text{N}=\text{N}-^{14}\text{N}-\text{CD}_3$ indicates that **H** is formed after cleavage of the N-N bond of N_2H_4 bound to FeMo-co and loss of NH_3 . Quadrupole coupling parameters for this cofactor-bound NH_x fragment indicate it is not NH_3 , whose three-fold symmetry would yield $\eta \sim 0$, and thus must be NH_2 .

With these findings, it is possible to propose a complete unification of reaction pathway and LT scheme. In the LT scheme the MoFe protein is optimally activated for N_2 binding at the E_4 stage, in which MoFe protein has accumulated four reducing equivalents and four protons. Our studies (19) further show that the four reducing equivalents of E_4 exist in the form of two (Fe-bridging) hydrides, presumably with an additional two protons bound to sulfide (20). As illustrated, in **Figure 3-3**, N_2 binding to FeMo-co of E_4 is accompanied by the loss of two reducing equivalents and two protons

as H₂ (Eq. 3-1), leaving FeMo-co activated by two reducing equivalents and two protons, presumably in the form of one hydride and one proton.

Recently, we concluded that the subsequent catalytic stages follow an ‘Alternating’ (**A**) pathway, in which the two N atoms of N₂ are hydrogenated alternately and the first NH₃ is released after N₂ has been hydrogenated five times (**Figure 3-3**), rather than a ‘Distal’ pathway in which a specific nitrogen of N₂ is hydrogenated three times, then released as NH₃. We also noted (4) that the **A** pathway offers multiple ways to deal with the two reducing equivalents that remain on FeMo-co after N₂ binding. In the ‘Prompt’ (**P**) pathway, when N₂ binds to FeMo-co it is ‘nailed down’ by prompt hydrogenation, **Figure 3-3**, with N₂ binding, H₂ loss, and reduction to diazene all occurring at the E₄ kinetic stage of the LT scheme. In the ‘Late’ (**L**) model, the two reducing equivalents associated with FeMo-co after N₂ binding are delivered to substrate after one or more steps of hydrogenation. In the limiting version of **Figure 3-3**, this comes after hydrazine is formed. This only occurs at the final, E₈ kinetic stage of the LT scheme, and in this case N-N bond cleavage and release of the first NH₃, followed by conversion of the remaining bound NH₂ to NH₃ and its release all occur at E₈. Thus, as illustrated, a given state of N₂ hydrogenation can correspond to a different E_n state along the two **A** pathway branches.

The present results establish the identities of **H** and **I**, as well as their correspondence with E_n states along the **P** pathway of **Figure 3-3**, while unambiguously ruling out the limiting version of the **L** pathway. (i) As the same intermediate **H** is formed during turnover with the two diazenes and with hydrazine, the diazenes must have catalytically ‘caught up’ to hydrazine, and **H** must occur at or after the appearance of a

hydrazine-bound intermediate. (ii) As noted above, **H** contains FeMo-co in an integer-spin (NK) state, and thus corresponds to an E_n state with $n = \text{odd}$. As **H** is a common intermediate that contains a bound fragment of substrate, it must therefore correspond to E_5 or E_7 . But **H** cannot be either E_5 or E_7 on the **L** path *or* E_5 on the **P** pathway, for they all come *before* hydrazine appears (**Figure 3-3**). Indeed, in the **L** pathway of **Figure 3-3**, the MoFe protein is in the E_8 state at the binding of hydrazine and after, and thus FeMo-co is in a Kramers (half-integer-spin; odd-electron) spin state. As a result, no state on this pathway can correspond with the non-Kramers intermediate, **H**. (iii) We are left to conclude that **H** corresponds to the $[\text{NH}_2]^-$ -bound intermediate formed by N-N bond cleavage at the E_7 stage on the **P** pathway. By parallel arguments, the only possible assignment for the $S = 1/2$ state **I**, which we showed earlier to occur after N-N bond cleavage (8), is as E_8 : **I** must correspond to the final state in the catalytic process (**Figure 3-3**), in which the NH_3 product is bound to FeMo-co at its resting oxidation state, prior to release and regeneration of the resting-state form of the cofactor.

Although the above discussion focuses on the limiting version of the **L** pathway, the stabilization of bound substrate by prompt hydrogenation along the **P** pathway for N_2 reduction and the respective correspondences of **H** and **I** with E_7 and E_8 of this pathway greatly favor it over a version of the **L** pathway in which the reducing equivalents from E_4 are transferred to substrate at an intermediate stage of substrate reduction, E_{5-7} (**Figure 3-3**). The trapping of a product-bound intermediate **I** is analogous to the trapping of a bio-organometallic intermediate during turnover of the $\alpha\text{-70}^{\text{Val}\rightarrow\text{Ala}}$ MoFe protein with the alkyne, propargyl alcohol; this intermediate was shown to bind the allyl alcohol alkene product of reduction (21).

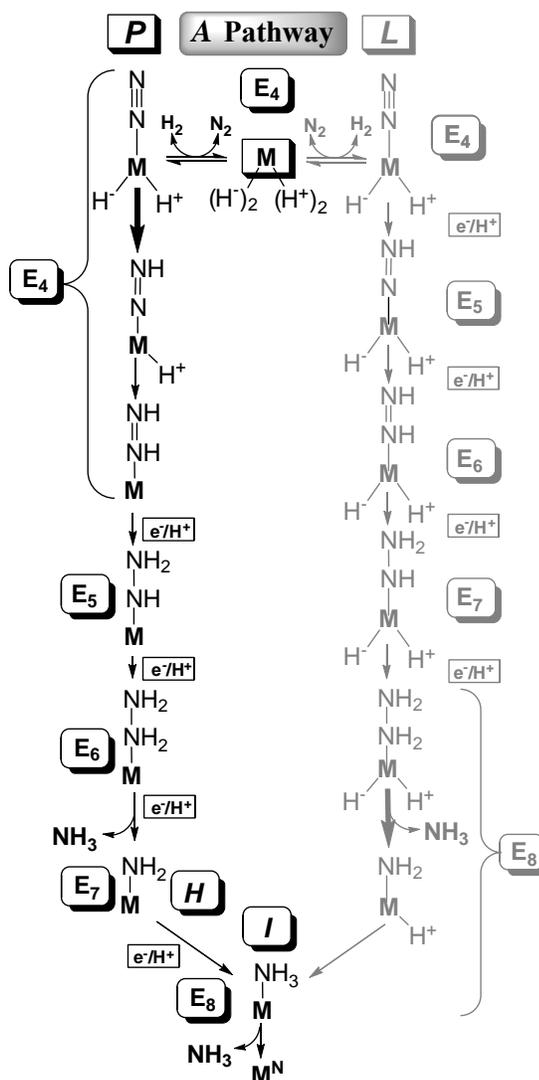


Figure 3-3. Integration of LT kinetic scheme with Alternating (A) pathways for N_2 reduction. *Note:* M denotes $FeMo-co$ in its entirety and substrate-derived species are drawn to indicate stoichiometry only; nothing is implied as to mode of substrate binding. Bold arrows indicate transfer to substrate of hydride remaining after N_2 binding in E_4 ; **P** represents ‘Prompt’ and **L** ‘Late’ transfer; as this pathway is ruled out by experiment, it is in gray. E_n states, $n = \text{even}$, are Kramers states; $n = \text{odd}$ are non-Kramers. M^N denotes resting-state $FeMo-co$. Individual charges are not assigned to M and any substrate fragment, but they sum to the charge on resting $FeMo-co$.

A final mechanistic question to be addressed is: how do the hydrogenated reaction intermediates, diazene and hydrazine, join the N_2 reduction pathway? Key to this issue is the finding that H_2 inhibits the reduction of diazene (22), but not hydrazine (23). We take that to mean that H_2 and diazene bind competitively, as do H_2 and N_2 (2, 5, 6), but that this is not the case for hydrazine. Provisionally, we further take the simplest view, that under turnover, diazene and hydrazine each join the N_2 reduction pathway at a their own characteristic entry point, and then proceeds to generate both ***H*** and ***I***. These two assumptions alone lead to the scheme of **Figure 3-4**. In this scheme, diazene binds to E_2 with the release of H_2 , and enters the N_2 pathway as the final form of the E_4 state. In contrast, N_2H_4 instead binds to E_1 , as is proposed for another two-electron substrate, C_2H_2 (2, 5, 6), and joins the N_2 pathway at a stage corresponding to E_7 in the N_2 reduction scheme.

The proposed identification of nitrogenous intermediate states ***H*** and ***I*** and their correlation with LT stages E_7 and E_8 , plus their incorporation in the ‘Prompt-Alternating’ pathway of **Figure 3-3**, represent a unification of the nitrogenase reaction pathway and the LT kinetic scheme into a draft mechanism for N_2 reduction by nitrogenase. We view this scheme as a ‘draft’ because of the numerous additional questions it poses. Among the key issues are the electron/proton ‘inventory’ that relates the redox levels of the substrate and metal-ion core, along with the site of protonation, in individual E_n states subsequent to N_2 binding. For example, consider reduction of N_2 to diazene at the E_4 stage. This is shown as occurring by hydride transfer followed by protonation, but there are other alternatives. Likewise, it is postulated in **Figure 3-3** that E_5 contains a diazenido ligand, yet there are alternative ways to form this species, as well as other formulations of that

Materials and Methods

Sample preparation followed freeze-quench procedures previously described (22, 24, 25); the 35 GHz CW (26) and pulsed (27) EPR spectrometers also have been described. Fourier transforms were performed with Bruker software, Win-EPR.

References

1. Christiansen J, Dean DR, Seefeldt LC (2001) Mechanistic features of the Mo-containing nitrogenase. *Annu Rev Plant Physiol Plant Mol Biol* 52:269-295.
2. Burgess BK, Lowe DJ (1996) Mechanism of molybdenum nitrogenase. *Chem Rev* 96:2983-3011.
3. Seefeldt LC, Hoffman BM, Dean DR (2009) Mechanism of Mo-dependent nitrogenase. *Annu Rev Biochem* 78:701-722.
4. Hoffman BM, Dean DR, Seefeldt LC (2009) Climbing nitrogenase: Towards the mechanism of enzymatic nitrogen fixation. *Acc Chem Res* 42:609-619.
5. Thorneley RNF, Lowe DJ (1985) Kinetics and mechanism of the nitrogenase enzyme system. *Molybdenum Enzymes*, ed Spiro TG (Wiley-Interscience, New York), Metal Ions in Biology, 7, pp 89-116.
6. Wilson PE, Nyborg AC, Watt GD (2001) Duplication and extension of the Thorneley and Lowe kinetic model for *Klebsiella pneumoniae* nitrogenase catalysis using a MATHEMATICA software platform. *Biophys Chem* 91:281-304.
7. Thorneley RNF, Eady RR, Lowe DJ (1978) Biological nitrogen fixation by way of an enzyme-bound dinitrogen-hydride intermediate. *Nature* 272:557-558.
8. Lukoyanov D, et al. (2011) ENDOR/HYSCORE studies of the common intermediate trapped during nitrogenase reduction of N_2H_2 , CH_3N_2H , and N_2H_4 support an alternating reaction pathway for N_2 reduction. *J Am Chem Soc* 133:11655-11664.
9. Yoo SJ, Angove HC, Papaefthymiou V, Burgess BK, Muenck E (2000) Moessbauer study of the MoFe protein of nitrogenase from *Azotobacter vinelandii* using selective ^{57}Fe enrichment of the M-centers. *J Am Chem Soc* 122(20):4926-4936.
10. Hendrich MP, Debrunner PG (1989) Integer-spin electron paramagnetic resonance of iron proteins. *Biophys J* 56:489-506.

11. Münck E, Surerus K, Hendrich MP (1993) Combining Mössbauer spectroscopy with integer spin electron paramagnetic resonance. *Methods Enzymol Part C* 227:463-479.
12. Hoffman BM, et al. (1994) ESEEM and ENDOR magnetic resonance studies of the non-Kramers doublet in the integer-spin diiron(II) forms of two methane monooxygenase hydroxylases and hemerythrin azide. *J Am Chem Soc* 116:6023-6024.
13. Fisher K, Newton WE, Lowe DJ (2001) Electron paramagnetic resonance analysis of different *Azotobacter vinelandii* nitrogenase MoFe-protein conformations generated during enzyme turnover: Evidence for S = 3/2 spin states from reduced MoFe-protein intermediates. *Biochemistry* 40:3333-3339.
14. Griffith JS (1963) Spin Hamiltonian for even-electron systems having even multiplicity. *Phys Rev* 132:316-319.
15. Hoffman BM (1994) ENDOR and ESEEM of a non-Kramers doublet in an integer-spin system. *J Phys Chem* 98:11657-11665.
16. Sturgeon BE, et al. (1997) Non-Kramers ESEEM of integer-spin diferrous carboxylate-bridged clusters in proteins. *J Am Chem Soc* 119:375-386.
17. Doan PE, Hoffman BM (2000) How important is parallel-mode EPR in electron spin echo envelope modulation studies of non-Kramers systems? *Inorg Chim Acta* 297:400-403.
18. Forgeron MAM, Wasylshen RE (2008) Molybdenum magnetic shielding and quadrupolar tensors for a series of molybdate salts: a solid-state ⁹⁵Mo NMR study. *Phys Chem Chem Phys* 10:574-581.
19. Lukoyanov D, Barney BM, Dean DR, Seefeldt LC, Hoffman BM (2007) Connecting nitrogenase intermediates with the kinetic scheme for N₂ reduction by a relaxation protocol and identification of the N₂ binding state. *Proc Natl Acad Sci USA* 104:1451-1455.
20. Lukoyanov D, Yang Z-Y, Dean DR, Seefeldt LC, Hoffman BM (2010) Is Mo involved in hydride binding by the four-electron reduced (E₄) intermediate of the nitrogenase MoFe protein? *J Am Chem Soc* 132:2526-2527.
21. Lee H-I, et al. (2004) An organometallic intermediate during alkyne reduction by nitrogenase. *J Am Chem Soc* 126:9563-9569.
22. Barney BM, et al. (2007) Diazene (HN=NH) is a substrate for nitrogenase: Insights into the pathway of N₂ reduction. *Biochemistry* 46:6784-6794.

23. Davis LC (1980) Hydrazine as a substrate and inhibitor of *Azotobacter vinelandii* nitrogenase. *Arch Biochem Biophys* 204:270-276.
24. Barney BM, et al. (2005) Trapping a hydrazine reduction intermediate on the nitrogenase active site. *Biochemistry* 44:8030-8037.
25. Barney BM, et al. (2006) A methyldiazene (HN=N-CH₃)-derived species bound to the nitrogenase active-site FeMo cofactor: Implications for mechanism. *Proc Natl Acad Sci USA* 103:17113-17118.
26. Werst MM, Davoust CE, Hoffman BM (1991) Ligand spin densities in blue copper proteins by Q-band ¹H and ¹⁴N ENDOR spectroscopy. *J Am Chem Soc* 113:1533-1538.
27. Zipse H, et al. (2009) Structure of the nucleotide radical formed during reaction of CDP/TTP with the E441Q-a2b2 of *E. coli* ribonucleotide reductase. *J Am Chem Soc* 131:200-211.

CHAPTER 4

IS MO INVOLVED IN HYDRIDE BINDING BY THE FOUR-ELECTRON REDUCED
(E₄) INTERMEDIATE OF THE NITROGENASE MOFE PROTEIN?⁴

The X-ray structure¹ of the nitrogenase² molybdenum-iron (MoFe) protein reveals the active-site FeMo-cofactor (FeMo-co) to be an unprecedented [Fe₇S₉MoX; homocitrate] cluster, **Figure 4-1**, but does not define the location of substrate binding and reduction. Mo is an obvious candidate, as it is the catalytic metal in the only known inorganic metal complexes that catalytically reduce N₂.³ However, Fe is no less a candidate, given that it is the catalytic metal in the commercial Haber-Bosch process for NH₃ formation and that there are V and Fe nitrogenases that reduce N₂ but do not have Mo.⁴

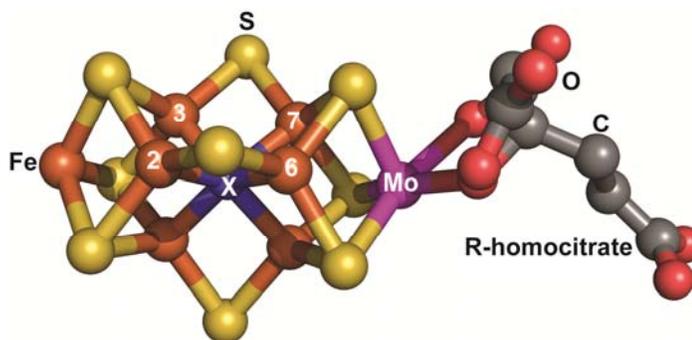


Figure 4-1. FeMo-co from PDB coordinate file 1M1N.pdb: Fe, rust; Mo, magenta; S, yellow; C, dark gray; O, red; X, blue.

⁴ Reproduced with permission from [Dmitriy Lukoyanov, Zhi-Yong Yang, Dennis R. Dean, Lance C. Seefeldt, and Brian M. Hoffman (2010) *Journal of The American Chemical Society* **132**(8), 2526-2527]. Copyright [2010] American Chemical Society.

Recent studies revealed the importance of substrate interactions at the 4Fe-4S face of FeMo-co defined by Fe atoms 2, 3, 6, and 7. Of particular importance, increasing the size of the sidechain of residue α -70^{Val}, which lies over Fe6, by substitution with isoleucine leaves the reactivity of FeMo-co toward proton reduction unaltered, but severely restricts the reduction of nitrogenous and alkyne substrates.^{5,6} Although the changed substrate preferences of the α -70^{Ile} variant implicate Fe as the site of substrate binding, they do not preclude migration of substrate-derived moieties between metal atoms during reduction. As a result, we have initiated studies that directly probe the involvement of Mo during catalytic turnover.

The resting state wild type (WT) MoFe protein (E_0) shows a rhombic EPR spectrum from $S = 3/2$ FeMo-co that is conventionally treated in terms of a fictitious spin $S' = 1/2$ with g -tensor, $\mathbf{g}' = [4.32, 3.64, 2.0]$. When the α -70^{Ile} MoFe protein is freeze-trapped during H^+ reduction under Ar, the majority of its E_0 EPR signal disappears and is replaced by the $S = 1/2$ signal ($g_{\parallel} = 2.15, g_{2,3} = 2.01, 1.97$) of an intermediate that has been shown to be the pivotal E_4 MoFe state that is activated for N_2 binding and reduction through the accumulation of 4 electrons/protons by FeMo-co.^{7,8} ENDOR studies of E_4 showed that it contains two hydrides bound to FeMo-co.⁹ We here report a ⁹⁵Mo ENDOR study that determines whether Mo is involved in hydride binding.

The bound hydrides of E_4 have a large isotropic hyperfine coupling, $a_{iso} \approx 24$ MHz and an anisotropic contribution, $\mathbf{T} = \pm[-13.3, 0.7, 12.7]$ MHz, that exhibits almost complete rhombicity, defined by the form, $\mathbf{T}_{rh} \approx \pm[t, 0, -t]$. This form rules out terminal hydrides, which would have a roughly axial \mathbf{T} ,¹⁰ and suggests that the bound hydrides

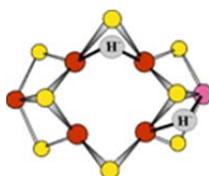


Chart 4-1. Representative hydride bridging modes.

bridge two metal ions,¹¹ as Fe-H-Fe and/or Mo-H-Fe fragments (**Chart 4-1**), with Mo-H-Fe₆ suggested by the indications that Fe₆ participates in binding alkyne substrates.^{5,6}

Equations presented earlier for the anisotropic hyperfine interaction matrix, **T**, of a nucleus that undergoes through-space dipolar interactions to the two metal ions of a spin-coupled dinuclear center¹² are straightforwardly generalized to describe an M₁-H-M₂ fragment in which M₁, M₂ are part of the multi-metallic spin-coupled FeMo-co center. For a given M₁-H-M₂ geometry, the components of **T** become a function of the coefficients [*K*₁, *K*₂] that describe the projection of the total cluster spin on the local metal-ion spins. These equations are now applied to E₄.

Consider a hydride bound as a Mo-H-Fe fragment with the 2.7 Å Mo-Fe separation characteristic of FeMo-co and Fe-H and Mo-H bond-lengths of ~ 1.66 Å and ~ 1.78 Å respectively, the most probable values for all Fe-H-M and Mo-H-M fragments in the Cambridge Structural Database. The observed **T** of E₄ can be matched only for [*K*_{Fe}, *K*_{Mo}] ~ ±[0.4-0.5, 0.4-0.3] and ~ ±[~0.3, -0.2], values that do not vary substantially with bond lengths. In short, Mo involvement in the hydride binding would require |*K*_{Mo}| ≥ 0.2. The *K* for an ion can be experimentally measured as the ratio of the isotropic hyperfine coupling, *a*_{iso}, for the spin-coupled metal ion to *a*_{iso}⁰, that for the ion in the absence of spin coupling: $K = a_{iso}/a_{iso}^0$. We here determine *K*_{Mo} for the E₄ intermediate state through

ENDOR measurements of ^{95}Mo enriched MoFe protein, further comparing the results with those for the E_0 resting state.

The EPR spectrum of α -70^{lle} MoFe in its E_0 state shows two $S = 3/2$ E_0 signals: one with $g_1(a)' = 4.36$ ($S' = 1/2$) corresponds to the signal for WT enzyme; the other has a slightly higher value, $g_1(b)' = 4.53$. These signals have been assigned to alternate conformations of amino acids near FeMo-co.^{5,6}

Early ^{95}Mo CW X-band ENDOR measurements indicated that resting-state WT MoFe protein contains a diamagnetic Mo(IV), an assignment based on its small hyperfine coupling, $a_{iso} \approx 6$ MHz (expressed in terms of the true, $S = 3/2$) and its quadrupolar interaction.¹³ **Figure 4-2, left**, shows 35 GHz Davies pulsed ENDOR¹⁴ signals collected¹⁵ at g_1' from the resting-state α -70^{lle} MoFe protein with ^{95}Mo in natural-abundance (15.8%) and isotopically enriched ($\sim 95\%$ ^{95}Mo).¹⁶ As the signals are ~ 6 times stronger for the enriched sample they can be assigned, as before, to the $m_I = \pm 1/2$ transitions of ^{95}Mo ($I = 5/2$).

The ^{95}Mo spectrum from α -70^{lle} MoFe protein collected at $g_1(b)' = 4.53$ shows a ν_+/ ν_- doublet ($\nu_{\pm} = |\pm A'/2 + \nu_{\text{Mo}}|$) associated with the perturbed (b) conformation; it is centered at an effective hyperfine coupling, $A'(b)/2 = 7.01$ MHz, and split by $2\nu_{\text{Mo}}$, which is larger than the intrinsic value for the ^{95}Mo Larmor frequency, $2\nu_{\text{Mo}}^0$. The difference, $(\nu_{\text{Mo}}^0 - \nu_{\text{Mo}})$, is caused by the pseudo-nuclear Zeeman effect and can be used to calculate the zero-field splitting (Δ) between the ground $m_S = \pm 1/2$ and excited $m_S = \pm 3/2$ doublets of the $S = 3/2$ state:¹⁷ $\Delta(b) = 9.6 \text{ cm}^{-1}$, notably less than $\Delta = 12.5 \text{ cm}^{-1}$ previously reported for WT enzyme.¹⁷

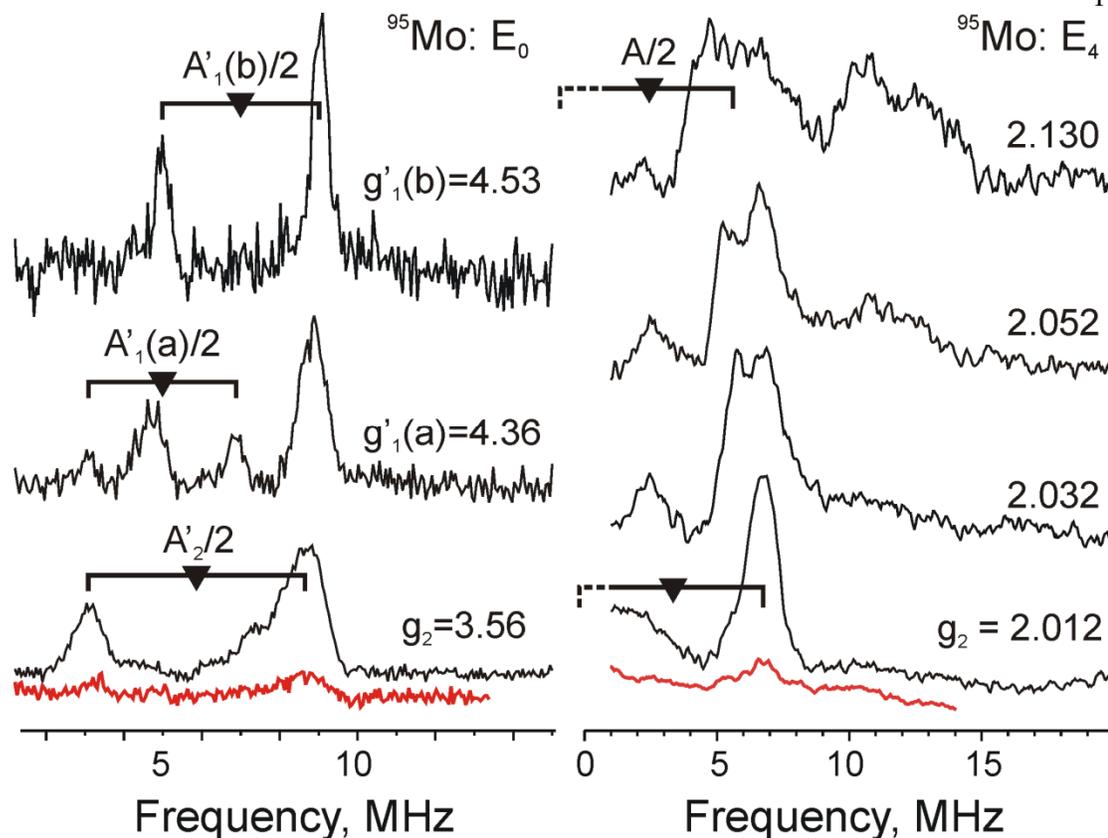


Figure 4-2. (Left) Davies ^{95}Mo -ENDOR spectra of ^{95}Mo -enriched (black) and natural-abundance (red) α -70 $^{116}\text{MoFe}$ protein in the resting state. (Right) CW ^{95}Mo -ENDOR spectra of ^{95}Mo -enriched (black) and natural-abundance (red) α -70 $^{116}\text{MoFe}$ protein in E_4 intermediate state. Brackets in left and right patterns indicate frequencies for ν_{\pm} doublets, as described in text. *Conditions.* $T = 2$ K. *Pulsed:* microwave frequency, ~ 34.78 GHz, Davies sequence, $\pi/2 = 40$ ns, $\tau = 600$ ns, RF 40 μs , random hop acquisition, 2 K, 350-1500 scans. *CW:* microwave frequency, ~ 35.1 GHz; modulation amplitude, 4 G; time constant, 64 ms; RF sweep speed, 1 MHz/sec; RF bandwidth -broadened to 100 kHz.

When the field is increased to $g_1(a)' = 4.36$, the (b) doublet persists with little change in coupling while a doublet from the (a) conformer appears (**Figure 4-2**). Its hyperfine coupling, $A'(a)/2 = 4.98$ MHz, and the zero-field splitting $\Delta(a) = 11.8$ cm⁻¹ are essentially the same as for WT enzyme. Correction of the ⁹⁵Mo hyperfine couplings (A' ; $S' = 1/2$) at g_1' to those for the true $S = 3/2$ spin ($A = (g_e/g_1')A'$) yields, $A(a) = 4.57$ MHz, $A(b) = 6.19$ MHz. Spectra collected across the EPR spectrum of WT MoFe protein show the hyperfine coupling to be roughly isotropic, with $a_{iso} \approx 6$ MHz ($S = 3/2$);¹³ a similar set of spectra for the (a) conformation of the α -70^{Ile} variant yields an equivalent value, while that for the (b) conformation is larger, ~ 7 MHz. Surprisingly, this increase is larger than that for the $\Delta NifV$ mutant,¹³ which contains a FeMo-co with homocitrate replaced by citrate.¹ These measurements thus reveal that structural perturbations in the vicinity of Fe6 caused by the α -70^{Val→Ile} modification are sensed at Mo.

Figure 4-2, right, shows 35 GHz CW ENDOR spectra¹⁸ of ⁹⁵Mo-enriched intermediate E₄ obtained at several g -values. The signals seen with the enriched sample again can be assigned to ⁹⁵Mo from their absence in natural-abundance spectra. The ⁹⁵Mo spectrum obtained at $g_2 = 2.012$ shows a sharp ν_+ feature associated with an $m_1 = \pm 1/2$, doublet centered $A/2 = 3$ MHz (true $S = 1/2$) and split by $2\nu_{Mo}^0$; the ν_- feature falls at ~ 0 MHz and is not detected. As the g -value of observation is increased, the ν_+ feature moves to lower frequency; it first splits, then broadens, with the coupling decreasing to $A/2 \sim 1.5$ MHz by $g \sim g_{||}$; in addition, satellite transitions associated with $m_1 = \pm 3/2, 5/2$ transitions appear and increase in frequency. Regardless of whether the observed splitting arises from hyperfine anisotropy or from the presence of two conformers, simulations show that the isotropic ⁹⁵Mo coupling is $a_{iso} \approx 4$ MHz, *less* than that for the resting state.

The decrease in a_{iso} for ^{95}Mo of E_4 from the already small value in resting state MoFe protein strongly suggests that the resting Mo(IV) is not one-electron reduced during the accumulation of the four electrons of E_4 . In any case, the effective K for Mo is very small; a value, $a_{iso}^0 \geq 100$ MHz is indicated by studies of mononuclear Mo complexes^{19,20} and yields for E_4 an effective spin-coupling coefficient no greater than, $|K_{\text{Mo}}| = |a_{iso}/a_{iso}^0| \leq 0.04$, at least 5-fold less than the lower bound, $|K_{\text{Mo}}| \geq 0.2$ required for Mo to be involved in forming a Mo-H-Fe, hydride. As the hydride couplings also are both far too large, given the value of $|K_{\text{Mo}}|$, and of the wrong symmetry to be associated with a terminal hydride on Mo,¹⁰ we may thus conclude that Mo does *not* participate in binding a hydride of the catalytically central E_4 intermediate, and that only Fe ions are involved. Nonetheless, the response of the Mo coupling to subtle conformational changes in E_0 and to the formation of E_4 suggest that Mo is intimately involved in tuning the geometric and electronic properties of FeMo-co in these states. Similar investigations of Mo involvement in other intermediates are planned.

REFERENCES

- (1) Rees, D. C.; Tezcan, F. A.; Haynes, C. A.; Walton, M. Y.; Andrade, S.; Einsle, O.; Howard, J. B. *Phil. Trans. R. Soc. A* **2005**, *363*, 971-984.
- (2) Burgess, B. K.; Lowe, D. J. *Chem. Rev.* **1996**, *96*, 2983-3011.
- (3) Schrock, R. R. *Acc. Chem. Res.* **2005**, *38*, 955-962.
- (4) Eady, R. R. *Chem. Rev.* **1996**, *96*, 3013-3030.
- (5) Igarashi, R. Y.; Dos Santos, P. C.; Niehaus, W. G.; Dance, I. G.; Dean, D. R.; Seefeldt, L. C. *J. Biol. Chem.* **2004**, *279*, 34770-34775.
- (6) Seefeldt, L. C.; Hoffman, B. M.; Dean, D. R. *Annu. Rev. Biochem.* **2009**, *78*, 701-722.

- (7) Lukoyanov, D.; Barney, B. M.; Dean, D. R.; Seefeldt, L. C.; Hoffman, B. M. *Proc. Natl. Acad. Sci. U.S.A.* **2007**, *104*, 1451-1455.
- (8) Hoffman, B. M.; Dean, D. R.; Seefeldt, L. C. *Acc. Chem. Res.* **2009**, *42*, 609-619.
- (9) Igarashi, R. Y.; Laryukhin, M.; Santos, P. C. D.; Lee, H.-I.; Dean, D. R.; Seefeldt, L. C.; Hoffman, B. M. *J. Am. Chem. Soc.* **2005**, *127*, 6231-6241.
- (10) Kinney, R. A.; Hettterscheid, D. G. H.; Hanna, B. S.; Schrock, R. R.; Hoffman, B. M. *Inorg. Chem.* **2010**, *49*, 704-713.
- (11) DeRose, V. J.; Liu, K. E.; Kurtz, D. M., Jr.; Hoffman, B. M.; Lippard, S. J. *J. Am. Chem. Soc.* **1993**, *115*, 6440-6441.
- (12) Willems, J.-P.; Lee, H.-I.; Burdi, D.; Doan, P. E.; Stubbe, J.; Hoffman, B. M. *J. Am. Chem. Soc.* **1997**, *119*, 9816-9824.
- (13) Venters, R. A.; Nelson, M. J.; McLean, P. A.; True, A. E.; Levy, M. A.; Hoffman, B. M.; Orme-Johnson, W. H. *J. Am. Chem. Soc.* **1986**, *108*, 3487-3498.
- (14) Schweiger, A.; Jeschke, G. *Principles of Pulse Electron Paramagnetic Resonance*; Oxford University Press: Oxford, UK, 2001.
- (15) Zipse, H.; Artin, E.; Wnuk, S.; Lohman, G. J. S.; Martino, D.; Griffin, R. G.; Kacprzak, S.; Kaupp, M.; Hoffman, B.; Bennati, M.; Stubbe, J.; Lees, N. *J. Am. Chem. Soc.* **2009**, *131*, 200-211.
- (16) *Azotobacter vinelandii* strain DJ1373 was grown and nitrogenase was expressed and purified as described previously (Ref 9), except that $^{95}\text{MoO}_4^{2-}$ was used in the growth media. ^{95}Mo metal (>95%) was heated to 600°C, and the condensed crystals of $^{95}\text{MoO}_3$ were dissolved in 5 M NaOH, yielding $^{95}\text{MoO}_4^{2-}$.
- (17) True, A. E.; Nelson, M. J.; Venters, R. A.; Orme-Johnson, W. H.; Hoffman, B. M. *J. Am. Chem. Soc.* **1988**, *110*, 1935-1943.
- (18) Werst, M. M.; Davoust, C. E.; Hoffman, B. M. *J. Am. Chem. Soc.* **1991**, *113*, 1533-1538.
- (19) Averill, B. A.; Orme-Johnson, W. H. *Inorg. Chem.* **2002**, *19*, 1702-1705.
- (20) Wilson, G. L.; Greenwood, R. J.; Pilbrow, J. R.; Spence, J. T.; Wedd, A. G. *J. Am. Chem. Soc.* **2002**, *113*, 6803-6812.

CHAPTER 5

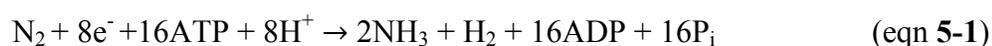
ACETYLENE INTERCEPTION OF INTERMEDIATES REVEALS IMPORTANT
ROLES OF METAL HYDRIDES IN NITROGENASE CATALYSIS⁵**Abstract**

Nitrogenase accumulates four electrons/protons on its active site FeMo-cofactor (designated E₄) before N₂ binds, with subsequent addition of four more electrons/protons to yield two NH₃ and one H₂. It has recently been demonstrated that the E₄ state of FeMo-cofactor contains two iron bridged hydrides (Fe-H-Fe), offering an explanation for how electrons and protons are accumulated on FeMo-cofactor and suggesting a key role for metal hydrides in the substrate reduction mechanism. Here, it is demonstrated that FeMo-cofactor can be loaded with deuterides (Fe-D-Fe) from D₂ by turning over nitrogenase under N₂ and D₂ and that this state can be intercepted by the substrate acetylene, yielding mono- and di-deuterated ethylene (C₂H₃D and C₂H₂D₂) as products. Observation of these products provides direct experimental confirmation for a proposed reductive elimination mechanism of N₂ reduction catalyzed by nitrogenase that involves metal hydrides. Moreover, these results reveal the direct involvement of metal hydride in hydrogenation of substrates.

⁵ Coauthored by Zhi-Yong Yang, Nimesh Khadka, Dmitriy Lukoyanov, Brian M. Hoffman, Dennis R. Dean, and Lance C. Seefeldt, *manuscript in preparation*.

Introduction

Biological nitrogen fixation — the reduction of dinitrogen (N₂) to two ammonia (NH₃) molecules — is primarily catalyzed by the Mo-dependent nitrogenases (1–6). These enzymes comprise an electron-delivery Fe protein and MoFe protein, carrier of the catalytic FeMo-cofactor. The nitrogenase catalyzed reaction has a limiting stoichiometry as shown in equation **5-1** (1, 7).



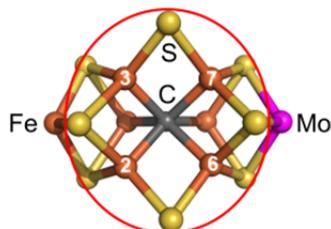
This equation conveys one of the most puzzling aspects of nitrogenase function, the obligatory formation of one H₂ per mole of N₂ reduced, resulting in the apparent ‘waste’ of two reducing equivalents and four ATP (1, 7–9). A kinetic framework for nitrogenase function that incorporates the stoichiometry of **eqn. 5-1** is provided by the Lowe-Thorneley (LT) model (1, 8, 10), which describes transformations among catalytic intermediates (denoted E_{*n*}) where *n* is the number of electrons and protons (*n* = 0–8) delivered to MoFe protein. N₂ binding is coupled to H₂ production and requires activation of the MoFe protein to the key E₄ state, in which FeMo-cofactor has accumulated four electrons and four protons, which are stored as two hydrides that bridge Fe atoms (Fe–H–Fe) and two protons putatively bound to sulfide (**Figure 5-1**) (11–14).

We recently presented a draft mechanism for nitrogen fixation whose keystone is a proposed reason for obligatory H₂ production (5). H₂ is produced by reductive elimination (15–18) of the two bridging hydrides of E₄ during N₂ binding (**Figure 5-1**) (5). This yields N₂ bound to doubly reduced FeMo-cofactor with two protons, and thereby is activated to promptly deliver two e⁻/H⁺ to N₂, generating diazene (HN=NH) bound to FeMo-cofactor (5). The reductive activation of FeMo-cofactor for N₂ binding

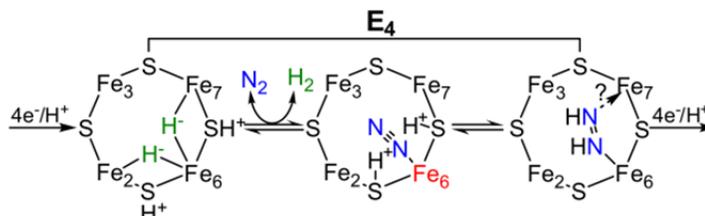
and reduction that thus underlies obligatory H₂ formation (i) provides a compelling rationale for the *apparently* wasteful stoichiometry of **eqn. 5-1** and (ii) uniquely satisfies key constraints imposed by turnover under N₂ plus D₂ or T₂ (1, 19–26). In particular, although D₂ or T₂ do not by themselves react with nitrogenase during turnover, as schematized in **Figure 5-1**, they can be incorporated into FeMo-cofactor during reduction of N₂ by reversing the N₂ binding equilibrium (27), reacting with FeMo-cofactor to release N₂ and generate the (Fe-(D⁻/T⁻)-Fe)₂ E₄ intermediate, which can relax in two steps to form two HD or HT *without* D⁺/T⁺ exchange with solvent (5, 19).

This reductive elimination (*re*) mechanism for H₂ release upon N₂ binding (**Figure 5-1B**) makes *testable* predictions. As indicated in **Figure 5-1C**, this mechanism predicts that during turnover under D₂/N₂, reaction of the E₄[N₂/N₂H₂] intermediate with D₂ would generate dideutero-E₄ (E₄(2D)), which can relax to monodeutero-E₂ (E₂(D)) with loss of HD (5, 28). Neither of these two deuterated enzymatic intermediates could otherwise form in H₂O buffer, as D₂ does not react with nitrogenase during reduction of any other substrate than N₂ (19, 26, 29). As indicated in **Figure 5-1C**, the formation of E₂(D) and E₄(2D) might be revealed by intercepting them with the non-physiological substrate acetylene (C₂H₂) (30, 31) to generate deuterated ethylenes (C₂H₃D and C₂H₂D₂, respectively). There is no report on the production of deuterated ethylenes from reduction of acetylene in the presence of D₂ (1), thus the formation of these deuterated ethylenes during turnover under C₂H₂/D₂/N₂ would thus provide definitive support for the reductive elimination mechanism.

A FeMo-cofactor



B Reductive elimination mechanism



C Deuteration of acetylene

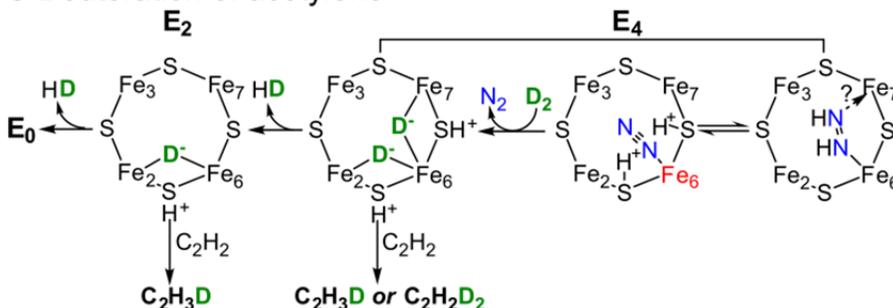


Figure 5-1. FeMo-cofactor and key mechanistic steps. **(A)** FeMo-cofactor inorganic core with Mo in magenta, Fe in rust, S in yellow, and C in gray. The structure and numbering of Fe atoms are based on the protein database file PDB:1M1N. The face composed of Fe atoms 2, 3, 6, and 7 is noted with a red circle. **(B)** Proposed reductive elimination (*re*) mechanism for N_2 binding at E_4 with reductive elimination of H_2 and hydrogenation of N_2 to generate a metal bound diazene intermediate. Colors are N in blue and H in green. Fe_6 in red indicates the Fe^0 valence state. **(C)** Predicted steps for the N_2 -dependent formation of 2HD (right to left) during relaxation of $E_4(2D)$ formed by D_2 displacement of N_2 . The possible interception of the key $E_4(2D)$ and $E_2(D)$ intermediates by acetylene to produce C_2H_3D and $C_2H_2D_2$ is shown.

Results

The earlier finding that HD is formed during turnover of nitrogenase under a mixture of D_2/N_2 , but not under D_2 alone (20–23, 25), can be explained by the *re* mechanism in which N_2 is displaced from the $E_4[N_2/N_2H_2]$ intermediate by D_2 (**Figure 1**) (5, 23), which undergoes oxidative addition to form the $E_4(2D)$ state containing two Fe-bridging deuterides (Fe-D-Fe) that are not exchangeable with solvent (11). In the absence of reactions with other substrates, this intermediate could then relax to the resting E_0 level in a two-step process: (i) release of HD to form $E_2(D)$; (ii) release of a second HD to form E_0 . The $E_4(2D)$ and $E_2(D)$ deuterated intermediates of **Figure 5-1** are unique to the *re* mechanism (5), and in an attempt to intercept them, and thereby reveal their presence, turnover conditions were created that favor HD formation (0.25 atm N_2 and 0.7 atm D_2) (20), but included a small amount of ^{13}C -acetylene (typically 0.02 atm). As illustrated in **Figure 5-1** and discussed below in detail, reduction of C_2H_2 by $E_4(2D)$ and $E_2(D)$ are predicted to yield $C_2H_2D_2$ and C_2H_3D , respectively. These studies employed $^{13}C_2H_2$ as the starting material to avoid confusion from the small but significant natural abundance of ^{13}C (1.07%) (32) in acetylene.

Most of the ethylene formed in both the presence and absence of N_2 or D_2 is $^{13}C_2H_4$, which is detected by mass spectrometry (MS) as a peak with mass/charge (m/z) of 30, following separation from other gases by gas chromatography (GC). The ethylene clearly forms by the normal acetylene reduction process, with the two solvent protons added to C_2H_2 coming from solvent without intervention of D_2 or N_2 . However, deuterated ethylenes were also formed with the full $^{13}C_2H_2/D_2/N_2$ reaction mixture. As expected from prior work, they were not formed when N_2 was not included (**Figure 5-2**).

A substantial amount of mono-deuterated ethylene ($^{13}\text{C}_2\text{H}_3\text{D}$; $m/z = 31$) was detected, a species that can only have been produced by $^{13}\text{C}_2\text{H}_2$ intercepting $\text{E}_2(\text{D})$ or $\text{E}_4(2\text{D})$ (**Figure 5-1**). The rate of $^{13}\text{C}_2\text{H}_3\text{D}$ formation was found to be ~ 27 nmol $\text{C}_2\text{H}_3\text{D}/\text{nmol MoFe}$ protein over 20 min, about 2% of the amount of $^{13}\text{C}_2\text{H}_4$ generated. Also detected was a product with m/z of 32, corresponding to $^{13}\text{C}_2\text{H}_2\text{D}_2$ (**Figure 5-2**), with a lower, though still significant production rate of ~ 1.9 nmol $^{13}\text{C}_2\text{H}_2\text{D}_2/\text{nmol MoFe}$ protein over 20 min. This species can only have been produced by $^{13}\text{C}_2\text{H}_2$ intercepting $\text{E}_4(2\text{D})$ (**Figure 5-1**), the intermediate formed through N_2 replacement by D_2 , which oxidatively adds to FeMo-cofactor (5).

Reduction of acetylene and N_2 are mutually exclusive, with complicated inhibition kinetics between these two substrates (33). Therefore, it was of interest to determine the effect of varying the C_2H_2 partial pressure on the formation of $\text{C}_2\text{H}_3\text{D}$ and $\text{C}_2\text{H}_2\text{D}_2$ at a fixed N_2 and D_2 concentration. As the partial pressure of C_2H_2 is increased, the amounts of $\text{C}_2\text{H}_3\text{D}$ and $\text{C}_2\text{H}_2\text{D}_2$ both decrease as a fraction of the total acetylene reduction, with a stronger decrease in the production of $\text{C}_2\text{H}_3\text{D}$ (**Figure 5-3**). The overall suppression of deuterated ethylene products can be understood as the result of increased capture by C_2H_2 of less reduced states than $\text{E}_4[\text{N}_2/\text{N}_2\text{H}_2]$, thereby preventing the formation of this state and its reaction with D_2 , which leads to the creation of deuterated ethylenes. However, with increasing C_2H_2 concentration, the $\text{E}_4(2\text{D})$ that nonetheless does form will react with increasing C_2H_2 , somewhat ameliorating the suppression of $\text{C}_2\text{H}_2\text{D}_2$. This process would further suppress $\text{C}_2\text{H}_3\text{D}$ production, as it competes with HD release by $\text{E}_4(2\text{D})$ to form the $\text{E}_2(\text{D})$ state whose reaction with C_2H_2 generates $\text{C}_2\text{H}_3\text{D}$.

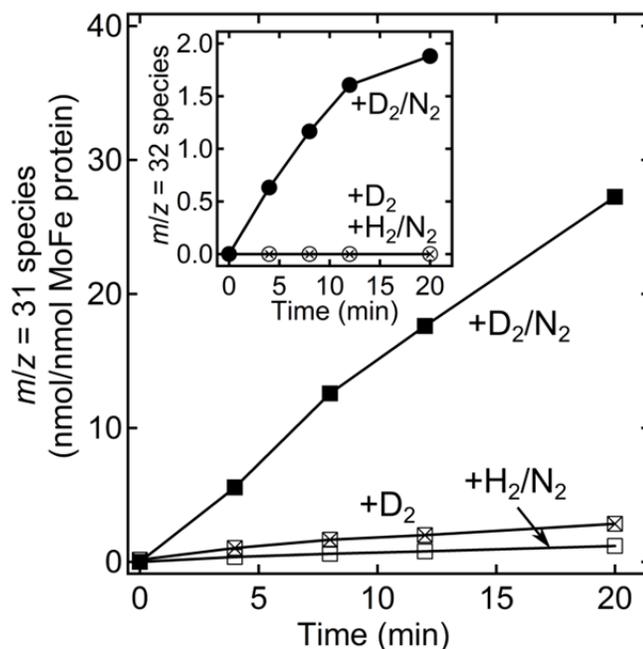


Figure 5-2. Time-dependent formation of mono- and di-deutero ^{13}C -ethylene catalyzed by nitrogenase. Shown is the formation of monodeutero- ^{13}C -ethylene ($^{13}\text{C}_2\text{H}_3\text{D}$) as a function of time determined by GC/MS monitoring of $m/z = 31$ starting with $^{13}\text{C}_2\text{H}_2$ and including D_2 and N_2 (■), just D_2 (⊠), or H_2 and N_2 (□). The inset shows the formation of dideutero- ^{13}C -ethylene ($^{13}\text{C}_2\text{H}_2\text{D}_2$, $m/z = 32$) monitored at $m/z = 32$ starting with $^{13}\text{C}_2\text{H}_2$ and including D_2 and N_2 (●), just D_2 (⊗), or H_2 and N_2 (○). The assays were conducted with partial pressures of 0.02 atm $^{13}\text{C}_2\text{H}_2$, 0.25 atm N_2 , and 0.7 atm H_2/D_2 , where present. The molar ratio between Fe protein and MoFe protein was 2:1. All assays were incubated at 30°C.

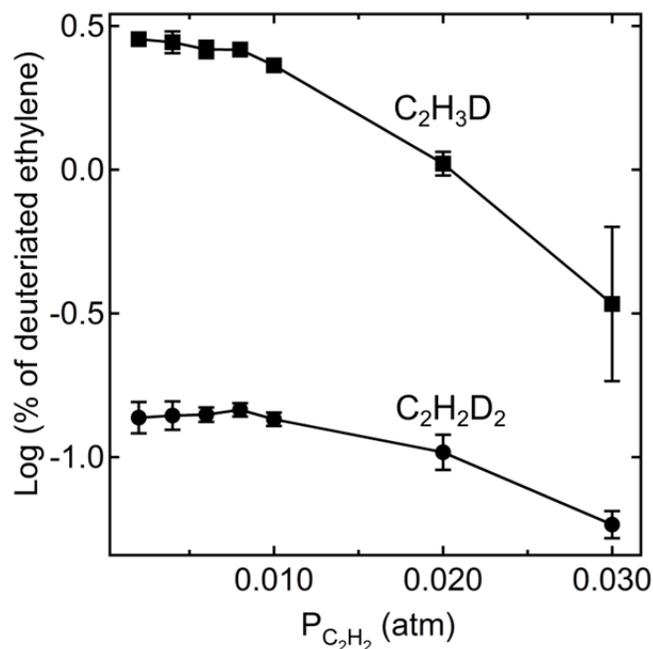


Figure 5-3. Deuterated ethylene formation as a function of acetylene partial pressure.

The log of the percentage of maximum formation of monodeuterated (C_2H_3D) or dideuterated ($C_2H_2D_2$) ethylene is plotted as a function of the partial pressure of acetylene.

The partial pressure of D_2 was 0.7 atm and the partial pressure of N_2 was 0.2 atm. The molar ratio of Fe protein and MoFe protein was 4:1. Assay conditions as in Figure 2, except all assays were incubated at 30°C for 60 min.

Davis *et al.* showed that increasing the partial pressure of H_2 increasingly diverts nitrogenase from reduction of N_2 to reduction of C_2H_2 (34), an observation interpreted as resulting from increased reaction of H_2 with $E_4[N_2/N_2H_2]$, displacing N_2 and suppressing the formation of NH_3 . The *re* mechanism further predicts that in the presence of D_2 , the displacement of N_2 generates $E_4(2D)$, which can release HD to form $E_2(D)$ (**Figure 5-1**); reaction of C_2H_2 with those deuterated E-states would yield $C_2H_2D_2$ and C_2H_3D ,

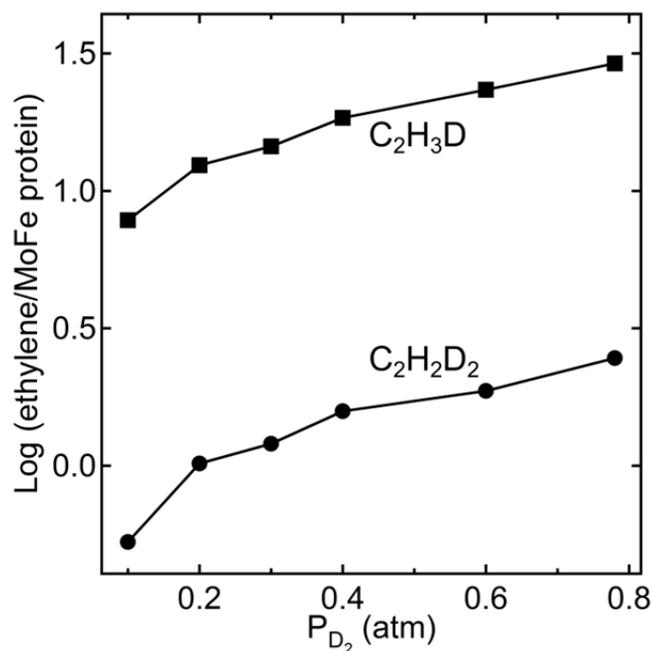


Figure 5-4. Deuterated ethylene formation as a function of D_2 partial pressure. The amounts of C_2H_3D and $C_2H_2D_2$ formed versus the partial pressure of D_2 are shown. The partial pressure of C_2H_2 and N_2 were 0.02 and 0.2 atm, respectively. The molar ratio of Fe protein to MoFe protein was 4:1. Assay conditions as in **Figure 5-3**.

respectively, as described in the previous paragraph. Correspondingly, as shown in **Figure 5-4**, the formation of both C_2H_3D and $C_2H_2D_2$ increase in parallel with increasing D_2 partial pressure, as expected from this analysis.

The yield of C_2H_3D and $C_2H_2D_2$ similarly increase in parallel with increasing partial pressure of N_2 (**Figure 5-5**). This can be explained by enhanced formation of $E_4[N_2/N_2H_2]$ by reaction of N_2 with E_4 . Increased formation of $E_4[N_2/N_2H_2]$ in turn would enhance reaction with D_2 to form $E_4(2D)$, which can be intercepted by acetylene to form deuterated ethylenes (**Figure 5-1**). These observations from N_2 and D_2 partial pressure

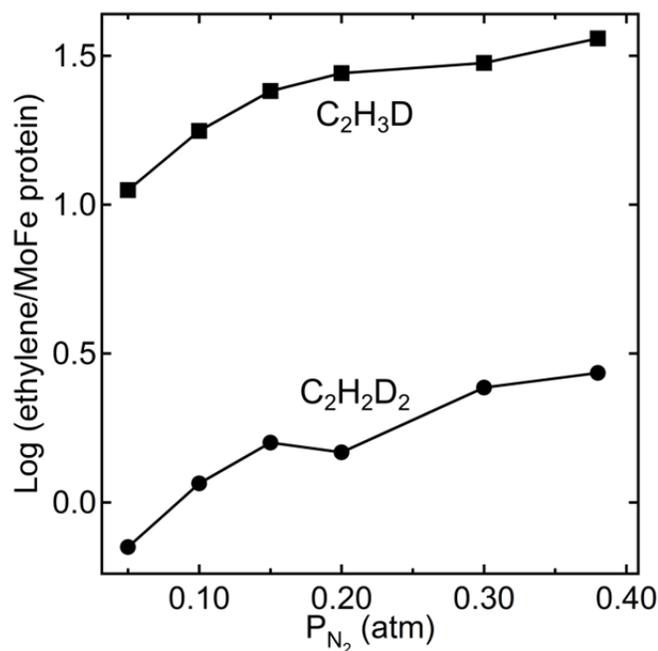


Figure 5-5. Deuterated ethylene formation as a function of N_2 partial pressure. The amounts of C_2H_3D and $C_2H_2D_2$ formed as a function of the partial pressure of N_2 is shown. The partial pressure of C_2H_2 was 0.02 atm and D_2 was 0.6 atm. The molar ratio of Fe protein to MoFe protein was 4:1. All assays were incubated at 30°C for 60 min.

studies is consistent the previous observation of the effects of N_2 and D_2 partial pressure on HD formation reaction (20–22).

The rate of electron flow through nitrogenase (called electron flux) is known to affect product distribution for other substrates (1). The electron flux is easily controlled by altering the molar ratio of Fe protein to MoFe protein ($[Fe\text{ protein}]:[MoFe\text{ protein}]$), the electron flux increasing with this ratio. In earlier studies, it was observed that varying the electron flux affects the HD formation rate (20). The current experiments show that as the flux is increased from 2:1 to 32:1 in the presence of $C_2H_2/D_2/N_2$ (0.02 atm C_2H_2 , 0.68

atm D_2 , and 0.3 atm N_2), the amounts of the two deuterated ethylene products decrease with a stronger effect on the $C_2H_2D_2$ than that on the C_2H_3D in the lower electron flux range (**Figure 5-6**). This observation is consistent with the higher flux enhancing electron delivery to the $E_4[N_2/N_2H_2]$ intermediate, sending it along the catalytic pathway to NH_3 production and thus shortening the window-time for the formation of $E_4(2D)$ intermediate and competitively decreasing the formation of the deuterated ethylenes (20).

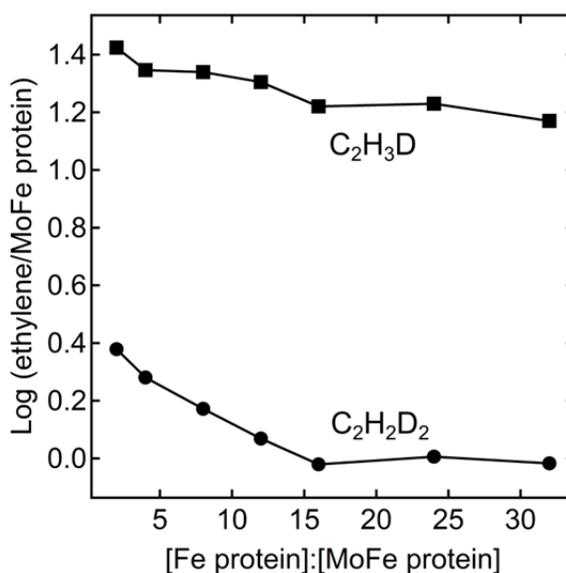


Figure 5-6. Deuterated ethylene formation as a function of electron flux. The amounts of C_2H_3D and $C_2H_2D_2$ formed as a function of the electron flux, as characterized by the ratio of Fe protein to MoFe protein, is shown. The partial pressure of C_2H_2 was 0.02 atm, D_2 was 0.68 atm, and N_2 was 0.3 atm. The molar ratio of Fe protein to MoFe protein was 4:1. The molar ratio of Fe protein to MoFe protein varied from 2:1 to 32:1. All assays were incubated at 30 °C for 60 min.

Discussion

Upon formulating the *re* mechanism for the activation of FeMo-cofactor to reduce N_2 (**Figure 5-1**) (5), we noted that addition of C_2H_2 to an N_2/D_2 reaction mixture offers a rigorous test of the mechanism. The test is founded on a defining characteristic of nitrogenase catalysis, an exact distinction between hydrons (L; L = H/D/T) associated with the gaseous diatomics, L_2 , and those derived from solvent water. Thus, (i) when nitrogenase in protic buffer is turned over under N_2/D_2 , gaseous D_2 can displace N_2 from the $E_4(N_2/N_2H_2)$ state (**Figure 5-1**), stoichiometrically yielding two HD; (ii) however, there is essentially no loss of T^+ to solvent (*ca.* 2%) during the corresponding turnover under N_2/T_2 (19). This and other observations clearly show that diatomic L_2 is not used to reduce N_2 during turnover under N_2/L_2 (in particular, T incorporated into the ammonia product of N_2 fixation would exchange with solvent (5)). (iii) Likewise, when any other substrate is being reduced by nitrogenase, if diatomic L_2 is added to the reaction mixture it is not used to reduce the substrate (1, 35). *In particular*, there is no report on the production of deuterated ethylenes from reduction of acetylene in the presence of D_2 (1).

With this foundation, we recognized that the *re* mechanism predicts that turnover under $C_2H_2/D_2/N_2$ should not only incorporate H from solvent to generate C_2H_4 by the normal reduction process, but through the agency of the added N_2 also should for the first time breach the separation of gaseous D_2 from solvent protons by generating *both* C_2H_3D or $C_2H_2D_2$, as follows. According to the *re* mechanism, **Figure 5-1**, when turnover is carried out under N_2/D_2 , D_2 can intercept $E_4(N_2/N_2H_2)$, replacing the N_2 and undergoing oxidative addition to generate $E_4(2D)$ (5). We recognized that this state in fact can be expected to react with C_2H_2 to form $C_2H_2D_2$, with a plausible mechanism (**Figure 5-7A**)

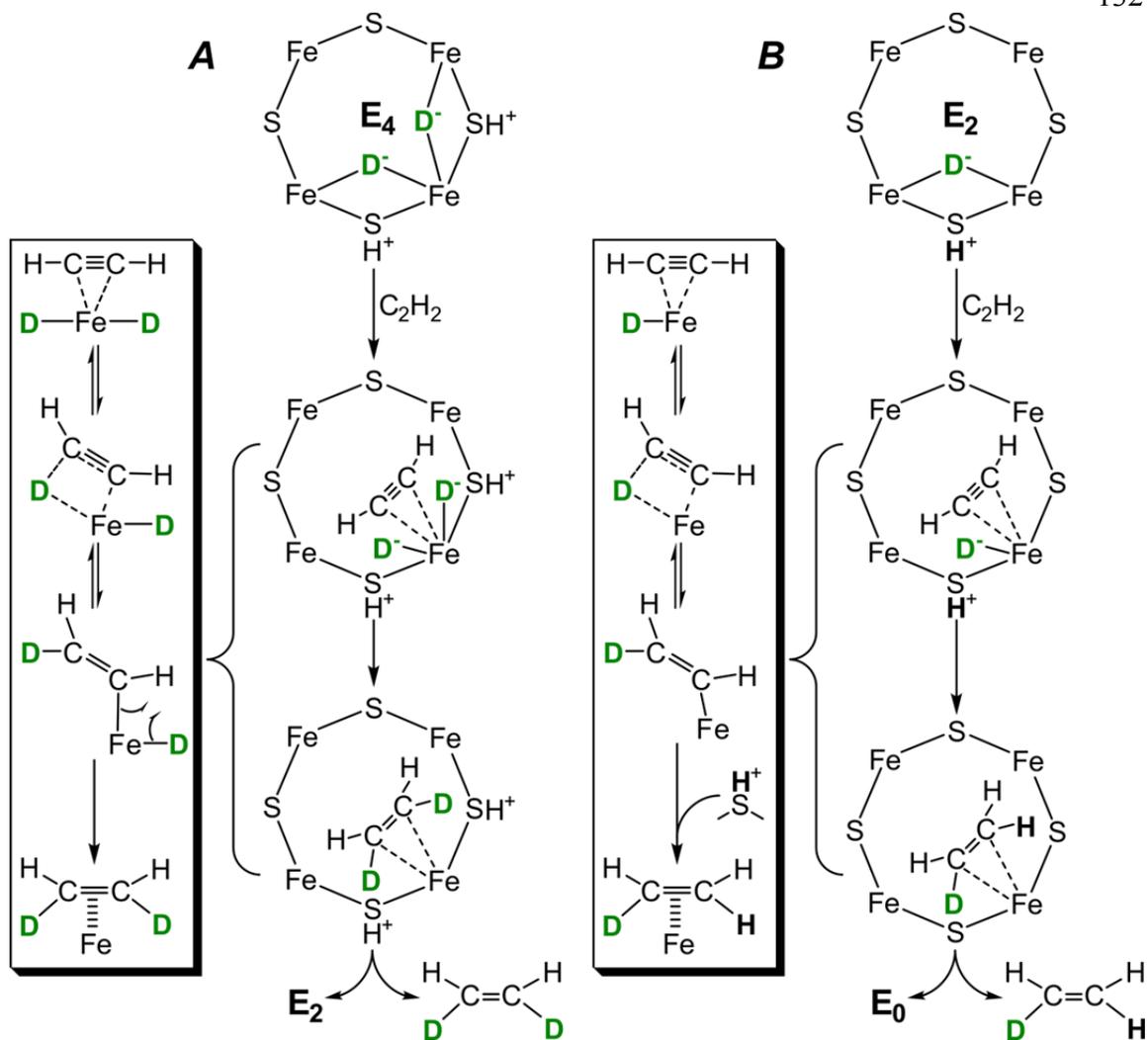


Figure 5-7. Proposed acetylene interception mechanisms. **(A)** $C_2H_2D_2$ formation from $E_4(2D)$ through acetylene insertion into metal-deuteride bond followed by reductive elimination from Fe-bound vinyl and hydride ligands. **(B)** C_2H_3D formation from $E_2(D)$ through acetylene insertion and protonation of the vinyl ligand. Deuteride is highlighted in green.

involving terminalization of an Fe-D⁻-Fe bridge of E₄, migratory insertion of bound C₂H₂ into the Fe-D⁻ bond to form an Fe-vinyl intermediate (36), followed by reductive elimination (15) of C₂H₂D₂.

The E₄(2D) state would also relax through the loss of HD to form E₂(D), an E₂ state whose unique isotopic composition can be generated in no other way under applied assay conditions (5). Interception of the E₂(D) thus produced by C₂H₂ would then generate C₂H₃D, with **Figure 5-7B** presenting a plausible mechanism: hydride terminalization and insertion, followed by vinyl protonation (15). The E₂(D) can be reduced by two more electrons to form a E₄ state with one bridging hydride and one bridging deuteride (E₄(HD)), from which acetylene can also be reduced to form C₂H₃D through a reductive elimination mechanism (**Figure 5-7A**). A full reaction pathway for acetylene interception of deuteride intermediates is illustrated in **Figure 5-8**.

To test these predictions of an unprecedented involvement of gaseous D₂ in substrate reduction we have carried out C₂H₂ reduction under N₂/D₂/C₂H₂ gas mixtures and under varying electron flux, with turnover under N₂/H₂/C₂H₂ as control. As expected, the control reactions of turnover under N₂/H₂/¹³C₂H₂ and D₂/¹³C₂H₂ generates only ¹³C₂H₄, with a trace amount of ¹³C₂H₃D from the natural abundance of deuterium or contaminating level of N₂ in reaction system and without any detectable ¹³C₂H₂D₂ (**Figure 5-2**). In contrast, ¹³C₂H₂ reduction by nitrogenase under a N₂/D₂/¹³C₂H₂ gas mixture in fact produces substantial yields of, ¹³C₂H₃D and lesser, though still significant, yields of ¹³C₂H₂D₂ (**Figure 5-2**). The measured yield of C₂H₃D indicates that under the conditions of electron flux and D₂/N₂ partial pressures employed, formation of C₂H₃D occurs up to about 7% as often as accumulation of an additional electron by E₄(N₂/N₂H₂)

directs this state down the N₂ reduction pathway to NH₃ production. The even lower yield of C₂H₂D₂ likely indicates that the probability for binding and reduction of C₂H₂ by E₄(2D) is substantially lower than that for the relaxation to E₂(D) through loss of HD (**Figure 5-1**). These observations are enriched by the dependence of the yields of C₂H₃D and C₂H₂D₂ on the partial pressures of C₂H₂, D₂, N₂, and electron flux, **Figures 5-3 to 5-6**, all of which are shown in **Results** section, above, to be understandable in terms of the *re* mechanism for FeMo-cofactor activation for N₂ binding and reduction, **Figure 5-1**.

It is of keen interest to note that the reduction of C₂H₂ to C₂H₃D by reaction with E₂(D) formally corresponds to the reduction of C₂H₂ by the HD that otherwise would form during relaxation of E₂(D) to E₀ (**Figure 5-1C**), a perspective that highlights the contrast between this result, achieved in the presence of N₂. Elaborating on this perspective, the formation of HD during turnover under N₂/D₂, with stoichiometry (1), $D_2 + 2H^+(aq) + 2e^- \rightarrow 2HD$, can be seen to correspond to the catalytic reduction of D₂ by nitrogenase with N₂ as cocatalyst, a reaction that does not proceed without N₂. Likewise, although C₂H₂D₂ of course is well known to form during nitrogenase reduction of C₂D₂ in H₂O buffer (or C₂H₂ in D₂O buffer) (6, 36), observation of this species during turnover under N₂/D₂/C₂H₂ is remarkable because the stoichiometry of the reaction corresponds to the unprecedented reduction of C₂H₂ by gaseous D₂, $C_2H_2 + D_2 \rightarrow C_2H_2D_2$, as catalyzed by nitrogenase with N₂ as cocatalyst.

Other than supporting the *re* mechanism (5) we proposed for N₂ binding, obligatory H₂ evolution, and HD formation, the generation of C₂H₃D and C₂H₂D₂ observed in this study can also help us understand some other important mechanistic

aspects in nitrogenase catalysis, including the hydrogenation mechanism of substrates (6) and complicated enzyme kinetics reported before (1, 33).

Since the incorporation of D into C_2H_3D and $C_2H_2D_2$ is exclusively from D_2 -derived deuteride intermediates, this observation is the first piece of experimental evidence for the direct involvement of metal-hydride intermediates in hydrogenation of substrate other than proton reduction (1, 6, 8, 11, 37). The mechanism for hydrogenation of acetylene could be different at different steps (**Figure 5-7**) (6), including migratory acetylene insertion into a metal-hydride bond as the first step, and reductive elimination of the vinyl intermediate and a second metal-hydride bond or solvent protonation of the vinyl ligand to produce the product ethylene (6, 15).

Acetylene interception of metal-hydride intermediates found here might explain several important observations related to acetylene serving as an inhibitor and substrate of nitrogenase: (a) acetylene at saturating concentrations can completely inhibit proton reduction catalyzed by wild-type nitrogenase (38), due to the acetylene interception of metal hydrides that is destined to make H_2 (6); (b) acetylene is a noncompetitive inhibitor of N_2 reduction, and N_2 is a competitive inhibitor of acetylene reduction for wild-type nitrogenase (39). The nonreciprocal inhibition pattern can be explained by acetylene interception of the metal-hydride intermediates (*e.g.* $E_2(H)$ and $E_4(2H)$) preceding N_2 binding and reduction by wild-type nitrogenase (33).

The results from this study also explained the observations by Davis *et al.* that the presence of hydrogen diverted nitrogenase from production of NH_3 to increased production of C_2H_4 (34).

Our results also strongly suggest a direct involvement of metal-hydride as part of the hydrogenation reactions of other substrate reduction, which could be a common feature of nitrogenase catalysis. However, we still could not exclude other hydrogenation mechanisms such as sequential protonation of substrate-derived anionic ligands bound to FeMo-cofactor. It's clear that more work need to be done to understand the hydrogenation mechanism of substrate reduction catalyzed by nitrogenase.

In LT model for acetylene reduction, acetylene was suggested to bind to E_1 and E_2 state and ethylene is released when the third electron is accumulated in MoFe protein (8, 10). Our data clearly indicates that acetylene can be reduced at the E_4 level (**Figure 5-7A**). The reason that this reaction had never been considered before perhaps because the reaction at the E_4 state could not be distinguished from reaction at the E_2 state when C_2H_2 is reduced in the absence of N_2 , which is required to enable gaseous D_2 to enter the catalytic process (5).

In summary, there are many conclusions can be made from this study. (i) The unprecedented incorporation of D from D_2 into the nitrogenase reduction products $C_2H_2D_2$ and C_2H_3D during turnover under $C_2H_2/D_2/N_2$ by nitrogenase in H_2O provides clear evidence that the *re* mechanism is responsible for the activation of FeMo-cofactor for reduction of N_2 during nitrogen fixation, **Figure 5-1**. (ii) Under these turnover conditions nitrogenase catalytically (a) reduces D_2 to 2HD by electrons and solvent protons, with N_2 as cocatalyst, and (b) reduces C_2H_2 to $C_2H_2D_2$ by D_2 , both with N_2 as cocatalyst. (iii) Metal hydride intermediates at E_2 and E_4 states are directly involved in hydrogenation of acetylene through different mechanisms at different steps. The same hydrogenation mechanism could be true for the reduction of other substrates catalyzed by

nitrogenase. (iv) Acetylene interception of hydride intermediates explains why proton reduction can be completely inhibited and N_2 is *non-competitively* inhibited by acetylene for wild-type nitrogenase.

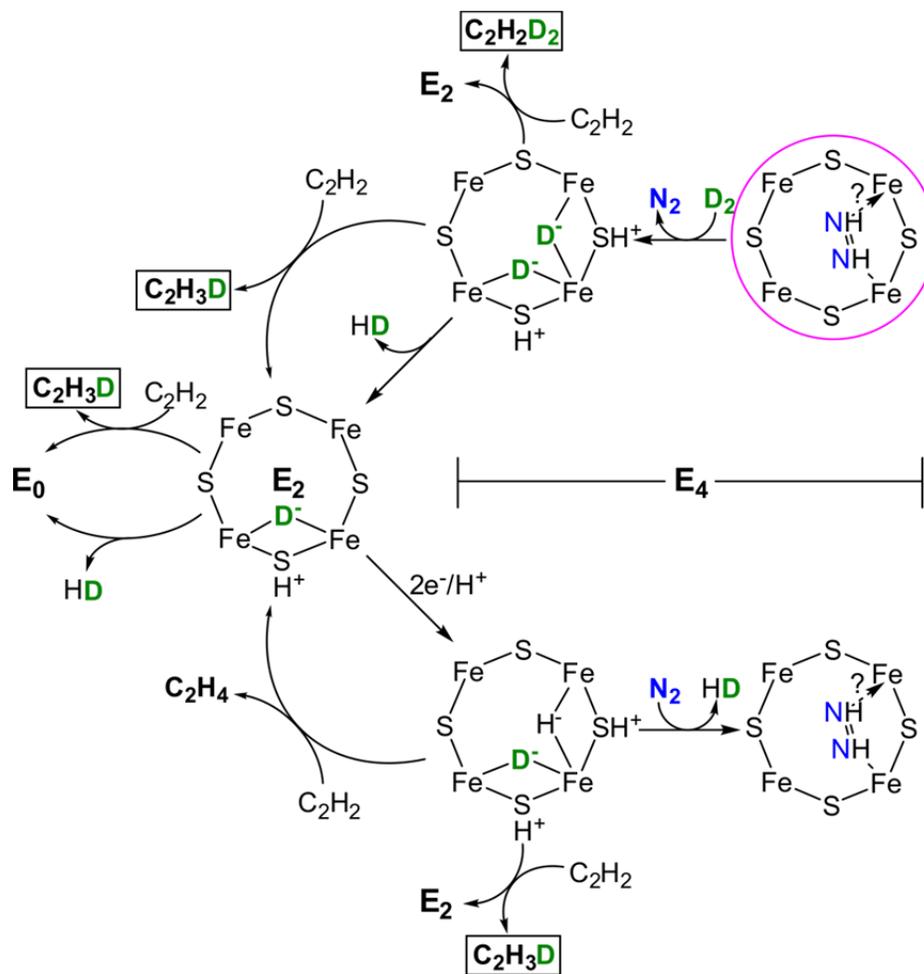


Figure 5-8. A full reaction pattern for acetylene interception of deuteride containing nitrogenase intermediates. The proposed diazene intermediate is shown in a magenta circle. The question mark indicates the uncertainty of the binding mode of the diazene ligand, which could be either terminal or bridging. Colors: N in blue and D in green.

Materials and Methods

Chemical reagents and protein purification. Gases were purchased from Air Liquide (Plumsteadville, PA and Houston, TX). Ultrapure helium was purchased from Airgas (Denver, CO). Ethylene (99.9%) was obtained from Praxair Inc. (Danbury, CT). ^{13}C -acetylene (99 atom % ^{13}C) and D_2 (99.8 atom % D) were purchased from Sigma-Aldrich (St. Louis, MO) and Isotec (Miamisburg, OH), respectively. All other reagents were obtained from Sigma-Aldrich (St. Louis, MO) or Fisher Scientific (Fair Lawn, NJ), and were used without further purification, unless specified otherwise. *Azotobacter vinelandii* strains DJ1260 (hydrogenase gene cluster removed, ΔHup) and DJ884 (R187I in *nifD*, ΔHup) were grown as previously described (40). The wild-type nitrogenase MoFe protein (DJ1260) and Fe protein (DJ884) were expressed and purified as previously reported (40, 41). The wild-type MoFe protein in this study contains a seven-His tag addition near the carboxy-terminal end of the α -subunit. Protein concentrations were determined by the Biuret assay using bovine serum albumin as standard. The purities of these proteins were estimated to >95% based on denaturing polyacrylamide gel separation with Coomassie blue staining. Manipulation of proteins, solutions, and buffers was done in septum-sealed serum vials under an argon atmosphere on a Schlenk vacuum line. All gases and liquid transfers used gas-tight syringes.

Assay methods. All assays were conducted in 9.4-mL serum vials with gases added before addition of 1.1 mL of an anaerobic “assay buffer” consisting of 90 mM sodium dithionite, a MgATP regenerating system (13.4 mM MgCl_2 , 10 mM ATP, 60 mM phosphocreatine, 1.2 mg/mL bovine serum albumin, and 0.4 mg/mL creatine phosphokinase) in a 100 mM MOPS buffer, pH 7.0. Prior to all assays, the MoFe protein

was added and the vials were equilibrated for about 20 min. The gas overpressure was released before initiating the assays. Reactions were initiated by the addition of Fe protein and the reaction was allowed to proceed at 30°C for 60 min, unless noted otherwise. Reactions were quenched by the addition of 300 μ L of 400 mM EDTA, pH = 8.0, solution. For the acetylene partial pressure dependence study, 3.3 mL of the assay buffer was used with acetylene partial pressures from 0.002-0.008 atm with the same protein concentrations as described below. For analysis of the partial pressure dependence of acetylene, N₂, and D₂, all samples contained 1.0 mg of wild-type MoFe protein and 1.0 mg of Fe protein in 1.1 mL of “assay buffer”. For the electron flux dependence study, 1.0 mg of MoFe protein was used and the Fe protein varied from 0.5 mg to 8.0 mg in 1.1 mL of assay buffer. In the time course study using ¹³C₂H₂, 1.0 mg of wild-type MoFe protein and 0.5 mg of Fe protein in 1.1 mL of assay buffer. The acetylene partial pressure dependence study was done in triplicate.

GC-MS measurement of products. Ethylene was quantated by analysis of the headspace gas with a Shimadzu GC-2010 gas chromatograph (GC) equipped with a programmed temperature vaporization (PTV) injector and a Shimadzu GCMS-QP2010S mass spectrometer (MS) in selected ion monitoring (SIM) mode using electron ionization (EI) as the ion source. Separation of ethylene from other gases was achieved with a Rt-Alumina BOND/KCl column (30 m, 0.32 mm ID, and 5.0 μ m film thickness) (Restek, Belafonte, PA). The injector and column temperatures were set to 35°C. Ultra-pure helium was used as the carrier gas set at a linear velocity of 60 cm/s. For each injection, 100 or 150 μ L of headspace gas was directly injected into the PTV injector. When ¹²C-acetylene (C₂H₂) was the substrate, ethylene (C₂H₄, mass 28) was monitored at $m/z = 28$

(m), with minor species being 29 (m+1) and 30 (m+2) resulting from natural abundance ^2H (D) and ^{13}C (32) in the acetylene. For samples using $^{13}\text{C}_2\text{H}_2$, ethylene ($^{13}\text{C}_2\text{H}_4$, mass 30) was monitored as $m/z = 30$ (m) with minor products detected at 31 (m+1) and 32 (m+2) from natural abundance ^2H . When the reaction was run with D_2 in place of H_2 , the ethylene products C_2DH_3 (mass 29) and $\text{C}_2\text{D}_2\text{H}_2$ (mass 30) or $^{13}\text{C}_2\text{DH}_3$ (mass 31) and $^{13}\text{C}_2\text{D}_2\text{H}_2$ (mass 32) were detected. Ethylene was quantified from the peak area using a standard curve generated with known amounts of ethylene in argon.

It was taken that all isotopomers of ethylene had the same retention time and that the ionization and fragmentation efficiency of all isotopomers was the same. Intensities for all ethylene peaks were established by subtraction of the signal background at that retention time. Error propagation was calculated using the online calculator (42).

References

1. Burgess BK, Lowe DJ (1996) Mechanism of molybdenum nitrogenase. *Chem Rev* 96:2983–3012.
2. Seefeldt LC, Hoffman BM, Dean DR (2009) Mechanism of Mo-dependent nitrogenase. *Annu Rev Biochem* 78:701–722.
3. Hoffman BM, Dean DR, Seefeldt LC (2009) Climbing nitrogenase: Toward a mechanism of enzymatic nitrogen fixation. *Acc Chem Res* 42:609–619.
4. Seefeldt LC, Hoffman BM, Dean DR (2012) Electron transfer in nitrogenase catalysis. *Curr Opin Chem Biol* 16:19–25.
5. Hoffman BM, Lukoyanov D, Dean DR, Seefeldt LC (2013) Nitrogenase: A draft mechanism. *Acc Chem Res* 46:587–595.
6. Seefeldt LC, Yang Z-Y, Duval S, Dean DR (2013) Nitrogenase reduction of carbon-containing compounds. *Biochim Biophys Acta* <http://dx.doi.org/10.1016/j.bbabi.2013.04.003>.
7. Simpson FB, Burris RH (1984) A nitrogen pressure of 50 atmospheres does not prevent evolution of hydrogen by nitrogenase. *Science* 224:1095–1097.

8. Thorneley RNF, Lowe DJ (1985) in *Molybdenum Enzymes*, ed Spiro TG (Wiley, New York), pp 221–284.
9. Peters JC, Mehn MP (2006) in *Activation of Small Molecules: Organometallic and Bioinorganic Perspectives*, ed Tolman WB (Wiley-VCH Verlag GmbH & Co. KGaA, Weinheim, Germany), pp 81–119.
10. Wilson P, Nyborg A, Watt G (2001) Duplication and extension of the Thorneley and Lowe kinetic model for *Klebsiella pneumoniae* nitrogenase catalysis using a MATHEMATICA software platform. *Biophys Chem* 91:281–304.
11. Igarashi RY, et al. (2005) Trapping H⁻ bound to the nitrogenase FeMo-cofactor active site during H₂ evolution: Characterization by ENDOR spectroscopy. *J Am Chem Soc* 127:6231–6241.
12. Lukoyanov D, Yang Z-Y, Dean DR, Seefeldt LC, Hoffman BM (2010) Is Mo involved in hydride binding by the four-electron reduced (E₄) intermediate of the nitrogenase MoFe protein? *J Am Chem Soc* 132:2526–2527.
13. Doan PE, et al. (2011) ⁵⁷Fe ENDOR spectroscopy and “Electron Inventory” analysis of the nitrogenase E₄ intermediate suggest the metal-ion core of FeMo-cofactor cycles through only one redox couple. *J Am Chem Soc* 133:17329–17340.
14. Kinney RA, Saouma CT, Peters JC, Hoffman BM (2012) Modeling the signatures of hydrides in metalloenzymes: ENDOR analysis of a di-iron Fe(μ-NH)(μ-H)Fe core. *J Am Chem Soc* 134:12637–12647.
15. Crabtree RH (2009) *The Organometallic Chemistry of the Transition Metals* (Wiley, Hoboken, NJ), 5th Ed.
16. Ballmann J, Munhá RF, Fryzuk MD (2010) The hydride route to the preparation of dinitrogen complexes. *Chem Commun* 46:1013–1025.
17. Peruzzini M, Poli R eds. (2001) *Recent Advances in Hydride Chemistry* (Elsevier Science B. V., Amsterdam, The Netherlands).
18. Kubas GJ (2007) Fundamentals of H₂ binding and reactivity on transition metals underlying hydrogenase function and H₂ production and storage. *Chem Rev* 107:4152–4205.
19. Burgess B, Wherland S, Newton W, Stiefel E (1981) Nitrogenase reactivity: Insight into the nitrogen-fixing process through hydrogen-inhibition and HD-forming reactions. *Biochemistry* 20:5140–5146.
20. Guth JH, Burris RH (1983) Inhibition of nitrogenase-catalyzed NH₃ formation by H₂. *Biochemistry* 22:5111–5122.

21. Li J-L, Burris RH (1983) Influence of pN_2 and pD_2 on HD formation by various nitrogenases. *Biochemistry* 22:4472–4480.
22. Jensen BB, Burris RH (1985) Effect of high pN_2 and high pD_2 on ammonia production, hydrogen evolution, and hydrogen deuteride formation by nitrogenases. *Biochemistry* 24:1141–1147.
23. Fisher K, Dilworth MJ, Newton WE (2000) Differential effects on N_2 binding and reduction, HD formation, and azide reduction with α -195^{His}- and α -191^{Gln}-substituted MoFe proteins of *Azotobacter vinelandii* nitrogenase. *Biochemistry* 39:15570–15577.
24. Wherland S, Burgess BK, Stiefel EI, Newton WE (1981) Nitrogenase reactivity: effects of component ratio on electron flow and distribution during nitrogen fixation. *Biochemistry* 20:5132–5140.
25. Dilworth MJ, Fisher K, Kim CH, Newton WE (1998) Effects on substrate reduction of substitution of histidine-195 by glutamine in the α -subunit of the MoFe protein of *Azotobacter vinelandii* nitrogenase. *Biochemistry* 37:17495–17505.
26. Jackson EK, Parshall GW, Hardy RWF (1968) Hydrogen reactions of nitrogenase. Formation of the molecule HD by nitrogenase and by an inorganic model. *J Biol Chem* 243:4952–4958.
27. Lowe DJ, Thorneley RN (1984) The mechanism of *Klebsiella pneumoniae* nitrogenase action: The determination of rate constants required for the simulation of the kinetics of N_2 reduction and H_2 evolution. *Biochem J* 224:895–901.
28. Lukoyanov D, Barney BM, Dean DR, Seefeldt LC, Hoffman BM (2007) Connecting nitrogenase intermediates with the kinetic scheme for N_2 reduction by a relaxation protocol and identification of the N_2 binding state. *Proc Natl Acad Sci USA* 104:1451–1455.
29. Hoch GE, Schneider KC, Burris RH (1960) Hydrogen evolution and exchange, and conversion of N_2O to N_2 by soybean root nodules. *Biochim Biophys Acta* 37:273–279.
30. Schöllhorn R, Burris RH (1967) Acetylene as a competitive inhibitor of N_2 fixation. *Proc Natl Acad Sci USA* 58:213–216.
31. Dilworth MJ (1966) Acetylene reduction by nitrogen-fixing preparations from *Clostridium pasteurianum*. *Biochim Biophys Acta* 127:285–294.
32. Böhlke JK, et al. (2005) Isotopic compositions of the elements, 2001. *J Phys Chem Ref Data* 34:57–67.

33. Seefeldt LC, Dance IG, Dean DR (2004) Substrate interactions with nitrogenase: Fe versus Mo. *Biochemistry* 43:1401–1409.
34. Davis LC, Shah VK, Brill WJ (1975) Nitrogenase: VII. Effect of component ratio, ATP and H₂, on the distribution of electrons to alternative substrates. *Biochim Biophys Acta* 403:67–78.
35. Lee CC, Hu Y, Ribbe MW (2011) Tracing the hydrogen source of hydrocarbons formed by vanadium nitrogenase. *Angew Chem Int Ed* 50:5545–5547.
36. Benton PMC, Christiansen J, Dean DR, Seefeldt LC (2001) Stereospecificity of acetylene reduction catalyzed by nitrogenase. *J Am Chem Soc* 123:1822–1827.
37. Lowe DJ, Thorneley RNF (1984) The mechanism of *Klebsiella pneumoniae* nitrogenase action. Pre-steady-state kinetics of H₂ formation. *Biochem J* 224:877–886.
38. Hardy RW, Burns RC, Parshall GW (1971) in *Bioinorganic Chemistry*, eds Dessy R, Dillard J, Taylor L (American Chemical Society, Washington, D. C.), pp 219–247.
39. Rivera-Ortiz JM, Burris RH (1975) Interactions among substrates and inhibitors of nitrogenase. *J Bacteriol* 123:537–545.
40. Christiansen J, Goodwin PJ, Lanzilotta WN, Seefeldt LC, Dean DR (1998) Catalytic and biophysical properties of a nitrogenase apo-MoFe protein produced by a *nifB*-deletion mutant of *Azotobacter vinelandii*. *Biochemistry* 37:12611–12623.
41. Seefeldt LC, Mortenson LE (1993) Increasing nitrogenase catalytic efficiency for MgATP by changing serine 16 of its Fe protein to threonine: Use of Mn²⁺ to show interaction of serine 16 with Mg²⁺. *Protein Sci* 2:93–102.
42. Error propagation was calculated using the online calculator: <http://laffers.net/tools/error-propagation-calculator/>.

CHAPTER 6

STERIC CONTROL OF THE HI-CO MOFE NITROGENASE COMPLEX REVEALED
BY STOPPED-FLOW INFRARED SPECTROSCOPY⁶

Here, we present the impact of substitution for the α -70^{Val} residue of *Azotobacter vinelandii* nitrogenase MoFe protein on the hi-CO complex as monitored by stopped-flow infrared (SF-IR) spectroscopy. Nitrogenase is a bacterial metalloenzyme system whose physiological function is to catalyze the reduction of dinitrogen to ammonia^[1,2] with a concomitant reduction of 2H⁺ to H₂ and hydrolysis of MgATP. X-ray crystallography on MoFe nitrogenase reveals the active-site FeMo-cofactor to be an unprecedented [Fe₇S₉MoX:homocitrate] cluster, (**Figure 6-1**).^[3,4] However, simple inspection of this structure does not provide an obvious location for substrate binding or any indication of the subsequent mechanism for substrate reduction. Mechanisms focused on substrate binding to either Mo and Fe sites have been proposed as have combination approaches that involve migration of substrate-derived moieties between metal atoms during reduction.^[5-8]

A series of recent studies have revealed the importance of substrate interactions at the 4Fe-4S face of FeMo-co defined by Fe atoms 2, 3, 6, and 7. These have analyzed the impact of modulating the steric influence of the uncharged α -70^{Val} residue, which lies over Fe6 (**Figure 6-1**).^[6] Reducing the size of the sidechain by substitution with alanine or glycine allows the reduction of significantly larger alkyne substrates such as propargyl alcohol,^[9-11] while increasing its size by substitution with isoleucine severely restricts the

⁶ Coauthored by Zhi-Yong Yang, Lance C. Seefeldt, Dennis R. Dean, Stephen P. Cramer, and Simon J. George (2011) *Angewandte Chemie International Edition* **50**(1), 272-275. Copyright © [2011] WILEY-VCH Verlag GmbH & Co. KGaA, Weinheim. Reprinted with permission.

reduction of nitrogenous and alkyne substrates while leaving the reactivity towards proton reduction unaltered.^[12,13] The clear implication of these results, and especially those from α -70^{Ile}, is to implicate the Fe 2-3-6-7 face as the region for initial substrate binding.

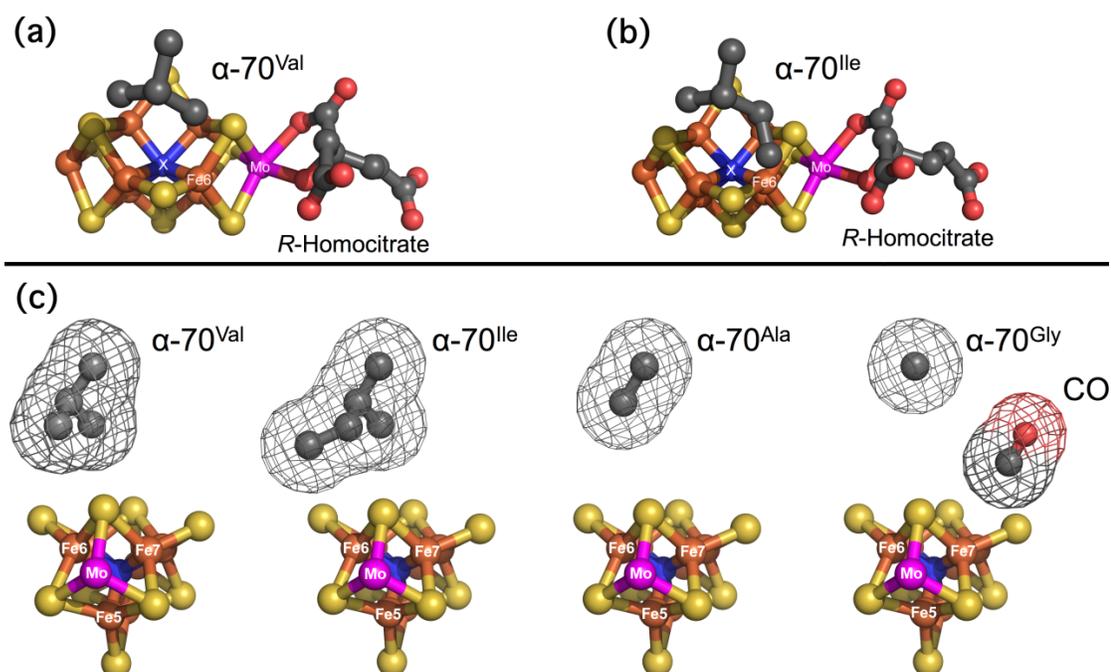


Figure 6-1. FeMo-co showing the position and potential steric influence of the α -70 residue over the Fe 6 atom on the Fe 2, 3, 6, 7 face. a) Side view of α -70^{Val}. b) Side view of α -70^{Ile}. c) End view of (left to right) α -70^{Val}, α -70^{Ile}, α -70^{Ala}, α -70^{Gly}. The wireframe indicates the van der Waals radii of the sidechains. A CO molecule is included for size comparison. Fe, rust; Mo, magenta; S, yellow; C, dark gray; O, red; X, blue. Structures built from PDB files: 1M1N.pdb^[3] and 3K1A.pdb.^[13]

CO is a valuable probe of the ligand binding properties of the FeMo-co active site.

The molecule is a potent non-competitive inhibitor of the enzyme's ability to reduce dinitrogen and other multiply bonded molecules,^[14,15] although recent work has shown that for the vanadium enzyme it can be a slow substrate.^[16] It does not, however, inhibit enzyme turnover and MgATP hydrolysis, and the electron flux through the enzyme is redirected to increasing the rate of reduction of 2H^+ to H_2 .

The binding chemistry of CO to MoFe nitrogenase is known to be complex and dependent on the partial pressure or concentration of CO present.^[17,18] Electron paramagnetic resonance (EPR) and electron-nuclear double resonance (ENDOR) studies have identified three bound states: under limiting [CO] conditions (< 0.08 atm in the gas phase or $< 1:1$ [CO]:[FeMo-co] in solution) the "lo-CO" state forms, which is proposed to comprise a single CO bound to the FeMo-cofactor, while under excess [CO] or under a high partial pressure of the gas, two EPR signals are observed, termed "hi-CO" and "hi(5)-CO". Each signal is proposed to comprise at least two CO molecules bound to separate sites on the cofactor.^[17,18]

Significant insight into CO binding to nitrogenase is possible by SF-IR spectroscopy, which has the enormous advantage of being a real-time room temperature technique.^[19-21] Under lo-CO conditions, SF-IR measurements on both *Klebsiella pneumoniae* and *A. vinelandii* MoFe enzymes show a transient $\nu(\text{C}\equiv\text{O})$ band at 1904 cm^{-1} which corresponds to a single CO terminally bound to a metal site, which converts on the minute timescale to an infrared (IR) band at 1715 cm^{-1} which presumably arises from a bridged or protonated bound CO species.^[20,21] By contrast, under hi-CO conditions complex spectra are seen with $\nu(\text{C}\equiv\text{O})$ bands at 1960 , 1936 , 1906 and 1880 cm^{-1} , all of

which most likely arise from terminally bound CO species at more than one metal site.^[19,20] Further insight has been gained from spectroelectrochemical IR studies of the isolated FeMo-cofactor in *N*-methyl formamide (NMF:FeMo-co), which also reveals lo-CO and hi-CO behavior. The lo-CO state has redox dependent $\nu(\text{C}\equiv\text{O})$ bands at 1835 and 1808 cm^{-1} that are assigned to bridged CO groups, while hi-CO has bands at 1885 and 1920 cm^{-1} , assigned to terminally bound CO on Fe and Mo, respectively.^[22]

Here we use SF-IR to examine the sensitivity of the hi-CO complex to steric changes in the uncharged α -70 sidechain. The results for *A. vinelandii* wild-type MoFe protein (α -70^{Val}) together with those from the α -70^{Gly}, α -70^{Ala} and α -70^{Ile} variants are summarized in **Figure 6-2** and **Table 6-1**. These data were all generated by reacting a 1:4 molar ratio of MoFe:Fe proteins with a buffered solution of MgATP saturated with CO, giving 50 μM FeMo-cofactor centers and 0.5 mM CO after mixing.

The spectrum of the wild-type (α -70^{Val}) complex (**Figure 6-2a, top**) is consistent with those previously reported.^[19,20] The time courses, **Figure 6-2b**, allow us to assign the spectrum to a mixture of two distinct hi-CO forms and the lo-CO complex. The first hi-CO form comprises the intense band at 1936 cm^{-1} and the weaker band at 1880 cm^{-1} . These bands share the same time course and so it is reasonable to assign them to the same species. This species forms slowly, reaching a maximum intensity at ~ 150 s before slowly decaying (not shown) so we term it “slow hi-CO.” The second hi-CO form is characterized in this region by a single observed band at 1960 cm^{-1} . We term this “fast hi-CO” as it initially appears quickly, within 10 s, and decays more slowly than the 1936 cm^{-1} band. The band at 1906 cm^{-1} mostly likely corresponds to the lo-CO complex and reaches maximum intensity within 8 seconds before decaying slowly to about 50%

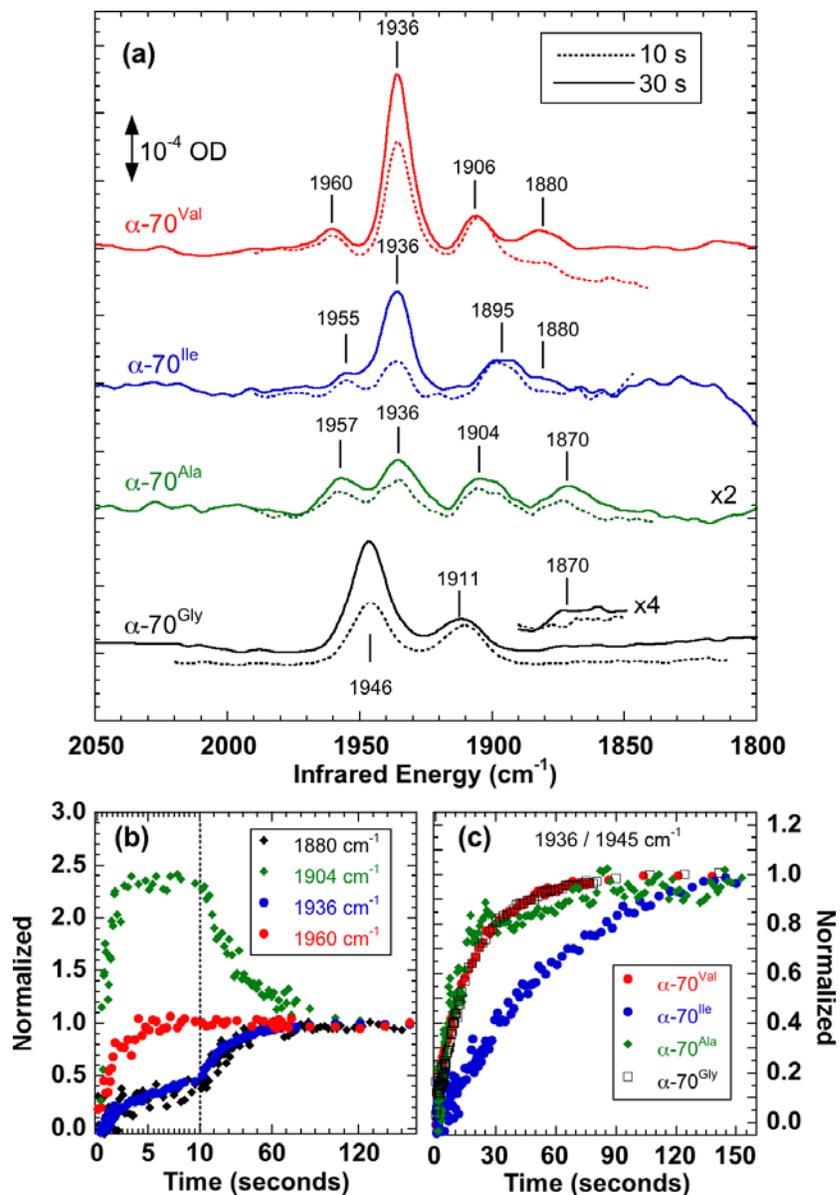


Figure 6-2. Transient IR spectra of the *A. vinelandii* MoFe nitrogenase hi-CO complex showing the effect of varying the size of the α -70 sidechain. a) Spectra averaged 25–35 s (solid line) and 6–14 s (broken line) after mixing. b) Time courses for wild-type (α -70^{Val}) measured at 1880, 1904, 1936 and 1960 cm^{-1} . c) Comparison of time courses at 1936 cm^{-1} (α -70^{Val}, α -70^{Ile}, α -70^{Ala}) and 1945 cm^{-1} (α -70^{Gly}). Intensities in (b) and (c) are normalized at 150 s.

Table 6-1. Assignment of observed IR bands

α -70 variant	Lo-CO (cm ⁻¹)	Slow Hi-CO (cm ⁻¹)	Fast Hi-CO (cm ⁻¹)
Val ^[a]	1906	1936	1880
Ile	1895	1936	1880
Ala	1904	1936	1870
Gly	1911	1946	1870
			n/o ^[b]

[a] Wild-type. [b] not observed or not resolved.

maximum size. Interestingly, the time course of the lo-CO decay is similar to the time course of formation of the slow hi-CO species suggesting that the slow hi-CO species may in part result from further CO binding to the 1906 cm⁻¹ lo-CO species.

Changing the size of the uncharged α -70^{Val} isopropyl sidechain modifies the energies and intensities of the IR bands, **Figure 6-2**, however, there is consistently a visual correspondence with the wild-type spectrum, suggesting that both the two hi-CO species and the lo-CO band are still present. Band energies and assignments are presented in **Table 6-1**. Substitution with a methyl group in α -70^{Ala} reduces all the band intensities and shifts their energies. Interestingly, the intense band at 1936 cm⁻¹ is substantially attenuated so that it now has similar intensity to the other bands. Similarly, increasing sidechain size to isobutyl in α -70^{Ile} also weakens the spectrum and again shifts the bands. Of particular interest is the α -70^{Gly} variant where the sidechain is replaced by a hydrogen atom thereby eliminating any steric effect. In this case, not only are all the slow hi-CO and lo-CO bands shifted in energy, but unlike the other variants, they are also broadened; for example, the bandwidth of the large slow hi-CO band increases from 10.5 to 15.5 cm⁻¹ (FWHM). The fast hi-CO band is not observed although it is possible that it is obscured by the intense 1946 cm⁻¹ band.

The apparent correlation of the hi-CO bands in the variant spectra with those in the wild-type spectrum is confirmed through the similarity in their time-dependence. When observed, the fast hi-CO band close to 1960 cm^{-1} is essentially formed within 10 s in each case. Similarly, in each variant, the 2 slow hi-CO bands have the same time dependence, **Figure 6-2a**. The kinetics of formation of the slow hi-CO species are of particular interest. As shown in **Figure 6-2c**, the formation time-course for the wild-type, the $\alpha\text{-70}^{\text{Gly}}$ and the $\alpha\text{-70}^{\text{Ala}}$ variants are virtually identical, but for $\alpha\text{-70}^{\text{Ile}}$ it is significantly slower. This can be rationalized in terms of the larger sidechain impeding access to the CO binding site.

The principal conclusion that can be drawn from these data is that the Fe 2-3-6-7 face of the FeMo-cofactor is likely responsible for binding most if not all the CO ligands giving rise to the observed IR bands. This arises from observation that the $\alpha\text{-70}$ sidechain exerts steric control on the energies, conformation freedom and/or the formation kinetics on each of the four observed bands in at least one variant. The potential steric influence of this residue on the Fe 2-3-6-7 face is clear from **Figure 6-1**. However, the data do not indicate a change in overall pattern of CO binding; it is clear that the slow hi-CO and the lo-CO species are present in all the spectra in **Figure 6-2**, while the fast hi-CO is observed in three of them and could well be present in them all. This is consistent with a model where CO molecules are bound to the same metal sites in each variant protein, but that the CO ligands are clustered about, and sterically influenced by, the $\alpha\text{-70}$ aliphatic sidechain. Changing the sidechain size changes the angles and freedom of movement of the metal-CO bonds, which in turn impacts the energies and intensities of the $\nu(\text{C}\equiv\text{O})$ stretching vibrations. Increasing the sidechain size in $\alpha\text{-70}^{\text{Ile}}$ impedes binding at one site

at least. The α -70^{Gly} spectrum is particularly interesting, as the observed broadening of the IR bands is consistent with the bound CO groups being conformationally less constrained by the protein environment when the α -70 sidechain is reduced to a hydrogen atom.

An alternative hypothesis is that modifying the α -70 sidechain causes the FeMo-cofactor to move within the protein pocket with a concomitant impact on CO binding elsewhere on the cofactor. This is largely excluded by the recent crystal structure of α -70^{Ile}, which shows close overall structural agreement with that of wild-type α -70^{Val} with near identity in the positions of most of the amino acids in the FeMo-cofactor binding pocket.^[13]

There are a number of secondary conclusions. First, as noted previously^[19, 20], the energies of all the bands observed in **Figure 6-2** indicate that they most likely comprise $\nu(\text{C}\equiv\text{O})$ stretches from terminally bound metal-CO species. It is possible that the 1880 cm^{-1} band arises from a CO bridging two metal sites through the C atom as $\nu(\text{C}=\text{O})$ stretches from such complexes have been observed to occur up to 1898 cm^{-1} .^[23] We consider this unlikely, however, as bridging CO species in other iron-sulfur systems exhibit $\nu(\text{C}=\text{O})$ at significantly lower energies; FeFe hydrogenase, for example, has bridging $\nu(\text{C}=\text{O})$ bands between 1850 – 1800 cm^{-1} .^[24] However, we cannot exclude the possibility of additional bridging CO or even protonated formyl groups as these could produce bands below the 1800 cm^{-1} limit of our measurements.

Second, the sensitivity of all the observed $\nu(\text{C}\equiv\text{O})$ bands to α -70 substitution confirms that they all arise from CO bound to the active site FeMo-co. Finally, it is implicit from the principal conclusion that it is unlikely that the observed CO is bound to

Fe atoms 4 or 5. The possibility that a CO may be bound to the Mo is also unlikely, however this is more difficult to rigorously exclude, as the Mo is adjacent to the Fe 2-3-6-7 face and its associated α -70 residue, and it has been proposed that CO can bind to the Mo in NMF:FeMo-co with $\nu(\text{C}\equiv\text{O})$ energies similar to those in **Table 6-1**.^[22]

These data comprise the first spectroscopic observations of the impact of varying the α -70 residue on the physical properties of ligands bound to FeMo-cofactor. This turn localizes the likely binding sites of the CO ligands to the Fe 2-3-6-7 face of the FeMo-cofactor, confirming the importance of both this region of the cofactor and the α -70 sidechain. This work also shows the value of CO as a probe of nitrogenase mechanism as CO inhibition clearly involves a dynamic and complex chemistry at the FeMo-co active site. The hi-CO state is of particular use as it comprises multiple CO molecules bound to more than one metal site and this means it can explore the array of available high and low affinity binding sites on FeMo-co. A complete understanding of nitrogenase-CO chemistry will undoubtedly give substantial insight into the mechanism of this intriguing enzyme system.

Experimental Section

Spectroscopic quantities of wild-type and variant MoFe nitrogenase were prepared as previously described.^[11] FTIR spectra were measured using a modified Bruker IFS/66s FTIR spectrometer interfaced to a home-built stopped-flow drive system with the sample cuvette and drive system maintained inside an anaerobic chamber ($\text{O}_2 < 1.1$ ppm) as described elsewhere.^[20] The IR cuvette was thermostated at 25°C. For these measurements, one side of the drive system was loaded with the protein mixture with the

other containing a buffered solution of MgATP saturated with CO. IR spectra were collected between 2200-1800 cm^{-1} only because a narrow band optical filter was used to enhance sensitivity. Spectra were measured at 4 cm^{-1} resolution. The IR cuvette path length was calibrated at 47.6 μm . Appropriate corrections were made for water vapor contamination. The α -70^{Ala} and α -70^{Ile} spectra in **Figure 6-2a** required arbitrary background corrections to make them flat.

References

- [1] B. K. Burgess, D. J. Lowe, *Chem. Rev.* **1996**, *96*, 2983.
- [2] J. W. Peters, R. K. Szilagyi, *Curr. Opin. Chem. Biol.* **2006**, *10*, 101.
- [3] O. Einsle, F. A. Tezcan, S. L. A. Andrade, B. Schmid, M. Yoshida, J. B. Howard, D. C. Rees, *Science* **2002**, *297*, 1696.
- [4] D. C. Rees, F. A. Tezcan, C. A. Haynes, M. Y. Walton, S. Andrade, O. Einsle, J. B. Howard, *Philos. Trans. Roy. Soc. Lon. A.* **2005**, *363*, 971.
- [5] R. Y. Igarashi, L. C. Seefeldt, *Crit. Rev. Biochem. Mol. Biol.* **2003**, *38*, 351.
- [6] L. C. Seefeldt, B. M. Hoffman, D. R. Dean, *Annu. Rev. Biochem.* **2009**, *78*, 701.
- [7] D. Lukoyanov, Z. Y. Yang, D. R. Dean, L. C. Seefeldt, B. M. Hoffman, *J. Am. Chem. Soc.* **2010**, *132*, 2526.
- [8] L. C. Seefeldt, I. G. Dance, D. R. Dean, *Biochemistry.* **2004**, *43*, 1401.
- [9] P. M. C. Benton, M. Laryukhin, S. M. Mayer, B. M. Hoffman, D. R. Dean, L. C. Seefeldt, *Biochemistry.* **2003**, *42*, 9102.
- [10] R. Y. Igarashi, P. C. Dos Santos, W. G. Niehaus, I. G. Dance, D. R. Dean, L. C. Seefeldt, *J. Biol. Chem.* **2004**, *279*, 34770.
- [11] P. C. Dos Santos, S. M. Mayer, B. M. Barney, L. C. Seefeldt, D. R. Dean, *J. Inorg. Biochem.* **2007**, *101*, 1642.
- [12] B. M. Barney, R. Y. Igarashi, P. C. Dos Santos, D. R. Dean, L. C. Seefeldt, *J. Biol. Chem.* **2004**, *279*, 53621.

- [13] R. Sarma, B. M. Barney, S. Keable, D. R. Dean, L. C. Seefeldt, J. W. Peters, *J. Inorg. Biochem.* **2010**, *104*, 385.
- [14] J. C. Hwang, C. H. Chen, R. H. Burris, *Biochim. Biophys. Acta* **1973**, *292*, 256.
- [15] D. N. Pham, B. K. Burgess, *Biochemistry.* **1993**, *32*, 13725.
- [16] C. C. Lee, Y. Hu, M. W. Ribbe, *Science* **2010**, *329*, 642.
- [17] H.-I. Lee, L. M. Cameron, B. J. Hales, B. M. Hoffman, *J. Am. Chem. Soc.* **1997**, *119*, 10121.
- [18] Z. Maskos, K. Fisher, M. Sørli, W. E. Newton, B. J. Hales, *J. Biol. Inorg. Chem.* **2005**, *10*, 394.
- [19] S. J. George, G. A. Ashby, C. W. Wharton, R. N. F. Thorneley, *J. Am. Chem. Soc.* **1997**, *119*, 6450
- [20] R. N. F. Thorneley, S. J. George, in *Prokaryotic Nitrogen Fixation: A Model System for Analysis of a Biological Process*. (Ed.: E. W. Triplett), Horizon Scientific Press, Wymondham, UK., **2000**, p. 81.
- [21] J. D. Tolland, R. N. F. Thorneley, *Biochemistry* **2005**, *44*, 9520.
- [22] C. J. Pickett, K. A. Vincent, S. K. Ibrahim, C. A. Gormal, B. E. Smith, S. P. Best, *Chem. Eur. J.* **2003**, *9*, 76.
- [23] D. M. Adams, *Metal-Ligand and Related Vibrations*, Edward Arnold, London, **1967**.
- [24] W. Roseboom, A. L. De Lacey, V. M. Fernandez, E. C. Hatchikian, S. P. J. Albracht, *J. Biol. Inorg. Chem.* **2006**, *11*, 102.

CHAPTER 7

MOLYBDENUM NITROGENASE CATALYZES THE REDUCTION AND
COUPLING OF CO TO FORM HYDROCARBONS⁷

The molybdenum-dependent nitrogenase catalyzes the multi-electron reduction of protons and N₂ to yield H₂ and 2NH₃. It also catalyzes the reduction of a number of non-physiological doubly and triply bonded small molecules (*e.g.* C₂H₂, N₂O). Carbon monoxide (CO) is not reduced by the wild-type molybdenum nitrogenase, but instead inhibits the reduction of all substrates catalyzed by nitrogenase except protons. Here, we report that when the nitrogenase MoFe protein α -Val⁷⁰ residue is substituted by alanine or glycine, the resulting variant proteins will catalyze the reduction and coupling of CO to form methane (CH₄), ethane (C₂H₆), ethylene (C₂H₄), propene (C₃H₆), and propane (C₃H₈). The rates and ratios of hydrocarbon production from CO can be adjusted by changing the flux of electrons through nitrogenase, by substitution of other amino acids located near FeMo-cofactor, or by changing the partial pressure of CO. Increasing the partial pressure of CO shifted the product ratio in favor of the longer chain alkanes and alkenes. The implications of these findings in understanding the nitrogenase mechanism and the relationship to Fischer-Tropsch production of hydrocarbons from CO are discussed.

⁷ This research was originally published in *The Journal of Biological Chemistry*. Zhi-Yong Yang, Dennis R. Dean, and Lance C. Seefeldt. Molybdenum nitrogenase catalyzes the reduction and coupling of CO to form hydrocarbons. *The Journal of Biological Chemistry*. 2011; 286:19417-19421. © the American Society for Biochemistry and Molecular Biology.

Nitrogenase is the bacterial enzyme responsible for the biological reduction of N_2 to ammonia, accounting for more than half of the input of fixed nitrogen into the biogeochemical nitrogen cycle (1). Three different nitrogenases have been identified, with each being coded for by unique sets of genes (2, 3). The three nitrogenase systems are composed of a smaller protein called the Fe protein and a larger protein called the MoFe protein, VFe protein, or FeFe protein, depending on the metal composition of the corresponding cofactors. The Fe protein serves as a reductant of the larger protein, with electron transfer from the Fe protein being coupled to the hydrolysis of 2 MgATP molecules for each electron transferred (4). The nitrogenase system containing Mo is the most widely occurring and is preferentially expressed if sufficient Mo is present in the cell growth medium, with the other nitrogenases being expressed secondarily if Mo is deficient (3, 5).

All three nitrogenase systems catalyze the reduction of N_2 to ammonia and the reduction of protons to H_2 . In addition, all three systems catalyze the reduction of a range of other small molecules that contain double and triple bonds, such as acetylene (C_2H_2) to ethylene (C_2H_4), with different rates and ratios of products being observed for the three systems (2). Carbon monoxide (CO) is a well established inhibitor of all three nitrogenase systems, where it inhibits the reduction of all known substrates except protons (2, 6, 7). Recently, Lee et al. (8) discovered that the vanadium nitrogenase system can reduce and couple CO at low rates to form the hydrocarbons ethane, ethylene, and propane. The molybdenum nitrogenase was not observed to catalyze any detectable reduction of CO to hydrocarbons.

We have recently shown that the substrate range for the molybdenum nitrogenase can be expanded to larger substrates by substitution of an amino acid residue located near the active site FeMo-cofactor (α -Val⁷⁰) (9, 10). In light of our ability to change the substrate range of nitrogenase, and the observation of CO reduction and coupling by the vanadium nitrogenase, it was of interest to determine if CO might be reduced and coupled to form hydrocarbons in the molybdenum nitrogenase having amino acid substitutions at the α -Val⁷⁰ residue.

Experimental procedures

Reagents and protein purification—All reagents were obtained from Sigma-Aldrich (St. Louis, MO) or Fisher Scientific (Fair Lawn, NJ), and were used without further purification, unless specified otherwise. CO was purchased from Matheson Tri-Gas (Basking Ridge, NJ) with a purity of $\geq 99.9\%$. Ethylene (99.9%) was obtained from Praxair Inc. (Danbury, CT). Methane gas was obtained from household natural gas line containing about 3% ethane as an impurity. Propane gas was obtained from a propane fuel tank with an estimated purity of 86%. All other gases were from Air Liquide (Plumsteadville, PA). *Azotobacter vinelandii* strains DJ1260 (wild-type, WT, or α -Val⁷⁰), DJ997 (α -Gln¹⁹⁵), DJ1310 (α -Ala⁷⁰), DJ1316 (α -Ala⁷⁰/ α -Gln¹⁹⁵), DJ1313 (α -Gly⁷⁰), DJ1391 (α -Ala⁷⁰/ α -His⁹⁶), and DJ1495 (α -Ala⁷⁰/ α -Ala¹⁹¹) were grown and the corresponding nitrogenase MoFe proteins were expressed and purified as previously described (11). All MoFe proteins in this study contain a seven-His tag addition near the carboxy-terminal end of the α -subunit. The purification of these proteins was accomplished by following the previously developed zinc affinity purification protocol (11). Protein concentrations were determined by the Biuret assay using bovine serum

albumin as standard. The purities of these proteins were >95% based on SDS-PAGE analysis with Coomassie Blue staining. Manipulation of proteins and buffers was done in septum-sealed serum vials under an argon atmosphere or on a Schlenk vacuum line. All gases and liquid transfers used gas-tight syringes.

Carbon monoxide reduction assays—Unless stated otherwise, CO reduction assays were conducted in serum vials having a 9.4-mL total volume and containing 1 mL of an assay buffer consisting of 200 mM MOPS, pH 7.0, with MgATP and a MgATP regenerating system (13.4 mM MgCl₂, 10 mM ATP, 60 mM phosphocreatine, 1.3 mg/mL bovine serum albumin, and 0.4 mg/mL creatine phosphokinase). After the solution was made anaerobic, 150 μL of 1 M dithionite solution and the MoFe protein were added. Reactions were initiated by the addition of Fe protein and incubated at 30°C. Reactions were quenched by the addition of 300 μL of 400 mM EDTA, pH = 8.0, solution. All assays were done under 1 atm of CO pressure except for wild-type and α-Gln¹⁹⁵ MoFe proteins (0.106 atm of CO for these two cases). Methane (CH₄), ethylene (C₂H₄), and ethane (C₂H₆) were quantified by gas chromatography by injection of 200 μL of the gas phase of the reaction vial (400 μL for wild-type and α-Ala⁷⁰/α-Gln¹⁹⁵ MoFe samples) into a Shimadzu GC-8A equipped with a flame ionization detector fitted with a 30 cm × 0.3 cm Porapak N column with nitrogen as the carrier gas. The injection/detection temperature was set to 180°C, and the column temperature was set to 110°C. The standard curves with high linearity were created using methane, ethylene, and ethane gases diluted with argon in 9.4-mL serum vials. Propane (C₃H₈) and propene (C₃H₆) were quantified by gas chromatography by injection of 100 μL of the gas phase of the reaction vial into a Shimadzu GC-2010 gas chromatograph equipped with a flame ionization

detector fitted with a Rt-Alumina BOND/KCl column (30 m, 0.32 mm inner diameter, and 5 μm film thickness) (Restek, Belafonte, PA). Helium was used as the carrier gas set at a linear velocity of 45 cm/s. The injection/detection temperature was set to 200°C, and the column temperature was set to 60°C. Identification of three- and four-carbon hydrocarbons were confirmed by mass spectroscopy (GCMS-QP2010S, Shimadzu Scientific). After addition of 300 μL of EDTA solution, the total liquid volumes in the standard vials were the same as those in CO reduction assay vials.

For the electron flux dependence study, 1 mg of MoFe protein was used for each assay vial. Molar ratios of Fe protein to MoFe protein from 4:1 to 20:1 were tested. All these assays were incubated for 2 hours before quenching with EDTA. For time dependence measurements and CO pressure dependence studies, the amount of MoFe protein and the electron flux for different mutants was varied.

Results

Reduction of CO by $\alpha\text{-Ala}^{70}$ substituted MoFe proteins—Consistent with the earlier report (8), we find that the wild-type MoFe protein shows no catalytic production of hydrocarbons by reduction and coupling of CO when analyzed over 90 min under turnover conditions. In contrast, when the MoFe protein residue $\alpha\text{-Ala}^{70}$ was substituted by alanine ($\alpha\text{-Ala}^{70}$) or glycine ($\alpha\text{-Gly}^{70}$), the variant MoFe proteins were found to reduce and couple CO to hydrocarbons in a reaction dependent on the presence of Fe protein, MgATP, and reductant (**Figure 7-1**). Four hydrocarbon products were quantified for both

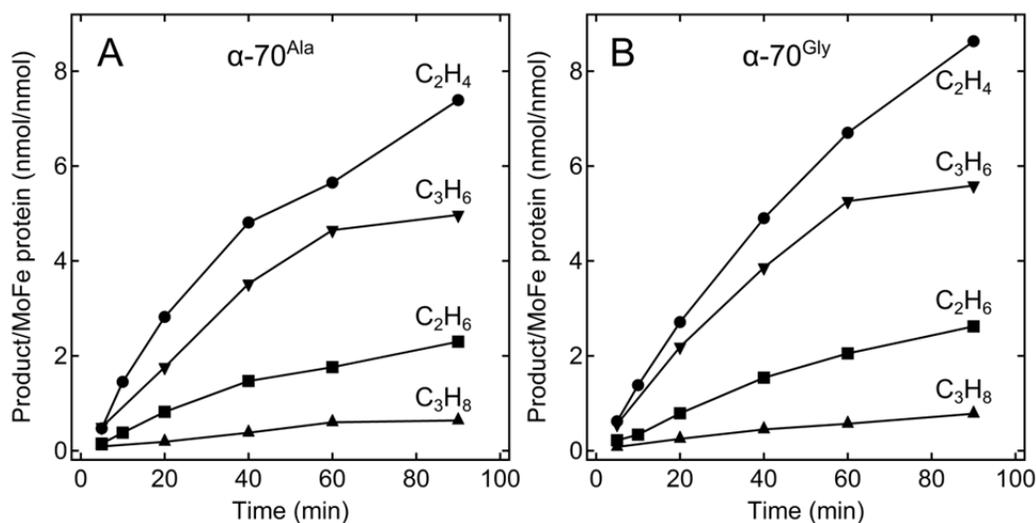


Figure 7-1. Time course of hydrocarbon production by the α -Ala⁷⁰ and α -Gly⁷⁰ substituted MoFe proteins. The quantity of (●) ethylene (C₂H₄), (■) ethane (C₂H₆), (▼) propene (C₃H₆), and (▲) propane (C₃H₈) produced per MoFe protein (nmol product per nmol MoFe protein) as a function of time is shown for the α -Ala⁷⁰ (A), and α -Gly⁷⁰ (B) MoFe nitrogenases. Assay conditions are described under “Experimental Procedures.”

the α -Ala⁷⁰ and α -Gly⁷⁰ MoFe proteins: the alkanes ethane (C₂H₆) and propane (C₃H₈) and the alkenes ethylene (C₂H₄) and propene (C₃H₆). For both proteins, the highest yielding product was ethylene, followed by propene, ethane, and propane. The amounts of hydrocarbons produced were approximately 7 nmol ethylene (C₂H₄)/nmol MoFe protein, 4 nmol propene (C₃H₆)/nmol MoFe protein, 2 nmol ethane (C₂H₆)/nmol MoFe protein, and 1 nmol propane (C₃H₈)/nmol MoFe protein over 60 min. Three of these products (ethylene, ethane, and propane) were reported for CO reduction by the vanadium nitrogenase system (8), although the relative ratio of products and rates of

production were different between the two nitrogenase systems. For the vanadium nitrogenase, product production rates were 140 nmols ethylene/nmol VFe protein, 1.5 nmol propane/nmol VFe protein, and 5 nmols ethane/nmol VFe protein over 60 min. No propene product was reported for the vanadium nitrogenase, whereas this was the second most abundant product in the molybdenum nitrogenase.

Effects of additional amino acid substitutions—In addition to the pivotal role of α -Val⁷⁰ in defining substrate binding to FeMo-cofactor, we have earlier shown that two additional amino acids located near FeMo-cofactor, α -Arg⁹⁶ and α -Gln¹⁹¹, can affect substrate binding (12, 13). Substituting these amino acids by histidine or alanine, respectively, has been shown to further expand the substrate range of nitrogenase to include even longer chain alkynes. We therefore examined the doubly substituted α -Ala⁷⁰/ α -His⁹⁶ and α -Ala⁷⁰/ α -Ala¹⁹¹ MoFe proteins to test if they might reduce and couple CO. Both of the doubly substituted MoFe proteins showed an altered product profile for hydrocarbon production, with the yield of the longer chain products propane and propene rising significantly (**Figure 7-2**). For the α -Ala⁷⁰/ α -Ala¹⁹¹ MoFe protein, 8 nmol of propene were accumulated per nmol of MoFe protein over 60 min. A trace of methane (CH₄) was also detected as a product of CO reduction for both doubly substituted MoFe proteins, whereas methane was not detected for any of the singly substituted MoFe protein variants. The doubly substituted MoFe proteins demonstrated a non-linear production of products, suggesting possible inactivation of these enzymes during the course of the assay.

The amino acid α -His¹⁹⁵ is located near FeMo-cofactor and has been implicated in the delivery of protons for the reduction of nitrogenous substrates (14, 15). We find that

when α -His¹⁹⁵ is substituted by glutamine in combination with the α -Ala⁷⁰ substitution, the rates of product formation for CO reduction and coupling are greatly decreased (Figure 7-3), consistent with the possibility that α -His¹⁹⁵ functions to deliver protons for the reduction of CO.

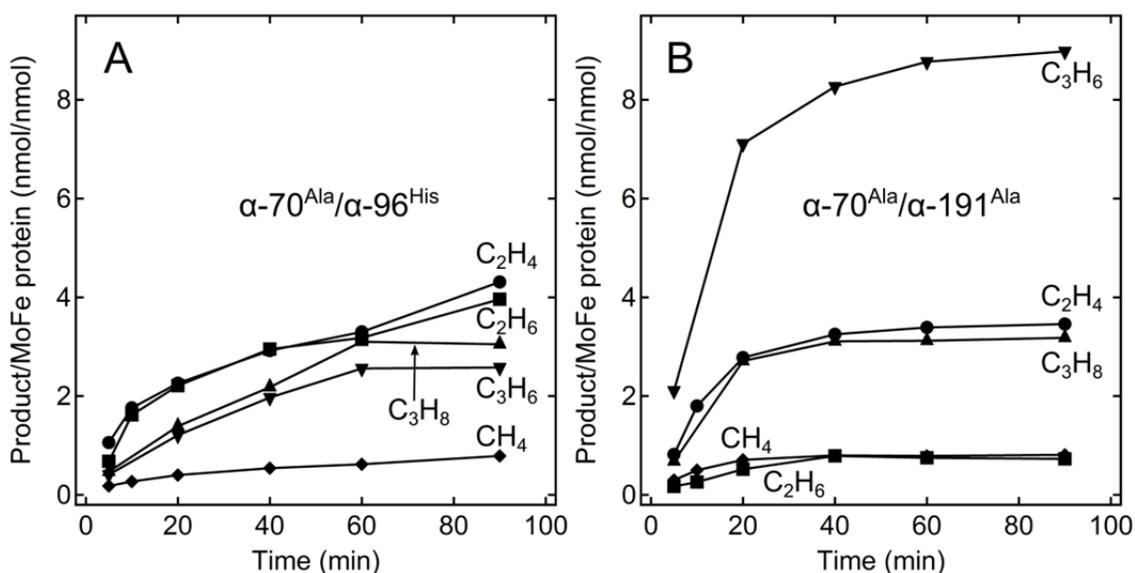


Figure 7-2. Time course of hydrocarbon production by the α -Ala⁷⁰/ α -His⁹⁶ and α -Ala⁷⁰/ α -Ala¹⁹¹ substituted MoFe proteins. The quantity of (◆) methane (CH₄), (●) ethylene (C₂H₄), (■) ethane (C₂H₆), (▼) propene (C₃H₆), and (▲) propane (C₃H₈) produced per MoFe protein (nmol product per nmol MoFe protein) as a function of time is shown for the α -Ala⁷⁰/ α -His⁹⁶ (A) and α -Ala⁷⁰/ α -Ala¹⁹¹ (B) MoFe nitrogenases.

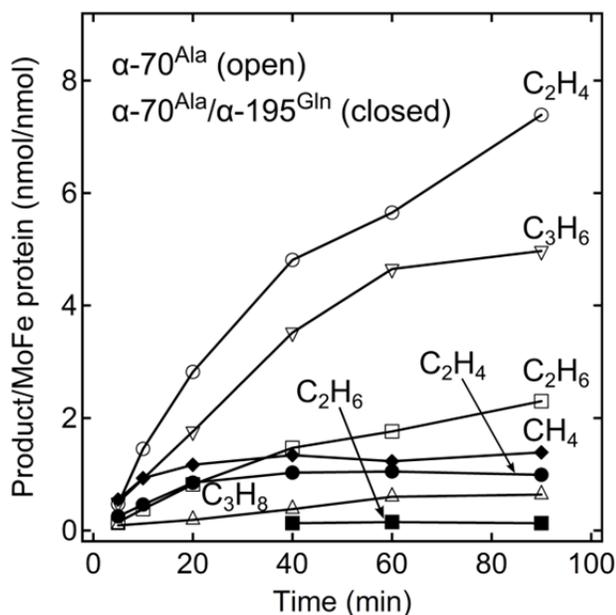


Figure 7-3. Time course of hydrocarbon production by the α -Ala⁷⁰ and α -Ala⁷⁰/ α -Gln¹⁹⁵ substituted MoFe proteins. The quantity of (*circles*) ethylene (C₂H₄), (*squares*) ethane (C₂H₆), (*inverted triangles*) propene (C₃H₆), and (*triangles*) propane (C₃H₈) produced per MoFe protein (nmol product per nmol MoFe protein) as a function of time is shown for the α -Ala⁷⁰ (*open symbols*) and α -Ala⁷⁰/ α -Gln¹⁹⁵ MoFe proteins (*closed symbols*).

Influence of electron flux on product ratio—Electron flux in nitrogenase is defined as the rate of total electrons flowing through the enzyme going to substrates. The flux can be controlled by varying the ratio of Fe protein to MoFe protein, with a low ratio corresponding to low flux and a higher ratio corresponding to higher flux (2). Increasing electron flux affected the product profile for the α -Ala⁷⁰, α -Gly⁷⁰, and α -Ala⁷⁰/ α -His⁹⁶ MoFe proteins (**Figure 7-4**). In each case, however, ethylene remained the most abundant product over the range tested.

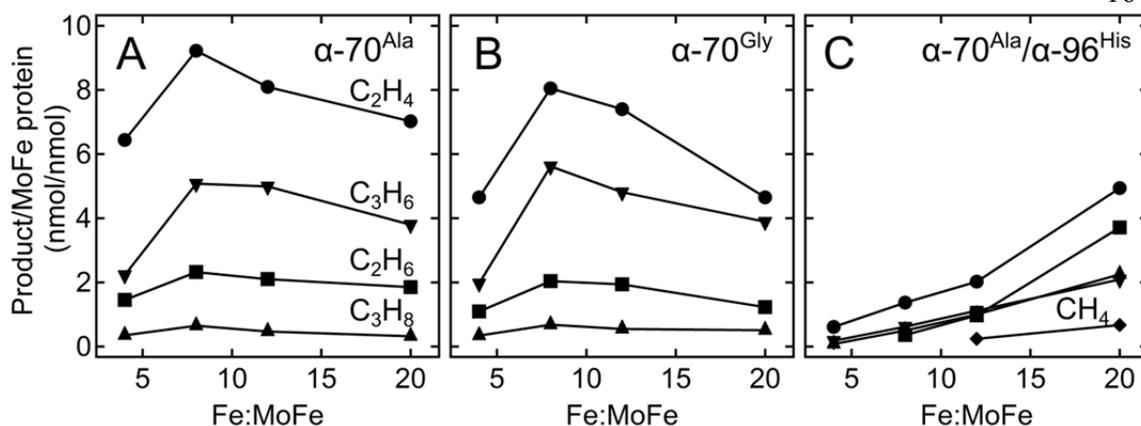


Figure 7-4. Electron flux dependence on CO reduction product profile. The quantity of (\blacklozenge) methane (CH_4), (\bullet) ethylene (C_2H_4), (\blacksquare) ethane (C_2H_6), (\blacktriangledown) propene (C_3H_6), and (\blacktriangle) propane (C_3H_8) produced per MoFe protein (nmol product per nmol MoFe protein) is shown as a function of the molar ratio of Fe protein to MoFe protein for the $\alpha\text{-Ala}^{70}$ (A), $\alpha\text{-Gly}^{70}$ (B), and $\alpha\text{-Ala}^{70}/\alpha\text{-His}^{96}$ (C) MoFe proteins. The time of the assay was 120 min.

Influence of CO partial pressure on product profile—Varying the partial pressure of CO has been shown to result in different numbers of CO bound to FeMo-cofactor (6, 16). Under low concentrations of CO (~ 0.08 atm partial pressure), a single CO species binds to FeMo-cofactor, referred to as the low CO state. At partial pressures of CO above 0.4 atm, two CO molecules bind to FeMo-cofactor, referred to the high CO state (17). It was therefore of interest to determine if varying the partial pressure of CO might also alter the product profile for CO reduction and coupling. As can be seen in **Figure 7-5**, the partial pressure of CO significantly changes the product profile for the four MoFe protein variants examined ($\alpha\text{-Ala}^{70}$, $\alpha\text{-Gly}^{70}$, $\alpha\text{-Ala}^{70}/\alpha\text{-His}^{96}$, $\alpha\text{-Ala}^{70}/\alpha\text{-Ala}^{191}$ MoFe proteins). At lower CO partial pressure (0.08 atm), the shorter chain C2 products are favored. At

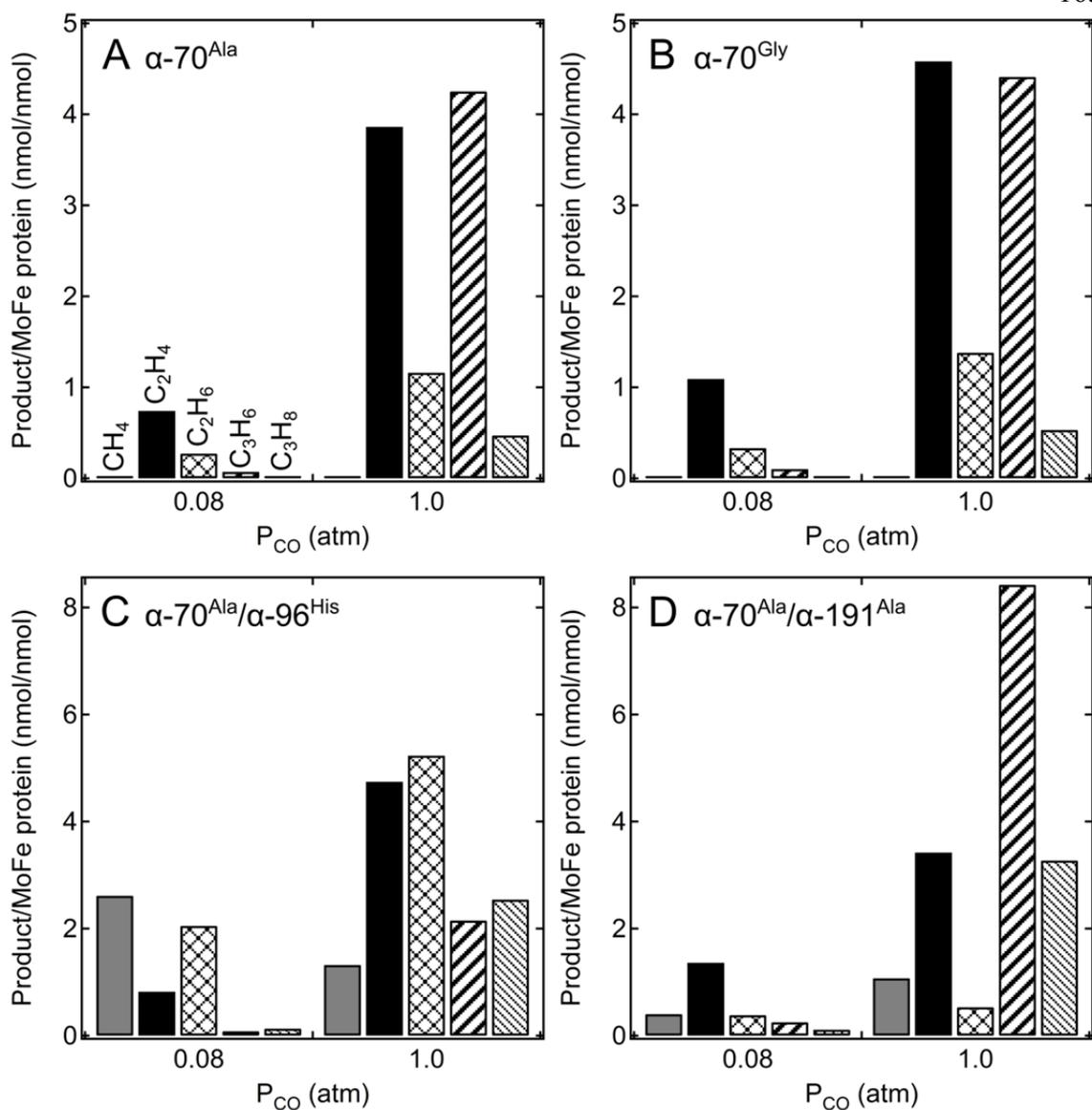


Figure 7-5. CO pressure dependence on CO reduction product profile. Shown are the methane (CH_4), ethylene (C_2H_4), ethane (C_2H_6), propene (C_3H_6), and propane (C_3H_8) production per MoFe protein (nmol product per nmol of MoFe protein) under either low CO (0.08 atm) or high CO (1.0 atm) for the $\alpha-Ala^{70}$ (A), $\alpha-Gly^{70}$ (B), $\alpha-Ala^{70}/\alpha-His^{96}$ (C), and $\alpha-Ala^{70}/\alpha-Ala^{191}$ (D) MoFe proteins. Assay time is 60 min. P_{CO} , Partial pressure of CO.

this low CO concentration, the α -Ala⁷⁰/ α -His⁹⁶ MoFe protein also showed a significant methane production rate. At high CO partial pressure (1.0 atm), the product profile shifted in favor of the longer chain C3 hydrocarbons.

Discussion

Earlier spectroscopic studies of CO bound to nitrogenase indicate that there are two CO binding sites on FeMo-cofactor (6). At low CO concentrations, only one CO is bound, whereas at higher CO concentrations two CO molecules are bound (17-19). The observation that CO can be reduced to 2 and 3 carbon containing hydrocarbons demands that the two CO binding sites on FeMo-cofactor are close enough to allow a coupling reaction that would result in the formation of C2 and C3 hydrocarbon products. This fact, coupled with the parallels between this reaction and the Fischer-Tropsch reaction (20-23), suggest a possible mechanism for CO reduction and coupling by nitrogenase (**Figure 7-6**). Initially, two CO molecules would chemisorb to two adjacent metal (**Figure 7-6**, *black circles*) atoms of FeMo-cofactor. Available spectroscopic studies on CO bound to FeMo-cofactor indicate that the CO molecules are bound to iron atoms located in the waist region of FeMo-cofactor (19, 24, 25). Reduction of the two metal bound CO molecules by protons and electrons (hydrogen) with loss of water would result in the formation of metal bound -CH_x and -CH_y groups. Analogous intermediates have been proposed in a mechanism for the Fischer-Tropsch reaction (22). The two metal bound -CH_x groups could either be further reduced/protonated, resulting in release of methane, or a coupling reaction could result in the formation of a CH_x-CH_y species bound to one metal. This species could yield ethylene or ethane or a third CO could bind to and be reduced at the

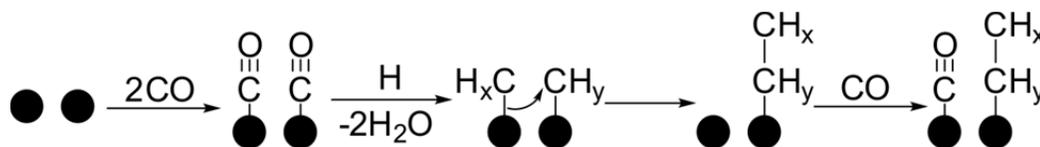


Figure 7-6. Schematic representation of a possible CO-derived hydrocarbon formation at the nitrogenase active site. *Black circles* represent CO binding sites, presumably Fe atoms, upon which two CO can bind. Following reduction to semi-reduced states ($-\text{CH}_x$ and $-\text{CH}_y$), coupling can occur, resulting in formation of a $\text{CH}_x\text{-CH}_y$ species. The binding of additional CO molecules can lead to further chain elongation.

open metal site, leading to the formation of C3 or longer hydrocarbons. Traces of longer chain (C4) hydrocarbon products were detected from molybdenum nitrogenase reduction and coupling of CO molecules that were tentatively assigned by mass spectroscopy as isobutene and *n*-butane (data not shown).

In this mechanism, it is expected that higher CO concentrations would favor two bound CO molecules, which in turn would favor formation of longer chain hydrocarbons (e.g., propene and propane) consistent with the observations here. Nevertheless, even under low CO concentrations that have been assigned to a single CO bound to FeMo-cofactor, we still observe C2 and C3 products, consistent with CO binding at both sites even at the lower CO concentrations.

Essential for the CO reduction reactions is the delivery of protons. For the Fischer-Tropsch reduction of CO, hydrogen atoms come from H_2 . For nitrogenase catalyzed reduction, protons appear to come from multiple sites, although $\alpha\text{-His}$ ¹⁹⁵ residue located near FeMo-cofactor has been shown to play a critical role in proton

delivery for reduction of nitrogenous substrates (14, 15). Substitution of this residue with the amino acid glutamine effectively eliminates N₂ reduction, even though N₂ still binds to FeMo-cofactor in the substituted MoFe protein (14, 15). Such an inability to reduce N₂ is likely due to a disruption in the proton delivery needed for substrate reduction. To test if α -His¹⁹⁵ might also be responsible for delivery of protons for CO reduction, the α -Gln¹⁹⁵ substitution was introduced into the α -Ala⁷⁰ MoFe protein. The resulting doubly substituted MoFe protein showed significantly lowered CO reduction rates for all products, consistent with the α -His¹⁹⁵ being responsible for much, but not all, of the proton delivery for CO reduction in the MoFe protein.

One of the goals for Fischer-Tropsch chemistry is finding catalysts and conditions that favor the formation of the higher value, longer chain hydrocarbons like propene and propane (23). Here we report that introduction of additional amino acid substitutions near FeMo-cofactor and increasing the CO concentration can significantly shift the product profile of nitrogenase CO reduction and coupling in favor of production of these longer chain hydrocarbons. Thus, the molybdenum nitrogenase offers an experimentally tractable system for examining mechanistic features that favor the production of longer chain hydrocarbons from CO that might be translated to the development of small molecule metal complexes that catalyze such reactions.

In summary, we report that when the active site of the molybdenum nitrogenase is exposed by substitution of α -Val⁷⁰, CO can be reduced and coupled to yield the hydrocarbons methane, ethylene, ethane, propene, and propane. Further, it is found that the relative ratio of products can be manipulated by altering other amino acids, electron flux or the CO concentration.

References

1. Smil, V. (2004) *Enriching the Earth: Fritz Haber, Carl Bosch, and the Transformation of World Food Production*, The MIT Press, Cambridge, MA
2. Burgess, B. K., and Lowe, D. J. (1996) *Chem. Rev.* **96**, 2983-3012
3. Eady, R. R. (1996) *Chem. Rev.* **96**, 3013-3030
4. Howard, J. B., and Rees, D. C. (1994) *Annu. Rev. Biochem.* **63**, 235-264
5. Joerger, R. D., and Bishop, P. E. (1988) *Crit. Rev. Microbiol.* **16**, 1-14
6. Davis, L. C., Henzl, M. T., Burris, R. H., and Orme-Johnson, W. H. (1979) *Biochemistry* **18**, 4860-4869
7. Rivera-Ortiz, J. M., and Burris, R. H. (1975) *J. Bacteriol.* **123**, 537-545
8. Lee, C. C., Hu, Y., and Ribbe, M. W. (2010) *Science* **329**, 642
9. Dos Santos, P. C., Igarashi, R. Y., Lee, H., Hoffman, B. M., Seefeldt, L. C., and Dean, D. R. (2005) *Acc. Chem. Res.* **38**, 208-214
10. Seefeldt, L. C., Hoffman, B. M., and Dean, D. R. (2009) *Annu. Rev. Biochem.* **78**, 701-722
11. Christiansen, J., Goodwin, P. J., Lanzilotta, W. N., Seefeldt, L. C., and Dean, D. R. (1998) *Biochemistry* **37**, 12611-12623
12. Dos Santos, P. C., Mayer, S. M., Barney, B. M., Seefeldt, L. C., and Dean, D. R. (2007) *J. Inorg. Biochem.* **101**, 1642-1648
13. Benton, P. M., Mayer, S. M., Shao, J., Hoffman, B. M., Dean, D. R., and Seefeldt, L. C. (2001) *Biochemistry* **40**, 13816-13825
14. Kim, C. H., Newton, W. E., and Dean, D. R. (1995) *Biochemistry* **34**, 2798-2808
15. Fisher, K., Dilworth, M. J., and Newton, W. E. (2000) *Biochemistry* **39**, 15570-15577
16. Maskos, Z., Fisher, K., Sørli, M., Newton, W. E., and Hales, B. J. (2005) *J. Biol. Inorg. Chem.* **10**, 394-406
17. Lee, H., Cameron, L. M., Hales, B. J., and Hoffman, B. M. (1997) *J. Am. Chem. Soc.* **119**, 10121-10126
18. Lee, H., Sørli, M., Christiansen, J., Yang, T., Shao, J., Dean, D. R., Hales, B. J., and Hoffman, B. M. (2005) *J. Am. Chem. Soc.* **127**, 15880-15890

19. Christie, P. D., Lee, H., Cameron, L. M., Hales, B. J., Orme-Johnson, W. H., and Hoffman, B. M. (1996) *J. Am. Chem. Soc.* **118**, 8707-8709
20. Rofer-DePoorter, C. K. (1981) *Chem. Rev.* **81**, 447-474
21. Zhang, C., Zhao, G., Liu, K., Yang, Y., Xiang, H., and Li, Y. (2010) *J. Mol. Catal. A-Chem.* **328**, 35-43
22. Davis, B. H. (2009) *Catal. Today* **141**, 25–33
23. Khodakov, A. Y., Chu, W., and Fongarland, P. (2007) *Chem. Rev.* **107**, 1692-1744
24. Pollock, R. C., Lee, H., Cameron, L. M., DeRose, V. J., Hales, B. J., Orme-Johnson, W. H., and Hoffman, B. M. (1995) *J. Am. Chem. Soc.* **117**, 8686-8687
25. Yang, Z., Seefeldt, L. C., Dean, D. R., Cramer, S. P., and George, S. J. (2011) *Angew. Chem. Int. Ed.* **50**, 272-275

CHAPTER 8

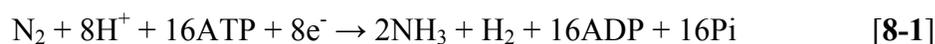
CARBON DIOXIDE REDUCTION TO METHANE AND COUPLING WITH
ACETYLENE TO FORM PROPYLENE CATALYZED BY REMODELED
NITROGENASE⁸

A doubly substituted form of the nitrogenase MoFe protein (α -70^{Val}→Ala, α -195^{His}→Gln) has the capacity to catalyze the reduction of carbon dioxide (CO₂) to yield methane (CH₄). Under optimized conditions, one nmole of the substituted MoFe protein catalyzes the formation of 21 nmole of CH₄ within 20 minutes. The catalytic rate is dependent on the partial pressure of CO₂ (or concentration of HCO₃⁻) and on the electron flux through nitrogenase. The doubly substituted MoFe protein also has the capacity to catalyze the unprecedented formation of propylene (H₂C=CH-CH₃) through the reductive coupling of CO₂ and acetylene (HC≡CH). In light of these observations, we suggest that an emerging understanding of the mechanistic features of nitrogenase could be relevant to the design of synthetic catalysts for CO₂ sequestration and formation of olefins.

⁸ Coauthored by Zhi-Yong Yang, Vivian R. Moure, Dennis R. Dean, and Lance C. Seefeldt (2012) *Proceedings of the National Academy of Sciences of the United States of America* **109**(48), 19644-19648.

Carbon dioxide (CO₂) is an abundant and stable form of carbon that is the product of respiration and burning of fossil fuels. As a result of these activities, the atmospheric concentration of CO₂, a greenhouse gas, has been rising over the last century contributing to global warming (1). There is strong interest in developing methods for sequestering CO₂ either by capturing it or by chemically converting it to valuable chemicals (2–5). Of particular interest are possible routes to reduction of CO₂ by multiple electrons to yield methanol (CH₃OH) and methane (CH₄), which are renewable fuels (2). The reduction of CO₂ is difficult, with a limited number of reports of metal-based compounds able to catalyze these reactions (6–13). In biology, only a few enzymes are known to reduce CO₂ (14–18), and none of these can catalyze the eight electron reduction to CH₄.

The bacterial Mo-dependent nitrogenase enzyme catalyzes the multi-electron/proton reduction of dinitrogen (N₂) to two ammonia (NH₃) at a metal cluster designated FeMo-cofactor [7Fe-9S-1Mo-1C-*R*-homocitrate] (**Figure 8-1**) in a reaction that requires ATP hydrolysis and evolution of H₂, with a minimal reaction stoichiometry shown in equation **8-1** (19–22).



Given that nitrogenase is effective at catalyzing the difficult multi-electron reduction of N₂, it was of interest to determine if this enzyme might also catalyze the reduction of CO₂ to the level of CH₄. Nitrogenase is known to have the capacity to reduce a variety of other small, relatively inert, doubly or triply bonded compounds, such as acetylene (HC≡CH) (19, 23). It has recently been shown that an alternative form of nitrogenase, which contains V in place of Mo in the active site cofactor, has the remarkable capacity to reduce CO and couple multiple CO molecules, yielding short chain alkenes and

Results

CO₂ reduction to CH₄ by remodeled nitrogenase. When the wild-type nitrogenase was tested for reduction of CO₂ to yield CH₄, no CH₄ above background could be detected over the course of 20 min (**Figure 8-2**). Earlier work has demonstrated that several amino acids having side chains that approach FeMo-cofactor play an important role in controlling substrate binding and reduction (20, 28). Among these residues are included α -70^{Val}, α -195^{His}, and α -191^{Gln} (**Figure 8-1**). Variant forms of the MoFe protein having α -70 substituted by Ala, α -195 substituted by Gln, or α -70 and α -191 both substituted by Ala showed no appreciable capacity for reduction of CO₂ to yield CH₄. In contrast, a doubly substituted MoFe protein, α -70^{Ala}/ α -195^{Gln}, was found to catalyze the formation of CH₄ from CO₂, forming up to 16 nmol of CH₄/nmol of MoFe protein over 20 min (**Figure 8-2**). The formation of CH₄ was absolutely dependent on the presence of CO₂, Fe protein, MoFe protein, and MgATP. The rate of CH₄ production was found to increase with increasing partial pressure of CO₂ up to 0.45 atm (**Figure D-S1**, APPENDIX D). A fit of these data to the Michaelis-Menten equation gave a K_m for CO₂ of 0.23 atm and a V_{max} of 21 nmol CH₄/nmol MoFe protein over 20 min. In a Bis-Tris buffer at pH 6.7, sodium bicarbonate (NaHCO₃) could also serve as a substrate for CH₄ formation, with a determined K_m of 16 mM for NaHCO₃ and V_{max} of 14 nmol CH₄/nmol MoFe protein over 20 min (**Figure D-S2**, APPENDIX D).

The rate of electron flow through nitrogenase (called electron flux) can be regulated by altering the ratio of Fe protein to MoFe protein (Fe protein:MoFe protein), with a low ratio corresponding to low electron flux and a high ratio corresponding to high electron flux. Under all conditions, the majority of electrons passing through nitrogenase

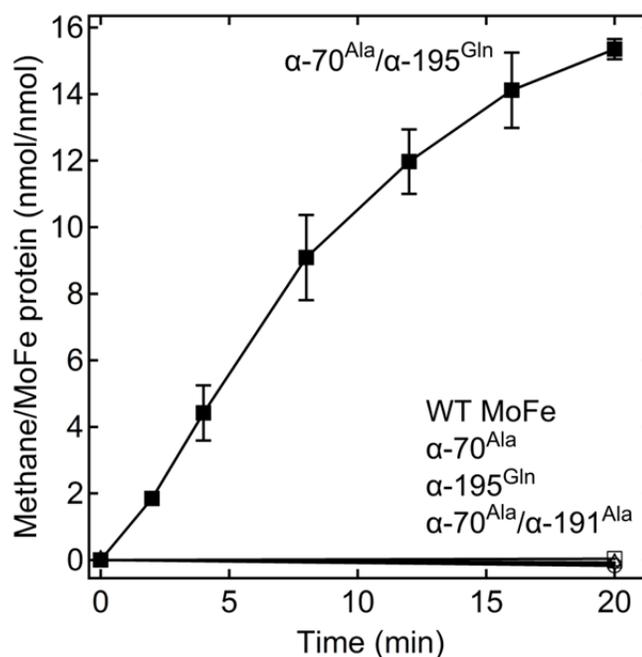


Figure 8-2. CH₄ formation as a function of time for different MoFe proteins. CO₂ reduction to CH₄ is shown as a function of time for the wild-type (○), α -70^{Ala} (◇), α -195^{Gln} (△), α -70^{Ala}/ α -191^{Ala} (□) and α -70^{Ala}/ α -195^{Gln} (■) MoFe proteins. The partial pressure of CO₂ was 0.45 atm, the concentration of MoFe protein was 0.5 mg/mL, and Fe protein was 3 mg/mL. The reaction temperature was 30°C. The complete assay for α -70^{Ala}/ α -195^{Gln} MoFe protein was done in triplicate, with SE bars shown.

in the presence of saturating CO₂ were found to reduce protons to make H₂ with relatively low rates of associated CH₄ formation (**Figure 8-3**). However, as the electron flux increased, the proportion of electrons passing to CO₂ reduction increased, reaching a maximum at a molar ratio of about 50 Fe protein per MoFe protein. At this highest flux, the molar ratio of H₂ formed per CH₄ formed was approximately 250:1. Given that proton reduction is a two-electron reduction and CO₂ reduction to CH₄ is an eight electron

reduction, up to 2% of the total electron flux passing through nitrogenase goes to CO₂ reduction to methane under these conditions.

The use of ¹²C- or ¹³C-enriched bicarbonate (HCO₃⁻) as substrate and product analysis by gas chromatography-mass spectrometry (GC-MS) confirmed that CH₄ formation was derived from added CO₂. When H¹²CO₃⁻ was the added substrate, a peak having the same retention time as methane showed a mass over charge (*m/z*) peak of 16, whereas no peak with *m/z* of 17 was observed (**Figure D-S3**, APPENDIX D). When H¹³CO₃⁻ was the substrate, a peak having the same retention time was found to have a *m/z* of 17, which can be ascribed to the molecular mass of ¹³CH₄. This result demonstrates that HCO₃⁻ or CO₂ is the substrate for CH₄ formation rather than some other component in the reaction mixture.

When the CO₂ reduction reaction catalyzed by the remodeled nitrogenase was performed in the presence of 0.30 mg/mL of deoxyhemoglobin, the amount of CH₄ formed was lowered by ~25% (**Figure D-S4**, APPENDIX D). Deoxyhemoglobin binds CO very rapidly (rate constant $k \approx 2 \times 10^5 \text{ M}^{-1} \text{ s}^{-1}$) and with a high affinity (dissociation constant $K_d \approx 50 \text{ nM}$) and would, therefore, bind any CO released into solution during CO₂ reduction by nitrogenase (27). While CO is expected to be an intermediate along the reaction pathway from CO₂ to CH₄, a relatively small lowering of the rate of formation of CH₄ from CO₂ when deoxyhemoglobin is included in reaction cocktail indicates that CO₂ reduction follows primarily a non-dissociative mechanism.

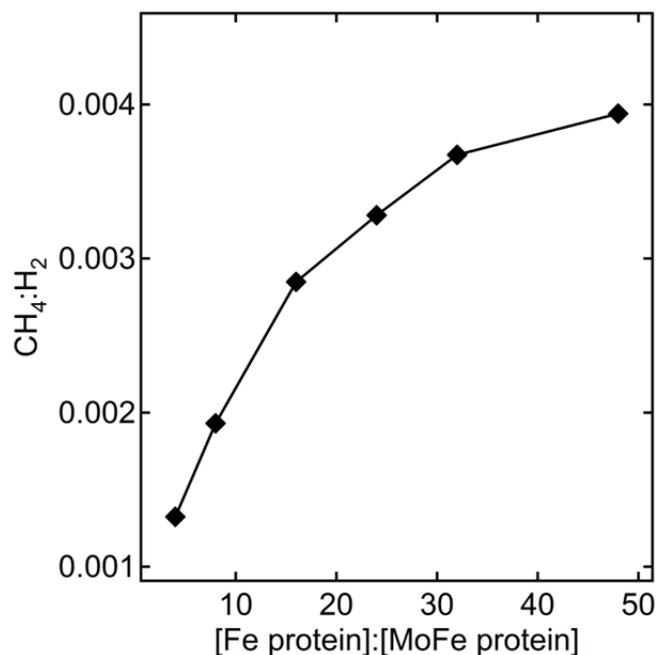


Figure 8-3. Electron flux dependence for CO₂ reduction to CH₄. The ratio CH₄ formed to H₂ formed is shown as a function of the electron flux through the α -70^{Ala}/ α -195^{Gln} MoFe protein for assays quenched after 20 min at 30°C. The partial pressure of CO₂ was 0.45 atm, the concentration of MoFe protein was 0.5 mg/mL, and Fe protein was varied from 0.5 to 6 mg/mL.

Several earlier studies revealed multiple inhibitor and substrate binding sites on FeMo-cofactor, including at least two binding sites for CO (29–33) and acetylene (31, 34, 35). Two adjacent binding sites can explain the earlier reports that two or three CO molecules can be reduced and coupled to form C₂ and C₃ hydrocarbon products (24, 26). It was therefore of interest to test if the doubly substituted MoFe protein could couple two or more CO₂ molecules to yield short chain hydrocarbons. Under the assay conditions examined, no C₂ or C₃ hydrocarbon products were detected above the

background when CO₂ was the sole C substrate. However, when a small amount of acetylene was added when CO₂ was used as substrate, the C₃ hydrocarbon propylene (H₂C=CH-CH₃) was detected as the major product and propane (H₃C-CH₂-CH₃) as a minor product. Propylene formation only occurred in a reaction with all components for a complete nitrogenase assay, revealing that propylene is formed by nitrogenase turnover. Interestingly, it was found that propylene formation was favored under relatively low electron flux conditions (4 Fe protein: 1 MoFe protein), with higher electron flux favoring CH₄ formation at the expense of propylene formation under 0.45 atm of CO₂ and 0.014 atm of acetylene (**Figure 8-4**). Under the optimal electron flux condition, the amount of propylene formed increased with increasing acetylene partial pressure up to 0.027 atm and then decreased rapidly at higher acetylene concentrations (**Figure 8-5**) likely due to inhibition of CO₂ reduction by acetylene. The results indicate there is an optimal concentration ratio between CO₂ and acetylene to achieve reductive coupling of the two molecules at a given electron flux. All possible combinations of electron flux and acetylene and CO₂ concentration have not been examined.

Formation of propylene from the reductive coupling of one CO₂ and one C₂H₂ was confirmed by GC-MS analysis. When H¹²CO₃⁻ and ¹²C₂H₂ were used as substrates, the propylene elution peak displayed a molecular ion peak with m/z of 42, which is ascribed to ¹²C₃H₆. Trace amounts of a fragment with a m/z of 43 was observed due to natural abundance of ¹³C and ²H. When H¹³CO₃⁻ was used together with ¹²C₂H₂, a molecular ion peak with m/z of 43 was detected at the same retention time as propylene, consistent with the coupling of one ¹³CO₂ with one ¹²C₂H₂ to form ¹³CH₃-¹²CH=¹²CH₂ (**Figure D-S5**, APPENDIX D).

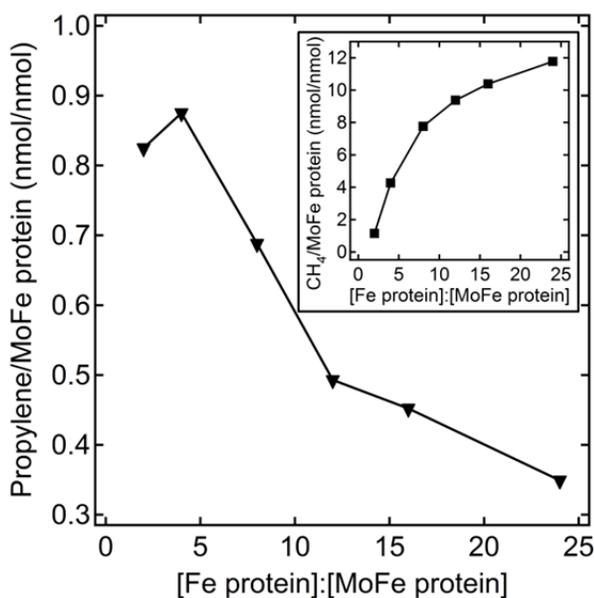
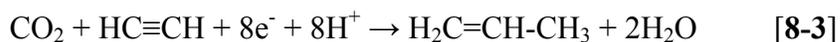


Figure 8-4. Propylene formation from CO₂ and acetylene as a function of electron flux. The amount of propylene formed as a function of electron flux is shown for the α -70^{Ala}/ α -195^{Gln} MoFe protein. The partial pressure of CO₂ was 0.45 atm and C₂H₂ was 0.014 atm. The concentration of MoFe protein was 0.5 mg/mL, and Fe protein was varied from 0.25 to 3 mg/mL. The reactions were incubated at 30°C for 60 min. The inset shows the CH₄ production as a function of electron flux.

Discussion

The discovery reported here that remodeled nitrogenase is able to reduce CO₂ by eight electrons to CH₄ (**eqn 8-2**) makes it unique among known enzyme catalyzed reactions. Further, the ability to reduce CO₂ and couple it to acetylene to form propylene (**eqn 8-3**) makes nitrogenase unique among all reported catalysts (5).



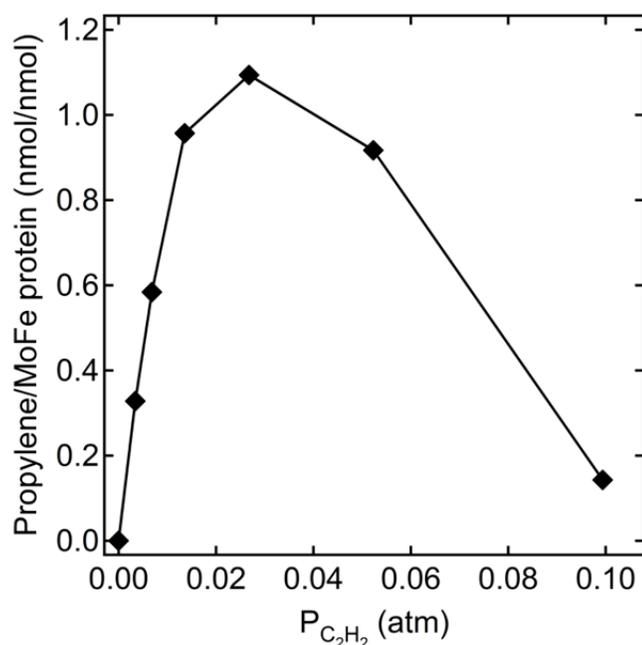


Figure 8-5. Propylene formation from CO₂ and acetylene. The dependence of propylene formation on the partial pressure of acetylene at a partial pressure of CO₂ of 0.40-0.45 atm is shown for the α -70^{Ala}/ α -195^{Gln} MoFe protein. The concentration of MoFe protein was 0.5 mg/mL, and Fe protein was 0.5 mg/mL. The reactions were incubated at 30°C for 60 min.

Propylene is an especially important hydrocarbon, being the starting point for the synthesis of a variety of polymers (36). A limited number of metal-based catalysts have been shown to reduce CO₂ to yield different reduction products including formate (HCOO⁻), carbon monoxide (CO), formaldehyde (CH₂O), methanol (CH₃OH) and methane (CH₄) (2, 6–13). Common features of homogeneous catalysts for CO₂ reduction to CH₄ are low reaction rates (e.g., turnover frequencies) and limited number of turnovers (e.g., turnover number) before inactivation of the catalyst (37, 38). Further, for

electrochemical reductions, a high overpotential is required, with production of H₂ as a waste of electron flux (39, 40). The nitrogenase catalyzed reduction of CO₂ to CH₄ reported here is comparable in turnover frequency (about 1 min⁻¹) and turnover number, with notable slowing of the reaction beyond 20 min. Nitrogenase also diverts most of its electron flux to H₂ formation, with only a small percentage going to CO₂ reduction. In contrast to the electrochemical catalysts, nitrogenase catalyzes these reactions at modest electrochemical potentials (dithionite is the reductant used in these experiments), however, it does require considerable energy input from the obligate hydrolysis of ATP.

No other known single enzyme can catalyze CO₂ reduction to CH₄. Methanogenic bacteria convert CO₂ to CH₄, but this is accomplished by the action of a consortium of enzymes functioning as part of a metabolic pathway (16). In acetogenic bacteria, CO₂ is converted to acetate by the action of several enzymes including CO dehydrogenase, which catalyzes the reversible interconversion of CO₂ and CO (41). Like nitrogenase, CO dehydrogenase also utilizes a complex metal cluster to achieve this reaction. Other enzymes have been shown to reduce CO₂ to formate or methanol (17, 18), but none to CH₄ as reported here for nitrogenase.

The reduction of CO₂ catalyzed by nitrogenase can be considered in the context of our current understanding of the mechanism for the reduction of the physiological substrate N₂ by 6 electrons to two ammonia molecules with two additional electrons being utilized to evolve H₂ (20, 28, 42). Several recent studies have added to earlier work in building a probable mechanism for how N₂ might be reduced at the active site FeMo-cofactor. One important insight relevant to the current discussion is the observation of metal-bound hydrides (determined as two hydrides bridging between Fe

atoms) as an integral part of the FeMo-cofactor reactivity toward N_2 (43–45). These metal bound hydrides ($M-H^-$) have been proposed to participate in the initial reduction of N_2 to the proposed intermediate diazene ($HN=NH$). Further reduction of the metal bound diazene to two ammonia molecules is proposed to involve successive addition of electrons and protons. An important observation regarding this mechanistic feature is that during N_2 reduction, the proposed reaction intermediates (diazene $HN=NH$ or hydrazine H_2N-NH_2) are not detected in appreciable quantities, indicating that intermediates remain bound to the active site until the final products are released. This phenomenon is likely explained by stabilization of key intermediates along the reaction pathway through appropriate functional groups, thereby minimizing kinetic barriers in going from N_2 to two ammonias. The observation reported here that nitrogenase can achieve the multi-electron reduction of CO_2 to CH_4 suggests that nitrogenase can also stabilize key intermediates along this reaction pathway through appropriate functional groups. Metal hydrides have been suggested to be involved in the initial steps of CO_2 reduction catalyzed by metal complexes (39), suggesting that nitrogenase might also achieve the two electron reduction of CO_2 by hydride insertion, in a process parallel to the one proposed for the initial steps in N_2 reduction. Whether or not partial reduction intermediates (e.g., formate or formaldehyde) are leaked from nitrogenase during CO_2 reduction is technically challenging to determine because accurate measurement of formate or formaldehyde in solutions containing dithionite is complicated by interference from dithionite.

Another key finding reported here is the need to remodel the protein environment around FeMo-cofactor to activate the reduction of CO_2 to CH_4 . Earlier studies have

illustrated that the protein environment immediately surrounding FeMo-cofactor control both the size of compounds that can be substrates and the reactivity of FeMo-cofactor toward those compounds (46). We earlier found that CO₂ could be reduced to CO by the wild-type MoFe protein (27), but very little further reduction products are detected suggesting that CO₂ had limited access to the active part of FeMo-cofactor in the wild-type enzyme and that the reaction cannot go forward beyond CO. The inability to go beyond CO could be due to steric constraints imposed by the active site on subsequent intermediates in the reaction pathway or the lack of functional groups to stabilize reaction intermediates. Such possibilities are supported by the requirement for amino acid substitutions to achieve CO₂ beyond CO all the way to CH₄ and the fact that the unsubstituted MoFe protein has an exceedingly poor capacity to reduce CO (24, 26).

A final notable observation from the current work is the capacity for reductive coupling of CO₂ with acetylene, to yield the 3C olefin propylene by the remodeled MoFe protein. Several earlier studies have suggested two binding sites on FeMo-cofactor. For example, it has been proposed that two CO molecules bind to FeMo-cofactor in the high CO concentration inhibited state (29–33). Likewise, two acetylene binding sites have been implicated from studies combining kinetics and amino acid substitutions (31, 34, 35). Finally, the finding that CO can be reduced and coupled to make C₂ and C₃ hydrocarbons is consistent with two adjacent binding sites (24, 26). Here, we report that CO₂ can be reduced to the level of CH₄ and coupled to acetylene, yielding predominately propylene. Up to 8% of the C₃ product during CO₂ and acetylene reduction catalyzed by nitrogenase is the C₃ product propane. Addition of ethylene to a reaction with CO₂ did not yield propane. This observation clearly suggests that both CO₂ and acetylene are

binding to the active site and both are being activated within the active site during the coupling reaction. This observation is best explained by two adjacent substrate activation sites, which can be populated to varying extents by changing the electron flux through nitrogenase and the partial pressures of CO₂ and acetylene. Reductive coupling of CO₂ to alkynes yielding oxygenated hydrocarbons (e.g., carboxylic acids) has been reported for metal catalysts (10, 47), but to our knowledge the production of olefins is unique to the reactions reported here.

In summary, the findings presented here initiate the understanding of how nitrogenase can reduce and couple CO₂ by multiple electrons to the industrially interesting CH₄ and propylene. The findings presented here begin to shed light on these reactions and provide insights into the broader context of how N₂ is reduced to ammonia. Future studies will be aimed at understanding how reaction barriers are lowered through stabilization of key reaction intermediates, which should provide guiding insights that can be utilized in the design of more robust catalysts for the reduction of CO₂ to various hydrocarbons.

Materials and Methods

Reagents and protein purification. All reagents were obtained from Sigma-Aldrich or Fisher Scientific and were used without further purification, unless specified otherwise. Sodium bicarbonate (NaHCO₃) was from Avantor Performance Materials. Sodium dithionite was purified to about 99% purity according to a published procedure (48). Gases were purchased from Air Liquide: CO₂, and acetylene. Methane gas was obtained from household natural gas line with an estimated purity of 97%. Propane gas was obtained from a propane fuel tank with an estimated purity of 86%. All other gases

were purchased from Air Liquide. *Azotobacter vinelandii* strains DJ1260 (wild-type, WT, or α -70^{Val}), DJ997 (α -195^{Gln}), DJ1310 (α -70^{Ala}), DJ1316 (α -70^{Ala}/ α -195^{Gln}), and DJ1495 (α -70^{Ala}/ α -191^{Ala}) were grown and the corresponding nitrogenase MoFe proteins were expressed and purified as previously described (49). All MoFe proteins in this study contain a seven-His tag addition near the carboxy-terminal end of the α -subunit. The purification of these proteins was accomplished according to a published purification protocol (50). Protein concentrations were determined by the Biuret assay using bovine serum albumin as standard. The purities of these proteins were >95% based on SDS/PAGE analysis with Coomassie staining. Manipulation of proteins and buffers was done in septum-sealed serum vials under an argon atmosphere or on a Schlenk vacuum line. All gases and liquid transfers used gas-tight syringes.

Carbon dioxide reduction assays. Using CO₂ as substrate, assays were conducted in 9.4-mL serum vials containing 2 mL of an assay buffer consisting of about 100 mM sodium dithionite, a MgATP regenerating system (13.4 mM MgCl₂, 10 mM ATP, 60 mM phosphocreatine, 0.6 mg/mL bovine serum albumin, and 0.4 mg/mL creatine phosphokinase) in a combination buffer of 33.3 mM MOPS, 33.3 mM MES, and 33.3 mM TAPS at pH 8.0 except for the CO₂ partial pressure dependence study, which was done in 100 mM Bis-Tris buffer, pH 6.7. After making the solution anaerobic, addition of CO₂ and equilibration between the gas phase and liquid phase for about 20 min, the MoFe protein were added. Then the assay vials were ventilated to atmospheric pressure. Reactions were initiated by the addition of Fe protein and incubated at 30°C. Reactions were quenched by the addition of 400 μ L of 400 mM EDTA at pH = 8.0 solution. When using NaHCO₃ as the substrate for reduction or coupling assays, the reaction mixture was

made by mixing a 100 mM Bis-Tris buffer (pH 6.7) containing all components as described above and a stock solution of NaHCO₃ dissolved in 100 mM Bis-Tris buffer (pH 6.7). For coupling reactions between CO₂ and C₂H₂, the three component buffer system (33.3 mM MOPS, 33.3 mM MES, and 33.3 mM TAPS, pH 8.0) was used. All pH values in this work were nominal values before mixing and/or equilibration with CO₂ gas or NaHCO₃ solution. Methane (CH₄), and propylene (C₃H₆) were quantified by gas chromatography by injection of 500 μL of the gas phase of the reaction vial into a Shimadzu GC-8A equipped with a flame ionization detector fitted with a 30 cm × 0.3 cm Porapak N column with nitrogen as the carrier gas. The injection/detection temperature was set to 180°C, and the column temperature was set to 110°C. The standard curves with high linearity were created using methane, and propane gases diluted with argon in 9.4-mL serum vials.

GC-MS analysis. The production of CH₄ from CO₂ reduction and C₃H₆ from the reductive coupling between CO₂ and C₂H₂ was confirmed on a Shimadzu GC-2010 gas chromatograph equipped with a programmed temperature vaporization (PTV) injector and a Shimadzu GCMS-QP2010S mass spectrometer by using ^{12/13}C-enriched NaHCO₃ as CO₂ source. Separation of methane was achieved with a GC-CARBONPLOT column [30 m, 0.32 mm inner diameter (ID), and 3.0 μm film thickness] (Agilent Technologies), and separation of propylene and propane was achieved with a Rt-Alumina BOND/KCl column (30 m, 0.32 mm ID, and 5.0 μm film thickness) (Restek). The injector and column temperatures were set to 35°C. Ultrapure helium was used as the carrier gas set at a linear velocity of 50 cm/s for methane separation and 60 cm/s for propylene separation. For separation of methane and propylene, 25 μL and 500 μL of headspace gases were

directly injected into the PTV injector, respectively. The mass spectrometer was operated in electron ionization and selected ion monitoring mode.

References

1. Mann ME (2012) *The Hockey Stick and the Climate Wars: Dispatches from the Front Lines* (Columbia University Press, New York).
2. Olah GA, Prakash GKS, Goepfert A (2011) Anthropogenic chemical carbon cycle for a sustainable future. *J Am Chem Soc* 133(33):12881–12898.
3. Lackner KS (2003) A guide to CO₂ sequestration. *Science* 300(5626):1677–1678.
4. Szulczewski ML, MacMinn CW, Herzog HJ, Juanes R (2012) Lifetime of carbon capture and storage as a climate-change mitigation technology. *Proc Natl Acad Sci USA* 109(14):5185–5189.
5. Omae I (2012) Recent developments in carbon dioxide utilization for the production of organic chemicals. *Coord Chem Rev* 256(13-14):1384–1405.
6. Rakowski Dubois M, Dubois DL (2009) Development of molecular electrocatalysts for CO₂ reduction and H₂ production/oxidation. *Acc Chem Res* 42(12):1974–1982.
7. Morris AJ, Meyer GJ, Fujita E (2009) Molecular approaches to the photocatalytic reduction of carbon dioxide for solar fuels. *Acc Chem Res* 42(12):1983–1994.
8. Olah GA (2005) Beyond oil and gas: the methanol economy. *Angew Chem Int Ed Engl* 44(18):2636–2639.
9. Cokoja M, Bruckmeier C, Rieger B, Herrmann WA, Kühn FE (2011) Transformation of carbon dioxide with homogeneous transition-metal catalysts: a molecular solution to a global challenge? *Angew Chem Int Ed Engl* 50(37):8510–8537.
10. Schaub T, Paciello RA (2011) A process for the synthesis of formic acid by CO₂ hydrogenation: thermodynamic aspects and the role of CO. *Angew Chem Int Ed Engl* 50(32):7278–7282.
11. Sakakura T, Choi J-C, Yasuda H (2007) Transformation of carbon dioxide. *Chem Rev* 107(6):2365–2387.
12. Wang W, Wang S, Ma X, Gong J (2011) Recent advances in catalytic hydrogenation of carbon dioxide. *Chem Soc Rev* 40(7):3703–3727.

13. Darensbourg DJ (2010) Chemistry of carbon dioxide relevant to its utilization: a personal perspective. *Inorg Chem* 49(23):10765–10780.
14. Reda T, Plugge CM, Abram NJ, Hirst J (2008) Reversible interconversion of carbon dioxide and formate by an electroactive enzyme. *Proc Natl Acad Sci USA* 105(31):10654–10658.
15. Ragsdale SW, Pierce E (2008) Acetogenesis and the Wood-Ljungdahl pathway of CO₂ fixation. *Biochim Biophys Acta* 1784(12):1873–1898.
16. Thauer RK, Kaster AK, Seedorf H, Buckel W, Hedderich R (2008) Methanogenic archaea: ecologically relevant differences in energy conservation. *Nature Rev Microbiol* 6(8):579–591.
17. Heo J, Skjeldal L, Staples CR, Ludden P (2002) Carbon monoxide dehydrogenase from *Rhodospirillum rubrum* produces formate. *J Biol Inorg Chem* 7(7-8):810–814.
18. Obert R, Dave BC (1999) Enzymatic conversion of carbon dioxide to methanol: enhanced methanol production in silica sol-gel matrices. *J Am Chem Soc* 121(51):12192–12193.
19. Burgess BK, Lowe DJ (1996) Mechanism of molybdenum nitrogenase. *Chem Rev* 96(7):2983–3012.
20. Seefeldt LC, Hoffman BM, Dean DR (2009) Mechanism of Mo-dependent nitrogenase. *Annu Rev Biochem* 78:701–722.
21. Spatzal T, et al. (2011) Evidence for interstitial carbon in nitrogenase FeMo cofactor. *Science* 334(6058):940.
22. Lancaster KM, et al. (2011) X-ray emission spectroscopy evidences a central carbon in the nitrogenase iron-molybdenum cofactor. *Science* 334(6058):974–977.
23. Rivera-Ortiz JM, Burris RH (1975) Interactions among substrates and inhibitors of nitrogenase. *J Bacteriol* 123(2):537–545.
24. Lee CC, Hu Y, Ribbe MW (2010) Vanadium nitrogenase reduces CO. *Science* 329(5992):642.
25. Hu Y, Lee CC, Ribbe MW (2011) Extending the carbon chain: Hydrocarbon formation catalyzed by vanadium/molybdenum nitrogenases. *Science* 333(6043):753–755.
26. Yang Z-Y, Dean DR, Seefeldt LC (2011) Molybdenum nitrogenase catalyzes the reduction and coupling of CO to form hydrocarbons. *J Biol Chem* 286(22):19417–19421.

27. Seefeldt LC, Rasche ME, Ensign SA (1995) Carbonyl sulfide and carbon dioxide as new substrates, and carbon disulfide as a new inhibitor, of nitrogenase. *Biochemistry* 34(16):5382–5389.
28. Seefeldt LC, Hoffman BM, Dean DR (2012) Electron transfer in nitrogenase catalysis. *Curr Opin Chem Biol* 16(1-2):19–25.
29. Lee H-I, Cameron LM, Hales BJ, Hoffman BM (1997) CO binding to the FeMo cofactor of CO-inhibited nitrogenase: ^{13}C and ^1H Q-band ENDOR investigation. *J Am Chem Soc* 119(42):10121–10126.
30. Pollock RC, et al. (1995) Investigation of CO bound to inhibited forms of nitrogenase MoFe protein by ^{13}C ENDOR. *J Am Chem Soc* 117(33):8686–8687.
31. Davis LC, Henzl MT, Burris RH, Orme-Johnson WH (1979) Iron-sulfur clusters in the molybdenum-iron protein component of nitrogenase. Electron paramagnetic resonance of the carbon monoxide inhibited state. *Biochemistry* 18(22):4860–4869.
32. Maskos Z, Fisher K, Sørliie M, Newton WE, Hales BJ (2005) Variant MoFe proteins of *Azotobacter vinelandii*: effects of carbon monoxide on electron paramagnetic resonance spectra generated during enzyme turnover. *J Biol Inorg Chem* 10(4):394–406.
33. Christie PD, et al. (1996) Identification of the CO-binding cluster in nitrogenase MoFe protein by ENDOR of ^{57}Fe isotopomers. *J Am Chem Soc* 118(36):8707–8709.
34. Shen J, Dean DR, Newton WE (1997) Evidence for multiple substrate-reduction sites and distinct inhibitor-binding sites from an altered *Azotobacter vinelandii* nitrogenase MoFe protein. *Biochemistry* 36(16):4884–4894.
35. Hwang JC, Chen CH, Burris RH (1973) Inhibition of nitrogenase-catalyzed reductions. *Biochim Biophys Acta* 292(1):256–270.
36. Olah GA, Molnár Á (2003) *Hydrocarbon Chemistry* (Wiley, Hoboken, NJ), 2nd Ed.
37. Matsuo T, Kawaguchi H (2006) From carbon dioxide to methane: homogeneous reduction of carbon dioxide with hydrosilanes catalyzed by zirconium–borane complexes. *J Am Chem Soc* 128(38):12362–12363.
38. Khandelwal M, Wehmschulte RJ (2012) Deoxygenative reduction of carbon dioxide to methane, toluene, and diphenylmethane with $[\text{Et}_2\text{Al}]^+$ as catalyst. *Angew Chem Int Ed Engl* 51(29):7323–7326.
39. Benson EE, Kubiak CP, Sathrum AJ, Smieja JM (2009) Electrocatalytic and homogeneous approaches to conversion of CO_2 to liquid fuels. *Chem Soc Rev* 38(1):89–99.

40. Cook TR, et al. (2010) Solar energy supply and storage for the legacy and nonlegacy worlds. *Chem Rev* 110(11):6474–6502.
41. Ragsdale SW (2008) Enzymology of the Wood-Ljungdahl pathway of acetogenesis. *Annals NY Acad Sci* 1125:129–136.
42. Hoffman BM, Dean DR, Seefeldt LC (2009) Climbing nitrogenase: Toward a mechanism of enzymatic nitrogen fixation. *Acc Chem Res* 42(5):609–619.
43. Lukoyanov D et al. (2012) Unification of reaction pathway and kinetic scheme for N₂ reduction catalyzed by nitrogenase. *Proc Natl Acad Sci USA* 109(15):5583–5587.
44. Lukoyanov D, Yang Z-Y, Dean DR, Seefeldt LC, Hoffman BM (2010) Is Mo involved in hydride binding by the four-electron reduced (E₄) intermediate of the nitrogenase MoFe protein? *J Am Chem Soc* 132(8):2526–2527.
45. Igarashi RY, et al. (2005) Trapping H⁺ bound to the nitrogenase FeMo-cofactor active site during H₂ evolution: Characterization by ENDOR spectroscopy. *J Am Chem Soc* 127(17):6231–6241.
46. Dos Santos PC, et al. (2005) Substrate interactions with the nitrogenase active site. *Acc Chem Res* 38(3):208–214.
47. Zhang Y, Riduan SN (2011) Catalytic hydrocarboxylation of alkenes and alkynes with CO₂. *Angew Chem Int Ed Engl* 50(28):6210–6212.
48. McKenna CE, Gutheil WG, Song W (1991) A method for preparing analytically pure sodium dithionite. dithionite quality and observed nitrogenase-specific activities. *Biochim Biophys Acta* 1075(1):109–117.
49. Barney BM, et al. (2007) Diazene (HN=NH) is a substrate for nitrogenase: Insights into the pathway of N₂ reduction. *Biochemistry* 46(23):6784–6794.
50. Christiansen J, Goodwin PJ, Lanzilotta WN, Seefeldt LC, Dean DR (1998) Catalytic and biophysical properties of a nitrogenase Apo-MoFe protein produced by a nifB-deletion mutant of *Azotobacter vinelandii*. *Biochemistry* 37(36):12611–12623.

CHAPTER 9

SUMMARY AND FUTURE DIRECTIONS

In Chapter 1, many outstanding mechanistic questions concerning different aspects of substrate binding and reduction mechanism of nitrogenase have been outlined. The results presented in this dissertation addressed some of these key questions and advanced the understanding of the mechanism of Mo-dependent nitrogenase from several perspectives. The detailed achievements from this dissertation are summarized as the followings.

1. Molybdenum nitrogenase catalyzed biological nitrogen fixation requires delivery of multiple electrons and protons through the interaction of the two component proteins (Fe protein and MoFe protein) and accumulating the reducing equivalents on the FeMo-cofactor to activate and break the $\text{N}\equiv\text{N}$ triple bond ($BDE = 944 \text{ KJ/mol}$, **Figure 9-1**) to form two NH_3 (1–4). During N_2 reduction catalyzed by Mo-dependent nitrogenase, one of the most important observations is that, once bound, N_2 is quantitatively converted to 2 NH_3 , without any semi-reduced intermediate species being “leaked” (5). Thus, nitrogenase is designed to efficiently bind N_2 and conduct multiple rounds of reduction and protonation without the release of any semi-reduced states. This feature, the ability to capture a substrate for multiple rounds of reduction, is important towards understanding how nitrogenase can achieve the multiple electron reduction of N_2 and other substrates (6). As I described in Chapter 1, this feature also makes it very hard to study the mechanism of N_2 reduction catalyzed by Mo-nitrogenase.

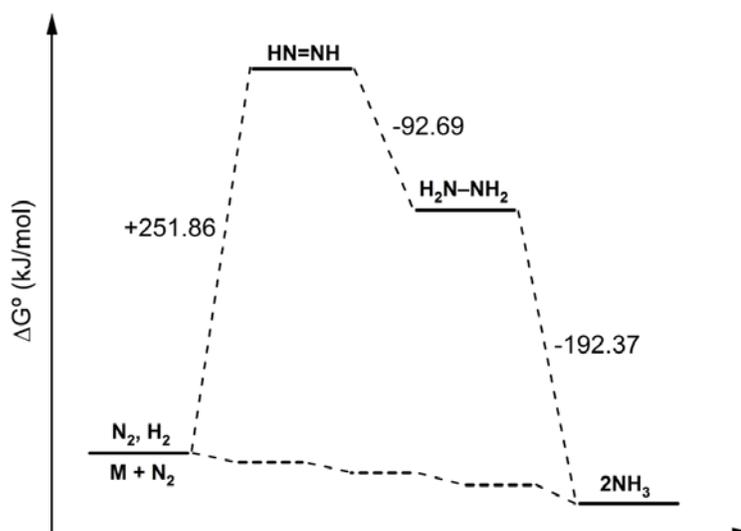


Figure 9-1. Standard Gibbs free energy change diagrams for N_2 reduction. Shown is the standard Gibbs free energy change (ΔG°) between intermediates for the N_2 reduction pathways. Also shown are possible energy states for metal bound intermediates (lower dashed traces in both panels). All reaction standard Gibbs free energy changes were calculated from known thermodynamic parameters for the reactants and products involved in the corresponding reaction (7–9).

N_2 reduction by molybdenum nitrogenase has been suggested to proceed by an alternating reduction mechanism. This is strongly supported by the characterization of an EPR-active common intermediate **I** ($S = 1/2$) and the newly discovered non-Kramers EPR active intermediate **H** ($S = 2$) characterized by ENDOR/ESEEM/HYSCORE with different isotopomers of methyl diazene, diazene, and hydrazine (Chapter 2 and 3). The molecular structures of substrates-derived ligands in **H** and **I** were assigned to an amide group ($-NH_2$) and ammonia (NH_3) ligand, respectively, after the cleavage of the N-N bonds of these substrates. The spin-states of intermediates **H** and **I** also suggested that the

redox states of the FeMo-cofactor in the two intermediates should be M^{1+} and M^N , respectively. Considering that these common intermediates are usually trapped in the samples containing a variety of different intermediates, the information of **H** and **I** could not be easily obtained from any other techniques. This shed light on the future direction for characterization of other intermediates during N_2 reduction. Application of these pulsed EPR techniques for characterization of freeze-trapped intermediates from other substrates might result in fruitful information for nitrogenase mechanism. After unifying the LT kinetic model with the “prompt” alternating pathway, the proposed draft mechanism of N_2 reduction has the suggested “electron inventory” for each intermediate from FeMo-cofactor bound N_2 to NH_3 .

2. The role of Mo atom during nitrogenase catalysis was directly studied for the first time. The results from ^{95}Mo -ENDOR study of the E_4 intermediate trapped by α -70^{lle} MoFe protein under Ar clearly revealed that the Mo does not interact with the two bridging hydride ligands and is not reduced in this intermediate (Chapter 4), further supporting the assignment of the two bridging hydrides to Fe-bridged hydrides [Fe-H-Fe].

3. In LT model, the role of the E_4 state is pivotal for N_2 binding and activation (10, 11) and N_2 -dependent HD formation catalyzed by molybdenum nitrogenase (12). Based on our progress in understanding the N_2 reduction mechanism (Chapter 2 and 3) and the characterization of the two-hydride E_4 intermediate (Chapter 4), a reductive elimination mechanism was proposed. In this mechanism, N_2 reversibly binds to the activated FeMo-cofactor formed by reductively elimination of one H_2 from two bridging hydrides at E_4 state. This reductive elimination mechanism explained key observations in

nitrogenase catalysis: (i) the obligatory evolution of one H₂ per N₂ reduced; (ii) all the constraints for N₂-dependent HD formation reactions (12).

One feature of this reductive elimination mechanism is that N₂ and H₂ can reversibly replace each other. In Chapter 5 of this dissertation, I described the formation of two iron-bridging deuteride intermediates, the dideutero-E₄ and the monodeutero-E₂, generated during turnover of wild-type molybdenum nitrogenase under D₂ and N₂. Intercepting these two intermediates with acetylene resulted in the formation of mono- and di-deuterated ethylene detected by GC-MS. The deuterium in the deuterated ethylenes is exclusively derived from the deuteride intermediates from D₂ binding and activation, not from the solvent. These results strongly support the proposed reductive elimination mechanism for N₂ binding and activation at the E₄ state.

Moreover, these results are the first experimental evidence that hydride intermediates could be directly involved in hydrogenation of acetylene. Many previous enzymology observations related to acetylene have been explained by acetylene interception of hydride intermediates at different E_n level (see Chapter 5). Considering the hydrogenation mechanism of substrate reduction is one important perspective (the last section in Chapter 1) (3), it should be one of the top priorities in nitrogenase research in the future. The strategy I developed in Chapter 5 might help to understand the hydrogenation mechanism of other substrates.

4. The steric effects of amino acid residue at α -70 position of MoFe protein on access of CO to the binding sites on FeMo-cofactor was studied by monitoring the kinetics of the formation and decay of nitrogenase-CO complexes using SF-FTIR as a real time technique (Chapter 6). The results revealed the formation of three nitrogenase-

CO complexes during turnover with different formation and decay kinetics. The formation of these species is slowed down when the larger isoleucine is at the α -70 position. These observations further support the previous conclusion that one or more Fe atoms on the 4Fe4S face “gated” by α -70-residue might be the substrate binding sites.

Different from EPR and ENDOR techniques, SF-FTIR can monitor the formation and decay of different intermediates at both EPR active and silent states in a real-time mode. Comparison of kinetics of formation and decay of different intermediates can help us to understand the mechanism of the conversion between different intermediates during substrate reduction. But there is one weakness of this technique. That is, the intermediate must be able to have distinguishable absorption bands in the IR energy region.

5. Prior to work in this dissertation, carbon monoxide was reported as an inhibitor of molybdenum nitrogenase, but not as a substrate. Recently, V-nitrogenase was found to catalyze the reduction and coupling of carbon monoxide to form C2 and C3 hydrocarbons at very low rate. In this dissertation, I expanded the nitrogenase reactivity toward CO using MoFe proteins having amino acid substitutions at α -70-position (Chapter 7). It was found that CO can be catalytically reduced and coupled to form C1-C3 hydrocarbons by these remodeled nitrogenases. This is the first observation that CO can serve as a substrate of molybdenum nitrogenase. The reductive coupling of multiple CO may be due to two adjacent binding sites on the 4Fe4S face “gated” by α -70-residue in MoFe protein.

In Chapter 8 of this dissertation, carbon dioxide (CO₂) was found to be catalytically reduced to form methane for the first time by a remodeled molybdenum nitrogenase (α -70^{Ala}/ α -195^{Gln} MoFe protein). Carbon dioxide reduction in the presence of acetylene resulted in the production of both propane and propylene, with propylene as the

major C3 product from the reductive coupling reaction of CO₂ and acetylene. The ability of remodeled nitrogenase to catalyze these two types of reactions makes it unique among known enzymes and all other reported catalysts.

All hydrocarbon products from nitrogenase-catalyzed CO and CO₂ reduction have important applications as fuels or important petrochemical starting materials. Considering that we are facing an energy-intense time and highly polluted environment, these nitrogenase-catalyzed reduction and coupling reactions of CO and CO₂ provide potential application of nitrogenase in developing a sustainable pathway for conversion of CO and CO₂ to fuels and other value-added chemicals. Our findings may also inspire other scientists to design and synthesize novel metallic catalysts for conversion and utilization of CO and CO₂.

In summary, several important advancements have been achieved concerning on substrate binding and reduction of molybdenum nitrogenase. However, there are still many questions left that need to be explored in the future. In the following sections of this chapter, I will discuss possible directions for understanding nitrogenase mechanism and expanding nitrogenase catalysis.

N₂ Reduction Mechanism

In the proposed draft reduction mechanism of N₂ reduction, one important question is what is the reaction for the formation of **H** and **I**. If **I** (E₈) is formed from produced NH₃ and resting state FeMo-cofactor, we should be able to see the same EPR signal by addition of ammonia to the sample in the resting state or under turnover conditions. Our recent data from these experiments did not show any formation of intermediate **I**. This result supports the assignment that **I** is generated after one more

electron reduction of **H** (E_1 or E_7). To further understand the relationship between **H** and **I**, rapid freeze quench technique can be used to study the formation kinetics of the two intermediates in future studies. The sequence of the appearance of the two intermediates and other possible intermediates might be able to help us understand how middle stage substrates diazene and methyldiazene catch up hydrazine to form the same intermediate species. Whereas, diazenes need to be reduced by three electrons to form **H**, and hydrazine needs to be reduced by one electron to cleave the N-N single bond to form **H**.

A relaxation protocol applying an EPR-monitored temperature step annealing experiment has been developed by Dr. Brian M. Hoffman's group and applied to study the kinetics of the two-bridging hydrides bound E_4 state (13), from which study a new-EPR active E_2 intermediate was observed during relaxation of the E_4 state back to the resting E_0 state. This two-step relaxation provided definitive evidence for the assignment of the two-hydride E_4 state. Application of this annealing method to nitrogenous intermediates **H** and **I** might be able to give us insightful information about the N_2 reduction cycle (**Figure 1-6**). Actually, our preliminary data from the annealing experiment of the intermediate **I** revealed a coincident relationship between the decay of the EPR signal ($S = 1/2$) and appearance of the resting state signal ($S = 3/2$). This is consistent with the assignment of **I** as E_8 .

Both intermediate **H** and **I** are late stage intermediates during N_2 reduction. Gaining insightful information of early stage intermediate is challenging. The observed trapped intermediate in N_2 reduction by wild-type molybdenum nitrogenase resulted in low yields (14), making it difficult to conduct thorough pulsed ENDOR studies, such as ESEEM and HYSCORE to fully characterize the intermediate. Recently, we found that

the relaxation rate of this intermediate is dependent on N_2 partial pressure. This might be caused by the inhibition effect of formed H_2 during turnover. Detailed study is in progress. How to enhance the yield of this intermediate is another direction for mechanistic study.

Hydrogenation Mechanism for Substrate Reduction

One important strategy to study the hydrogenation mechanism of substrate reduction could be the isotope effects for different substrates. An inverse isotope effect has been observed before when acrylonitrile was reduced in H_2O and D_2O reaction mixture (15). But the interpretation of the data is not convincing. Recently, this inverse isotope effect has also been observed in CO reduction to hydrocarbons (16). We also observed this inverse isotope effect for reduction of CO_2 to methane, N_2 to ammonia, and acetylene to ethylene. These isotope effects can be altered by changing the electron flux condition. The observation of these isotope effects might help us to study the hydrogenation mechanism of N_2 and other substrates. At the same time, if the reduction rate of the substrate is too fast, we observed a normal isotope effect, which suggests a shift change in rate limiting steps. To study the isotope effect, C-containing substrates might be a good choice because of the non-exchangeable property of the H/D atom in C-H/D bonds.

Substrate/Inhibitor Binding Sites and the Role of Mo

As reviewed in Chapter 1, more and more evidence has suggested that the 4Fe4S face gated by α -70 amino acid residue as the site of substrate binding. In Chapter 6, the SF-FTIR study of the hi-CO complexes also support this 4Fe4S site as the

substrate/inhibitor binding sites. In Chapter 4, ^{95}Mo -ENDOR study and analysis of hyperfine tensors in ENDOR spectra clearly resulted in a conclusion that Mo does not interact with the two hydrides and is not reduced in that intermediate. Considering these results are all observing either one specific state in a complex catalytic reaction involving many other states and intermediates, the possible role of Mo for binding and interacting with substrate/inhibitor or corresponding intermediates still could not be totally excluded. Recent observations from different studies involving the production or addition of ammonia gave us some hints that NH_3 or NH_4^+ might interact with the Mo site either through a hydrogen bonding or by replacing one of the ligand of Mo. For example, Mo-EXAFS study of the trapped intermediate *I* clearly displayed a disturbed Mo-EXAFS spectrum pattern compared to the resting state control and turnover control under Ar (**Figure 9-2**).

CO and CO₂ Reduction and Coupling Reactions

One common feature of those MoFe protein variants catalyzing reduction and coupling of CO and CO₂ is substitution of the valine at α -70 position in wild type MoFe protein by a smaller alanine or glycine (Chapter 7 and 8). Why can this substitution change the reactivity of nitrogenase towards CO? In Chapter 1, it was reported that CO does not inhibit the proton reduction by wild-type nitrogenase. Recently, our study of the CO inhibition of proton reduction catalyzed by different MoFe protein variants used in the reduction and coupling of CO and CO₂ (Chapter 7 and 8) revealed an intriguing and exciting observation (**Figure 9-3**). It is very clear that CO does not inhibit proton reduction catalyzed by wild-type MoFe and α -195^{Gln}, which cannot reduce CO. However, when the valine at α -70 position of MoFe protein was substituted by alanine or glycine,

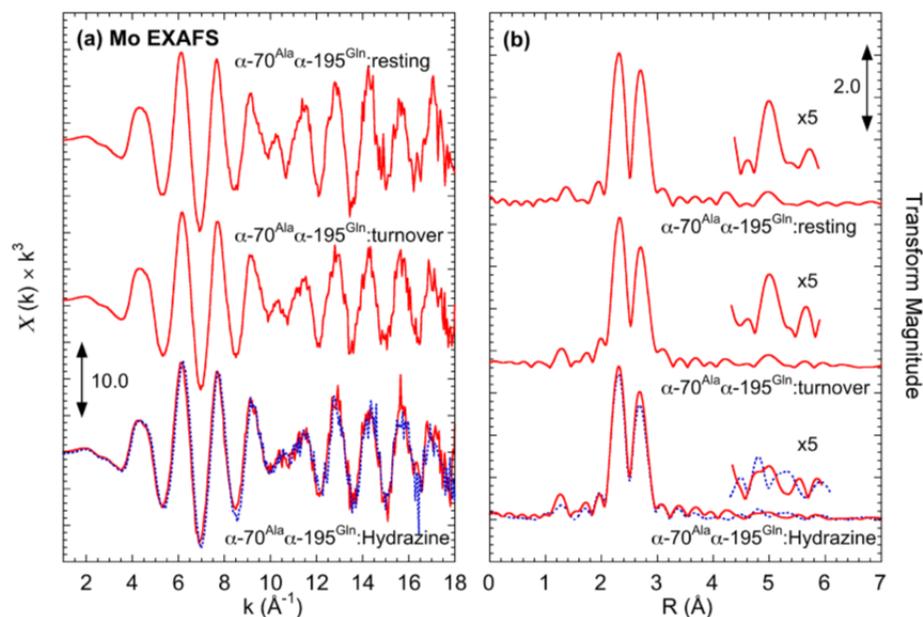


Figure 9-2. Mo-EXAFS spectra for α -70^{Ala}/ α -195^{Gln} MoFe protein at different states.

the resulted MoFe protein variants displayed CO inhibition of proton reduction by about 50%. This observation could lead to two conclusions: (i) opening up the cavity around 4Fe4S face next to α -70 position can allow CO to compete with one hydride binding site, which could not be used to produce H₂ anymore. Given that there are only two hydrides formed at E₄H₄ state, it is reasonable to conclude that at least one of the hydride ligand bind to the 4Fe4S face dominated by α -70 residue. (ii) the more freedom CO obtained in the larger cavity created by these CO-reducing variants allows CO to bind to a Fe atom which is next to the other hydride, which can participate in the activation and hydrogenation of the bound CO. This is consistent with the hydrogenation of acetylene described in Chapter 5.

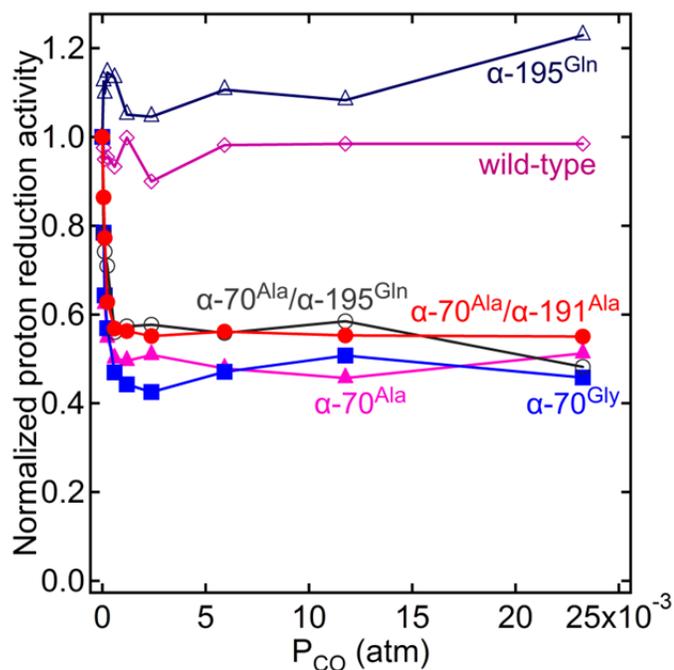


Figure 9-3. CO inhibition of proton reduction catalyzed by different MoFe proteins.

In the future, it is worth expanding the nitrogenase catalysis toward CO and CO₂ reduction and coupling reactions. The following directions might be valuable: (i) searching for other potential value-added products from reduction of CO/CO₂, such as formic acid and methanol; (ii) understanding the hydrogenation mechanism of CO and CO₂ reduction; (iii) improving the catalytic efficiency and selectivity of nitrogenase catalyzed reduction and coupling of CO and CO₂; (iv) studying the coupling reactions between CO/CO₂ with other small molecules for production of other value-added chemicals; (v) characterizing key intermediates along the reduction pathway of CO and CO₂, especially hydrogenated intermediates, and defining a mechanism for reduction and coupling reactions catalyzed by molybdenum nitrogenase.

References

1. MacKay, B. A., and Fryzuk, M. D. (2004) Dinitrogen coordination chemistry: On the biomimetic borderlands. *Chem. Rev.* **104**, 385–402
2. Hoffman, B. M., Dean, D. R., and Seefeldt, L. C. (2009) Climbing nitrogenase: Toward a mechanism of enzymatic nitrogen fixation. *Acc. Chem. Res.* **42**, 609–619
3. Hoffman, B. M., Lukoyanov, D., Dean, D. R., and Seefeldt, L. C. (2013) Nitrogenase: A draft mechanism. *Acc. Chem. Res.* **46**, 587–595
4. Seefeldt, L. C., Hoffman, B. M., and Dean, D. R. (2009) Mechanism of Mo-dependent nitrogenase. *Annu. Rev. Biochem.* **78**, 701–722
5. Thorneley, R. N. F., Eady, R. R., and Lowe, D. J. (1978) Biological nitrogen fixation by way of an enzyme-bound dinitrogen-hydride intermediate. *Nature* **272**, 557–558
6. Seefeldt, L. C., Yang, Z.-Y., Duval, S., and Dean, D. R. (2013) Nitrogenase reduction of carbon-containing compounds. *Biochim. Biophys. Acta*, <http://10.1016/j.bbabi.2013.04.003>
7. Gurvich, L. V. (1989) Reference books and data banks on the thermodynamic properties of individual substances. *Pure Appl. Chem.* **61**, 1027–1031
8. Linstrom, P. J., and Mallard, W. G. (eds.) (2005) *NIST Chemistry Webbook*, National Institute of Standards and Technology, Gaithersburg, MD
9. Dean, J. A. (ed.) (1999) *Lange's Handbook of Chemistry*, 15th Ed., McGraw-Hill, Inc., New York, NY
10. Thorneley, R. N. F., and Lowe, D. J. (1985) in *Molybdenum Enzymes* (Spiro, T. G., ed.) pp. 221–284, Wiley, New York
11. Wilson, P. E., Nyborg, A. C., and Watt, G. D. (2001) Duplication and extension of the Thorneley and Lowe kinetic model for *Klebsiella pneumoniae* nitrogenase catalysis using a MATHEMATICA software platform. *Biophys. Chem.* **91**, 281–304
12. Fisher, K., Dilworth, M. J., and Newton, W. E. (2000) Differential effects on N₂ binding and reduction, HD formation, and azide reduction with α -195^{His}- and α -191^{Gln}-substituted MoFe proteins of *Azotobacter vinelandii* nitrogenase. *Biochemistry* **39**, 15570–15577
13. Lukoyanov, D., Barney, B. M., Dean, D. R., Seefeldt, L. C., and Hoffman, B. M. (2007) Connecting nitrogenase intermediates with the kinetic scheme for N₂ reduction by a relaxation protocol and identification of the N₂ binding state. *Proc. Natl. Acad. Sci. U.S.A.* **104**, 1451–1455

14. Barney, B. M., Lukoyanov, D., Igarashi, R. Y., Laryukhin, M., Yang, T.-C., Dean, D. R., Hoffman, B. M., and Seefeldt, L. C. (2009) Trapping an intermediate of dinitrogen (N_2) reduction on nitrogenase. *Biochemistry* **48**, 9094–9102
15. Fuchsman, W. H., and Hardy, R. W. F. (1972) Nitrogenase-catalyzed acrylonitrile reductions. *Bioinorg. Chem.* **1**, 195–213
16. Hu, Y., Lee, C. C., and Ribbe, M. W. (2011) Extending the carbon chain: Hydrocarbon formation catalyzed by vanadium/molybdenum nitrogenases. *Science* **333**, 753–755

APPENDICES

APPENDIX A

COPYRIGHT PERMISSIONS

Zhiyong Yang
 Utah State University
 0300 Old Main Hill
 Logan, UT 84322-0300
 (435)-754-9690

Dr. Brett M. Barney
 304 BioAgEng Bldg
 University of Minnesota
 1390 Eckles Avenue
 St. Paul, MN 55108

Dear Dr. Barney,

I am currently preparing my dissertation and would like your permission to include the following articles of which you are a coauthor, as chapters. I will include an acknowledgment to each article on the first pages of the chapters. Please note that USU sends dissertations to Bell and Howell Dissertation services to be made available for reproduction.

Please indicate your approval for this request by signing in the space provided.

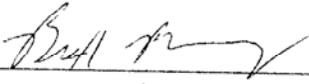
If you have any questions, please contact me.

Sincerely,

Zhiyong Yang

I hereby give permission to Zhiyong Yang to include the following articles, of which I am a coauthor, in his dissertation.

- (1) Lukoyanov, D., Yang, Z.-Y., Barney, B. M., Dean, D. R., Seefeldt, L. C., and Hoffman, B. M. (2012) Unification of reaction pathway and kinetic scheme for N_2 reduction catalyzed by nitrogenase. *Proc. Natl. Acad. Sci. U.S.A.* 109, 5583–5587.
 (2) Lukoyanov, D., Dikanov, S. A., Yang, Z.-Y., Barney, B. M., Samoilova, R. I., Narasimhulu, K. V., Dean, D. R., Seefeldt, L. C., and Hoffman, B. M. (2011) ENDOR/HYSCORE studies of the common intermediate trapped during nitrogenase reduction of N_2H_2 , CH_3N_2H , and N_2H_4 support an alternating reaction pathway for N_2 reduction. *J. Am. Chem. Soc.* 133, 11655–11664.

Signed 
 Date 11/26/13

Zhiyong Yang
Utah State University
0300 Old Main Hill
Logan, UT 84322-0300
(435)-754-9690

Dr. Dennis R. Dean
Department of Biochemistry
Virginia Polytechnic Institute and State University
Blacksburg, VA 24061

Dear Dr. Dean,

I am currently preparing my dissertation and would like your permission to include the following articles of which you are a coauthor, as chapters. I will include an acknowledgment to each article on the first page of the corresponding chapter. Please note that USU sends dissertations to Bell and Howell Dissertation services to be made available for reproduction.

Please indicate your approval for this request by signing in the space provided.

If you have any questions, please contact me.

Sincerely,

Zhiyong Yang

I hereby give permission to Zhiyong Yang to include the following articles, of which I am a coauthor, in his dissertation.

- (1) Yang, Z.-Y., Khadka, N., Lukoyanov, D., Hoffman, B. M., Dean, D. R., and Seefeldt, L. C. (2013) On reversible H₂ loss upon N₂ binding to FeMo-cofactor of nitrogenase. *Proc. Natl. Acad. Sci. U.S.A.* 110, 16327–16332.
- (2) Seefeldt, L. C., Yang, Z.-Y., Duval, S., and Dean, D. R. (2013) Nitrogenase reduction of carbon-containing compounds. *Biochim. Biophys. Acta* 1827, 1102–1111.
- (3) Yang, Z.-Y., Moure, V. R., Dean, D. R., and Seefeldt, L. C. (2012) Carbon dioxide reduction to methane and coupling with acetylene to form propylene catalyzed by remodeled nitrogenase. *Proc. Natl. Acad. Sci. U.S.A.* 109, 19644–19648.
- (4) Lukoyanov, D., Yang, Z.-Y., Barney, B. M., Dean, D. R., Seefeldt, L. C., and Hoffman, B. M. (2012) Unification of reaction pathway and kinetic scheme for N₂ reduction catalyzed by nitrogenase. *Proc. Natl. Acad. Sci. U.S.A.* 109, 5583–5587.

- (5) Yang, Z.-Y., Seefeldt, L. C., Dean, D. R., Cramer, S. P., and George, S. J. (2011) Steric control of the Hi-CO MoFe nitrogenase complex revealed by stopped-flow infrared spectroscopy. *Angew. Chem. Int. Ed.* 50, 272–275.
- (6) Yang, Z.-Y., Dean, D. R., and Seefeldt, L. C. (2011) Molybdenum nitrogenase catalyzes the reduction and coupling of CO to form hydrocarbons. *J. Biol. Chem.* 286, 19417–19421.
- (7) Lukoyanov, D., Dikanov, S. A., Yang, Z.-Y., Barney, B. M., Samoilova, R. I., Narasimhulu, K. V., Dean, D. R., Seefeldt, L. C., and Hoffman, B. M. (2011) ENDOR/HYSCORE studies of the common intermediate trapped during nitrogenase reduction of N_2H_2 , CH_3N_2H , and N_2H_4 support an alternating reaction pathway for N_2 reduction. *J. Am. Chem. Soc.* 133, 11655–11664.
- (8) Lukoyanov, D., Yang, Z.-Y., Dean, D. R., Seefeldt, L. C., and Hoffman, B. M. (2010) Is Mo involved in hydride binding by the four-electron reduced (E_4) intermediate of the nitrogenase MoFe protein? *J. Am. Chem. Soc.* 132, 2526–2527.

Signed

A handwritten signature in black ink that reads "Dan R. Dean". The signature is written in a cursive style with a horizontal line underneath the name.

Date November 25, 2013

Zhiyong Yang
Utah State University
0300 Old Main Hill
Logan, UT 84322-0300
(435)-754-9690

Dr. Brian M. Hoffman
Department of Chemistry and Molecular Biosciences
Northwestern University
Evanston, IL 60208

Dear Dr. Hoffman,

I am currently preparing my dissertation and would like your permission to include the following articles of which you are a coauthor, as chapters. I will include an acknowledgment to each article on the first page of the corresponding chapter. Please note that USU sends dissertations to Bell and Howell Dissertation services to be made available for reproduction.

Please indicate your approval for this request by signing in the space provided.

If you have any questions, please contact me.

Sincerely,

Zhiyong Yang

I hereby give permission to Zhiyong Yang to include the following articles, of which I am a coauthor, in his dissertation.

- (1) Yang, Z.-Y., Khadka, N., Lukoyanov, D., Hoffman, B. M., Dean, D. R., and Seefeldt, L. C. (2013) On reversible H₂ loss upon N₂ binding to FeMo-cofactor of nitrogenase. *Proc. Natl. Acad. Sci. U.S.A.* *110*, 16327–16332.
- (2) Lukoyanov, D., Yang, Z.-Y., Barney, B. M., Dean, D. R., Seefeldt, L. C., and Hoffman, B. M. (2012) Unification of reaction pathway and kinetic scheme for N₂ reduction catalyzed by nitrogenase. *Proc. Natl. Acad. Sci. U.S.A.* *109*, 5583–5587.
- (3) Lukoyanov, D., Dikanov, S. A., Yang, Z.-Y., Barney, B. M., Samoilova, R. I., Narasimhulu, K. V., Dean, D. R., Seefeldt, L. C., and Hoffman, B. M. (2011) ENDOR/HYSCORE studies of the common intermediate trapped during nitrogenase reduction of N₂H₂, CH₃N₂H, and N₂H₄ support an alternating reaction pathway for N₂ reduction. *J. Am. Chem. Soc.* *133*, 11655–11664.

(4) Lukoyanov, D., Yang, Z.-Y., Dean, D. R., Seefeldt, L. C., and Hoffman, B. M. (2010) Is Mo involved in hydride binding by the four-electron reduced (E_4) intermediate of the nitrogenase MoFe protein? *J. Am. Chem. Soc.* 132, 2526–2527.

Signed Brian Hoffman

Date 11/20/2013

Zhiyong Yang
Utah State University
0300 Old Main Hill
Logan, UT 84322-0300
(435)-754-9690

Dr. Simon J. George
Department of Chemistry
University of California, Davis
One Shields Avenue
Davis, CA 95616

Dear Simon,

I am currently preparing my dissertation and would like your permission to include the following article of which you are a coauthor, as a chapter. I will include an acknowledgment to the article on the first page of the chapter. Please note that USU sends dissertations to Bell and Howell Dissertation services to be made available for reproduction.

Please indicate your approval for this request by signing in the space provided.

If you have any questions, please contact me.

Sincerely,

Zhiyong Yang

I hereby give permission to Zhiyong Yang to include the following article, of which I am a coauthor, in his dissertation.

Yang, Z.-Y., Seefeldt, L. C., Dean, D. R., Cramer, S. P., and George, S. J. (2011) Steric control of the Hi-CO MoFe nitrogenase complex revealed by stopped-flow infrared spectroscopy. *Angew. Chem. Int. Ed.* 50, 272–275.

Signed 

Date November 18, 2013

Zhiyong Yang
Utah State University
0300 Old Main Hill
Logan, UT 84322-0300
(435)-754-9690

Dr. Dmitriy Lukoyanov
Department of Chemistry and Molecular Biosciences
Northwestern University
Evanston, IL 60208

Dear Dr. Lukoyanov,

I am currently preparing my dissertation and would like your permission to include the following articles of which you are a coauthor, as chapters. I will include an acknowledgment to each article on the first page of the corresponding chapter. Please note that USU sends dissertations to Bell and Howell Dissertation services to be made available for reproduction.

Please indicate your approval for this request by signing in the space provided.

If you have any questions, please contact me.

Sincerely,

Zhiyong Yang

I hereby give permission to Zhiyong Yang to include the following articles, of which I am a coauthor, in his dissertation.

- (1) Yang, Z.-Y., Khadka, N., Lukoyanov, D., Hoffman, B. M., Dean, D. R., and Seefeldt, L. C. (2013) On reversible H₂ loss upon N₂ binding to FeMo-cofactor of nitrogenase. *Proc. Natl. Acad. Sci. U.S.A.* 110, 16327–16332.
- (2) Lukoyanov, D., Yang, Z.-Y., Barney, B. M., Dean, D. R., Seefeldt, L. C., and Hoffman, B. M. (2012) Unification of reaction pathway and kinetic scheme for N₂ reduction catalyzed by nitrogenase. *Proc. Natl. Acad. Sci. U.S.A.* 109, 5583–5587.
- (3) Lukoyanov, D., Dikanov, S. A., Yang, Z.-Y., Barney, B. M., Samoilova, R. I., Narasimhulu, K. V., Dean, D. R., Seefeldt, L. C., and Hoffman, B. M. (2011) ENDOR/HYSCORE studies of the common intermediate trapped during nitrogenase reduction of N₂H₂, CH₃N₂H, and N₂H₄ support an alternating reaction pathway for N₂ reduction. *J. Am. Chem. Soc.* 133, 11655–11664.

(4) Lukoyanov, D., Yang, Z.-Y., Dean, D. R., Seefeldt, L. C., and Hoffman, B. M. (2010) Is Mo involved in hydride binding by the four-electron reduced (E_4) intermediate of the nitrogenase MoFe protein? *J. Am. Chem. Soc.* 132, 2526–2527.

Signed 
Date 11/19/2013

Zhiyong Yang
Utah State University
0300 Old Main Hill
Logan, UT 84322-0300
(435)-754-9690

Dr. Sergei A. Dikanov
Department of Veterinary Clinical Medicine
University of Illinois
Urbana, IL 61801

Dear Dr. Dikanov,

I am currently preparing my dissertation and would like your permission to include the following article of which you are a coauthor, as a chapter. I will include an acknowledgment to the article on the first page of the chapter. Please note that USU sends dissertations to Bell and Howell Dissertation services to be made available for reproduction.

Please indicate your approval for this request by signing in the space provided.

If you have any questions, please contact me.

Sincerely,

Zhiyong Yang

I hereby give permission to Zhiyong Yang to include the following article, of which I am a coauthor, in his dissertation.

Lukoyanov, D., Dikanov, S. A., Yang, Z.-Y., Barney, B. M., Samoilova, R. I., Narasimhulu, K. V., Dean, D. R., Seefeldt, L. C., and Hoffman, B. M. (2011) ENDOR/HYSCORE studies of the common intermediate trapped during nitrogenase reduction of N_2H_2 , CH_3N_2H , and N_2H_4 support an alternating reaction pathway for N_2 reduction. *J. Am. Chem. Soc.* 133, 11655–11664.

Signed  _____
Date 11/18/20013

Zhiyong Yang
Utah State University
0300 Old Main Hill
Logan, UT 84322-0300
(435)-754-9690

Dr. Kuppala V. Narasimhulu
Department of Veterinary Clinical Medicine
University of Illinois
Urbana, IL 61801

Dear Dr. Narasimhulu,

I am currently preparing my dissertation and would like your permission to include the following article of which you are a coauthor, as a chapter. I will include an acknowledgment to the article on the first page of the chapter. Please note that USU sends dissertations to Bell and Howell Dissertation services to be made available for reproduction.

Please indicate your approval for this request by signing in the space provided.

If you have any questions, please contact me.

Sincerely,

Zhiyong Yang

I hereby give permission to Zhiyong Yang to include the following article, of which I am a coauthor, in his dissertation.

Lukoyanov, D., Dikanov, S. A., Yang, Z.-Y., Barney, B. M., Samoilova, R. I., Narasimhulu, K. V., Dean, D. R., Seefeldt, L. C., and Hoffman, B. M. (2011) ENDOR/HYSCORE studies of the common intermediate trapped during nitrogenase reduction of N_2H_2 , CH_3N_2H , and N_2H_4 support an alternating reaction pathway for N_2 reduction. *J. Am. Chem. Soc.* 133, 11655–11664.

Signed



Date : November 19, 2013

Zhiyong Yang
 Utah State University
 0300 Old Main Hill
 Logan, UT 84322-0300
 (435)-754-9690

Dr. Rimma I. Samoilova
 Institute of Chemical Kinetics and Combustion
 Russian Academy of Sciences
 Novosibirsk 6300090, Russian Federation

Dear Dr. Samoilova,

I am currently preparing my dissertation and would like your permission to include the following article, of which you are a coauthor, as a chapter. I will include an acknowledgment to the article on the first page of the chapter. Please note that USC sends dissertations to Bell and Howell Dissertation services to be made available for reproduction.

Please indicate your approval for this request by signing in the space provided.

If you have any questions, please contact me.

Sincerely,

Zhiyong Yang

I hereby give permission to Zhiyong Yang to include the following article, of which I am a coauthor, in his dissertation.

Lukoyanov, D., Dikanov, S. A., Yang, Z.-Y., Barney, B. M., Samoilova, R. I., Narasimhulu, K. V., Dean, D. R., Seefeldt, L. C., and Hoffman, B. M. (2011) ENDOR/HYSCORE studies of the common intermediate trapped during nitrogenase reduction of N_2H_2 . CH_3N_2H , and N_2H_2 support an alternating reaction pathway for N_2 reduction. *J. Am. Chem. Soc.* 133, 11655–11664.

Signed *Rimma I. Samoilova*
 Samoilova, R.I. _____

Date 11/22/2013 _____

Zhiyong Yang
Utah State University
0300 Old Main Hill
Logan, UT 84322-0300
(435)-754-9690

Vivian R. Moure
Federal University of Parana
Department of Biochemistry and Molecular Biology
Centro Politecnico
PO box 19046
Curitiba, PR, Brazil 81531-980

Dear Dr. Moure,

I am currently preparing my dissertation and would like your permission to include the following article of which you are a coauthor, as a chapter. I will include an acknowledgment to the article on the first page of the chapter. Please note that USU sends dissertations to Bell and Howell Dissertation services to be made available for reproduction.

Please indicate your approval for this request by signing in the space provided.

If you have any questions, please contact me.

Sincerely,

Zhiyong Yang

I hereby give permission to Zhiyong Yang to include the following article, of which I am a coauthor, in his dissertation.

Yang, Z.-Y., Moure, V. R., Dean, D. R., and Seefeldt, L. C. (2012) Carbon dioxide reduction to methane and coupling with acetylene to form propylene catalyzed by remodeled nitrogenase. *Proc. Natl. Acad. Sci. U.S.A.* 109, 19644–19648.

Signed Vivian Rotens moure

Date November 18, 2013

Zhiyong Yang
Utah State University
0300 Old Main Hill
Logan, UT 84322-0300
(208)-690-9433

Simon Duval
Utah State University
0300 Old Main Hill
Logan, UT 84322-0300

Dear Dr. Duval,

I am currently preparing my dissertation and would like your permission to include the following article of which you are a coauthor, as a chapter. I will include an acknowledgment to the article on the first page of the chapter. Please note that USU sends dissertations to Bell and Howell Dissertation services to be made available for reproduction.

Please indicate your approval for this request by signing in the space provided.

If you have any questions, please contact me.

Sincerely,

Zhiyong Yang

I hereby give permission to Zhiyong Yang to include the following article, of which I am a coauthor, in his dissertation.

Seefeldt, L. C., Yang, Z.-Y., Duval, S., and Dean, D. R. (2013) Nitrogenase reduction of carbon-containing compounds. *Biochim. Biophys. Acta*,
<http://dx.doi.org/10.1016/j.bbabbio.2013.04.003>.

Signed  _____

Date 6/27/2013 _____

Zhiyong Yang
Utah State University
0300 Old Main Hill
Logan, UT 84322-0300
(435)-754-9690

Nimesh Khadka
Utah State University
0300 Old Main Hill
Logan, UT 84322-0300

Dear Nimesh,

I am currently preparing my dissertation and would like your permission to include the following article of which you are a coauthor, as a chapter. I will include an acknowledgment to the article on the first page of the chapter. Please note that USU sends dissertations to Bell and Howell Dissertation services to be made available for reproduction.

Please indicate your approval for this request by signing in the space provided.

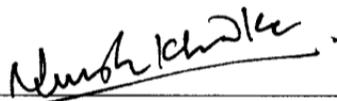
If you have any questions, please contact me.

Sincerely,

Zhiyong Yang

I hereby give permission to Zhiyong Yang to include the following article, of which I am a coauthor, in his dissertation.

Yang, Z.-Y., Khadka, N., Lukoyanov, D., Hoffman, B. M., Dean, D. R., and Seefeldt, L. C. (2013) On reversible H₂ loss upon N₂ binding to FeMo-cofactor of nitrogenase. *Proc. Natl. Acad. Sci. U.S.A.* 110, 16327–16332.

Signed 
Date 12/02/2013

Zhiyong Yang
Utah State University
0300 Old Main Hill
Logan, UT 84322-0300
(435)-754-9690

Karamatullah Danyal
Utah State University
0300 Old Main Hill
Logan, UT 84322-0300

Dear Karamatullah,

I am currently preparing my dissertation and would like your permission to include the following article of which you are a coauthor, as a chapter. I will include an acknowledgment to the article on the first page of the chapter. Please note that USU sends dissertations to Bell and Howell Dissertation services to be made available for reproduction.

Please indicate your approval for this request by signing in the space provided.

If you have any questions, please contact me.

Sincerely,

Zhiyong Yang

I hereby give permission to Zhiyong Yang to include the following article, of which I am a coauthor, in his dissertation.

Yang, Z.-Y., Danyal, K., and Seefeldt, L. C. (2011) Mechanism of Mo-dependent nitrogenase, in *Nitrogen Fixation* (Ribbe, M. W., Ed.), pp 9–29. Humana Press, Totowa, NJ.

Signed



Date

11/25/2013



May 24, 2013

Springer reference

Nitrogen Fixation
 Methods in Molecular Biology Volume 766, 2011
 ISBN 978-1-61779-194-9_2
 pp 9-29 "Mechanism of Mo-Dependent Nitrogenase" by
 Zhi-Yong Yang, Karamatullah Danyal, Lance C. Seefeldt

Your project

University: Utah State University
Title: "Substrate binding and reduction mechanism of molybdenum nitrogenase"

With reference to your request to reuse material in which Springer Science+Business Media controls the copyright, our permission is granted free of charge under the following conditions:

Springer material

- represents original material which does not carry references to other sources (if material in question refers with a credit to another source, authorization from that source is required as well);
- requires full credit (book title, year of publication, page, chapter title, name(s) of author(s), original copyright notice) is given to the publication in which the material was originally published by adding: "With kind permission of Springer Science+Business Media";
- may not be altered in any manner.

This permission

- is non-exclusive;
- is valid for one-time use only for the purpose of defending your thesis and with a maximum of 100 extra copies in paper.
- includes use in an electronic form, provided it is an author-created version of the thesis on his/her own website and his/her university's repository, including UMI (according to the definition on the Sherpa website: <http://www.sherpa.ac.uk/romeo/>);
- is subject to courtesy information to the corresponding author;
- is personal to you and may not be sublicensed, assigned, or transferred by you to any other person without Springer's written permission;
- is valid only when the conditions noted above are met.

Permission free of charge does not prejudice any rights we might have to charge for reproduction of our copyrighted material in the future.

Best regards,

Rights and Permissions
 Springer-Verlag GmbH
 Tiergartenstr. 17
 69121 Heidelberg
 Germany
 E-mail: permissions.heidelberg@springer.com

ELSEVIER LICENSE
TERMS AND CONDITIONS

Jun 27, 2013

This is a License Agreement between Zhiyong Yang ("You") and Elsevier ("Elsevier") provided by Copyright Clearance Center ("CCC"). The license consists of your order details, the terms and conditions provided by Elsevier, and the payment terms and conditions.

All payments must be made in full to CCC. For payment instructions, please see information listed at the bottom of this form.

Supplier	Elsevier Limited The Boulevard, Langford Lane Kidlington, Oxford, OX5 1GB, UK
Registered Company Number	1982084
Customer name	Zhiyong Yang
Customer address	0300 Old Main Hill Logan, UT 84322
License number	3157700922727
License date	May 28, 2013
Licensed content publisher	Elsevier
Licensed content publication	Biochimica et Biophysica Acta (BBA) - Bioenergetics
Licensed content title	Nitrogenase reduction of carbon-containing compounds
Licensed content author	Lance C. Seefeldt, Zhi-Yong Yang, Simon Duval, Dennis R. Dean
Licensed content date	16 April 2013
Licensed content volume number	
Licensed content issue number	
Number of pages	1
Start Page	
End Page	
Type of Use	reuse in a thesis/dissertation
Portion	full article
Format	both print and electronic
Are you the author of this Elsevier article?	Yes

Will you be translating?	No
Order reference number	BBA
Title of your thesis/dissertation	Substrate binding and reduction mechanism of molybdenum nitrogenase
Expected completion date	Dec 2013
Estimated size (number of pages)	200
Elsevier VAT number	GB 494 6272 12
Permissions price	0.00 USD
VAT/Local Sales Tax	0.00 USD
Total	0.00 USD
Terms and Conditions	

INTRODUCTION

1. The publisher for this copyrighted material is Elsevier. By clicking "accept" in connection with completing this licensing transaction, you agree that the following terms and conditions apply to this transaction (along with the Billing and Payment terms and conditions established by Copyright Clearance Center, Inc. ("CCC"), at the time that you opened your Rightslink account and that are available at any time at <http://myaccount.copyright.com>).

GENERAL TERMS

2. Elsevier hereby grants you permission to reproduce the aforementioned material subject to the terms and conditions indicated.

3. Acknowledgement: If any part of the material to be used (for example, figures) has appeared in our publication with credit or acknowledgement to another source, permission must also be sought from that source. If such permission is not obtained then that material may not be included in your publication/copies. Suitable acknowledgement to the source must be made, either as a footnote or in a reference list at the end of your publication, as follows:

“Reprinted from Publication title, Vol /edition number, Author(s), Title of article / title of chapter, Pages No., Copyright (Year), with permission from Elsevier [OR APPLICABLE SOCIETY COPYRIGHT OWNER].” Also Lancet special credit - “Reprinted from The Lancet, Vol. number, Author(s), Title of article, Pages No., Copyright (Year), with permission from Elsevier.”

4. Reproduction of this material is confined to the purpose and/or media for which permission is hereby given.

5. Altering/Modifying Material: Not Permitted. However figures and illustrations may be altered/adapted minimally to serve your work. Any other abbreviations, additions,

deletions and/or any other alterations shall be made only with prior written authorization of Elsevier Ltd. (Please contact Elsevier at permissions@elsevier.com)

6. If the permission fee for the requested use of our material is waived in this instance, please be advised that your future requests for Elsevier materials may attract a fee.

7. Reservation of Rights: Publisher reserves all rights not specifically granted in the combination of (i) the license details provided by you and accepted in the course of this licensing transaction, (ii) these terms and conditions and (iii) CCC's Billing and Payment terms and conditions.

8. License Contingent Upon Payment: While you may exercise the rights licensed immediately upon issuance of the license at the end of the licensing process for the transaction, provided that you have disclosed complete and accurate details of your proposed use, no license is finally effective unless and until full payment is received from you (either by publisher or by CCC) as provided in CCC's Billing and Payment terms and conditions. If full payment is not received on a timely basis, then any license preliminarily granted shall be deemed automatically revoked and shall be void as if never granted. Further, in the event that you breach any of these terms and conditions or any of CCC's Billing and Payment terms and conditions, the license is automatically revoked and shall be void as if never granted. Use of materials as described in a revoked license, as well as any use of the materials beyond the scope of an unrevoked license, may constitute copyright infringement and publisher reserves the right to take any and all action to protect its copyright in the materials.

9. Warranties: Publisher makes no representations or warranties with respect to the licensed material.

10. Indemnity: You hereby indemnify and agree to hold harmless publisher and CCC, and their respective officers, directors, employees and agents, from and against any and all claims arising out of your use of the licensed material other than as specifically authorized pursuant to this license.

11. No Transfer of License: This license is personal to you and may not be sublicensed, assigned, or transferred by you to any other person without publisher's written permission.

12. No Amendment Except in Writing: This license may not be amended except in a writing signed by both parties (or, in the case of publisher, by CCC on publisher's behalf).

13. Objection to Contrary Terms: Publisher hereby objects to any terms contained in any purchase order, acknowledgment, check endorsement or other writing prepared by you, which terms are inconsistent with these terms and conditions or CCC's Billing and Payment terms and conditions. These terms and conditions, together with CCC's Billing

and Payment terms and conditions (which are incorporated herein), comprise the entire agreement between you and publisher (and CCC) concerning this licensing transaction. In the event of any conflict between your obligations established by these terms and conditions and those established by CCC's Billing and Payment terms and conditions, these terms and conditions shall control.

14. **Revocation:** Elsevier or Copyright Clearance Center may deny the permissions described in this License at their sole discretion, for any reason or no reason, with a full refund payable to you. Notice of such denial will be made using the contact information provided by you. Failure to receive such notice will not alter or invalidate the denial. In no event will Elsevier or Copyright Clearance Center be responsible or liable for any costs, expenses or damage incurred by you as a result of a denial of your permission request, other than a refund of the amount(s) paid by you to Elsevier and/or Copyright Clearance Center for denied permissions.

LIMITED LICENSE

The following terms and conditions apply only to specific license types:

15. **Translation:** This permission is granted for non-exclusive world **English** rights only unless your license was granted for translation rights. If you licensed translation rights you may only translate this content into the languages you requested. A professional translator must perform all translations and reproduce the content word for word preserving the integrity of the article. If this license is to re-use 1 or 2 figures then permission is granted for non-exclusive world rights in all languages.

16. **Website:** The following terms and conditions apply to electronic reserve and author websites:

Electronic reserve: If licensed material is to be posted to website, the web site is to be password-protected and made available only to bona fide students registered on a relevant course if:

This license was made in connection with a course,

This permission is granted for 1 year only. You may obtain a license for future website posting,

All content posted to the web site must maintain the copyright information line on the bottom of each image,

A hyper-text must be included to the Homepage of the journal from which you are licensing at <http://www.sciencedirect.com/science/journal/xxxxx> or the Elsevier homepage for books at <http://www.elsevier.com> , and

Central Storage: This license does not include permission for a scanned version of the material to be stored in a central repository such as that provided by Heron/XanEdu.

17. **Author website** for journals with the following additional clauses:

All content posted to the web site must maintain the copyright information line on the

bottom of each image, and the permission granted is limited to the personal version of your paper. You are not allowed to download and post the published electronic version of your article (whether PDF or HTML, proof or final version), nor may you scan the printed edition to create an electronic version. A hyper-text must be included to the Homepage of the journal from which you are licensing at <http://www.sciencedirect.com/science/journal/xxxxx> . As part of our normal production process, you will receive an e-mail notice when your article appears on Elsevier's online service ScienceDirect (www.sciencedirect.com). That e-mail will include the article's Digital Object Identifier (DOI). This number provides the electronic link to the published article and should be included in the posting of your personal version. We ask that you wait until you receive this e-mail and have the DOI to do any posting.

Central Storage: This license does not include permission for a scanned version of the material to be stored in a central repository such as that provided by Heron/XanEdu.

18. **Author website** for books with the following additional clauses:

Authors are permitted to place a brief summary of their work online only.

A hyper-text must be included to the Elsevier homepage at <http://www.elsevier.com> . All content posted to the web site must maintain the copyright information line on the bottom of each image. You are not allowed to download and post the published electronic version of your chapter, nor may you scan the printed edition to create an electronic version.

Central Storage: This license does not include permission for a scanned version of the material to be stored in a central repository such as that provided by Heron/XanEdu.

19. **Website** (regular and for author): A hyper-text must be included to the Homepage of the journal from which you are licensing at <http://www.sciencedirect.com/science/journal/xxxxx>. or for books to the Elsevier homepage at <http://www.elsevier.com>

20. **Thesis/Dissertation**: If your license is for use in a thesis/dissertation your thesis may be submitted to your institution in either print or electronic form. Should your thesis be published commercially, please reapply for permission. These requirements include permission for the Library and Archives of Canada to supply single copies, on demand, of the complete thesis and include permission for UMI to supply single copies, on demand, of the complete thesis. Should your thesis be published commercially, please reapply for permission.

21. **Other Conditions**: Permission is granted to submit your article in both print and electronic format. This license permits you to post this Elsevier article online if it is embedded within your thesis. You are also permitted to post your Author Accepted Manuscript online however posting of the final published article is prohibited. Please refer to Elsevier's Posting Policy for further information:

<http://www.elsevier.com/wps/find/authors.authors/postingpolicy>

v1.6

If you would like to pay for this license now, please remit this license along with your payment made payable to "COPYRIGHT CLEARANCE CENTER" otherwise you will be invoiced within 48 hours of the license date. Payment should be in the form of a check or money order referencing your account number and this invoice number RLNK501030599.

Once you receive your invoice for this order, you may pay your invoice by credit card. Please follow instructions provided at that time.

**Make Payment To:
Copyright Clearance Center
Dept 001
P.O. Box 843006
Boston, MA 02284-3006**

For suggestions or comments regarding this order, contact RightsLink Customer Support: customercare@copyright.com or +1-877-622-5543 (toll free in the US) or +1-978-646-2777.

Gratis licenses (referencing \$0 in the Total field) are free. Please retain this printable license for your reference. No payment is required.

Thu, Jun 27, 2013 at
12:22 PM

Zhiyong Yang <zhiyong.yang@aggiemail.usu.edu>

To: permissions@elsevier.com

Dear Sir/Madam,

I am Zhiyong Yang, a graduate student in Utah State University, Utah, USA. Now I am working on my dissertation and want to use part of paper (text, table and some figures), of which I am one of the coauthor for the Introduction chapter in my PhD dissertation. I already got the reprint permission through Copyright Clearance Center (See attached doc file).

Specifically, I do need to modify Table 1. a little bit to add some nitrogen substrates into it. So I can write the introduction chapter with a good logic and arrangement to cover other aspects of nitrogenase research. I also need to use some of the text parts and incorporate them into different sections in the same chapter. I am not sure whether the attached license allows me to do this or not. *If not, I am writing this email to require a written permission which allows me to use the material described above.*

My concern in the attached permission is the Entry 5 in General Terms section. Would you like to help me figure this out?

Looking forward to hearing from you soon. I appreciate your help.

Best regards,
Zhiyong Yang

Shridhar, Lakshmi Priya (ELS-CHN)

<l.shridhar@elsevier.com>

Wed, Jul 3, 2013 at 5:30

AM

To: "zhiyong.yang@aggiemail.usu.edu" <zhiyong.yang@aggiemail.usu.edu>

Dear Zhiyong

Thank you for your email below. The terms and conditions of the Rightslink license do actually include the following text which allows for minor modifications:

5. Altering/Modifying Material: Not permitted. However, figures and illustrations may be altered/adapted minimally to serve your work.

However, I can confirm that we are happy for you to modify the material as requested. If you have any further queries regarding this please don't hesitate to contact us.

Regards

Lakshmi Priya

Global Rights Department

Elsevier
(A division of Reed Elsevier India Pvt. Ltd.)

International Tech Park | Crest – 12th Floor | Taramani Road | Taramani | Chennai 600
113 | India

Tel: [+91 44 42994660](tel:+914442994660) | Fax: [+91 44 42994701](tel:+914442994701)

E-mail: l.shridhar@elsevier.com | url: www.elsevier.com

American Chemical Society's Policy on Theses and Dissertations

If your university requires you to obtain permission, you must use the RightsLink permission system. See RightsLink instructions at <http://pubs.acs.org/page/copyright/permissions.html>.

This is regarding request for permission to include **your** paper(s) or portions of text from **your** paper(s) in your thesis. Permission is now automatically granted; please pay special attention to the **implications** paragraph below. The Copyright Subcommittee of the Joint Board/Council Committees on Publications approved the following:

Copyright permission for published and submitted material from theses and dissertations

ACS extends blanket permission to students to include in their theses and dissertations their own articles, or portions thereof, that have been published in ACS journals or submitted to ACS journals for publication, provided that the ACS copyright credit line is noted on the appropriate page(s).

Publishing **implications** of electronic publication of theses and dissertation material

Students and their mentors should be aware that posting of theses and dissertation material on the Web prior to submission of material from that thesis or dissertation to an ACS journal may affect publication in that journal. Whether Web posting is considered prior publication may be evaluated on a case-by-case basis by the journal's editor. If an ACS journal editor considers Web posting to be "prior publication", the paper will not be accepted for publication in that journal. If you intend to submit your unpublished paper to ACS for publication, check with the appropriate editor prior to posting your manuscript electronically.

Reuse/Republication of the Entire Work in Theses or Collections: Authors may reuse all or part of the Submitted, Accepted or Published Work in a thesis or dissertation that the author writes and is required to submit to satisfy the criteria of degree-granting institutions. Such reuse is permitted subject to the ACS' "Ethical Guidelines to Publication of Chemical Research" (<http://pubs.acs.org/page/policy/ethics/index.html>); the author should secure written confirmation (via letter or email) from the respective ACS journal editor(s) to avoid potential conflicts with journal prior publication*/embargo policies. Appropriate citation of the Published Work must be made. If the thesis or dissertation to be published is in electronic format, a direct link to the Published Work must also be included using the ACS Articles on Request author-directed link – see <http://pubs.acs.org/page/policy/articlesonrequest/index.html>

* Prior publication policies of ACS journals are posted on the ACS website at <http://pubs.acs.org/page/policy/prior/index.html>

If your paper has **not** yet been published by ACS, please print the following credit line on the first page of your article: "Reproduced (or 'Reproduced in part') with permission from [JOURNAL NAME], in press (or 'submitted for publication'). Unpublished work copyright [CURRENT YEAR] American Chemical Society." Include appropriate information.

If your paper has already been published by ACS and you want to include the text or portions of the text in your thesis/dissertation, please print the ACS copyright credit line on the first page of your article: "Reproduced (or 'Reproduced in part') with permission from [FULL REFERENCE CITATION.] Copyright [YEAR] American Chemical Society." Include appropriate information.

Submission to a Dissertation Distributor: If you plan to submit your thesis to UMI or to another dissertation distributor, you should not include the unpublished ACS paper in your thesis if the thesis will be disseminated electronically, until ACS has published your paper. After publication of the paper by ACS, you may release the entire thesis (**not the individual ACS article by itself**) for electronic dissemination through the distributor; ACS's copyright credit line should be printed on the first page of the ACS paper.

10/10/03, 01/15/04, 06/07/06, 04/07/10, 08/24/10, 02/28/11

Copyright and License to Publish

Beginning with articles submitted in Volume 106 (2009) the author(s) retains copyright to individual articles, and the National Academy of Sciences of the United States of America retains an exclusive license to publish these articles and holds copyright to the collective work. Volumes 90–105 copyright © (1993–2008) by the National Academy of Sciences. Volumes 1–89 (1915–1992), the author(s) retains copyright to individual articles, and the National Academy of Sciences holds copyright to the collective work.

The PNAS listing on the Sherpa RoMEO publisher copyright policies & self-archiving detail pages can be found [here](#).

Requests for Permission to Reprint

Requests for permission should be made in writing. For the fastest response time, please send your request via e-mail to PNASPermissions@nas.edu. If necessary, requests may be faxed to 202-334-2739 or mailed to:

PNAS Permissions Editor
500 Fifth Street, NW
NAS 340
Washington, DC 20001 USA

Anyone may, without requesting permission, use original figures or tables published in PNAS for noncommercial and educational use (i.e., in a review article, in a book that is not for sale) provided that the original source and the applicable copyright notice are cited.

For permission to reprint material in volumes 1–89 (1915–1992), requests should be addressed to the original authors, who hold the copyright. The full journal reference must be cited.

For permission to reprint material in volumes 90–present (1993–2012), requests must be sent via e-mail, fax, or mail and include the following information about the original material:

1. Your full name, affiliation, and title
2. Your complete mailing address, phone number, fax number, and e-mail address
3. PNAS volume number, issue number, and issue date
4. PNAS article title
5. PNAS authors' names
6. Page numbers of items to be reprinted
7. Figure/table number or portion of text to be reprinted

Also include the following information about the intended use of the material:

1. Title of work in which PNAS material will appear
2. Authors/editors of work
3. Publisher of work
4. Retail price of work
5. Number of copies of work to be produced
6. Intended audience
7. Whether work is for nonprofit or commercial use

PNAS authors need not obtain permission for the following cases: (1) to use their original figures or tables in their future works; (2) to make copies of their papers for their own personal use, including classroom use, or for the personal use of colleagues, provided those copies are not for sale and are not distributed in a systematic way; (3) to include their papers as part of their dissertations; or (4) to use all or part of their articles in printed compilations of their own works. Citation of the original source must be included and copies must include the applicable copyright notice of the original report.

Authors whose work will be reused should be notified. PNAS cannot supply original artwork. Use of PNAS material must not imply any endorsement by PNAS or the National Academy of Sciences. The full journal reference must be cited and, for articles published in Volumes 90–105 (1993–2008), "Copyright (copyright year) National Academy of Sciences, USA."

Requests for Permission to Photocopy

For permission to photocopy beyond that permitted by Section 107 or 108 of the US Copyright Law, contact:

[Copyright Clearance Center](#)
222 Rosewood Drive
Danvers, MA 01923 USA
Phone: 1-978-750-8400
Fax: 1-978-750-4770
E-mail: info@copyright.com

Authorization to photocopy items for the internal or personal use of specific clients is granted by The National Academy of Sciences provided that the proper fee is paid directly to CCC.

[11/12]

JOHN WILEY AND SONS LICENSE
TERMS AND CONDITIONS

Jun 27, 2013

This is a License Agreement between Zhiyong Yang ("You") and John Wiley and Sons ("John Wiley and Sons") provided by Copyright Clearance Center ("CCC"). The license consists of your order details, the terms and conditions provided by John Wiley and Sons, and the payment terms and conditions.

All payments must be made in full to CCC. For payment instructions, please see information listed at the bottom of this form.

License Number	3143830278541
License date	May 07, 2013
Licensed content publisher	John Wiley and Sons
Licensed content publication	Angewandte Chemie International Edition
Licensed content title	Steric Control of the Hi-CO MoFe Nitrogenase Complex Revealed by Stopped-Flow Infrared Spectroscopy
Licensed copyright line	Copyright © 2011 WILEY-VCH Verlag GmbH & Co. KGaA, Weinheim
Licensed content author	Zhi-Yong Yang, Lance C. Seefeldt, Dennis R. Dean, Stephen P. Cramer, Simon J. George
Licensed content date	Nov 30, 2010
Start page	272
End page	275
Type of use	Dissertation/Thesis
Requestor type	Author of this Wiley article
Format	Print and electronic
Portion	Full article
Will you be translating?	No
Order reference number	Wiley
Total	0.00 USD
Terms and Conditions	

TERMS AND CONDITIONS

This copyrighted material is owned by or exclusively licensed to John Wiley & Sons, Inc. or one of its group companies (each a "Wiley Company") or a society for whom a Wiley Company has exclusive publishing rights in relation to a particular journal (collectively "WILEY"). By clicking "accept" in connection with completing this licensing transaction, you agree that the following terms and conditions apply to this transaction (along with the billing and payment terms and conditions established by the Copyright Clearance Center

Inc., ("CCC's Billing and Payment terms and conditions"), at the time that you opened your RightsLink account (these are available at any time at <http://myaccount.copyright.com>).

Terms and Conditions

1. The materials you have requested permission to reproduce (the "Materials") are protected by copyright.
2. You are hereby granted a personal, non-exclusive, non-sublicensable, non-transferable, worldwide, limited license to reproduce the Materials for the purpose specified in the licensing process. This license is for a one-time use only with a maximum distribution equal to the number that you identified in the licensing process. Any form of republication granted by this license must be completed within two years of the date of the grant of this license (although copies prepared before may be distributed thereafter). The Materials shall not be used in any other manner or for any other purpose. Permission is granted subject to an appropriate acknowledgement given to the author, title of the material/book/journal and the publisher. You shall also duplicate the copyright notice that appears in the Wiley publication in your use of the Material. Permission is also granted on the understanding that nowhere in the text is a previously published source acknowledged for all or part of this Material. Any third party material is expressly excluded from this permission.
3. With respect to the Materials, all rights are reserved. Except as expressly granted by the terms of the license, no part of the Materials may be copied, modified, adapted (except for minor reformatting required by the new Publication), translated, reproduced, transferred or distributed, in any form or by any means, and no derivative works may be made based on the Materials without the prior permission of the respective copyright owner. You may not alter, remove or suppress in any manner any copyright, trademark or other notices displayed by the Materials. You may not license, rent, sell, loan, lease, pledge, offer as security, transfer or assign the Materials, or any of the rights granted to you hereunder to any other person.
4. The Materials and all of the intellectual property rights therein shall at all times remain the exclusive property of John Wiley & Sons Inc or one of its related companies (WILEY) or their respective licensors, and your interest therein is only that of having possession of and the right to reproduce the Materials pursuant to Section 2 herein during the continuance of this Agreement. You agree that you own no right, title or interest in or to the Materials or any of the intellectual property rights therein. You shall have no rights hereunder other than the license as provided for above in Section 2. No right, license or interest to any trademark, trade name, service mark or other branding ("Marks") of WILEY or its licensors is granted hereunder, and you agree that you shall not assert any

such right, license or interest with respect thereto.

5. NEITHER WILEY NOR ITS LICENSORS MAKES ANY WARRANTY OR REPRESENTATION OF ANY KIND TO YOU OR ANY THIRD PARTY, EXPRESS, IMPLIED OR STATUTORY, WITH RESPECT TO THE MATERIALS OR THE ACCURACY OF ANY INFORMATION CONTAINED IN THE MATERIALS, INCLUDING, WITHOUT LIMITATION, ANY IMPLIED WARRANTY OF MERCHANTABILITY, ACCURACY, SATISFACTORY QUALITY, FITNESS FOR A PARTICULAR PURPOSE, USABILITY, INTEGRATION OR NON-INFRINGEMENT AND ALL SUCH WARRANTIES ARE HEREBY EXCLUDED BY WILEY AND ITS LICENSORS AND WAIVED BY YOU.

6. WILEY shall have the right to terminate this Agreement immediately upon breach of this Agreement by you.

7. You shall indemnify, defend and hold harmless WILEY, its Licensors and their respective directors, officers, agents and employees, from and against any actual or threatened claims, demands, causes of action or proceedings arising from any breach of this Agreement by you.

8. IN NO EVENT SHALL WILEY OR ITS LICENSORS BE LIABLE TO YOU OR ANY OTHER PARTY OR ANY OTHER PERSON OR ENTITY FOR ANY SPECIAL, CONSEQUENTIAL, INCIDENTAL, INDIRECT, EXEMPLARY OR PUNITIVE DAMAGES, HOWEVER CAUSED, ARISING OUT OF OR IN CONNECTION WITH THE DOWNLOADING, PROVISIONING, VIEWING OR USE OF THE MATERIALS REGARDLESS OF THE FORM OF ACTION, WHETHER FOR BREACH OF CONTRACT, BREACH OF WARRANTY, TORT, NEGLIGENCE, INFRINGEMENT OR OTHERWISE (INCLUDING, WITHOUT LIMITATION, DAMAGES BASED ON LOSS OF PROFITS, DATA, FILES, USE, BUSINESS OPPORTUNITY OR CLAIMS OF THIRD PARTIES), AND WHETHER OR NOT THE PARTY HAS BEEN ADVISED OF THE POSSIBILITY OF SUCH DAMAGES. THIS LIMITATION SHALL APPLY NOTWITHSTANDING ANY FAILURE OF ESSENTIAL PURPOSE OF ANY LIMITED REMEDY PROVIDED HEREIN.

9. Should any provision of this Agreement be held by a court of competent jurisdiction to be illegal, invalid, or unenforceable, that provision shall be deemed amended to achieve as nearly as possible the same economic effect as the original provision, and the legality, validity and enforceability of the remaining provisions of this Agreement shall not be affected or impaired thereby.

10. The failure of either party to enforce any term or condition of this Agreement shall not constitute a waiver of either party's right to enforce each and every term and condition of this Agreement. No breach under this agreement shall be deemed waived or excused by either party unless such waiver or consent is in writing signed by the party granting such waiver or consent. The waiver by or consent of a party to a breach of any provision of this

Agreement shall not operate or be construed as a waiver of or consent to any other or subsequent breach by such other party.

11. This Agreement may not be assigned (including by operation of law or otherwise) by you without WILEY's prior written consent.

12. Any fee required for this permission shall be non-refundable after thirty (30) days from receipt

13. These terms and conditions together with CCC's Billing and Payment terms and conditions (which are incorporated herein) form the entire agreement between you and WILEY concerning this licensing transaction and (in the absence of fraud) supersedes all prior agreements and representations of the parties, oral or written. This Agreement may not be amended except in writing signed by both parties. This Agreement shall be binding upon and inure to the benefit of the parties' successors, legal representatives, and authorized assigns.

14. In the event of any conflict between your obligations established by these terms and conditions and those established by CCC's Billing and Payment terms and conditions, these terms and conditions shall prevail.

15. WILEY expressly reserves all rights not specifically granted in the combination of (i) the license details provided by you and accepted in the course of this licensing transaction, (ii) these terms and conditions and (iii) CCC's Billing and Payment terms and conditions.

16. This Agreement will be void if the Type of Use, Format, Circulation, or Requestor Type was misrepresented during the licensing process.

17. This Agreement shall be governed by and construed in accordance with the laws of the State of New York, USA, without regards to such state's conflict of law rules. Any legal action, suit or proceeding arising out of or relating to these Terms and Conditions or the breach thereof shall be instituted in a court of competent jurisdiction in New York County in the State of New York in the United States of America and each party hereby consents and submits to the personal jurisdiction of such court, waives any objection to venue in such court and consents to service of process by registered or certified mail, return receipt requested, at the last known address of such party.

Wiley Open Access Terms and Conditions

Wiley publishes Open Access articles in both its Wiley Open Access Journals program [<http://www.wileyopenaccess.com/view/index.html>] and as Online Open articles in its subscription journals. The majority of Wiley Open Access Journals have adopted the [Creative Commons Attribution License](#) (CC BY) which permits the unrestricted use, distribution, reproduction, adaptation and commercial exploitation of the article in any

medium. No permission is required to use the article in this way provided that the article is properly cited and other license terms are observed. A small number of Wiley Open Access journals have retained the [Creative Commons Attribution Non Commercial License](#) (CC BY-NC), which permits use, distribution and reproduction in any medium, provided the original work is properly cited and is not used for commercial purposes.

Online Open articles - Authors selecting Online Open are, unless particular exceptions apply, offered a choice of Creative Commons licenses. They may therefore select from the CC BY, the CC BY-NC and the [Attribution-NoDerivatives](#) (CC BY-NC-ND). The CC BY-NC-ND is more restrictive than the CC BY-NC as it does not permit adaptations or modifications without rights holder consent.

Wiley Open Access articles are protected by copyright and are posted to repositories and websites in accordance with the terms of the applicable Creative Commons license referenced on the article. At the time of deposit, Wiley Open Access articles include all changes made during peer review, copyediting, and publishing. Repositories and websites that host the article are responsible for incorporating any publisher-supplied amendments or retractions issued subsequently.

Wiley Open Access articles are also available without charge on Wiley's publishing platform, **Wiley Online Library** or any successor sites.

Conditions applicable to all Wiley Open Access articles:

- The authors' moral rights must not be compromised. These rights include the right of "paternity" (also known as "attribution" - the right for the author to be identified as such) and "integrity" (the right for the author not to have the work altered in such a way that the author's reputation or integrity may be damaged).
- Where content in the article is identified as belonging to a third party, it is the obligation of the user to ensure that any reuse complies with the copyright policies of the owner of that content.
- If article content is copied, downloaded or otherwise reused for research and other purposes as permitted, a link to the appropriate bibliographic citation (authors, journal, article title, volume, issue, page numbers, DOI and the link to the definitive published version on Wiley Online Library) should be maintained. Copyright notices and disclaimers must not be deleted.
 - Creative Commons licenses are copyright licenses and do not confer any other rights, including but not limited to trademark or patent rights.
- Any translations, for which a prior translation agreement with Wiley has not been agreed, must prominently display the statement: "This is an unofficial translation of an article that appeared in a Wiley publication. The publisher has not endorsed

this translation."

Conditions applicable to non-commercial licenses (CC BY-NC and CC BY-NC-ND)

For non-commercial and non-promotional purposes individual non-commercial users may access, download, copy, display and redistribute to colleagues Wiley Open Access articles. In addition, articles adopting the CC BY-NC may be adapted, translated, and text- and data-mined subject to the conditions above.

Use by commercial "for-profit" organizations

Use of non-commercial Wiley Open Access articles for commercial, promotional, or marketing purposes requires further explicit permission from Wiley and will be subject to a fee. Commercial purposes include:

- Copying or downloading of articles, or linking to such articles for further redistribution, sale or licensing;
- Copying, downloading or posting by a site or service that incorporates advertising with such content;
- The inclusion or incorporation of article content in other works or services (other than normal quotations with an appropriate citation) that is then available for sale or licensing, for a fee (for example, a compilation produced for marketing purposes, inclusion in a sales pack)
- Use of article content (other than normal quotations with appropriate citation) by for-profit organizations for promotional purposes
- Linking to article content in e-mails redistributed for promotional, marketing or educational purposes;
- Use for the purposes of monetary reward by means of sale, resale, license, loan, transfer or other form of commercial exploitation such as marketing products
- Print reprints of Wiley Open Access articles can be purchased from: corporatesales@wiley.com

The modification or adaptation for any purpose of an article referencing the CC BY-NC-ND License requires consent which can be requested from RightsLink@wiley.com .

Other Terms and Conditions:

BY CLICKING ON THE "I AGREE..." BOX, YOU ACKNOWLEDGE THAT YOU HAVE READ AND FULLY UNDERSTAND EACH OF THE SECTIONS OF AND PROVISIONS SET FORTH IN THIS AGREEMENT AND THAT YOU ARE IN AGREEMENT WITH AND ARE WILLING TO ACCEPT ALL OF YOUR OBLIGATIONS AS SET FORTH IN THIS AGREEMENT.

v1.8

If you would like to pay for this license now, please remit this license along with your payment made payable to "COPYRIGHT CLEARANCE CENTER" otherwise you will be invoiced within 48 hours of the license date. Payment should be in the form of a check or money order referencing your account number and this invoice number 501016364.

Once you receive your invoice for this order, you may pay your invoice by credit card. Please follow instructions provided at that time.

Make Payment To:

Copyright Clearance Center

Dept 001

P.O. Box 843006

Boston, MA 02284-3006

For suggestions or comments regarding this order, contact RightsLink Customer Support: customercare@copyright.com or +1-877-622-5543 (toll free in the US) or +1-978-646-2777.

Gratis licenses (referencing \$0 in the Total field) are free. Please retain this printable license for your reference. No payment is required.

Copyright Permission Policy

These guidelines apply to the reuse of articles, figures, charts and photos in the *Journal of Biological Chemistry*, *Molecular & Cellular Proteomics* and the *Journal of Lipid Research*.

For authors reusing their own material:

Authors need NOT contact the journal to obtain rights to reuse their own material. They are automatically granted permission to do the following:

- Reuse the article in print collections of their own writing.
- Present a work orally in its entirety.
- Use an article in a thesis and/or dissertation.
- Reproduce an article for use in the author's courses. (If the author is employed by an academic institution, that institution also may reproduce the article for teaching purposes.)
- Reuse a figure, photo and/or table in future commercial and noncommercial works.
- Post a copy of the paper in PDF that you submitted via BenchPress.
- Link to the journal site containing the final edited PDFs created by the publisher.

EXCEPTION: If authors select the Author's Choice publishing option:

- The final version of the manuscript will be covered under the Creative Commons Attribution license (CC BY), the most accommodating of licenses offered. [Click here for details.](#)
- The final version of the manuscript will be released immediately on the publisher's website and PubMed Central.

Please note that authors must include the following citation when using material that appeared in an ASBMB journal:

"This research was originally published in Journal Name. Author(s). Title. Journal Name . Year; Vol:pp-pp. © the American Society for Biochemistry and Molecular Biology."

For other parties using material for noncommercial use:

Other parties are welcome to copy, distribute, transmit and adapt the work — at no cost and without permission — for noncommercial use as long as they attribute the work to the original source using the citation above.

Examples of noncommercial use include:

- Reproducing a figure for educational purposes, such as schoolwork or lecture presentations, with attribution.
- Appending a reprinted article to a Ph.D. dissertation, with attribution.

For other parties using material for commercial use:

Navigate to the article of interest and click the "Request Permissions" button on the middle navigation bar. (See diagram at right.) It will walk you through the steps for obtaining permission for reuse.

Examples of commercial use by parties other than authors include:

- Reproducing a figure in a book published by a commercial publisher.
- Reproducing a figure in a journal article published by a commercial publisher.

Updated Nov. 10, 2009

APPENDIX B

SUPPORTING INFORMATION FOR CHAPTER 2

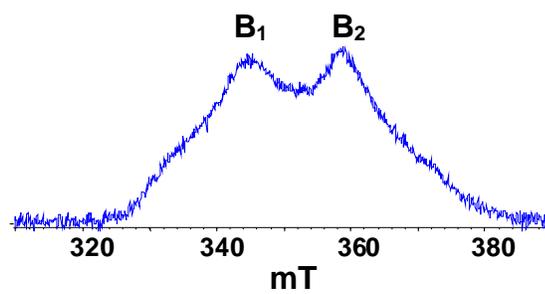


Figure B-S1. Two-pulse field-sweep ESE spectra of intermediate **I** ($l(\text{N}_2\text{H}_4)$) recorded with $\tau = 200$ ns. Microwave frequency is 9.702 GHz.

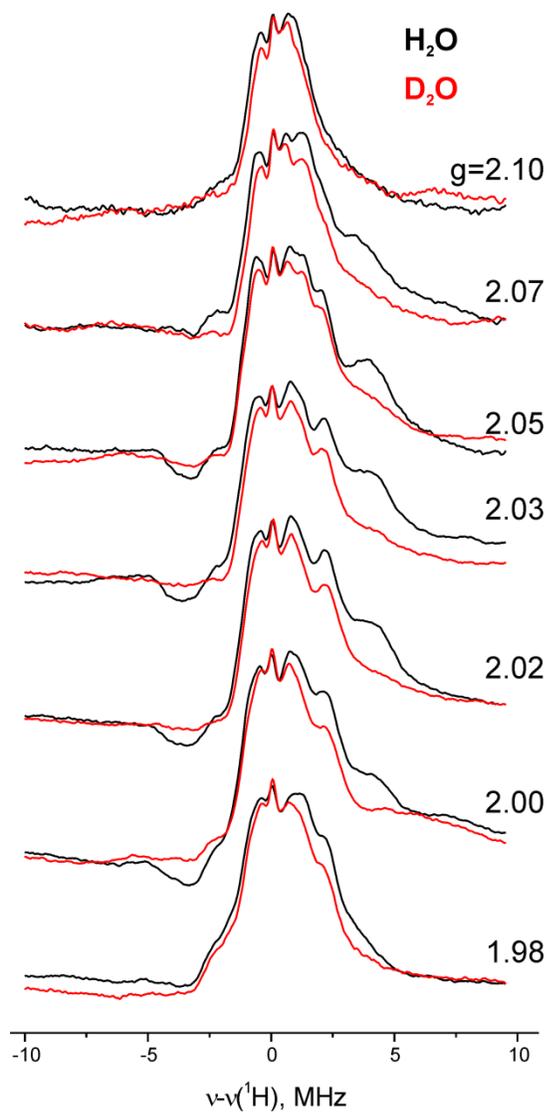


Figure B-S2. Field dependence of 35 GHz CW ¹H ENDOR spectra of **I** (l(N₂H₄)) obtained for samples prepared in H₂O (black) and D₂O (red) buffers. Conditions: microwave frequency, 35.002 GHz (H₂O), 35.096 GHz (D₂O); modulation amplitude, 2.5 G; time constant, 64 ms; bandwidth of RF broadened to 100 kHz; RF sweep speed, 1 MHz/s, 50-100 scans; temperature, 2 K.

1D Four-Pulse ESEEM

Additional information about the exchangeable proton(s) was obtained from 1D four-pulse ESEEM spectra (**Figure B-S3**). These spectra contain lines in the region of the double proton Larmor frequency ($2\nu_H \sim 28\text{-}29$ MHz) that are sum-combination harmonics ($\nu_\alpha + \nu_\beta$) of two basic frequencies ν_α and ν_β . These harmonics are not created in HYSCORE experiments, and the approach is particularly useful for the resolution of protons with different anisotropic couplings.³⁵

The four-pulse ESEEM spectrum of the **I** intermediate recorded at the low-field edge of the spectrum (329 mT, $g = 2.106$) contains two well-resolved lines in the region of the proton $2\nu_H$, as shown in **Figure B-S3A**. The most intense line represents the contribution of weakly coupled protons from the protein environment with $(\nu_\alpha + \nu_\beta) \cong 2\nu_H$. The spectrum also reveals a peak of lower intensity shifted from $2\nu_H$ to higher frequencies by ~ 0.9 MHz. This feature is greatly diminished in the spectrum of the sample prepared in D_2O , indicating that it contains a major contribution from the exchangeable proton(s) seen in ENDOR and as cross-peaks **2** (with larger deviation from antidiagonal) in the HYSCORE spectra. The resolved shifted peak was observed in the narrow interval up to field 332 mT ($g = 2.0876$). In orientation-selected spectra the shift depends on the part of the spectra excited by microwave pulses. The resolved shifted line was observed at the low-field edge of the EPR spectrum when the magnetic field is directed along g_1 axis, i.e. the single-crystal like conditions. In this case the shift of the sum combination line is described by the relation,^{35, 36}

$$\Delta = 9/4(T^2/\nu_H) \sin^2\theta \cos^2\theta \quad (\text{S1})$$

in which θ is the angle between the unique axes of g-tensor and hyperfine tensors in axial approximation. For $\Delta = 0.9$ MHz and $T = 4.6$ MHz obtained from HYSORE spectra analysis, **eq S1** gives an estimate that $\sin^2\theta \sim \cos^2\theta \sim 1/2$. This result indicates that either the orientation-selection at X band is not effective enough even near the edge of the spectrum or that θ is about 45° ; the latter agrees with the ENDOR measurements.

At the higher fields, **Figure B-S3B**, the sum combination peak at $2\nu_H$ is accompanied by unresolved shoulder that extends up to 0.8-0.9 MHz. This behavior is consistent with increase of intensity and width of the cross-peaks **1** (along the diagonal) in HYSORE spectra.

Analysis of ^1H and ^{15}N HYSORE spectra.

The contour lineshape in the powder 2D spectrum from $I = 1/2$ nuclei such as ^1H and ^{15}N Zeeman frequency, ν_1) for axial hyperfine interactions is described (Dikanov, S.A. and Bowman, M.K. (1995) *J. Magn. Reson. A* **116**, 125-128) by equation:

$$\nu_1^2 = Q\nu_2^2 + G \quad (\text{S2})$$

$$\text{where } Q = \frac{T + 2a - 4\nu_1}{T + 2a + 4\nu_1} \quad \text{and} \quad G = 2\nu_1 \left(\frac{4\nu_1^2 - a^2 + 2T^2 - aT}{T + 2a + 4\nu_1} \right)$$

For each cross-peak contour, the frequency values along the ridge can be plotted as ν_1^2 versus ν_2^2 , transforming the contour lineshape into a straight line segment whose slope and intercept are proportional to Q and G , respectively. These values can then be used to obtain two possible solutions of isotropic (a) and anisotropic (T) couplings with the same value of $|2a + T|$ and interchanged $A_\perp = |a - T|$ and $A_\parallel = |a + 2T|$.

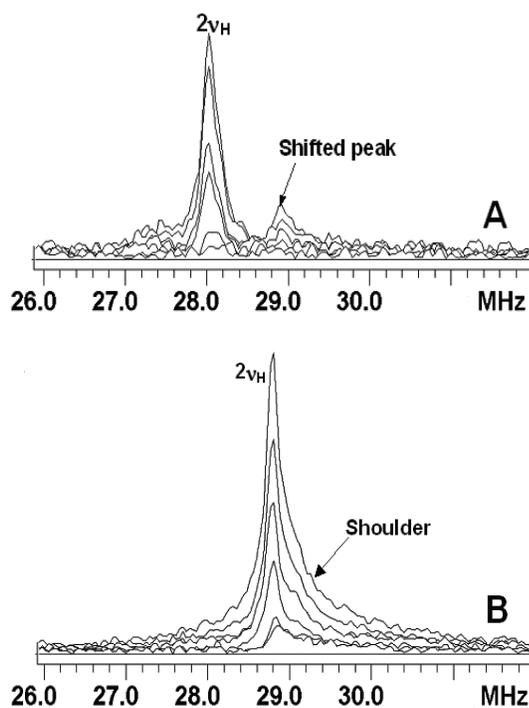


Figure B-S3. Stacked presentations of sets of four-pulse ESEEM spectra of $l(\text{N}_2\text{H}_4)$ intermediate. The spectra show the modulus of the Fourier transform along the time (T) axis for different times between first and second pulses, τ . The initial time τ is 100 ns in the farthest trace, and was increased by 12 ns in successive traces. Microwave frequency and magnetic field were 9.6995 GHz and 329.0 mT ($g = 2.106$) (A), 9.7004 GHz and 338.0 mT ($g = 2.05$) (B).

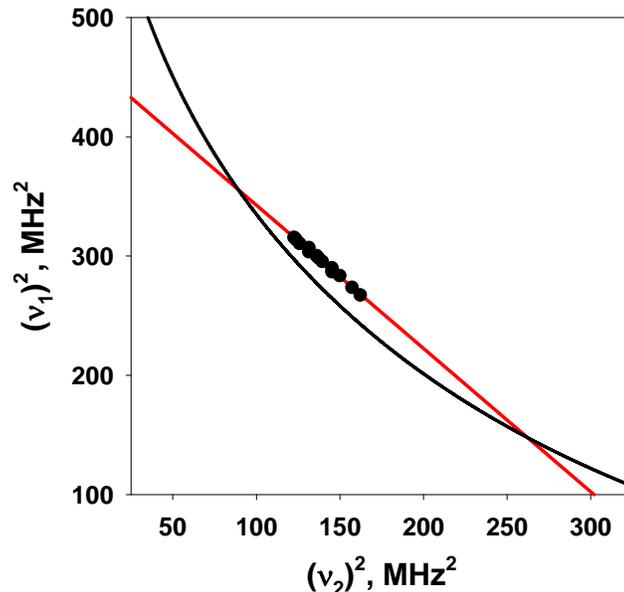


Figure B-S4. ^1H HYSCORE. The example of the cross-peaks **2** from the spectrum in **Figure B-S3A**. The coordinates v_1 and v_2 of arbitrary points along the ridge of cross-peaks **2** were plotted as sets of values for v_1^2 versus v_2^2 . The points have been fitted by linear regression (*red line*) to give the slope $Q = -1.20$ (0.03) and intercept $G = 462.8$ (3.8) MHz^2 . **Eq S1** with these coefficients define two solutions: $T = 4.6$ MHz and $a = -4.9$ MHz; $T = 4.6$ MHz and $a = 0.3$ MHz (signs are relative). In addition, the curve $|v_1 + v_2| = 2v_1$ (using $v_1 = 14.136$ MHz corresponding to the proton Zeeman frequency in the field 332 mT) is plotted in **Figure B-S4** to explain the nature of the two solutions determined by **Eq. (S1)**. The points at which the curve crosses each extrapolated straight line correspond to the nuclear frequencies v_α and v_β at canonical orientations. For an axial hyperfine tensor, there are two possible assignments of the parallel or perpendicular orientations and consequently, two sets of hyperfine tensors, one for each assignment. This approach gives hyperfine couplings a and T identical to those determined from the slope and intercept.

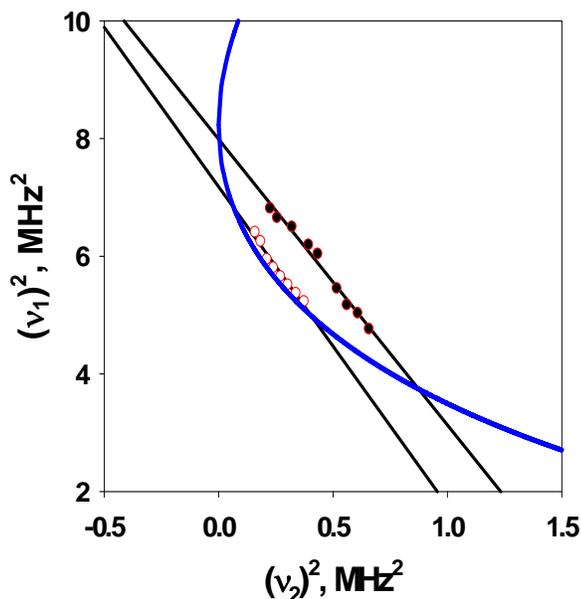


Figure B-S5. ¹H HYSCORE. The $((\nu_1)^2$ vs. $(\nu_2)^2$) plot for two arcs forming the ¹⁵N cross-feature seen in **Figure 2-8C**.

For the nonaxial hyperfine tensor, the cross-peak contour lineshape from single nitrogen in powder sample is a triangle with the corners located at the $|\nu_1+\nu_2|=2\nu_1$ line (*blue line* in the figure) (Dikanov, S. A.; Tyryshkin, A. M.; Bowman, M. K. *J. Magn. Reson.* **2000**, *144*, 228-242). The coordinates of the corners determine the principal values of the hyperfine tensor A_i ($i=1,2,3$) via the relations $[(\nu_1 + A_i/2)^2, (\nu_1 - A_i/2)^2]$, $A_i = a + T_i$. However, the spectrum in Figure 9C is orientation-selected one where only limited part of orientations forms the lineshape. It suggests that the observed arcs only part of the total lineshape, which would be observed in hypothetical case of complete excitation of all orientations. Theoretical prediction suggests that linear regressions of these arcs should give the estimate of two crossing points with the $|\nu_1+\nu_2|=2\nu_1$ line for each arc. If

two resolved arcs forming a cross-feature are resulted from non-axial tensor then two straight lines in coordinates $((v_1)^2$ vs. $(v_2)^2$) corresponding to these arcs should cross on $|v_1+v_2|=2v_1$ curve (or at least near this curve in the analysis of real spectrum). However, the regression lines of the points from two arcs are crossing somewhere far away from the $|v_1+v_2|=2v_1$ line indicating that this cross-feature is not produced by single nitrogen with nonaxial hyperfine tensor. If suggest that two arcs are produced by different nitrogens then their regression parameters $Q = -4.859 (0.22)$, $G = 7.991 (0.1) \text{ MHz}^2$ and $Q = -5.41 (0.387)$, $G = 7.18 (0.1) \text{ MHz}^2$ define two possibilities for each tensor in axial approximation, respectively: $T = 0.6 \text{ MHz}$ and $a = -2.2 \text{ MHz}$, $T = 0.6 \text{ MHz}$ and $a = 1.6 \text{ MHz}$; and $T = 0.25 \text{ MHz}$ and $a = -2.1 \text{ MHz}$ and $T = 0.25 \text{ MHz}$ and $a = -1.85 \text{ MHz}$.

APPENDIX C

SUPPORTING INFORMATION FOR CHAPTER 6

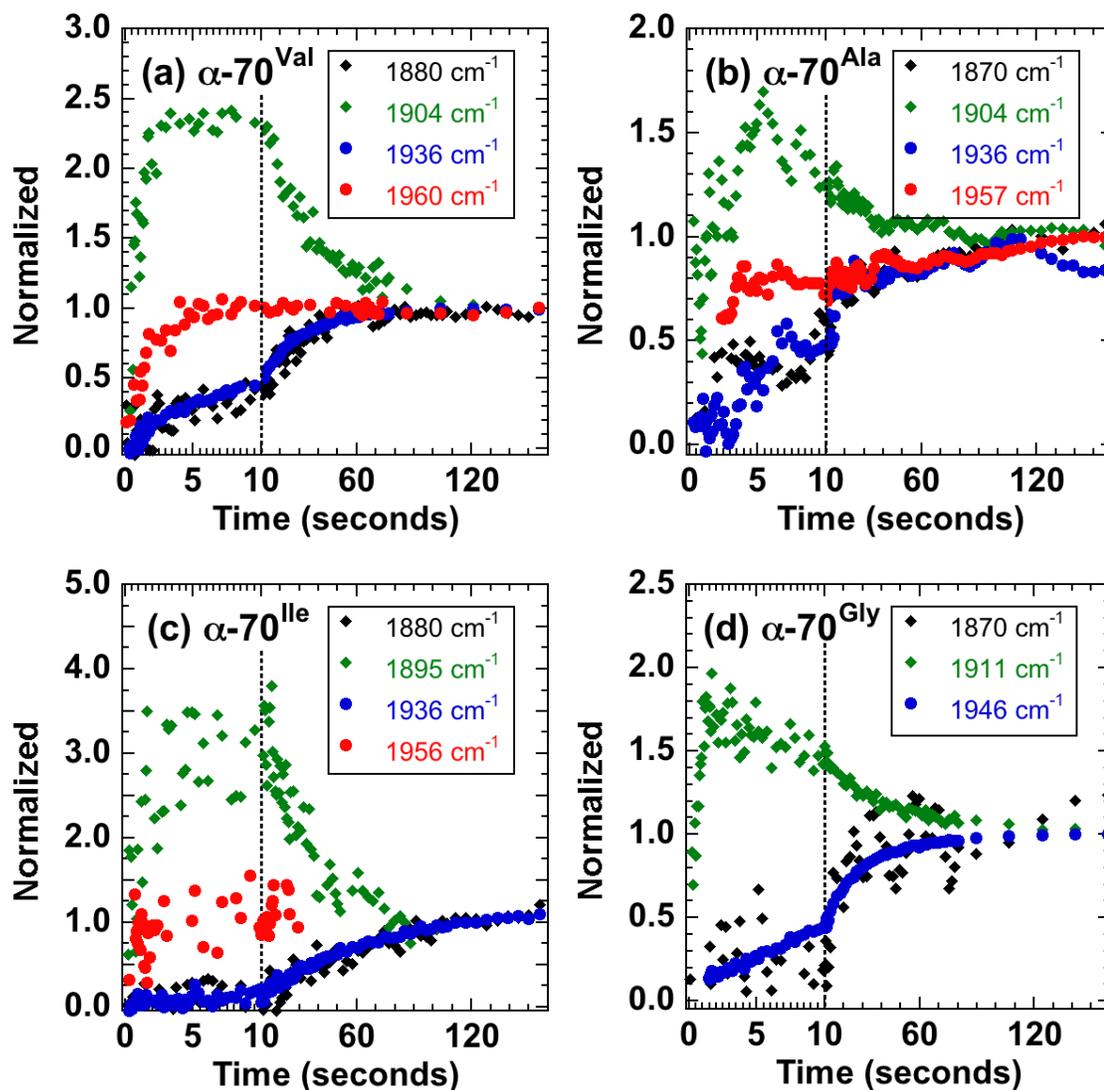


Figure C-S1. Time courses from transient IR spectra of the *A. vinelandii* MoFe nitrogenase hi-CO complex showing the effect of varying the size of the α -70 sidechain. Spectra are in **Figure 6-2a**. (a) Wild-type (α -70^{Val}) measured at 1880, 1904, 1936, 1960 cm^{-1} . This is the same as **Figure 6-2b**. (b) α -70^{Ala} at 1870, 1904, 1936, 1957 cm^{-1} . (c) α -70^{Ile} at 1880, 1895, 1936, 1956 cm^{-1} . The band at 1956 cm^{-1} was obscured by the 1936 cm^{-1} band at long times. (d) α -70^{Gly} at 1870, 1911, 1946 cm^{-1} . Intensities are normalized at (a-c) 150 s or (d) 120 s.

APPENDIX D

SUPPORTING INFORMATION FOR CHAPTER 8

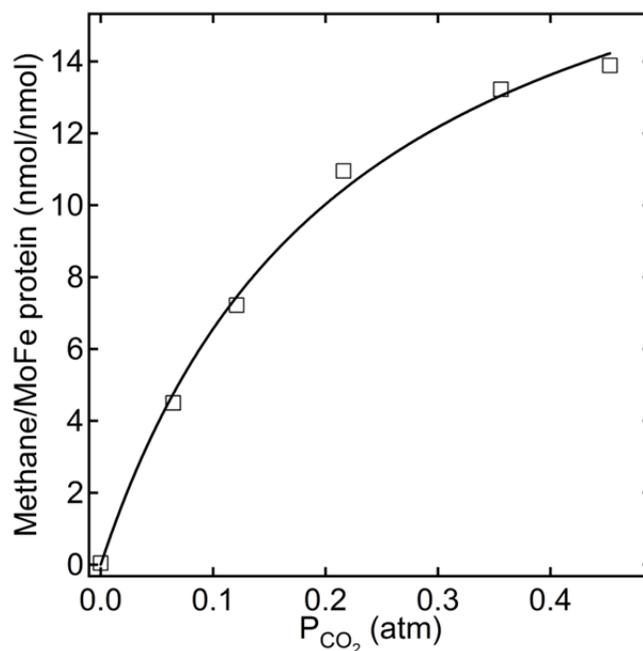


Figure D-S1. Dependence of CH₄ formation on partial pressure of CO₂. Methane production is shown under different partial pressure of CO₂ catalyzed by α -70^{Ala}/ α -195^{Gln} MoFe protein. The concentration of MoFe protein was 0.5 mg/mL, and Fe protein was 3 mg/mL. The reactions were incubated at 30°C for 20 min. The data were fitted to the Michaelis-Menten equation, yielding V_{\max} of 21 nmol CH₄/nmol MoFe protein and K_m of 0.23 atm of CO₂.

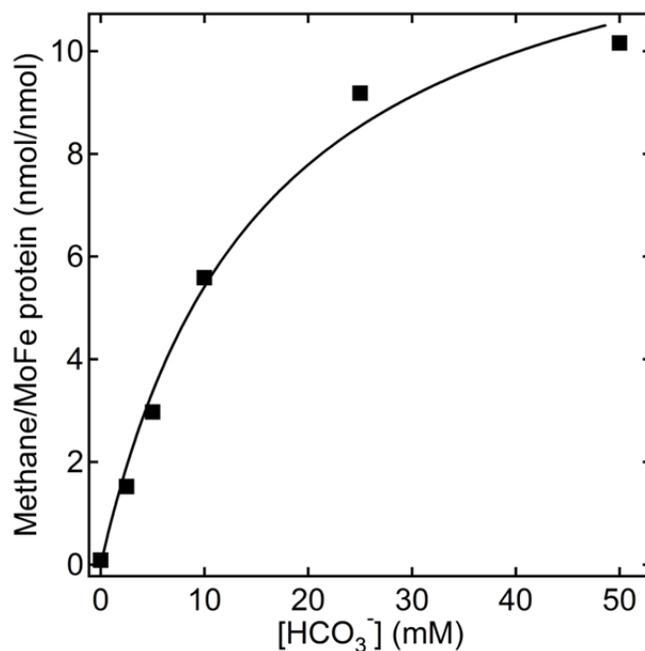


Figure D-S2. Dependence of CH₄ formation on concentration of HCO₃⁻. The amount of CH₄ formed as a function of the concentration of HCO₃⁻ is shown for the α -70^{Ala}/ α -195^{Gln} MoFe protein. The assay contained 3 mg/mL of Fe protein and 0.5 mg/mL of MoFe protein. The assay was at 30°C for 20 min. The data were fit to the Michaelis-Menten equation, yielding V_{\max} of 14 nmol CH₄/nmol MoFe protein and K_m of 16 mM of HCO₃⁻.

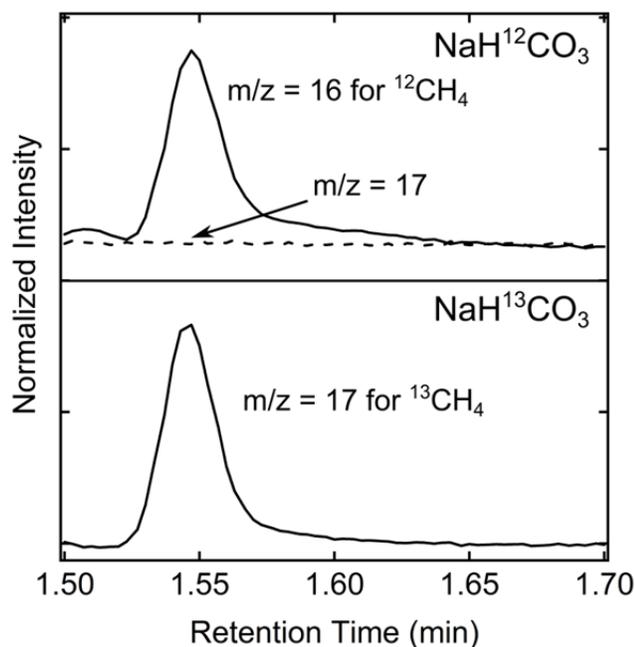


Figure D-S3. GC-MS analysis of methane. A portion of the gas mixture of an assay with α -70^{Ala}/ α -195^{Gln} MoFe protein and CO₂ was separated by gas chromatography, with detection by mass spectrometry. H¹²CO₃⁻ (upper graph) or H¹³CO₃⁻ (lower graph) were used as substrate. The peak eluting at 1.55 min was analyzed for molecular ion peak of ¹²CH₄ or ¹³CH₄ with a mass over charge ratio (m/z) of 16 or 17, as indicated.

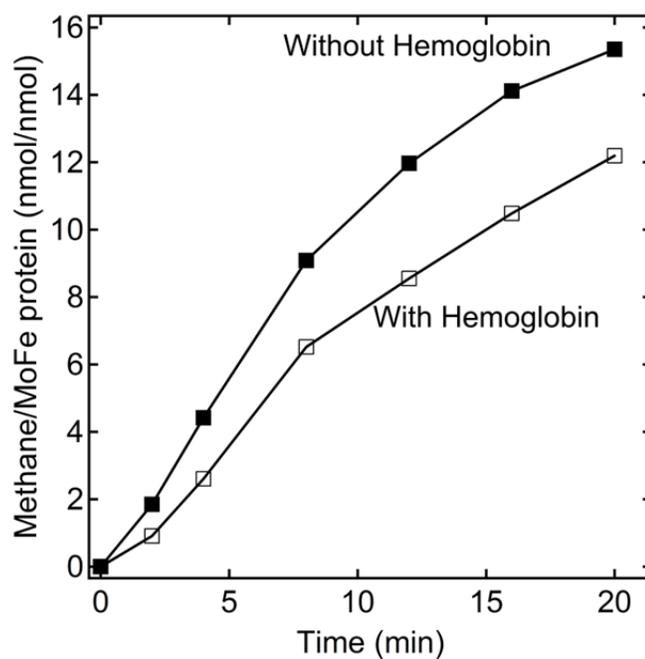


Figure D-S4. Effect of hemoglobin on CH₄ formation. The formation of CH₄ for the α -⁷⁰Ala/ α -¹⁹⁵Gln MoFe protein is shown as a function of time either without (■) or with 0.3 mg/mL hemoglobin (□). The partial pressure of CO₂ was 0.45 atm, the concentration of MoFe protein was 0.5 mg/mL, and Fe protein was 3 mg/mL. The reactions were conducted at 30°C for 20 min.




Figure D-S5. GC-MS analysis of propylene. A portion of the gas mixture of an assay with α -70^{Ala}/ α -195^{Gln} MoFe protein with CO₂ and acetylene was separated by gas chromatography, with detection by mass spectrometry. H¹²CO₃⁻ (upper graph) or H¹³CO₃⁻ (lower graph) and ¹²C₂H₂ were used as substrates. The peak eluting around 9.4 min was analyzed for molecular ion peak of ¹²C₃H₆ or ¹³CH₃-¹²CH=¹²CH₂ with a mass over charge ratio (m/z) of 42 or 43, as indicated.

CURRICULUM VITAE

Zhiyong Yang

Department of Chemistry and Biochemistry

Utah State University

0300 Old Main Hill

Logan, UT 84322-0300

E-mail: zhiyong.yang@aggiemail.usu.edu or usuyang@gmail.com

Lab Phone: (435) 797-7392

Cell Phone: (435) 754-9690

Education

08/2007-present *Ph. D. candidate in Biochemistry*, Department of Chemistry and Biochemistry, Utah State University, Logan, Utah, USA. Advisor: Prof. Lance C. Seefeldt

Dissertation title: Substrate Binding and Reduction Mechanism of Molybdenum Nitrogenase

12/2006 *Ph. D. in Organic Chemistry*, State Key Laboratory of Elemento-Organic Chemistry and Department of Chemistry, Nankai University, Tianjin, China. Supervisor: Prof. Licheng Song

Dissertation title: New Types of Models for the [FeFe] Hydrogenase Active Site: Synthesis, Structures and Functions.

07/2001 *B. Sc. in Chemistry*, Department of Chemistry, Nankai University, Tianjin, China. Advisors: Prof. Licheng Song and Prof. Qingmei Hu.

Thesis title: Investigations on Synthesis, Structures and Reactions of New Type of Acyclic and Macrocyclic Double Butterfly-Shaped Fe/S Cluster Complexes.

Publications

1. **Zhi-Yong Yang**, Nimesh Khadka, Dmitriy Lukoyanov, Brian M. Hoffman*, Dennis R. Dean*, and Lance C. Seefeldt*. "On reversible H₂ loss upon N₂ binding to FeMo-cofactor of nitrogenase." *Proc. Natl. Acad. Sci. USA*, **2013**, *110*, 16327-16332.
2. Lance C. Seefeldt*, **Zhi-Yong Yang**, Simon Duval, and Dennis R. Dean*. "Nitrogenase reduction of carbon-containing substrates." *Biochim. Biophys. Acta* **2013**, *1827*, 1102-1111.
3. Vivian R. Moure, Karamatullah Danyal, **Zhi-Yong Yang**, Shannon Wendroth, Marcelo Müller-Santos, Fabio O. Pedrosa, Marcelo, Scarduelli, Edileusa C. M. Gerhardt, Luciano F. Huergo, Emanuel M. Souza* and Lance C. Seefeldt*. "The nitrogenase regulatory enzyme dinitrogenase reductase ADP-ribosyltransferase

- (DraT) is activated by direct interaction with the signal transduction protein GlnB.” *J. Bacteriol.* **2013**, *195*, 279-286.
4. **Zhi-Yong Yang**, Vivian R. Moure, Dennis R. Dean, and Lance C. Seefeldt*. “CO₂ reduction to methane and coupling with acetylene forming propene catalyzed by remodeled nitrogenase.” *Proc. Natl. Acad. Sci. USA*, **2012**, *109*, 19644-19648. (This research was highlighted by Standard-Examiner, the Herald Journal, Utah State Today, and the Utah Statesman, and some other websites.)
 5. Dmitriy Lukoyanov, **Zhi-Yong Yang**, Brett M. Barney, Dennis R. Dean*, Lance C. Seefeldt*, and Brian M. Hoffman*. “Unification of reaction pathway and kinetic scheme for N₂ reduction catalyzed by nitrogenase.” *Proc. Natl. Acad. Sci. USA*, **2012**, *109*, 5583-5587. (This research was highlighted by the Salt Lake Tribune, the Herald Journal, Utah State Today, and the Utah Statesman.)
 6. Dmitriy Lukoyanov, Sergei Dikanov*, **Zhi-Yong Yang**, Brett M. Barney, Rimma I. Samoilova, Kuppala V. Narasimhulu, Dennis R. Dean*, Lance C. Seefeldt*, and Brian M. Hoffman*. “ENDOR/HYSCORE studies of the common intermediate trapped during nitrogenase reduction of N₂H₂, CH₃N₂H, and N₂H₄ support an alternating reaction pathway for N₂ reduction.” *J. Am. Chem. Soc.* **2011**, *133*, 11655-11664.
 7. **Zhi-Yong Yang**, Dennis R. Dean, and Lance C. Seefeldt*. “Molybdenum nitrogenase catalyzes the reduction and coupling of CO to form hydrocarbons.” *J. Biol. Chem.* **2011**, *286*, 19417-19421. (This paper has been selected as the paper of the week (top 1%), and was highlighted by the American Society for Biochemistry and Molecular Biology, the Salt Lake Tribune, the Herald Journal, Utah State Today, College of Science of USU and some other websites. The first author was profiled by the Journal of Biological Chemistry.)
 8. **Zhi-Yong Yang**, Lance C. Seefeldt, Dennis R. Dean, Stephen P. Cramer, and Simon J. George*. “Steric control of the hi-CO MoFe nitrogenase complex revealed by stopped-flow infrared spectroscopy.” *Angew. Chem. Int. Ed.* **2011**, *50*, 272-275.
 9. Dmitriy Lukoyanov, **Zhi-Yong Yang**, Dennis R. Dean*, Lance C. Seefeldt*, and Brian M. Hoffman*. “Is Mo involved in hydride binding by the four-electron reduced (E₄) intermediate of the nitrogenase MoFe protein?” *J. Am. Chem. Soc.* **2010**, *132*, 2525-2527.
 10. Li-Cheng Song, Qing-Shan Li, **Zhi-Yong Yang**, Yu-Juan Hua, Hong-Zhu Bian, and Qing-Mei Hu. “Synthesis and characterization of diiron thiadithiolate complexes related to the active site of [FeFe]-hydrogenases.” *Eur. J. Inorg. Chem.* **2010**, 1119-1128.
 11. Li-Cheng Song *, Chang-Gong Li, Jian-Hua Ge, **Zhi-Yong Yang**, Hu-Ting Wang, Juan Zhang, and Qing-Mei Hu. “Synthesis and structural characterization of the mono- and diphosphine-containing diiron propanedithiolate complexes related to [FeFe]-hydrogenases. Biomimetic H₂ evolution catalyzed by (μ-PDT)Fe₂(CO)₄ [(Ph₂P)₂N(n-Pr)].” *J. Inorg. Biochem.* **2008**, *102*, 1973-1979.
 12. Li-Cheng Song, * Bang-Shao Yin, Yu-Long Li, Li-Qun Zhao, Jian-Hua Ge, **Zhi-**

- Yong Yang**, and Qing-Mei Hu. "Synthesis, structural characterization, and some properties of new N-functionally substituted diiron azadithiolate complexes as biomimetic models of iron-only hydrogenases." *Organometallics* **2007**, *26*, 4921-4929.
13. Li-Cheng Song, * **Zhi-Yong Yang**, Yu-Juan Hua, Hu-Ting Wang, Yang Liu, and Qing-Mei Hu. "Diiron thiadithiolates as active site models for the iron-only hydrogenases: Synthesis, structures, and catalytic H₂ production." *Organometallics* **2007**, *26*, 2106-2110.
 14. Li-Cheng Song, * **Zhi-Yong Yang**, Hong-Zhu Bian, Yang Liu, Hu-Ting Wang, Xu-Feng Liu, and Qing-Mei Hu. "Diiron oxadithiolate type models for the active site of iron-only hydrogenases and biomimetic hydrogen evolution catalyzed by Fe₂(μ-SCH₂OCH₂S-μ)(CO)₆." *Organometallics* **2005**, *24*, 6126-6135.
 15. Li-Cheng Song, * **Zhi-Yong Yang**, Hong-Zhu Bian, and Qing-Mei Hu. "Novel single and double diiron oxadithiolates as models for the active site of [Fe]-only hydrogenases." *Organometallics* **2004**, *23*, 3082-3084.
 16. Li-Cheng Song, * Hong-Tao Fan, Qing-Mei Hu, **Zhi-Yong Yang**, Yi Sun, and Feng-Hua Gong. "Formation and chemical reactivities of a new type of double-butterfly [$\{\text{Fe}_2(\mu\text{-CO})(\text{CO})_6\}_2(\mu\text{-SZS-}\mu)\}^{2-}$]: Synthesis and structural studies on novel linear and macrocyclic butterfly Fe/E (E = S, Se) cluster complexes." *Chem. Eur. J.* **2003**, *9*, 170-180.
 17. Li-Cheng Song, * Qing-Mei Hu, Hong-Tao Fan, Ming-Yi Tang, **Zhi-Yong Yang**, and Guo-Liang Lu. "Reactions of butterfly complex anions of the type $[(\mu\text{-RTe})(\mu\text{-CO})\text{Fe}_2(\text{CO})_6]^-$ with electrophiles. A new route to $\mu_4\text{-Se}$ containing double-butterfly clusters. Crystal structures of $(\mu\text{-}p\text{-MeC}_6\text{H}_4\text{Te})(\mu\text{-PhCH}_2\text{SC}=\text{S})\text{Fe}_2(\text{CO})_6$ and $[(\mu\text{-RTe})\text{Fe}_2(\text{CO})_6]_2(\mu_4\text{-Se})$ (R = Ph, *p*-BrC₆H₄)." *Organometallics* **2002**, *21*, 2468-2472.

Book Chapters

1. **Zhi-Yong Yang**, Karamatullah Danyal, and Lance C. Seefeldt*. "Mechanism of Mo-dependent Nitrogenase" In *Methods in Molecular Biology-Nitrogen Fixation*, Markus W. Ribbe (Editor), Humana Press, New York, USA, **2011**, 766, 9-29.
2. Karamatullah Danyal, **Zhi-Yong Yang**, and Lance C. Seefeldt*. "Electron Paramagnetic Resonance (EPR) Spectroscopy and Nitrogenase" In *Methods in Molecular Biology-Nitrogen Fixation*, Markus W. Ribbe (Editor), Humana Press, New York, USA, **2011**, 766, 191-205.

Poster Presentations

1. "Steric effects of hi-CO nitrogenase probed by stopped-flow infra-red spectroscopy." *Gordon Research Conferences: Iron-Sulfur Enzymes*, Colby-Sawyer College, New London, NH, USA, June **2010**.

2. “Testing the site of substrate binding on nitrogenase cofactor by ^{95}Mo ENDOR spectroscopy.” *52nd Rocky Mountain Conference on Analytical Chemistry, Snowmass Conference Center, Snowmass, CO, USA, August 2010.*
3. “Mo-nitrogenase catalyzes reductive coupling reaction of carbon monoxide and carbon dioxide to form hydrocarbons.” *1st Hansen Biochemistry Retreat, Logan, UT, USA, September 2011.*
4. “Unification of N_2 reduction pathway and Lowe-Thorneley kinetic scheme catalyzed by nitrogenase.” *Gordon Research Conferences: Iron-Sulfur Enzymes, Mount Holyoke College, South Hadley, MA, USA, June 2012.*
5. “ CO_2 reduction to methane and coupling with acetylene to form propylene catalyzed by remodeled nitrogenase.” *2nd Hansen Biochemistry Retreat, Logan, UT, USA, September 2012.*
6. “An insight into nitrogenase catalyzed H/D exchange reaction.” *2nd Hansen Biochemistry Retreat, Logan, UT, USA, September 2012.*

Research and Teaching Experience

Graduate Research Assistant, 08/2007-present, Department of Chemistry and Biochemistry, Utah State University, Logan, Utah, USA. Worked on a research project focusing on figuring out the mechanism of nitrogen fixation catalyzed by molybdenum nitrogenase, and initiated a project using carbon-containing substrates as probes to understand the mechanism of molybdenum nitrogenase.

Graduate Teaching Assistant, 08/2007-05/2010, Department of Chemistry and Biochemistry, Utah State University, Logan, Utah, USA. Served as a teaching assistant in general chemistry laboratory classes.

Research Scientist, 12/2006-03/2007, Shanghai ChemPartner Co., Ltd., Shanghai, China. Synthesized and characterized a series of pharmaceutical lead compounds for the customer company.

Graduate Research Assistant, 09/2001-09/2006, Department of Chemistry, Nankai University, Tianjin, China. Initiated and established the biomimetic chemical research of [FeFe]-hydrogenase in the laboratories of Prof. Licheng Song.

Undergraduate Research Assistant, Summer 1999 and 03/2000-06/2001, Department of Chemistry, Nankai University in the laboratories of Prof. Guocai Deng, Prof. Jingjiang Liu and Prof. Licheng Song, respectively.

Research Interests

- Biochemistry and Biomimetic chemistry of metalloenzymes, especially hydrogenases, nitrogenases, and CO-dehydrogenases;

- Mechanisms of hydrogenases, nitrogenases, and other metalloenzymes relevant to natural hydrogen, nitrogen and carbon cycles.
- Organic, inorganic and bio-pharmaceutical chemistry.
- Development of novel metallic catalyst for conversion of carbon monoxide and carbon dioxide into fuels and value-added chemicals.
- Organometallic chemistry focusing on homonuclear or heteronuclear metal-metal multiple bonds and their reactivities.
- Organic reactions catalyzed by organometallic complexes.
- Activation of small molecules such as H₂, N₂, CO, CO₂, R₂C=CR₂, RC≡N and X-H bonds (X = C, N, Si, P and S) by transition metal complexes and related mechanisms.
- Chemistry of low-coordinated and low-valence transition metal complexes.

Awards and Honors

- 2012 *Graduate Student Travel Award*, Department of Chemistry and Biochemistry, Utah State University, Logan, UT, USA.
- 2010 *Graduate Student Travel Award*, Department of Chemistry and Biochemistry, Utah State University, Logan, UT, USA.
- 2005 *Donggang Scholarship*, Nankai University and Donggang Foundation in China
- 2003 *Donggang Scholarship*, Nankai University and Donggang Foundation in China
- 2002 *Donggang Scholarship*, Nankai University and Donggang Foundation in China
- 2001 *Outstanding Thesis Award*, Nankai University, Tianjin, China
- 2001 *Tri-A Student*, Nankai University, Tianjin, China
- 2000 *First-Class Award of the Fourth Experiment Competition*, Department of Chemistry, Nankai University, Tianjin, China
- 2000 *Third-Class Scholarship*, Nankai University, Tianjin, China
- 1999 *Second-Class Scholarship*, Nankai University, Tianjin, China
- 1999 *Tri-A Student*, Nankai University, Tianjin, China
- 1998 *First-Class Scholarship*, Nankai University, Tianjin, China
- 1998 *Tri-A Student*, Nankai University, Tianjin, China
- 1997 *First-Class Freshman Scholarship*, Nankai University, Tianjin, China

Professional Memberships

Member of the American Chemical Society (ACS), 2008-present.

Member of the American Association for the Advancement of Science (AAAS), 2009-present.